Advancing Lipidomics through Method Development, Data Processing, and its Applications in Cancer Research

by

Fernanda Sousa Monteiro

A thesis submitted in partial fulfillment of the requirements for the degree of

Doctor of Philosophy

Department of Chemistry
University of Alberta

© Fernanda Sousa Monteiro, 2024

Abstract

Lipidomics, a subfield of metabolomics, offers comprehensive insights into the lipid composition of biological systems. Lipids, comprising a broad class of biological molecules, are essential to several biological functions. They play critical roles in cell membrane formation, serving as signaling molecules and storing energy. Studying the lipidome can give insights into cellular processes and metabolic pathways. Several diseases affect lipid synthesis and metabolism, making lipidomics a valuable tool in health research. Understanding lipid changes caused by diseases can aid in biomarker research for early detection and disease progression. However, despite its potential, lipidomics requires more reliable and sensitive methods to enhance the profiling of biological samples.

Biological samples are susceptible to changes in their composition due to a broad range of factors, impacting lipid composition and adding uncertainty to quantitative analyses. To ensure a robust LC-MS workflow, it is crucial to maintain uniform sample concentrations, guaranteeing consistent instrument response. However, a standard method for lipid quantification has not been established in lipidomics. Often, metabolomics or proteomics techniques are used instead. Given the diverse characteristics of lipid samples, a specific method for lipid normalization is essential. The first part of this work focuses on developing a reliable Sulfo-Phospho-Vanillin (SPV) assay for normalizing samples in LC-MS lipidomics. This colorimetric method, optimized for better limits of detection and quantification, ensures accurate lipid measurements by reducing variability. Furthermore, this study also evaluates lipid profiles in human saliva, investigating the effects of different normalization methods on lipid annotations.

The second part of this work focused on developing a two-dimensional liquid chromatography-mass spectrometry (2DLC-MS) method. By optimizing the HILIC method and its integration with RPLC-MS, a robust 2DLC-MS framework was developed to overcome common analytical challenges in lipidomics, such as ion suppression and co-elution. This method showed improvements in peak resolution and reduction of ion suppression through a fractionation approach. Comparative analyses using different data processing software revealed varying levels of annotation accuracy, highlighting the importance of software selection in lipidomics studies. Moreover, Chapter V describes the development and optimization of a 1.0 mm inner diameter LC-MS method using Orbitrap for lipidomic profiling. The optimized method was validated using biological samples, demonstrating improved lipid coverage and peak resolution. Lastly, Chapter VI applies the methods developed in Chapters IV and V to investigate how cisplatin and rapamycin, two cancer drugs, alter lipid profiles in non-small cell lung cancer (NSCLC) cells. This chapter focuses on understanding the metabolic disruptions caused by these chemotherapeutic agents, providing a comprehensive lipidomic profile of A549 cells under different treatment conditions. The results reveal significant lipid composition and metabolism changes, highlighting the distinct and combined effects of cisplatin and rapamycin.

This work shows that more sensitive methods can improve lipid profiling and offer a comprehensive understanding of metabolic changes caused by diseases and treatments. The results described herein show the potential of lipidomics for biomarker discovery.

Preface

A version of Chapter II is currently being prepared for publication. This work was a collaboration with Dr. Adriana Zardini Buzatto (University of Calgary, Calgary, AB, CA). A version of this work was presented as a poster at the 69th American Society for Mass Spectrometry (ASMS) Conference on Mass Spectrometry and Allied Topics (October 31st to November 4th, 2021, Philadelphia, Pennsylvania, USA) as Fernanda Monteiro Queiroz, Adriana Zardini Buzatto and Liang Li; Sulfo-phospho-vanillin assay as a normalization method in LC-MS lipidomics. Another version of this chapter was presented at the 70th American Society for Mass Spectrometry (ASMS) Conference on Mass Spectrometry and Allied Topics (June 5th to June 9th, 2022, Minneapolis, Minnesota, USA) as Fernanda Monteiro Queiroz, Adriana Zardini Buzatto and Liang Li; Improving untargeted LC-MS cell lipidomics employing the Sulfo-phospho-vanillin method for sample normalization. I was responsible for saliva sample collection, experimental design and execution, data processing, interpretation, and writing. Dr. Li designed the experiments and supervised the project. Dr. Adriana Zardini Buzatto supervised experiments and interpreted data.

Chapter III was a collaboration with Dr. Adriana Zardini Buzatto (University of Calgary, Calgary, AB, CA). I was responsible for experimental design and execution, data processing, interpretation, and writing. Dr. Li designed the experiments and supervised the project. Dr. Adriana Zardini Buzatto was responsible for saliva sample collection and experimental design.

A version of Chapter IV is currently being prepared for publication. This work was a collaboration with Dr. Adriana Zardini Buzatto (University of Calgary, Calgary, AB, CA). A version of this work was presented as a poster at the 71st American Society for Mass Spectrometry (ASMS) Conference on Mass Spectrometry and Allied Topics (June 4th to June 8th, 2023, Houston,

Texas, USA) as Fernanda Monteiro, Adriana Zardini Buzatto and Liang Li; Development of an offline 2D-LC Lipidomics method. I was responsible for experimental design and execution, data processing, interpretation, and writing. Dr. Li designed the experiments and supervised the project. Dr. Adriana Zardini Buzatto supervised experiments and interpreted data.

A version of Chapter V is currently being prepared for publication. A version of this work was presented as a poster at the 72nd American Society for Mass Spectrometry (ASMS) Conference on Mass Spectrometry and Allied Topics (June 3rd to June 7th, 2023, Anaheim, California, USA) as Fernanda Sousa Monteiro and Liang Li; Optimization of a micro-LC-MS/MS method for untargeted Lipidomics. I was responsible for experimental design and execution, data processing, interpretation, and writing. Dr. Li designed the experiments and supervised the project.

Chapter VI was part of a comprehensive lipidomics and metabolomics study in collaboration with Cyrene Jonah Catenza. I was responsible for experimental design and execution, data processing, interpretation, and writing. Cyrene Jonah Catenza was responsible for experimental design and execution, data processing, interpretation, and writing. Dr. Li designed the experiments and supervised the project.

Appendices A, B, C, D, and E contain supporting figures for Chapters II, III, IV, V, and VI. Supplementary tables are available on the University of Alberta's Education and Research Archive (ERA) website under DOI: 10.7939/r3-27jx-mm98."

Acknowledgments

First, I would like to thank my supervisor Dr. Liang Li. This work could not have been completed without his guidance and support. Over the past five years, amidst various challenges, including a global pandemic, Dr. Li has encouraged me to strive for excellence and persevere through difficult times. I will forever be grateful for all the lessons and wisdom he shared. I would also like to thank my supervisory committee, Dr. Michael Serpe and Dr. John Vederas, for their comments and support during this journey.

I am also thankful to my current and past colleagues in the Li group, who made the past five years a more enjoyable experience. No words are enough to thank them for their on this journey. Their comments, questions, and feedback helped me navigate my research and prepare for several important milestones. A very special thank you to Adriana Zardini Buzatto, who gave me my initial training and introduction to lipidomics. To Gareth Lambkin, thank you for training me in cell culture procedures and advising me in navigating challenges in this field, and to all the staff at the Department of Chemistry at the University of Alberta.

This journey would not have been possible without the unconditional love and support my family and friends have given me throughout the years. My godfather, Wilson Ghetti, was the wisest person I have ever met. He instigated my curiosity and encouraged me to learn more about everything. My parents, Edson and Helena, never told me I could not do whatever I wanted to do or be whoever I wanted to be. Together with my brothers, Daniel and Matheus, they always encouraged me to pursue my dreams, even those they did not fully understand. I would also like to thank my host parents, Glenn Yarnell and Joan Giovannini, for teaching the 16-year-old me so

much about life and myself in what now seems such a short period. They became not just family but a constant source of inspiration and love. Erin Campbell and Hal Danchilla are kind, decent, unfailingly generous people. No words would be enough to thank everything they have done for me. I am extremely lucky to have them in my life. Last but certainly not least, I would like to thank my boyfriend, André. He has been my full-time cheerleader since day one, particularly in the last few months. His patience, understanding, and unwavering support have been invaluable - his ability to understand Python scripting was just a nice bonus! Thank you all for standing by my side; this work is as much yours as it is mine!

Table of Contents

List of Figures

List of Tables

List of Abbreviations

1DGC	One-dimensional gas chromatography
1DLC	One-dimensional liquid chromatography
2DGC	Two-dimensional gas chromatography
2DLC	Two-dimensional liquid chromatography
2DLC-MS	Two-Dimensional Liquid Chromatography-Mass Spectrometry
ACN	Acetonitrile
ALK	Anaplastic Lymphoma Kinase
Arb	Arbitrary Units
ASG	Acylsterylglycosides
BA	Bile acids and derivatives
BEH	Ethylene Bridged Hybrid
BPC	Base Peak Chromatogram
CAR	Acyl carnitines
CE	Cholesteryl Ester

Cer	Ceramide
CID	Collision induced dissociation
CL	Cardiolipin
CoA	Acyl CoAs
CSF	Cerebral Spinal Fluid
CSH	Charged Surface Hybrid
DCM	Dichloromethane
DDA	Data-dependent acquisition
DG	Diacylglycerol
DGDG	Digalactosyldiacylglycerol
DGMG	Digalactosylmonoacylglycerol
DMEM	Dulbecco's Modified Eagle Medium
DMSO	Dimethyl Sulfoxide
DNA	Deoxyribonucleic acid
EDTA	Ethylenediaminetetraacetic Acid

EGFR	Epidermal Growth Factor Receptor
EIC	Extracted Ion Chromatogram
EPA	Eicosapentaenoic acid
ESI	Electrospray Ionization
EtOH	Ethanol
FA	Fatty Acid
FA	Fatty Acyls
FAHFA	FA estolides
FAL	Fatty aldehydes
FBS	Fetal Bovine Serum
FC	Fold Change
FC	Free cholesterol
FOH	Fatty alcohols
GC	Gas chromatography
GL	Glycerolipids

GP	Glycerophospholipids
H-ESI	Heated Electrospray Ionization
HexCer	Hexosylceramide
HILIC	Hydrophilic Interaction Liquid Chromatography
HMDB	Human Metabolome Database
IC	Inhibitory Concentration
ID	Inner Diameter
ILCNC	International Lipid Classification and Nomenclature Committee
IMS	Ion Mobility Spectrometry
IPA	Isopropanol
IS	Internal Standard
IUPAC	International Union of Pure and Applied Chemistry
LC	Liquid chromatography
LC-MS	Liquid Chromatography-Mass Spectrometry
LDL	Low-density lipoprotein

LGP	Lysophospholipid
LLE	Liquid-Liquid Extraction
LOD	Limit of Detection
LOQ	Limit of Quantification
LPC	Lysophosphatidylcholine
LPE	Lysophosphatidylethanolamine
LPL	Lysophospholipids
m/z	Mass-to-Charge Ratio
MALDI	Matrix-Assisted Laser Desorption Ionization
MALDI-QIT-TOF	Matrix-assisted laser desorption/ionization-quadrupole ion trap-time of flight
MeOH	Methanol
MG	Monoacylglycerol
MGDG	Monogalactosyldiacylglycerol
MGMG	Monogalactosylmonoacylglycerol
MPA	Mobile Phase A

MPB	Mobile Phase B
MS	Mass Spectrometry
MS/MS	Tandem mass spectrometry
MSI	Mass spectrometry imaging
MTBE	Methyl tert-butyl ether
mTOR	mechanistic Target of Rapamycin
MUFA	Monosaturated fatty acids
NA	N-acyl amines
NAE	N-acyl ethanolamines
NAT	N-acyl taurines
N-mod PL	N-modified phospholipids
NMR	Nuclear Magnetic Resonance spectroscopy
NP	Normal Phase
NSCLC	Non-Small Cell Lung Cancer
Ox PL	Oxidized phospholipids

PA	Phosphatidic Acid
PBS	Phosphate-Buffered Saline
PC	Phosphatidylcholine
PC1	First principal component
PC2	Second principal component
PCA	Principal Component Analysis
PE	Phosphatidylethanolamine
PG	Phosphatidylglycerol
PI	Phosphatidylinositol
PIP	Phosphatidylinositol phosphates
PK	Polyketides
PKC	Protein kinase C
PL	Phospholipids
PLS-DA	Partial Least Square-Discriminant Analysis
PR	Prenol lipids

PS	Phosphatidylserine
PTFE	Polytetrafluoroethylene
PUFA	Polysaturated fatty acids
QC	Quality control
QToF	Quadrupole Time-of-Flight
QToF-MS	Quadruple Time-of-Flight Mass Spectrometry
RP	Reverse Phase
RPLC	Reverse Phase Liquid Chromatography
RPLC-MS	Reversed-Phase Liquid Chromatography-Mass Spectrometry
RSD	Relative Standard Deviation
S/N	Signal-to-noise ratio
S1P	Sphingosine-phosphates
SD	Standard deviation
SE	Steryl esters
SFA	Saturated fatty acids

SFC	Supercritical fluid chromatography
SFE	Short fatty ester
SG	Sterylglycosides
SL	Saccharolipids
SM	Sphingomyelin
SP	Sphingolipids
SPB	Sphingoid bases
SPV	Sulfo-phospho-vanillin
SQDG	Sulfoquinovosyldiacylglycerol
SQMG	Sulfoquinovosylmonoacylglycerol
ST	Sterols
TG	Triacylglycerol
TG-EST	Estolide
TIC	Total Ion Current
TIMS	Trapped Ion Mobility Spectrometry

TIMS-ToF	Trapped Ion Mobility Spectrometry Time-of-Flight Mass Spectrometry
TLC	Thin-layer chromatography
TLC	Total lipid concentration
TMC	Total metabolite concentration
TMIC	The Metabolomics Innovation Centre
ToF	Time-of-flight
UHPLC	Ultra High-Performance Liquid Chromatography
VIP	Variable Importance in Projection
WD	Wax Diesters
WE	Wax Esters

I

Chapter I: Introduction

1.1. Background on Lipidomics and Applications in Health Research

Lipidomics is a subfield of metabolomics focused on studying lipids in biological systems. It involves identifying and quantifying lipid molecules and their interactions with other lipids, proteins, and metabolites. It provides insights into the diverse roles these molecules play in biological systems, such as cell membranes, signaling pathways, and energy storage systems. Lipids are essential to cell structure, forming the lipid bilayer of cell membranes, which regulates the entry and exit of substances[1,2]. Additionally, lipids act as signaling molecules, mediating processes such as inflammation, cell growth, and cell death[1–3]. Lipid metabolism is crucial for energy storage and production, with fatty acids being a primary energy source during fasting or intense exercise. Lipids also form lipid rafts, microdomains in cell membranes that play a crucial role in signal transduction and protein sorting[1,4].

By evaluating how the lipidome changes, research can aid in discovering disease mechanisms for different conditions, such as cardiovascular diseases, diabetes, neurodegenerative disorders, and cancer[3,5–8]. Recent developments, such as Ion Mobility Mass Spectrometry (IMS), have enabled the precise identification and quantification of a wide range of lipid species. Additionally, advances in bioinformatics aid the analysis of complex lipidomics data, allowing researchers to identify lipid biomarkers associated with various diseases and to elucidate the underlying mechanisms of lipid metabolism[2,9–12].

High throughput lipidomics profiling has demonstrated specific phospholipid and sphingolipid alterations in metabolic disorders such as diabetes and obesity. These lipid changes can serve as early indicators of disease and progression, offering potential targets for therapeutic intervention[2,6,13,14]. In cancer research, lipid alterations were associated with cancer development and metastasis. Specific lipid species, such as ceramides and sphingolipids, regulate cell death and proliferation, highlighting their importance in cancer biology. Cancer cells often exhibit altered lipid profiles that can be used to distinguish between different cancer types and stages[15,16]. Additionally, lipidomics has made contributions to understanding neurodegenerative diseases. Lipid alterations in the brain and cerebrospinal fluid have been linked to conditions such as Alzheimer's disease and Parkinson's disease[5,17–19]. For example, changes in glycerophospholipid and sphingolipid metabolism have been associated with neuronal degeneration and cognitive decline, demonstrating how lipidomics can enhance modern medicine by identifying lipid-based biomarkers for disease diagnosis and treatment monitoring[20].

1.2. The Importance of Lipids

Over the years, lipid molecules have been defined differently, reflecting the complexity and diversity of these biomolecules. Despite many attempts to describe this class of molecules, a consensus on a single, all-encompassing definition still needs to be reached. Different sources provide varying descriptions based on their focus and scope of study. The IUPAC Gold Book defines lipids as "a loosely defined term for substances of biological origin that are soluble in nonpolar solvents”[21]. Similarly, biochemistry books have described this class as "a class of biological molecules defined by low solubility in water and high solubility in non-polar solvents"

or "a broad group of naturally occurring molecules that include fats, waxes, sterols, fat-soluble vitamins, monoglycerides, diglycerides, phospholipids, and others. They are characterized by their insolubility in water and solubility in nonpolar solvents"[22,23]. Despite these varying definitions, they all emphasize the solubility of lipids in nonpolar solvents and their insolubility in water, a key characteristic of their roles in biological systems[24,25].

1.2.1. Lipid Structures, Subclasses, and Biological Functions

LIPID MAPS is a comprehensive resource for lipid research supported by an association of international researchers. It aims to provide a structured classification system and extensive data on lipid molecules. LIPID MAPS categorizes lipids into eight subclasses based on their chemical structure and biological functions. These classes include fatty acyls (FA), glycerolipids (GL), glycerophospholipids (GP), sphingolipids (SP), sterol lipids (ST), prenol lipids (PR), saccharolipids (SL), and polyketides (PK)[26,27]. Structural examples for each of these subclasses can be found in Figure 1.1.

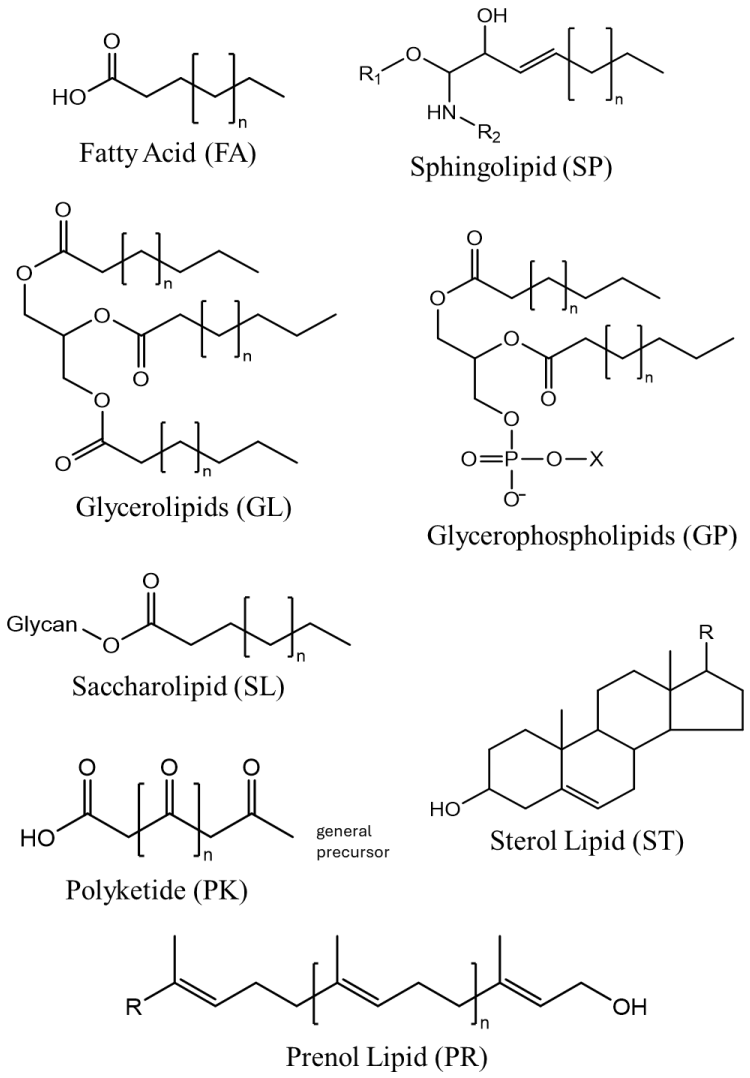

Figure 1.1. General Structures for each lipid subclass

1.2.2. Fatty acyls (FA) and Conjugates

Fatty acyls are fundamental building blocks of complex lipids, consisting of a hydrocarbon chain with a terminal carboxyl group. They are essential to various biological processes, including energy storage, cellular structure, and signaling pathways. They are categorized based on the presence or absence of double bonds and the number of carbon atoms in their structure[28–30]. Fatty

acyls typically have an even number of carbon atoms in mammalian samples because their biosynthetic pathway involves adding two-carbon units derived from acetyl-coenzyme A (CoA). Common even-chain fatty acids include palmitic acid (FA 16:0) and stearic acid (FA 18:0). Odd-chain fatty acids, such as pentadecanoic acid (FA 15:0) and heptadecanoic acid (FA 17:0), are less common and often originate from dietary sources or microbial fermentation in the gut. However, they have been studied for potential health benefits, including anti-inflammatory properties[29].

Moreover, FA lipids are also classified based on the presence or absence of double bonds. Saturated Fatty Acids (SFAs) are lipids that contain no double bonds, such as palmitic acid (FA 16:0) and stearic acid (FA 18:0). Saturated Fatty Acids are typically solid at room temperature and often found in animal fats and some plant oils. Monounsaturated Fatty Acids (MUFAs) contain only one double bond, such as oleic acid (FA 18:1), which is present in olive oil and is known for its beneficial effects on cardiovascular health, and palmitoleic acid (FA 16:1)[30,31]. Species with two or more double bonds are known as Polyunsaturated Fatty Acids (PUFAs). They can be further divided into omega-3 and omega-6 fatty acids based on the position of the first double bond from the methyl end. Examples of omega-3 FA include alpha-linolenic acid (FA 18:3) and eicosapentaenoic acid (EPA, FA 20:5), which are known for their anti-inflammatory properties and cardiovascular benefits[32]. Omega-6 fatty acids, such as linoleic acid (FA 18:2) and arachidonic acid (FA 20:4), play crucial roles in cell signaling and inflammation[32–35]. Figure 1.2 shows structural examples of SFAs, MUFAs, and PUFAs.

According to the LIPID MAPS database, Fatty acyls and conjugates can be further subdivided into 14 categories based on their structural characteristics: Fatty Acids (FA), Wax Esters (WE), Wax Diesters (WD), FA estolides (FAHFA), Short fatty ester (SFE), Fatty aldehydes

(FAL), Fatty alcohols (FOH), Acyl carnitines (CAR), Acyl CoAs (CoA), N-acyl amines (NA), N-acyl ethanolamines (NAE), N-acyl taurines (NAT), Eicosanoids, and Fatty acyl glycosides[27,36,37].

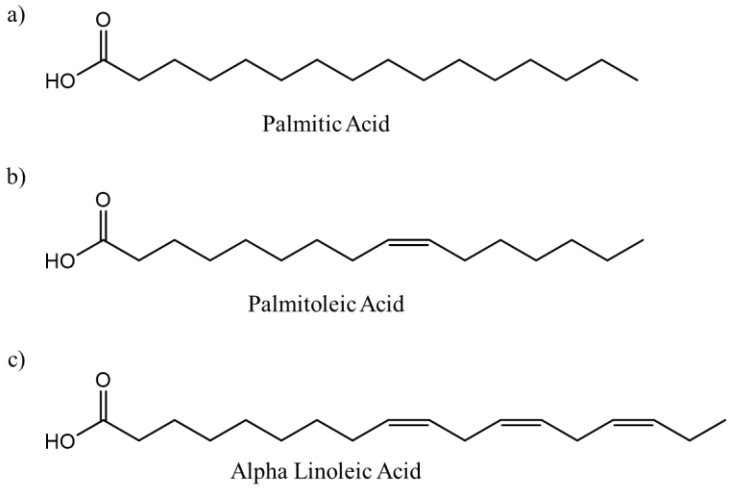

Figure 1.2. Structural examples of fatty acyls a) Saturated Fatty Acid (FA 16:0); b) Monounsaturated Fatty Acid (FA 16:1); and c) Polyunsaturated Fatty Acid (FA 18:2).

1.2.3. Glycerolipids (GL)

Comprised of at least one fatty acid chain esterified to a glycerol backbone, GLs play a role in energy storage and membrane structure. They are composed of glycerol, a three-carbon alcohol, that is the backbone to which fatty acids are esterified and characterized by the number of fatty acids attached to the glycerol backbone[2,38]. LIPID MAPS categorizes GLs into nine subclasses based on their chemical structure, as follows: Monoacylglyceride (MG), Diacylglyceride (DG), Triacylglyceride (TG), Estolide (TG-EST), Sulfoquinovosylmonoacylglycerol (SQMG), Monogalactosylmonoacylglycerol (MGMG), Digalactosylmonoacylglycerol (DGMG), Sulfoquinovosyldiacylglycerol (SQDG), Monogalactosyldiacylglycerol (MGDG),

Digalactosyldiacylglycerol (DGDG), with MG, DG and TG being the most common GL (Figure 1.3)[26,36,37].

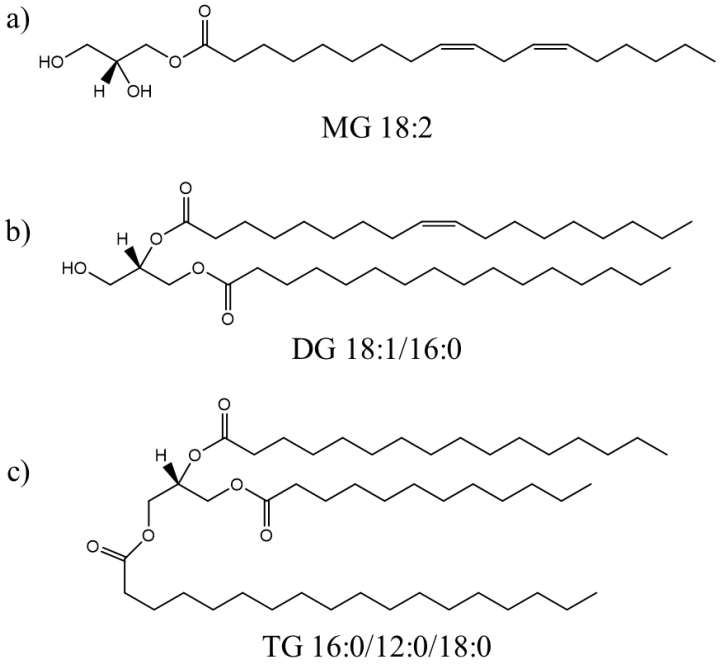

Figure 1.3. Structural examples of glycerolipids a) Monoacylglycerol (MG 18:2), b) Diacylglycerol (DG 18:1/16:0), and c) Triacylglycerol (TG 16:0/12:0/18:0).

Triacylglycerides are the most abundant glycerolipids. They consist of three fatty acid chains esterified to a glycerol molecule. These molecules are highly hydrophobic and stored as lipid droplets within adipocytes, the cells that make up adipose tissue. Triacylglycerides are one of the primary sources of energy storage in animals. In periods of energy excess, dietary fats are converted into TGs and stored in adipose tissue. During energy demand periods, TGs are hydrolyzed by lipases to release free fatty acids and glycerol into the bloodstream[39,40]. Besides their role in energy storage, TGs have other critical biological functions such as thermal insulation,

mechanical protection, and hormone production[40,41]. Excessive accumulation of TGs in adipose tissue leads to obesity, associated with an increased risk of metabolic disorders such as type 2 diabetes, cardiovascular diseases, and certain cancers[6,40,41].

Similarly, DG contains two fatty acid chains esterified to a glycerol molecule, and they are essential intermediates in the biosynthesis and metabolism of TG and phospholipids. They also act as signaling molecules, activating protein kinase C (PKC), which regulates various cellular processes, including growth, differentiation, and cell death. Studies have associated changes in DG metabolism and signaling with cancer[42,43]. Lastly, MG comprises a single fatty acid chain esterified to the glycerol backbone and plays a role as an intermediate in lipid metabolism. During digestion, TG is broken down into MG and free fatty acids, which are then absorbed by the intestinal cells and re-esterified into TGs for transport. Some MG can also act as signaling molecules interacting with cannabinoid receptors to regulate appetite, pain sensation, and immune response[44,45].

1.2.4. Glycerophospholipids (GP)

Glycerophospholipids are a major subclass of lipids consisting of the main components of cellular membranes, providing structural integrity and regulating membrane fluidity and permeability. They are comprised of a glycerol backbone, two fatty acid tails, and a phosphate group attached to a polar head group. According to LIPID MAPS, glycerophospholipids can be subdivided into four subcategories, namely Phospholipids (PL) and lysophospholipids (LPL), Phosphatidylinositol phosphates (PIP), N-modified phospholipids (N-mod PL) and Oxidized phospholipids (Ox PL)[1,36–38].

Phospholipids are the main components of cell membranes and play a crucial role in maintaining membrane structure and fluidity. Common phospholipids include phosphatidylcholine (PC), phosphatidylethanolamine (PE), phosphatidylserine (PS), phosphatidylinositol (PI), phosphatidylglycerol (PG), and cardiolipin (CL) (Figure 1.4). Each of these molecules has a distinct polar head group, which determines their specific functions in the membrane.

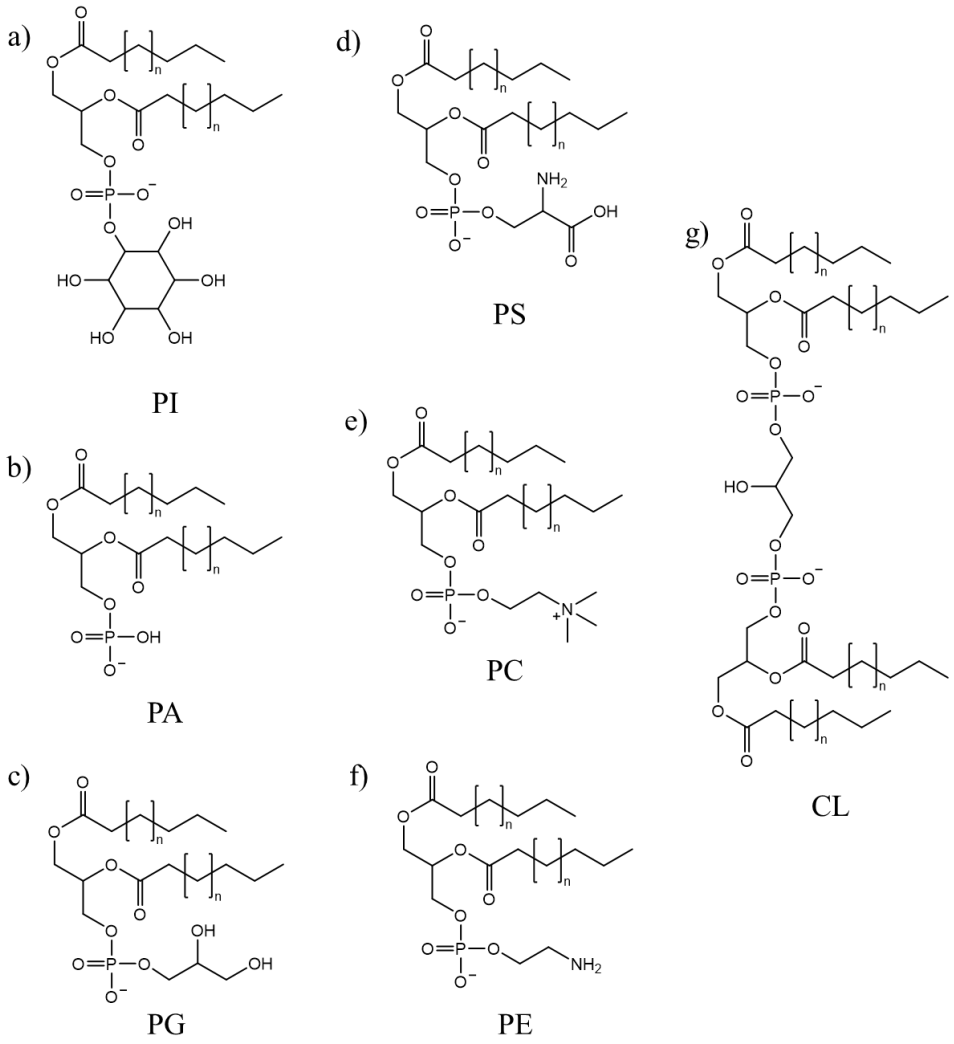

Figure 1.4. Structural examples of glycerophospholipids a) Phosphatidylinositol (PI), b) Phosphatic acid (PA), c) Phosphatidylglycerol (PG), d) Phosphatidylserine (PS), e) Phosphatidylcholine (PC), f) Phosphatidylserine (PE), and g) Cardiolipin (CL).

Phosphatidylcholine is the most abundant phospholipid and the main cellular membrane component. Phosphatidylethanolamine, the second most abundant, contributes to membrane curvature and fusion. Phosphatidylserine plays a role in cell signaling and apoptosis. Phosphatidylinositol and its derivatives, like PIP2, are important for signal transduction pathways. Phosphatidylglycerol is a key component of lung surfactant and is essential for proper lung function. It is involved in cardiolipin biosynthesis, predominantly found in the inner mitochondrial membrane, and plays a critical role in mitochondrial function and apoptosis[1,26,46].

Glycerophospholipids are synthesized in the endoplasmic reticulum and Golgi apparatus, where phosphatidic acid works as an intermediate. These lipids are important for membrane structure, cell signaling, lipid metabolism, and mitochondrial function. Alterations in glycerophospholipid metabolism are linked to various health issues, including cardiovascular diseases, neurodegenerative disorders, lung diseases, and mitochondrial dysfunctions[1,7,46,47].

Lysophospholipids are derived from phospholipids by the removal of one fatty acid chain. This results in a single fatty acid tail, making them highly amphipathic and capable of acting as potent signaling molecules. Lysophospholipids, such as lysophosphatidylcholine (LPC), are involved in inflammatory responses, modulate immune cell functions, and influence membrane curvature and permeability[48]. Phosphatidylinositol phosphates (PIPs) are phosphorylated derivatives of phosphatidylinositol (PI) and play an important role in cellular signaling by acting as docking sites for proteins involved in various pathways. Some PIPs, such as PI4P, PIP2, and PIP3, are involved in processes like signal transduction, membrane trafficking, and cytoskeletal dynamics[49].

N-modified phospholipids have been chemically modified by adding nitrogen-containing groups, altering their physical and chemical properties and affecting their function and interaction with other cellular components. They play roles in signaling and membrane dynamics, although specific examples and functions are less well characterized than other phospholipid subclasses[50]. Lastly, oxidized phospholipids (Ox PLs) undergo oxidative modifications, usually because of oxidative stress. These modifications can impact the structure and function of cellular membranes, leading to modified membrane properties and signaling pathways. Oxidized phospholipids are linked to various pathological processes, including inflammation, atherosclerosis, and cell death. They can serve as signaling molecules that modulate immune responses and other cellular processes[51].

1.2.5. Sphingolipids (SP)

A diverse class of lipid molecules, sphingolipids play a role in cellular structure and signaling. They are essential components of cell membranes, particularly in the brain and nervous system, and are involved in many cellular processes. Sphingolipids consist of a sphingoid base, such as sphingosine, linked to a fatty acid via an amide bond, forming a ceramide, the central building block of more complex sphingolipids[52]. LIPID MAPS subdivides sphingolipids into three categories: Sphingoid bases (SPB), Ceramides (Cer), and Phosphoceramides and Glycosphingolipids, as shown in Figure 1.5[26,36,37].

Ceramides are the simplest sphingolipids, and more complex sphingolipids are obtained from them. They are crucial in cell signaling, regulating apoptosis, cell growth, differentiation, and stress responses, besides being involved in the formation of lipid rafts[52]. Sphingomyelin (SM), a

phosphoceramide, is the most abundant sphingolipid in mammalian cell membranes, especially nerve cells. They consist of a ceramide backbone linked to a phosphocholine head group. Sphingomyelins are essential for maintaining membrane structure and function, and they play roles in signal transduction and cell recognition[46]. Glycosphingolipids are ceramides with one or more sugar molecules attached to them. They are further subdivided into cerebrosides, gangliosides, and globosides. Cerebrosides contain a single sugar moiety (glucose or galactose), while gangliosides have complex oligosaccharide chains with one or more sialic acids. Glycosphingolipids are involved in cell-cell communication, adhesion, and signal transduction and are abundant in the nervous system[52,53].

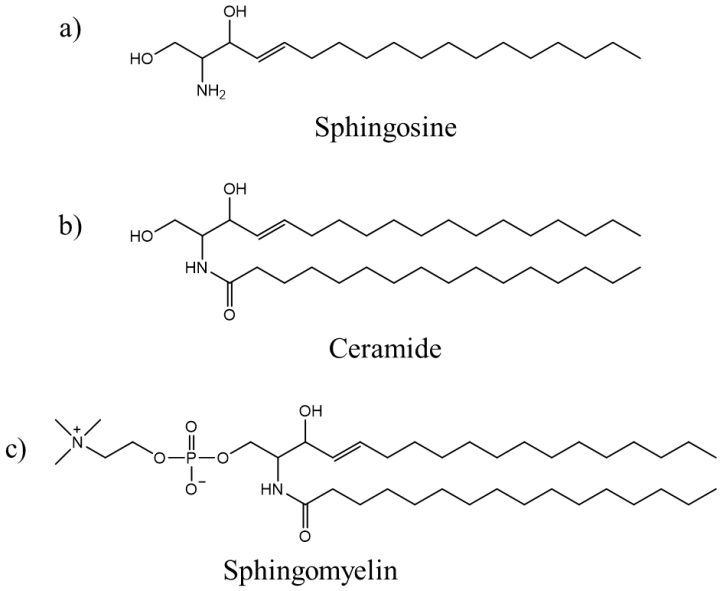

Figure 1.5. Structural examples of sphingolipids a) Sphingosine (SPB 16:1), b) Ceramide (Cer 16:1;O2/16:0), and c) Sphingomyelin (SM 16:1;O2/16:0).

Some neurological disorders have been associated with changes in sphingolipids concentration. For example, Gaucher's disease is characterized by the accumulation of

sphingolipids in the organism due to problems in their catabolic enzymes[54]. Studies have also linked sphingolipid metabolism to cancer progression by affecting cell growth, apoptosis, and metastasis. Ceramide and Sphingosine-phosphates (S1P) have opposing roles in regulating cell fate, with ceramide promoting apoptosis and S1P promoting survival and proliferation[55].

1.2.6. Sterol Lipids (ST)

Sterol lipids maintain cell membrane structure, modulate membrane fluidity, and serve as precursors for many biological molecules. Cholesterol is the most well-known sterol lipid and has several functions in the body. Sterol lipids are characterized by a common structure with a four-ring core called the cyclopentanoperhydrophenanthrene ring system. Cholesterol, for example, consists of this sterol backbone with a hydroxyl group at the 3-position and a hydrocarbon tail. This amphipathic nature allows cholesterol to insert into cell membranes, interacting with phospholipids and sphingolipids[1,56]. Examples of ST are shown in Figure 1.6.

Cholesterol is an important component of animal cell membranes, as it regulates membrane fluidity and permeability. This molecule interacts with the fatty acid tails of phospholipids, reducing membrane fluidity at high temperatures and preventing membrane solidification at low temperatures. This dual role helps maintain membrane integrity and function across a range of temperatures[1,56]. Additionally, cholesterol is a precursor for steroid hormones, including glucocorticoids, mineralocorticoids, and sex hormones (estrogens, androgens, and progesterone). These hormones are synthesized in the adrenal glands, ovaries, and testes and play critical roles in regulating metabolism, immune function, salt and water balance, and reproductive processes[57]. According to LIPID MAPS, sterol lipids can be classified into Free cholesterol (FC), Sterols (ST),

Cholesteryl esters (CE), Steryl esters (SE), Bile acids and derivatives (BA), Sterylglycosides (SG) and Acylsterylglycosides (ASG)[27,37].

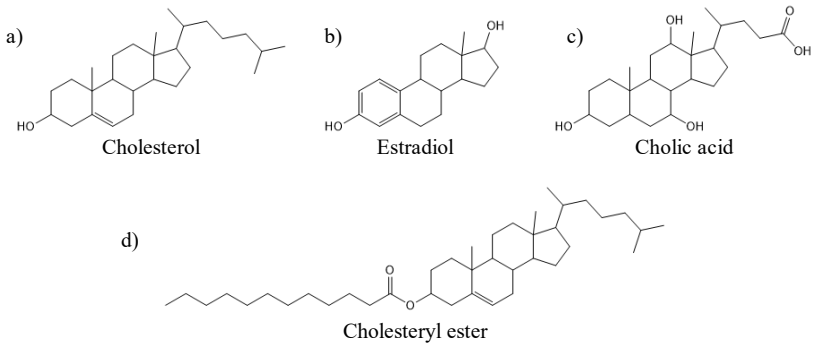

Figure 1.6. Structural examples of sterol lipids a) Cholesterol (ST 27:1;O), b) Estradiol (ST 18:3;O2), c) Cholic acid (ST 24:1;O5), and d) Cholesteryl Ester(CE 12:0).

In the liver, cholesterol is converted into bile acid, which is important for the digestion and absorption of dietary fats and fat-soluble vitamins. Bile acids act as detergents that emulsify fats, facilitating their breakdown and absorption[58]. Vitamin D, an important vitamin for maintaining calcium and phosphate homeostasis, promoting bone health, and supporting immune function, uses cholesterol for its synthesis in the body[59]. Studies have shown that high cholesterol levels increase the risk factors for cardiovascular diseases, such as coronary artery disease and stroke. Elevated levels of low-density lipoprotein (LDL) cholesterol contribute to the formation of atherosclerotic plaques, leading to vascular inflammation and blockage[60–62].

1.2.7. Prenol Lipids (PR)

Prenol lipids are a less common subclass of lipids synthesized from five-carbon isoprene units (C_5H_8) linked together in various ways to form linear or cyclic structures. These lipids are important in different biological processes, such as electron transport, and as precursors for vitamins and hormones, such as vitamin A (retinol), vitamin E (tocopherol), and vitamin K (phylloquinone)[24,63]. Figure 1.7 shows structural examples of the prenol lipids.

Because they are precursor molecules of vitamins, prenol lipids play an important role in cell protection from oxidative stress. Furthermore, deficiencies in vitamin K can lead to osteoporosis and bleeding disorders[64,65].

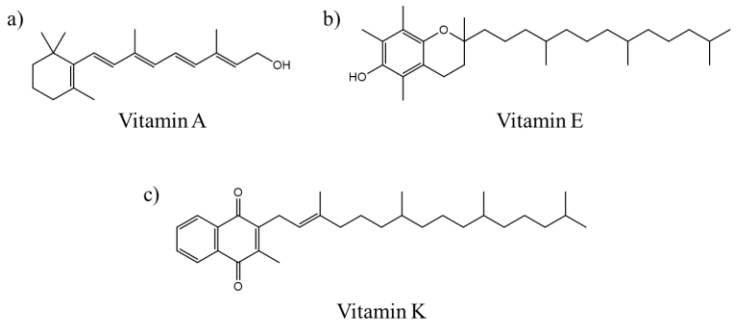

Figure 1.7. Structural examples of prenol lipids a) Vitamin A (Retinol, PR 20:5;O), b) Vitamin E (alpha-tocopherol, PR 29:3;O2), and c) Vitamin K2 (PR 41:10;O2).

1.2.8. Saccharolipids (SL)

Saccharolipids are a unique class of lipids characterized by the direct linkage of fatty acids to a sugar backbone. Although they play a significant role in bacterial physiology, these molecules

are often not included in lipidomics studies because of their high polarity and solubility in water. Saccharolipids can be further categorized into lipopolysaccharides and polyketides, each with distinct functions and applications[1,23,38].

Lipid A, a lipopolysaccharide, is essential for detecting and responding to Gram-negative bacterial infections. Excessive immune activation can lead to septic shock, which can be fatal. Moreover, polyketides are often used in antibiotics, which has led to the development of antibiotic resistance[66,67]. Some structural examples of SL are shown in Figure 1.8.

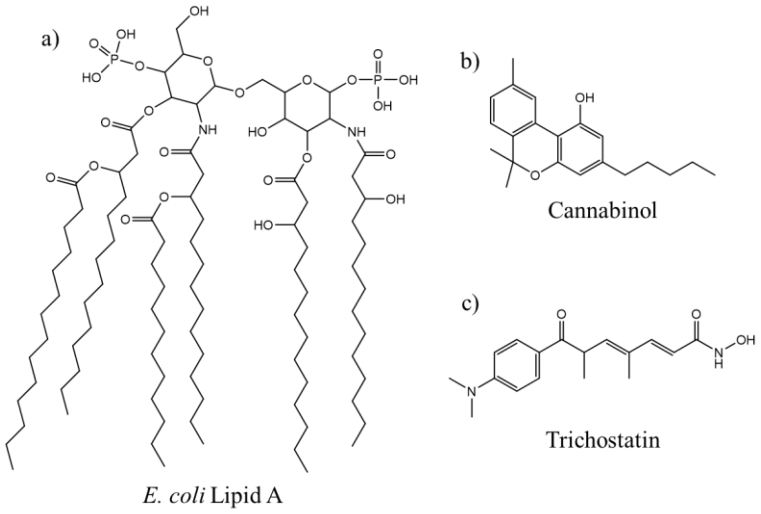

Figure 1.8. Structural examples of Saccharolipids a) E. coli Lipid A, b) Cannabinol, and c) Trichostatin.

1.3. Analytical Methods in Lipidomics

Research in lipidomics has evolved significantly since its beginning, yet it faces several challenges in comprehensively understanding and characterizing the lipidome. These challenges

arise from various sources, such as the diversity and complexity of lipid species to technical issues related to lipid extraction, stability, and quantification[38,68–70].

1.3.1. Sample Preparation and Storage

As described previously, lipid species are diverse molecules with different structures, biological functions, and physical chemical properties. Therefore, accurately detecting and quantifying these molecules can be challenging. Accurate and reproducible lipid extraction is an important step in lipidomics research. Although studies have shown some yield better results than others, no consensus on the most suitable method has been reached[2,38,68,71].

Lipid extraction protocols commonly use modified versions of the Bligh and Dyer or Folch method. However, some studies have also employed variations of the MTBE method. Both Bligh and Dyer and Folch's methods use a mixture of chloroform, methanol, and water to extract lipids, including phospholipids, glycolipids, and neutral lipids. Besides relying on chloroform, which is highly toxic, these methods suffer from the drawback that their organic layer is on the bottom, requiring a more experienced analyst[72,73]. On the other hand, the MTBE (methyl-tert-butyl ether) method uses a mixture of MTBE, methanol, and water, with lipids partitioning into the upper MTBE phase. This method offers a safer alternative that utilizes less toxic solvents, providing efficient extraction with simpler phase separation, though it may not extract very polar lipids as effectively[74].

Moreover, in lipidomics, accurate quantification is vital for accurately profiling the lipidome, understanding the biological processes, and identifying disease biomarkers. Variability in sample concentration can lead to inconsistencies and inaccuracies in the data. Hence, sample

normalization is important for obtaining accurate and comparable lipidomics data. This process involves adjusting the concentration of lipid samples to account for variations in sample size, extraction efficiency, and other factors that can affect lipid measurements. Normalization strategies such as total lipid normalization, internal standards, protein or DNA content, and cell number or tissue weight are commonly used. Furthermore, lipids are susceptible to oxidation and degradation during extraction, storage, and analysis. Therefore, strict quality controls are necessary to ensure proper sample handling and reproducible results, such as maintaining a stable and relatively low temperature. Lipid extracts can be stored at -20 °C, whereas samples should be stored at -80 °C for long-term storage. Furthermore, repeated freeze-thaw cycles can also cause lipid degradation through the formation of ice crystals and increased exposure to oxygen. To minimize these effects, lipid extracts should be subdivided into small aliquots before freezing, allowing only the amount needed for analysis to be thawed at a time and minimizing the number of freeze-thaw cycles for each aliquot[38,75–77].

1.3.2. Separation Methods

Separation techniques reduce the complexity of lipid mixtures, allowing a more accurate identification and quantification. The most common separation techniques used in lipidomics include liquid chromatography (LC), gas chromatography (GC), supercritical fluid chromatography (SFC), and thin-layer chromatography (TLC).

1.3.2.1.Liquid Chromatography (LC)

Liquid chromatography is one of the most widely used techniques in lipidomics due to its versatility and high resolution. Ultra-high-performance Liquid Chromatography (UHPLC) is an advanced form of LC that operates at higher pressures, providing faster and higher-resolution separations. This technique helps analyze lipid classes with subtle structural differences. Depending on the stationary and mobile phases, UHPLC can be characterized as Normal Phase (NP), Reversed Phase (RP), or Hydrophilic Interaction Liquid Chromatography (HILIC)[78–80].

In NP chromatography, the stationary phase, commonly silica, is polar, and the mobile phases, such as hexane or chloroform, are non-polar. NP chromatography can separate lipids based on their polarity in lipidomics, particularly neutral lipids such as TG, ST, and FA. Its drawbacks are solvent compatibility, safety concerns, limited applicability for polar lipids, reproducibility issues, and integration challenges with detection methods. Because of these limitations, the use of NP chromatography has been decreasing over the years[78].

Similarly to NP, RP chromatography is a polarity-based separation. However, this method employs a non-polar stationary phase, such as C18 or C8 columns, and a polar mobile phase, usually a mixture of water and organic solvents like methanol or acetonitrile. It is the most applied LC method in lipidomics research to separate lipids based on their hydrophobicity. While RP chromatography is highly effective for separating hydrophobic lipids and is widely used in lipidomics, its major drawback is its limited retention of hydrophilic lipids. Other issues, such as mobile phase compatibility and longer run times, should be evaluated before using RP[9,75,78,81].

Lastly, HILIC uses a polar stationary phase and a mobile phase with a high concentration of organic solvents, such as acetonitrile or methanol. Hudrophilic Interaction Liquid

Chromatography is an excellent technique for separating polar lipids, such as phospholipids and lysophospholipids, often poorly resolved by RP. However, its columns often require longer equilibration times, decreasing throughput, and its polar interactions can lead to peak tailing. Moreover, lipid subclasses with hydrophobic headgroups, such as TG, DG, and ST, are not well retained, making comprehensive lipidomics work challenging[78,79,82].

Recently, studies have proposed combining orthogonal separation methods to enhance separation in complex mixtures. Unlike conventional one-dimensional liquid chromatography (1DLC), which often struggles with the complexity and diversity of lipid species, two-dimensional liquid chromatography (2DLC) provides a higher resolving power by combining two distinct separation mechanisms, such as RPLC and HILIC. This approach allows for the effective separation of non-polar and polar lipids, thereby ensuring comprehensive lipid profiling. Two-dimensional liquid chromatography studies have shown a significantly higher number of lipid annotations compared to 1DLC, with peak capacities reaching 1784 versus 448, respectively. This increased peak capacity is crucial for detecting a broader range of lipid species. However, 2DLC also presents challenges, including higher complexity and cost, sophisticated instrumentation requirements, advanced data processing needs, and time-consuming method development[78,83,84].

1.3.2.2.Gas Chromatography (GC)

In gas chromatography, analytes are vaporized and carried through a column with an inert gas (*e.g.*, helium). They are separated based on their volatility and interactions with the stationary phase. Although some studies have used GC, it has not been widely used in lipidomics research because analytes need to be derivatized before analysis, making it time-consuming[84,85]. However,

recent studies have shown GC can be an effective technique for lipidomic profiling, including the analysis of FA and ST lipids[84,86,87].

Similarly to 2DLC, two-dimensional gas chromatography (2DGC) can enhance the separation and identification of complex lipid mixtures by combining two different GC separations, improving resolution and peak capacity. Some studies have used comprehensive 2DGC to analyze complex lipid mixtures, revealing lipid species that cannot be detected using traditional one-dimensional gas chromatography (1DGC)[88,89]. However, GC is unsuitable for non-volatile or thermally labile lipids, such as large phospholipids and glycolipids, requiring complementary techniques like liquid chromatography-mass spectrometry (LC-MS) for comprehensive lipid profiling[84,87,88].

1.3.2.3.Supercritical Fluid Chromatography (SFC)

In supercritical fluid chromatography, a supercritical fluid, commonly carbon dioxide (CO_2), is used as a mobile phase. By combining the properties of gases and liquids, SFC allows efficient and rapid separations with minimal environmental impact. Supercritical fluid chromatography provides high efficiency in separating lipid classes due to the low viscosity and high diffusivity of supercritical CO_2, yielding faster separations than traditional liquid chromatography (LC) with reduced column backpressure. It is particularly effective for non-polar lipids, including TGs, FA, and ST. Recent studies highlighted using SFC in lipidomics, such as the comprehensive profiling of lipids in biological samples and the analysis of lipid composition in olive oil[90–93].

Moreover, SFC is environmentally friendly, as supercritical CO_2 is nontoxic, nonflammable, and readily available, reducing the need for organic solvents and the risks associated with their use. However, challenges such as limited availability of suitable columns, time-consuming method development, and higher initial instrumentation costs exist[84,90,92].

1.3.2.4.Thin-Layer Chromatography (TLC)

Thin-layer chromatography is a cost-effective technique that can be used for preliminary lipid separation and qualitative analysis. Thin-Layer Chromatography can be useful for separating a wide range of lipid classes, including GP, GL, ST, and FA. It allows the visualization of lipid classes and subclasses based on their migration patterns and staining characteristics, and it is often used as a preparatory step for more advanced analytical techniques like LC or GC[84,94].

The most important limitations of TLC include lower separation resolution when compared to GC or LC, limited quantitative capabilities, and reproducibility issues because of variations in plate coating thickness, solvent composition, and environmental conditions. Studies have shown TLC's applicability in lipidomics, such as in combining a TLC-Blot system with matrix-assisted laser desorption/ionization-quadrupole ion trap-time of flight (MALDI-QIT-TOF) mass spectrometry (MS) for the analysis of human brain gangliosides. That study revealed changes in the composition of gangliosides in the hippocampus gray matter of patients with Alzheimer's disease compared to control patients[84,94,95].

1.3.3. Lipid Analysis

Different analytical techniques can be used in lipidomics studies, depending on the study's objectives, throughput, and availability. Each method will provide detailed information about lipid composition and structure, giving insights into lipid metabolism and its role in health and disease. The most common analytical techniques used in lipidomics include Nuclear Magnetic Resonance (NMR) spectroscopy and Mass Spectrometry (MS)[68,75,84].

1.3.3.1.Nuclear Magnetic Resonance (NMR)

Nuclear Magnetic Resonance spectroscopy is used for structural elucidation and quantification of lipids. It provides comprehensive information, enabling detailed analysis of lipid-lipid and lipid-protein interactions and complex lipid mixtures' composition and structural characteristics. NMR can provide detailed structural information about lipids, allowing for the identification of functional groups, double bonds, and the position of fatty acyl chains in GL, GP, and SP[84,96,97].

High-resolution NMR can differentiate between isomers and conformers of lipid molecules, which is important to understand their biological functions. Studies have shown the applicability of NMR for metabolomics and lipidomics. Besides structural elucidation and quantification, NMR can study lipid-lipid and lipid-protein interactions, giving insights into the dynamics and organization of lipids in biological membranes. Additionally, NMR allows for the study of lipid dynamics, including lipid molecule mobility and exchange rates[75,98,99].

1.3.3.2.Mass Spectrometry (MS)

Mass spectrometry is the analytical technique most commonly employed in lipidomics studies because of its high sensitivity, specificity, and ability to provide detailed structural information. Throughout the years, various MS techniques and configurations have been used in lipid analysis, each offering unique advantages for lipid identification, quantification, and structural elucidation. Different approaches have been used for lipidomic analysis. This section will cover some of the most used MS approaches in lipidomics[2,71,75,84].

Shotgun lipidomics is a direct infusion MS technique in which lipid extracts are introduced into the mass spectrometer without prior chromatographic separation. Studies have shown that shotgun analysis can yield comprehensive coverage of lipid species and high throughput. However, because it is not associated with a separation technique, it is prone to ion suppression[100].

Ionization techniques are crucial in lipidomics for generating ions from lipid molecules, enabling their analysis by a mass spectrometer. The most common ionization methods used in lipidomics include Electrospray Ionization (ESI) and Matrix-Assisted Laser Desorption Ionization (MALDI), each offering distinct advantages, and both have been extensively applied in lipidomics research[75,84,101]. Electrospray Ionization is a soft ionization technique that produces ions from large, polar molecules. It has often been used in lipidomics studies and is usually coupled with high-resolution mass spectrometers for lipid profiling. ESI is known for its gentle ionization process, which minimizes fragmentation and preserves the integrity of lipid species. It is compatible with several mass spectrometers, and its ability to provide detailed structural and quantitative information makes it essential in lipidomics research. Several studies have demonstrated high-sensitivity lipidomics methods using ESI. However, limitations include matrix effects, variability

in ionization efficiency for different lipid species, formation of multiple adducts, in-source fragmentation, and a limited ionization range for highly non-polar lipids[68,71,84,102–104].

Alternatively, MALDI is another soft ionization technique used in lipidomics. Matrix-Assisted Laser Desorption Ionization is used for imaging mass spectrometry (MSI), allowing for the spatial resolution of lipid species within biological tissues, making MALDI a powerful tool for studying the distribution and localization of lipids in various samples, including tissues and cell cultures. A recent lipidomics study used MALDI-MSI to investigate lipid metabolism alterations in A549 lung tumor spheroids treated with hydroxychloroquine, showing significant changes in the spatial arrangement of lipids within the proliferative and necrotic regions of the spheroids. Although MALDI has shown to be a powerful technique for lipidomics research, ionization efficiency and matrix effects must be considered to maximize its effectiveness[84,101,105].

Mass analyzers are crucial components of mass spectrometry, determining the mass-to-charge ratio of ions. Lipidomics' most used mass analyzers include Quadrupole Time-of-Flight (QToF) and Orbitrap[102,106,107]. The QToF mass spectrometer combines the quadrupole's mass filtering capabilities with the high resolution and mass accuracy of time-of-flight (ToF) analyzers. QToF-MS is a robust and cost-effective instrument with resolutions ranging from 30,000 to 60,000. Due to its sensitivity and fast data acquisition rates, it has often been used for targeted and untargeted lipidomics and metabolomic studies. However, frequent calibration is required to maintain mass accuracy, and it has a lower mass resolution than instruments like Orbitrap-MS, which can limit its ability to distinguish between closely related ion peaks[103,106].

On the other hand, the Orbitrap mass analyzer can offer ultra-high-resolution and accurate mass measurements. Orbitrap instruments provide superior sensitivity and resolution, which is

essential for accurately profiling lipids, especially low-abundance species. The high mass accuracy of Orbitrap instruments improves the reliability of lipid identification, reducing the chances of misidentification and allowing for the differentiation of isomeric and isobaric species. However, Orbitrap analyzers are generally more expensive than other mass spectrometers regarding initial purchase and maintenance costs. Additionally, while Orbitrap provides high-resolution and accurate mass measurements, it may not offer the same throughput as other mass spectrometers, such as QToF instruments[106,107].

Quadrupole Time-of-Flight and Orbitrap mass analyzers can perform tandem mass spectrometry (MS/MS), a technique for detailed structural elucidation that involves fragmenting lipid molecules and analyzing the resulting product ions[107,108]. Tandem mass spectrometry information is vital for lipid identification and structural elucidation. By fragmenting the lipid molecules, MS/MS can provide information about fatty acyl chain compositions and headgroups, aiding in understanding their biological roles and interactions. Moreover, MS/MS allows the differentiation of isomeric and isobaric species, which is important in lipidomics since many lipid species have similar masses[77,103,109]. Lipidomics studies often use MS/MS for lipid annotation and structural elucidation. However, it is essential to note that this technique does not offer information about double bonds and fatty acyl positions, limiting its accuracy[103,110]. Furthermore, both instruments allow for data-dependent acquisition (DDA, also known as auto-MS.MS) mode, which is critical for acquiring detailed structural information.

In auto MS/MS mode, a full-scan (MS1) spectrum is first acquired to detect all ions entering the mass spectrometer within the selected m/z range. The system automatically selects one m/z ion isolated within the quadrupole for the following scan. This isolated ion is then fragmented under

collision-induced fragmentation to obtain structural information for annotations (MS/MS or MS2 spectrum). Multiple MS2 spectra may be acquired for different precursor ions before the next full-scan (MS1) acquisition. The cycle time, or number of scans per cycle, includes one full scan (MS1) and a variable number of MS2 scans, depending on the acquisition rates set for the method. This value ensures an appropriate number of MS1 scans to define peak shapes (at least 5 points/peak). However, only a fraction of the detected ions are fragmented to generate MS2 spectra - usually, the peaks with the highest intensity[111,112].

Ion Mobility Spectrometry (IMS) adds another dimension of separation to mass spectrometry. It separates ions based on their mobility through a gas under the influence of an electric field. Lipidomics studies have used this technique to improve lipid separation because it can separate isomeric and isobaric lipid species, which can be challenging to distinguish using mass spectrometry alone. Moreover, IMS effectively improves the identification and characterization of lipids in biological samples[113,114]. An advanced form of IMS, Trapped Ion Mobility Spectrometry (TIMS), offers even greater separation capabilities. It provides unmatched sensitivity and resolution when combined with Time-of-Flight mass spectrometry. Trapped Ion Mobility Spectrometry Time-of-Flight Mass Spectrometry (TIMS-ToF) traps ions in an electric field and separates them based on mobility, followed by high-resolution mass analysis. A recent study used TIMS-ToF to improve the coverage and accuracy of untargeted lipidomics[115–117].

1.3.4. Data Processing and Analysis

A strict data processing routine must be established to obtain accurate lipidomics results. Lipidomics requires meticulous data processing to ensure that the data reflects biological variations

rather than technical artifacts. This is vital for understanding lipid functions, discovering biomarkers, and developing therapeutic strategies[68,75,106,108,118].

The acquired data needs to be aligned using tailored data processing software capable of handling complex datasets. These software tools usually have noise reduction, peak detection, alignment, mass recalibration, peak picking, and deconvolution functions. Over the years, different software has been used for lipidomics data processing, such as MetaboScape and MSDial. However, no consensus has been reached on the best software to use[11,119,120]. Because of the lack of consensus and to tailor it to their specific needs, some research groups have developed in-house software tools for lipidomics data processing[14,120].

1.3.4.1.Data Alignment and Normalization

Post-acquisition data normalization and scaling are used to correct systematic biases and variability so that the data can reflect biological changes. Technical variations, such as differences in sample preparation, instrument performance, and environmental conditions, can introduce significant errors in lipidomics data if not adequately addressed[38,71,75,118].

Normalization methods like Total Ion Current (TIC) and internal standard normalization are often used in lipidomics work. TIC normalization adjusts for variations in the total signal intensity across different runs by scaling each signal proportionally to the total signal intensity, helping to correct for differences in sample injection volume and ionization efficiency[9,75,118,121]. Internal standard (IS) normalization involves adding a known quantity of a compound or mixture of compounds not naturally present in the samples. The IS signal is then used to normalize the

signal for the naturally occurring lipid, correcting variabilities in sample preparation, instrument performance, and data acquisition[75,103,108].

Moreover, quality control (QC) procedures are used in these workflows to monitor instrument performance and data consistency, which helps identify and correct analytical drifts, assuring the quality of the data. QC samples are aliquots of a pooled sample representative of the entire study and are analyzed periodically throughout the batch run[75,103,108].

1.3.4.2.Lipid Identification and Annotation

Lipidomics data processing workflows often include lipid identification and annotation steps using spectral libraries and databases like the Human Metabolome Database (HMDB) and LipidBlast. Advanced algorithms match experimental spectra to database entries, considering mass accuracy, isotope distribution, fragmentation patterns, and retention times. However, accurate lipid identification and annotation remains a challenge in lipidomics because of the complexity and diversity of lipid species, potentially leading to ambiguous matches. The structural similarity among different lipid molecules often results in overlapping mass spectra, making it difficult to distinguish between them. Additionally, variations in experimental conditions, such as differences in instrumentation and sample preparation methods, can affect the reproducibility and accuracy of the results[108,118,122].

Most lipid libraries are *in silico* (*i.e.*, predicted by computers based on the expected fragmentation patterns of lipids). However, experimental spectra can vary with instrumental design, performance, settings, and convoluted spectra resulting from co-isolation of precursors with similar m/z values. Although this is a common and widely accepted practice within lipidomics,

annotations may suffer from low scores due to a mismatch between computer-predicted datasets and the obtained experimental spectra[120,123]. Furthermore, lipid annotation and lipid identification are two distinct processes in lipidomics. Lipid annotation involves assigning possible structures to observed features based on existing knowledge and *in silico* databases, often without definitive experimental confirmation. In contrast, lipid identification requires direct experimental evidence, such as experimental MS/MS spectra of lipid standards, to confirm the structure of a lipid molecule. This distinction is crucial for accurate lipidomic analysis and data interpretation[123].

For MS/MS matching, the precursor ions are identified with a strict m/z tolerance of 5.0 mDa. This high precision ensures that the ions selected for fragmentation are accurately matched to known lipid molecules. Tier 1 annotations require a high confidence level, with an MS/MS score threshold of 500, indicating a strong similarity between experimental and reference spectra. Tier 2 annotations, while still reliable, have a lower MS/MS score range of 100 to 500, reflecting a less confident match but still within acceptable limits. Features not annotated by MS/MS match proceed for putative annotation by mass match using the LIPID MAPS platform. This step involves searching for mass matches within a 5.0 mDa error margin[14,75,103,108,118,122].

Given the complexity of lipid molecules, lipidomics studies often use filtering systems to refine the annotations. For MS/MS annotations, these filters may include a retention time window based on IS and the possibility of the subclass ionization with that adduct. Furthermore, since the same feature may be annotated as multiple species because of isomers and isobars, tier-based filtering systems can be used to refine mass match annotations. Previous studies have used retention time filtering to ensure that the annotated species are within the expected retention time range for their lipid class; adduct detection to confirm the ionization pattern matches the expected adducts

for the lipid class; and annotation ranking, which ranks annotations based on the method characteristics and the biological sample context. This step considers the likelihood of each annotation, considering the lipid's chemical properties and its typical occurrence in the specific biological sample being analyzed. This tiered approach enhances the accuracy and reliability of lipid identification by systematically narrowing down potential annotations[75,103,110,118,122].

Nomenclature in lipidomics is another essential aspect of lipid identification and annotation. The systematic naming of lipids follows specific conventions that describe the structure and class of the lipid molecule. This nomenclature includes details such as the number of carbon atoms and double bonds in the fatty acyl chains, the type of head group, and any modifications to the lipid molecule. Consistent and accurate nomenclature is vital for clearly communicating lipidomics data and comparing results across different studies. The nomenclature employed herein is based on the guidelines of the International Lipid Classification and Nomenclature Committee, the Lipidomics Standards Initiative, and LIPID MAPS[27,37,75,118].

1.3.4.3.Statistical Analysis

Statistical analyses allow lipidomics studies to interpret complex data sets, identify significant patterns, and draw biological conclusions. However, searching for minor changes within thousands of random molecules can be challenging, especially given the complexity of lipidomics datasets. Due to a lack of reliable statistics and validation, the reproducibility and validity of omics data have been questioned. Understanding statistical models to avoid false performance-enhancing practices is, therefore, essential for high-quality results[118,124,125].

Scaling methods such as log transformation, Pareto scaling, and auto-scaling are crucial for stabilizing variance across different lipid species and improving data interpretation in multivariate statistical analyses. However, they should be carefully selected because each one will impact the dataset differently. Log transformation reduces data skewness and stabilizes variance, making the data more suitable for statistical analysis, especially when dealing with data spanning several orders of magnitude[124,126]. Pareto scaling balances the importance of large and small features in the data, ensuring that variables with higher variance do not dominate the analysis. By reducing the influence of highly variable features, Pareto scaling helps to highlight subtle but biologically significant changes across samples. Auto-scaling, known as unit variance scaling, centers each variable by subtracting the mean and dividing by the standard deviation. This approach gives variables equal weights, allowing for fair comparison across features. Auto-scaling is particularly useful when the data set contains variables with vastly different scales, ensuring that all features contribute equally to the analysis[124,127].

Multivariate statistical techniques such as Principal Component Analysis (PCA) and Partial Least Squares Discriminant Analysis (PLS-DA) are commonly used in lipidomics to explore complex datasets. PCA is an unsupervised method that reduces the dimensionality of the data while preserving as much variability as possible. It identifies patterns and clusters within the data, helping to visualize the relationships between different samples and lipid species. PCA simplifies the complexity of high-dimensional data while retaining its essential characteristics by transforming the data into a new coordinate system (*i.e.*, principal components), where the most significant variances lie on the first few principal components. This method is particularly effective in highlighting the underlying structure of the data, revealing correlations and trends that are not immediately apparent in the raw data[2,103,128]. Furthermore, PCA also provides a way to quantify

the variance explained by each principal component. By reducing the number of dimensions, PCA makes the data more manageable and facilitates analyses, such as clustering and classification. In this work, PCA score plots were mainly used to evaluate the reproducibility of the QC injections[108].

PLS-DA is a powerful tool for analyzing high-dimensional lipidomics data. Unlike PCA, which is unsupervised, PLS-DA incorporates response variable information during model building, increasing its ability to distinguish between groups. This statistical model can identify the variables (lipid species) that most contribute to the group separation, making it a powerful tool in biomarker discovery[129]. By maximizing the covariance between the lipidomics data and the class labels, PLS-DA provides a robust model that can classify samples accurately and highlight significant biomarkers. However, model validation is essential in PLS-DA analysis to ensure a robust and reliable result. R^2, or correlation coefficient, indicates how well the model explains the variability of the data. The predictive ability (Q^2) measures how well the model predicts the separation of the groups. There are no set values for R^2 and Q^2 to suggest a well-fitting and predictive model. However, significant differences between them indicate the model may be overfitted, especially in high-dimensional datasets with relatively few samples. Overfitting occurs when the model captures noise instead of the underlying data patterns, leading to poor generalization of new data. Permutation testing involves randomly shuffling the class labels and re-fitting the PLS-DA model to these permuted data sets. By comparing the model's performance with the original and permuted data, researchers can assess whether the observed classification is better than random chance, helping to identify potential overfitting and ensuring the model's predictive power is genuine[108,129,130].

Variable Importance in Projection (VIP) scores are an important output of PLS-DA, indicating the importance of each variable in the model. Variable Importance in Projection scores help identify the most significant variables contributing to the observed separation between different groups and are calculated based on the contribution of each variable to the model's total explained variance. High VIP scores indicate variables highly influential in separating the classes, making them potential biomarkers prioritized for further investigation[131].

Furthermore, univariate statistical methods analyze one variable simultaneously to assess its significance between different groups. In the following studies, t-tests and volcano plots were employed. The t-test compares the means of two groups and determines whether they are significantly different. This test calculates the ratio of the difference between group means to the variability of the groups, resulting in a t-statistic. This statistic is then compared to a critical value from the t-distribution to determine the p-value. A low p-value (typically less than 0.05) indicates that the observed difference is statistically significant and not due to random chance. Volcano plots, on the other hand, are scatter plots that visualize the results of t-tests by plotting the significance (p-value) against the magnitude of change (fold change) for each lipid species. Lipids with large fold changes and low p-values appear far from the origin, typically in the top left and top right corners, indicating significant differences between groups. Lipids near the center, with small fold changes and high p-values, are not significantly different. Studies use t-tests and volcano plots to visualize significantly altered lipid species, highlighting key lipids that may serve as potential biomarkers or targets for further study[108,131] .

1.4. Current Challenges and Limitations in Lipidomics Research

The importance of lipidomics has been increasing significantly in the past two decades, with significant advancements in analytical technologies, such as ultra-high-resolution mass spectrometers and improvements in LC systems and column technology. However, this field still faces several challenges that can impact the accuracy and reliability of lipidomic data, influencing the interpretation of biological processes and biomarker discovery.

Accurate and reproducible extraction and quantification of lipids from biological samples is still challenging. Sample normalization is essential to ensure consistency and comparability of results. However, conventional normalization methods, such as using protein or metabolite concentrations, may not be suitable for lipidomics due to the unique chemical properties of lipids. Furthermore, global lipidomics profiling has faced significant challenges in differentiating similar lipid species, either isomers and isobars or species with similar properties that coelute during LC separation. Isomers have the same molecular formula but different structural arrangements, while isobars have the same mass but different elemental compositions. These species often yield identical MS signals, making it difficult to distinguish them without high-resolution MS and advanced LC techniques. Coeluting species, which elute simultaneously during chromatographic separation, further complicate the annotation process. The lack of extensive and specialized databases for lipid analysis adds another layer of difficulty, as current databases may not cover the full range of possible lipid species or provide sufficient resolution for distinguishing similar compounds. Additionally, the existing software tools are often inadequate for comprehensive lipid analysis, lacking the power to annotate complex lipidomic data accurately. Improvements in chromatographic methods, high-resolution MS, and the development of more extensive and

accurate lipid databases and software tools are crucial to enhancing the accuracy of lipid identification and overall lipidomics research.

1.5. Thesis Objectives

The work described herein aimed to develop and optimize current lipidomics methods and apply those to improve the understanding of the role of lipids in biological systems. The first objective was to develop a normalization method targeting lipids and use it to reduce data variations from data collection and factors such as hydration and biological sex. Chapter II describes the development of the Sulfo-phospho-vanillin (SPV) assay, which can quantify lipids and normalize their concentrations before LC-MS analysis. Chapter III compared the effects of different sample normalization methods on the lipidomic profiling of human saliva. It compares the advantages and disadvantages of normalizing saliva samples using total metabolite concentration (TMC) and total lipid concentration (TLC, measured using the SPV method developed in Chapter II) before LC-MS analysis.

The second objective focused on improving separation and increasing annotation confidence for lipidomics studies. In Chapter IV, a HILIC method was developed to be used as the first separation dimension in a 2DLC-MS workflow. Lipid class elution profiles were accessed in both HILIC and RP, generating a comprehensive elution profile for each subclass and increasing the accuracy of our annotations. Moreover, a comparison of different software tools for lipidomics data processing was conducted in this chapter for a robust and reproducible data processing routine.

Chapter V focused on comparing the performance of QToF-MS and Orbitrap-MS in lipidomics studies to improve lipid separation and increase resolution. This chapter also describes

the development of an LC-MS method using a 1.0 mm inner diameter (ID) column. Lastly, Chapter VI evaluates the potential impacts of cisplatin and rapamycin on non-small cell lung cancer cells (NSCLC) using the methods developed in Chapters IV and V.

This study aimed to demonstrate the importance of lipid studies and the need for continuous improvement in the development of the lipidomics method. These improvements are crucial to generating more reliable and accurate results that can be used in biomedical sciences and biomarker discovery. By enhancing lipidomics methodologies, this research contributes to the broader understanding of lipid roles in health and disease, ultimately supporting the development of better diagnostic and therapeutic strategies.

II

Chapter II: Development of a Robust Sulfo-Phospho-Vanillin Assay for Sample Normalization in LC-MS-Based Lipidomics

2.1. Introduction

In recent years, the field of lipidomics has been rapidly advancing and gaining increased attention due to highly sensitive analytical techniques, such as liquid chromatography−mass spectrometry (LC-MS), which has been widely used for the exploration of biological processes and biomarker discovery[9,70,77,78,103,132]. However, the field still faces significant challenges, such as the lack of standardized protocols for sample preparation and variability in sample concentration, which can pose an issue for the accurate quantification of lipids and the establishment of a reliable LC-MS lipidomics workflow[133–136]. Studies reported the variability in lipid concentration between males and females, with levels of SM being higher in females than in males. Moreover, females were more susceptible to age-associated differences, with TG levels being significantly higher in older females than in young females, which can impact the results of lipidomics studies[136]. In response to the variability in lipid concentration across samples, relative lipid quantification emerges as a critical strategy to ensure consistent and accurate quantitative analysis[77,137].

Normalization procedures can be performed pre-analysis or post-analysis during data processing steps. Although post-analysis normalization is common in lipidomics (*e.g.*, normalization to the total or median peak intensity), it doesn't account for variations in extraction efficiencies and instrument response[103]. Hence, pre-analytical normalization, incorporated in

sample preparation steps, is an ideal approach for samples with high variations in lipid concentrations. In this context, normalization refers to adjusting the volumes or concentrations of individual samples to ensure a uniform level across all samples, facilitating a consistent basis for analysis. A suitable normalization method must be user-friendly, cost-effective, and ideally performed after initial sample preparation to correct for any variations introduced during this phase[77,137].

Nevertheless, looking for an optimal normalization method that can be accurately applied across different sample types has proven challenging. Over the years, different normalization approaches have been applied to biological samples, such as gravimetric analysis, fluorometry, cell counting, enzymatic reactions, and total protein or metabolite quantification, all of which come with their limitations[137–141]. Gravimetric analysis, while precise under ideal conditions, struggles with solvent residues and requires meticulous handling by skilled analysts. Fluorometry is susceptible to interference from naturally fluorescent substances within samples, which can lead to inaccurate lipid measurements. Cell counting fails to account for the variability in lipid content across cells of different sizes or stages of growth. Enzymatic reactions, specific to certain lipid types, might not reflect the complete lipid profile of a sample. Lastly, total protein or metabolite quantification assumes a constant ratio between protein and lipid content, which can vary significantly depending on the organism's metabolic state or environmental conditions[142–147].

These challenges show the complexity of accurately quantifying lipids across diverse biological samples, and in this context, the Sulfo-phospho-vanillin (SPV) method emerges as a promising alternative. Initially proposed in the 1930s, this colorimetric method is based on the reaction of a double bond with sulfuric acid (H_2SO_4), forming an intermediate, followed by its

reaction with the phospho-vanillin reagent. The product is a coloured compound, and lipid concentrations can be estimated based on colour development. This reaction has been downscaled and applied in different sample matrices, suggesting its potential[77,148–150]. Despite the multi-decade investigation into the mechanisms behind the SPV reaction, a consensus is yet to be reached. The most accepted mechanism was initially proposed in 1972 and involves a two-step reaction in which the H_2SO_4 reacts with the double bond present in the molecule to form a carbonium ion. Subsequently, the carbonium ion reacts with the phospho-vanillin carbonyl group to yield a pink-coloured compound (Figure 2.1). Although fatty acyl chains may have multiple double bonds, this study demonstrated higher derivatization efficiency for a single double bond per molecule. However, it is still possible for multiple double bonds to react within the same molecule, implying that although the reaction's efficiency peaks with a single interaction, the overall colorimetric response can be amplified by the presence of multiple reactive sites within a single molecule[151]. Moreover, a recent study postulated alternative pathways for carbonium ion formation in the presence of H_2SO_4 and the absence of double bonds[152].

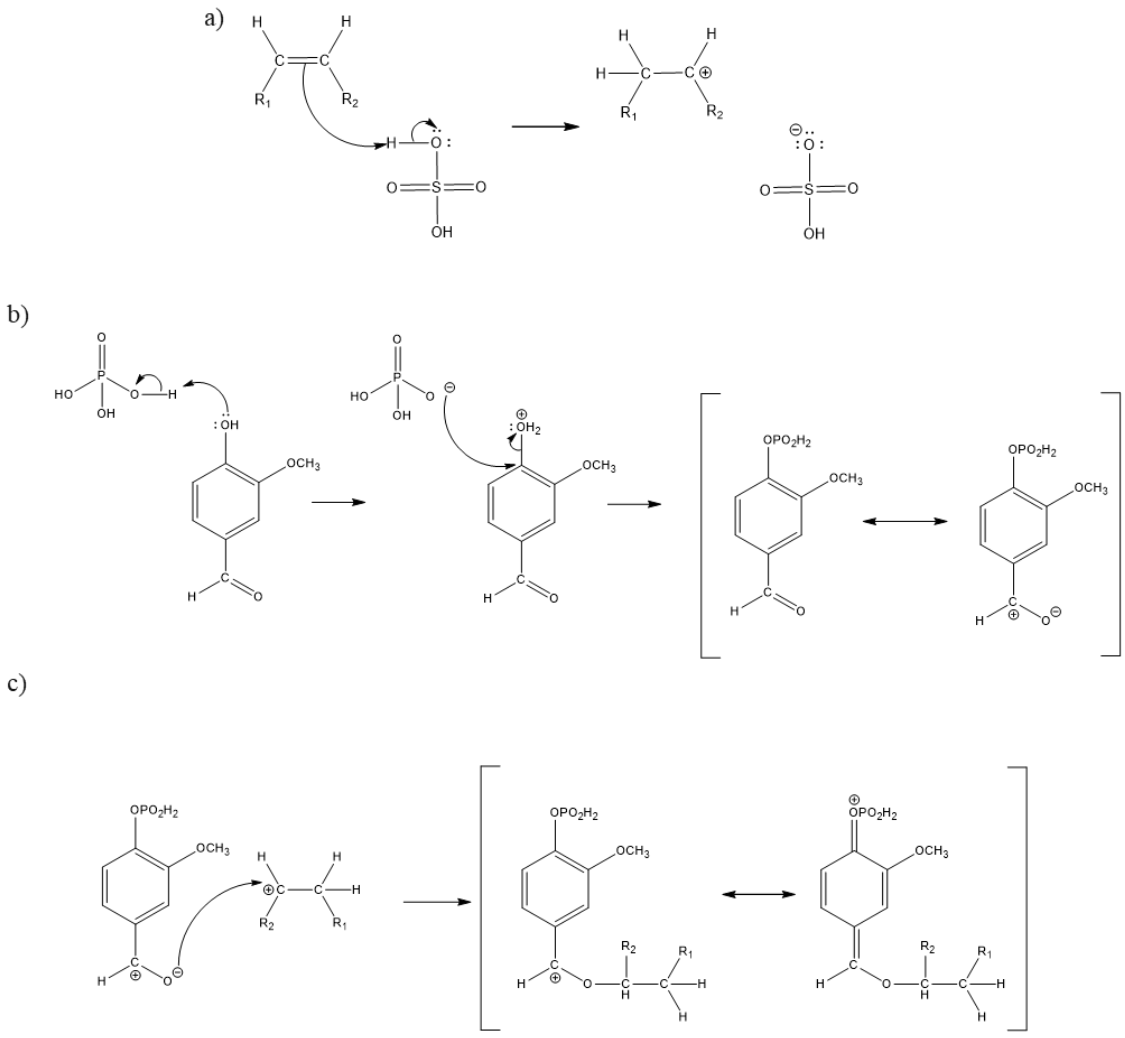

Figure 2.1 Proposed mechanism for the Sulfo-phospho-vanillin reaction. a) Formation of the carbonium ion; b) Formation of the phosphor-vanillin reagent; c) Reaction between the phosphor-vanillin reagent and the carbonium ion forming the pink-coloured product.

Nevertheless, the SPV method represents a viable alternative for normalizing total lipid content in biological samples. In lipid molecules, the double bonds are mainly located at the fatty acyl side chains, regardless of class or subclass. Furthermore, 35 to 60% of the mammalian lipidome is estimated to contain at least one double bond[13,33,34,153,154]. Hence, The SPV reaction is

an adaptable method with the potential to overcome challenges posed by lipid class and fatty-acyl chain, posing as a strong candidate for sample normalization in lipidomics studies[148,149,151,152].

In addition to normalizing samples, using an appropriate extraction method before LC-MS analysis is critical for achieving uniform instrumental responses, enabling precise and comparable lipidomic profiles. In addition to these challenges, the initial preparation of biological samples is also crucial, which may include the application of effective homogenization protocols or cell lysis techniques to ensure comprehensive lipid extraction. Effective cell lysis is often achieved using one of three methods: liquid-liquid extraction (LLE), freeze/thaw cycles, and ceramic bead-assisted extraction[155]. This step is crucial for managing the challenges associated with lipid analysis, such as variable responses to different lipid classes and the accurate detection of low-abundance lipids, while preventing issues like column saturation, sample carryover, and excessive ion suppression[108,137].

The present work focused on optimizing and applying the SPV method within our lipidomics LC-MS workflows. The main goal was to optimize the method to perform accurate relative lipid quantification in different sample matrices (*e.g.* human saliva and serum, and MCF-7 and A549 cell lines) such that it integrates seamlessly with our current lipidomics workflow while enhancing the method's sensitivity and reproducibility. Furthermore, we evaluated its performance in real-world samples to address possible nuances generated by biological matrix effects. Although previous studies have also proposed modifications to the SPV method, the optimizations proposed herein are tailored to the requirements of LC-MS-based lipidomic analysis, offering insights into the method's application and implications for accurate lipid quantification in a previously unexplored context[77,148,149].

2.2. Experimental

2.2.1. Reagents and Equipment

Ammonium formate (MS grade), oleic acid (99%), ethanol (95% v/v), vanillin, phosphoric acid (H_3PO_4, BioUltra, ≥85% (T)), and H_2SO_4, along with the deuterated lipid mix Splash Lipidomix Mass Spec Standard (provided by Avanti Polar Lipids, Alabaster, AL, USA) for internal standardization, were purchased from Sigma-Aldrich (St. Louis, Missouri, USA). High-purity LC-MS grade solvents such as acetonitrile (ACN), methanol (MeOH), dichloromethane (DCM), water, 2-propanol (IPA), and chloroform were purchased from Honeywell (Charlotte, North Carolina, USA).

2.2.2. Saliva Sample Collection and Processing

Saliva samples were gathered from two participants (one female and one male) across two consecutive days at three distinct times: morning, afternoon, and evening. The volunteers collected their saliva by spitting directly into sterile 50 mL polypropylene tubes. Morning collections were done after an overnight fast, without any water intake, while samples taken in the afternoon and evening were collected at least one hour after the participants' last meal or beverage. Additionally, all samples were collected no less than one hour after the volunteers had brushed their teeth. Following collection, the samples were centrifuged at 2,500 x g for 15 minutes. The resulting supernatant was divided into several aliquots and stored in sterile micro polypropylene tubes at -80 ºC pending further analysis[156].

2.2.3. Cell Culture

The method's performance was evaluated using two distinct cell lines: MCF-7 (ATCC HTB-22) and A549 (ATCC CCL-185). Each cell line was separately cultured in T-75 flasks under optimal conditions: MCF-7 cells in Dulbecco's Modified Eagle Medium (DMEM) and A549 cells in F-12k medium (Kaign's Modification of Ham's F-12 Medium). Both cultures were supplemented with 10% fetal bovine serum (FBS), maintained at 37 ºC in a humidified atmosphere containing 5% CO_2, and the medium was renewed every two to three days. The cells were harvested through trypsinization, which involved washing the cells with cold phosphate-buffered saline (PBS), incubating them with 3.0 mL of 0.25% trypsin/EDTA (Hyclone, Logan, Utah, USA) at 37 ºC and 5% CO_2 for 5 minutes, and quenching the reaction with 8 mL of growth medium. Subsequently, the cell suspensions were transferred to 15 mL sterile polypropylene tubes and centrifuged at 900 rpm for 7 minutes. The supernatant was aspirated off, leaving behind the cell pellet. For the MCF-7 line, one pellet was resuspended in 1 mL of growth medium and homogenized through gentle pipetting. The cell count was determined using a hemocytometer before aliquoting the cells into 2 mL sterile micro polypropylene tubes, each containing 1×10^5 to 3×10^6 cells. Other cultures were distributed into triplicate aliquots in 2 mL sterile micro polypropylene tubes without cell counting.

The aliquoted cells were then centrifuged at 900 rpm for 7 minutes to pellet them to remove the growth medium. The pellets were washed three times with 1 mL of cold PBS and dried under a gentle nitrogen stream before being stored at -80 ºC until further analysis.

2.2.4. SPV Method Optimization

An initial experiment was carried out using the refined method outlined by Cheng *et al.* (2011), which involved adding a maximum of 100 µL of lipid extract in 1:1 (v/v) DCM/MeOH into the well plate, followed by solvent evaporation[149]. Next, 100 µL of concentrated H_2SO_4 was added to the samples, which contained between 5 and 120 µg of lipids, which were then heated at 90 ºC for 20 minutes. After heating, 50 µL of phospho-vanillin reagent, which was prepared according to Knight *et al.* (1972) with modifications from Cheng *et al.* (2011) by dissolving vanillin to a final concentration of 0.2 mg/mL in a mixture of 2:18:5 of EtOH/H_2O/H_3PO_4, was introduced[108,149,151]. Upon visible colour development, the absorbance was measured at 540 nm. Based on these initial findings, several adjustments were made to tailor the method to our specific needs.

External calibration curves were constructed under each condition to optimize the method, and their performances were compared. The standard solution was prepared by diluting the oleic acid standard with 1:1 (v/v) DCM/MeOH to a concentration of 1 mg/mL. Volumes ranging from 2.5 to 17.5 µL of this solution were used to construct each calibration curve.

The first modification involved optimizing the incubation time and temperature after the addition of the phospho-vanillin reagent, testing conditions at room temperature (22 ºC), 40 ºC, 50 ºC, 60 ºC, and 80 ºC for durations of 20 or 80 minutes (initial conditions were 90 ºC for 20 minutes). Next, to minimize lipid sample dilution, we investigated varying volumes of H_2SO_4 (the initial 100 versus 50 µL) to minimize lipid sample dilution. Lastly, we explored different solvent mixtures for the lipid extract to find those that might offer benefits for potential future uses. The solvents assessed included a 2:1 chloroform/methanol (v/v) mixture, a 9:1 ratio of mobile phase A

(MPA) to mobile phase B (MPB) (with MPA consisting of 10 mM ammonium formate in a 50:40:10 mixture of MeOH, ACN, and H_2O, and MPB comprising 10 mM ammonium formate in a 95:5 mixture of IPA and H_2O), and a 9:1 MPA/MPB mix without ammonium formate.

The selection of optimal conditions was based on several criteria: improvements in detection and quantification limits, the linearity range, the volume of sample required, and the method's practicality for regular analysis. We used Student's t-tests to evaluate significant differences across all conditions, with a p-value of less than 0.05 considered statistically significant.

2.2.5. Sample Preparation

Lipid extraction for saliva and cell samples was performed using a modified version of the Folch liquid-liquid extraction protocol adapted to small sample volumes. Briefly, samples were vortexed with the Splash Lipidomix Mass Spec Standard (Avanti Polar Lipids, a mixture of 14 deuterated lipids in methanol, employed for internal standardization) and extracted with a mixture of 2:1 DCM/MeOH, followed by a clean-up step with water (8:4:3 DCM/MeOH/water). After 10 min equilibration at room temperature, the mixtures were centrifuged at 12,000 rpm and 4 ºC for 10 minutes. The bottom organic layer was employed for lipidomics[72,103]After extraction, an aliquot of the organic layer was evaporated to dryness and resuspended in chromatographic mobile phases before LC-MS injections. The resuspended samples were stored in polypropylene inserts placed inside autosampler vials sealed with a PTFE/silicone septum at 4 ºC for a minimum of 4 hours and a maximum of 24 hours before analysis.

2.2.5.1.Extraction of Lipids from Saliva Samples

A 225 µL saliva sample was mixed vigorously for 20 seconds with 1.1 µL of Splash Lipidomix Mass Spec Standard (Supp. Table 1) and 449 µL of methanol. After this initial mixing, 900 µL of DCM was added, followed by another 20-second vortex. Then, 113 µL of water was introduced to the mixture, which was vortexed for an additional 10 seconds and allowed to settle at room temperature for 10 minutes. The mixture was centrifuged at 12,000 rpm at 4 ºC for 10 minutes. From the separated organic layer, 720 µL was taken and evaporated under a gentle nitrogen stream at room temperature over 15 minutes. The resultant dry residue was reconstituted in a 17:3 mix of MPA/MPB to achieve a final volume of 45 µL. For quality control, a pooled saliva sample (QC), created by combining equal volume aliquots from all samples, was processed alongside every six-sample batch using the identical extraction methodology.

2.2.5.2.Extraction of Lipids from Cell Samples

Three techniques for cell lysis were evaluated to identify the best approach for extracting lipids from cells: LLE, freeze/thaw cycles, and ceramic bead-assisted extraction. In the LLE method, a dried MCF-7 cell pellet (with an approximate count of 6×10^5 cells) was processed using a method similar to that for saliva samples. In brief, cell pellets underwent extraction with 1.8 µL of Splash Lipidomix Mass Spec Standard, 38.2 µL of MeOH, 80 µL of DCM, and 30 µL of H_2O. Following equilibration and centrifugation, a portion of the organic phase (68 µL) was dried under a gentle stream of nitrogen for 15 minutes and reconstituted in a 9:1 mix of MPA/MPB to a total volume of 45 µL.

For the freeze/thaw cycle approach, cell pellets were initially suspended in 30 µL of a 1:1 MeOH/H_2O mixture. The samples were quickly frozen in liquid nitrogen for 2 minutes and then thawed in water for 2 minutes with vortexing, a process that was repeated three times. The lysed cells were then subjected to the same extraction steps as in the LLE method.

In the ceramic bead-assisted extraction method, three ceramic beads were added to the vial containing the cell pellet. After adding each solvent, samples were homogenized using a tissue homogenizer for one cycle at 4.5 m/s for 20 seconds and then processed as described in the LLE protocol.

Following the determination of the most effective extraction technique, all further extractions were conducted under these optimal conditions. Independent of the initial cell count, cell samples were extracted to a final volume of 150 µL, utilizing 5.0 µL of Splash Lipidomix Mass Spec Standard (Avanti), 128.3 µL of MeOH, 266.7 µL of DCM, and 100 µL of H_2O. The dried extracts were then reconstituted in a 9:1 mixture of MPA/MPB to a final volume of 150 µL. For quality control (QC), pooled cell samples were processed using the identical protocol as the test samples.

2.2.6. Determination of Total Lipid Content for Sample Normalization

Before conducting LC-MS analysis, the lipid concentrations of the extracts were assessed using the optimized SPV method. A 15 µL portion of each lipid extract (organic layer) was dried under a gentle nitrogen stream. Subsequently, 50 µL of concentrated H_2SO_4 was added to the residue, followed by incubation at 90 ºC for 20 minutes and then cooling at -20 ºC for 10 minutes. To the samples, 50 µL of the phospho-vanillin reagent (consisting of 17% H_3PO_4 and 0.2 mg/mL

vanillin) was added, and the mixture was incubated at 60 ºC for 20 minutes. After incubation, the absorbances of the samples were measured using a microplate reader at 540 nm[149]. Lipid quantification was carried out using oleic acid as the external calibration standard. An analytical curve was constructed by utilizing various volumes (ranging from 2 to 20 µL) of a 1 mg/mL stock solution of oleic acid, which was then diluted to a final volume of 100 µL with H_2SO_4 and the phospho-vanillin reagent, maintaining the same ratio as for the samples.

2.2.7. LC-MS Analysis

After quantifying total lipids, saliva sample normalization was conducted by injecting an optimal mole amount determined using a pooled sample for LC-MS analyses. Injection volumes ranged from 2 to 16 µL for positive and negative ion modes, with the pooled sample injection volumes set at 4 and 10 µL, respectively.

On the other hand, some MCF-7 cell samples, whose total cell counts had been previously determined, were used to estimate the cell count in all other samples. Once the cell count was estimated, each sample was diluted to achieve 8.6×10^4 cell equivalents/µL across all samples. Injection volumes were set at 3 µL for positive and 12 µL for negative ion modes. The need for different normalization approaches comes from differences in sample handling, such as the large injection volumes (*i.e.*, over 12 µL) required to inject a uniform amount of moles for the saliva samples, which could lead to significant peak broadening[157].

Lipid extracts underwent analysis via reversed-phase ultra-high-performance liquid chromatography (UHPLC) coupled to a high-resolution quadrupole-time-of-flight (QToF) mass spectrometer with an electrospray ionization (ESI) source. Chromatographic separation was

carried out using a Dionex 3000 system and a Waters Acquity CSH Premier C18 column. The mobile phases consisted of MPA: 10 mM ammonium formate in 50:40:10 ACN/MeOH/H_2O and MPB: 10 mM ammonium formate in 95:5 IPA/H_2O. A gradient separation lasting 22 minutes (starting at 5% MPB and reaching 95% MPB at 18 minutes) was followed by a 10-minute re-equilibration period. The flow rate was set at 250 µL/min, with a column temperature of 45 °C. MS/MS qualitative information was obtained for all sample injections using auto-MS/MS, with a cycle time of 1.2 seconds and active exclusion of precursors detected for more than three consecutive spectra within 0.50-minute intervals. Injection volumes were adjusted for each polarity and application based on ionization performance and experimental goals. Cell sample extracts were injected in volumes of 3 µL and 12 µL in the positive and negative ionization modes, respectively. Saliva samples were profiled comprehensively by injecting 3.47×10^{-6} mol in the positive ionization mode and 5.78×10^{-6} mol in the negative ionization mode.

Samples and blanks were prepared and injected randomly, but normalized and non-normalized samples were consistently injected on the same day. To ensure consistent quality control, a pool of aliquots from all samples was used for quality control (QC) and injected with each batch of 10 samples.

2.2.8. Data Processing and Lipid Annotation

MetaboScape 4.0 (Bruker Daltonics, Billerica, MA, USA) was used to analyze saliva samples with a minimum intensity cut-off set at 5,000 counts for positive ionization and 4,000 counts for negative ionization. Positive and negative ionization for cell pellets had a minimum intensity cut-off of 5,000 counts. Chromatograms were aligned using a minimum peak length of

six spectra, m/z re-calibration with sodium formate calibrant solution, a m/z tolerance of 5.0 mDa, and a retention time tolerance of 10 seconds. Isotopes and adducts were removed within a correlation threshold of 0.8. Recursive extraction was employed to search for features with missing values in over 20% of injections without applying the minimum intensity limit to the raw data. Aligned features were filtered based on detection in over 80% of injections in at least one group. Missing features were substituted using the minimum group intensity for features detected in more than 50% of injections within each group and the global minimum intensity for features detected in less than 50% of injections within each group.

Lipid annotation followed a three-tier putative annotation approach. Tiers 1 and 2 relied on acquired tandem mass spectrometry (MS/MS) spectra, while tier 3 annotations were based on mass matches in features previously not annotated. Lipid annotation protocols adhered to guidelines established by the Lipidomics Standards Initiative. Tier 1 and Tier 2 annotations utilized the MS-Dial LipidBlast library (https://fiehnlab.ucdavis.edu/projects/LipidBlast), the Human Metabolome Database (https://hmdb.ca), and the MassBank of North America LC−MS/MS libraries (https://mona.fiehnlab.ucdavis.edu) combined with MetaboScape 4.0 software. Tier 1 annotations had a precursor m/z tolerance of 5.0 mDa and an MS/MS score threshold of 500, while Tier 2 annotations had an MS/MS score between 100 and 500. All features not previously annotated by MS/MS match were searched against the LipidMaps database for mass-match annotation (tier 3 with m/z error smaller than 5.0 mDa). Due to the nature of lipid molecules, multiple isomers and isobars are possible within the mass tolerance of 5.0 mDa; therefore, we used a 5-tier system to ensure more accurate annotations. All annotation possibilities were filtered based on retention time and adduct detection and subsequently ranked according to the characteristics of the employed

method and biological fluids. The filtering system used herein has been previously described and employed by Buzatto *et al.* (2020)[108]. This study did not evaluate the positions of double bonds and stereospecific configurations of glycerol derivatives. Annotated lipids were categorized into subclasses and seven main categories following the classification system proposed by the International Lipid Classification and Nomenclature Committee, the Lipidomics Standards Initiative, and the LIPID MAPS database. Internal standards added during lipid extraction were identified based on retention time and accurate m/z values.

2.2.9. Post-acquisition Normalization and Statistics

Analytical curves generated for the SPV method optimization were evaluated based on their reproducibility, repeatability, limit of detection (LOD), limit of quantification (LOQ), and sensibility (m). The following formulas determined detection and quantification limits, where SD is the standard deviation of the curve's response.

$$\mathrm{LOD} = {}^{3 \times \mathrm{SD}}/_{\mathrm{m}}$$

$$\mathrm{LOQ} = {}^{10 \times \mathrm{SD}}/_{\mathrm{m}}$$

Hypothesis testing by Student's t-test was used to compare the sensitivity of the optimized SPV protocols with a confidence interval of 95%. The null hypothesis stated no difference between the sensitivities, whereas the alternative hypothesis stated that the difference was significant ($p>0.05$).

Isotope-labeled standards were utilized to mitigate ion suppression effects and other variations that might arise during sample handling. Class-matched normalization was performed

by associating each annotated lipid with an internal standard belonging to the same or most similar lipid subclass. Thus, the annotated lipids were normalized using one of the 14 deuterated standards present in the Splash Lipidomix Mass Spec Standard. However, features not previously annotated, whose lipid subclass remains unknown, were excluded from any statistical analyses.

The annotated lipids were matched with the most similar deuterated internal standard, and normalized intensities were calculated by dividing the original peak intensity (*i.e.*, peak height) of the annotated lipid by the peak intensity of the matched internal standard. Subsequently, the dataset was normalized by the summed intensity ratios (total intensity) for all annotated features within each sample and auto-scaled before statistical analysis using MetaboAnalyst 5.0. Features exhibiting low experimental reproducibility (RSD > 30% for QCs) were excluded before statistical analysis.

Statistical analysis involved Principal Component Analysis (PCA) and partial least square-discriminant analysis (PLS-DA). The PCA and PLS-DA score plots in this study showcase experimental replicates for each sample, with the clustering among quality control samples indicating technical reproducibility. PLS-DA models were assessed through leave-one-out cross-validation and permutation tests (1,000 permutations), with R^2, Q^2, and p-values provided in figure captions.

2.3. Results and Discussions

2.3.1. SPV Method Optimization

We first attempted to replicate the work by Cheng *et al.* (2011) to better understand their original optimization of the SPV method[149]. The procedure employed vegetable oils, such as canola oil (cooking grade), as a lipid standard to build analytical curves to quantify total lipid content. The methodology was originally described for less than 100 µL aliquots of lipid extract. A sample aliquot with a canola oil concentration of 15 mg/mL and volumes varying from 0.5 to 30 µL was loaded into a microplate and evaporated to dryness. The residue was mixed with 100 µL of concentrated H_2SO_4 and incubated at 90 ºC for 20 minutes, then cooling down at -20 ºC for 10 minutes. 50 µL of the phospho-vanillin reagent (0.2 mg/mL vanillin in 17% H_3PO_4) was added to the sample. After visual colour development (pink hue), the absorbance was determined using a microplate reader at 540 nm. The original paper mentioned 10 minutes for colour development after the addition of the phospho-vanillin reagent; however, we were unable to fully reproduce their results with said incubation time. A longer incubation of 80 min (Figure 2.2) was required to achieve similar sensitivities for the calibration curve published initially by Cheng *et al.* (2011)[149–151,158].

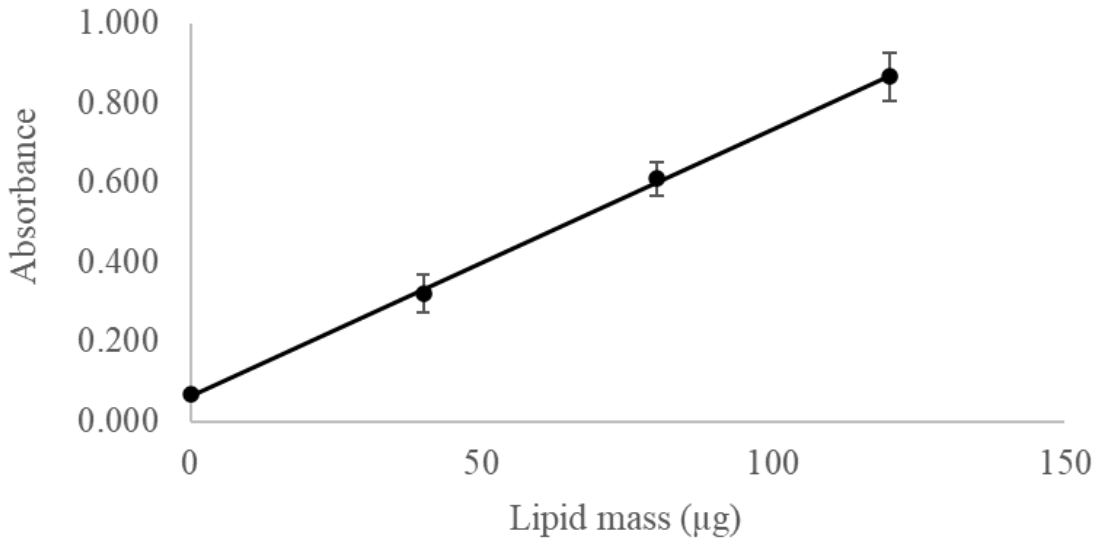

Figure 2.2. Reproduced results of the analysis carried out by Cheng *et al.* (2011) using canola oil as the calibrant standard. (m= 0.0067 and R^2=0.9994).

Although we replicated the published results after altering the incubation time, the 80-minute interval is unpractical for routine analyses. Furthermore, using commercially available vegetable oils is not ideal for quantifying lipids due to low purity and undefined composition. Therefore, we decided to optimize the methodology.

First, we replaced the commercial vegetal oil with a high-purity lipid standard for calibration. In this study, we investigated the composition of human saliva and epithelial cell samples; thus, an ideal standard would be a lipid found or closely related to human metabolism. Oleic acid is a monosaturated fatty acid (FA 18:1) commonly found in significant amounts in human biofluids, such as breast milk and saliva, making it a suitable calibrant[159]. All optimizations were performed using oleic acid as the external calibrant standard, and the x-axis units were

changed from lipid mass (µg) to concentration (mM), considering suitability for future applications.

Second, we evaluated the effect of different incubation conditions. Previous reports in the literature have indicated that heating after adding the phospho-vanillin reagent could improve sensitivity[148,150,158]. Hence, we evaluated the method's performance in different temperatures, ranging from 40 to 80 °C with an incubation time of 20 minutes (Figure 2.3).

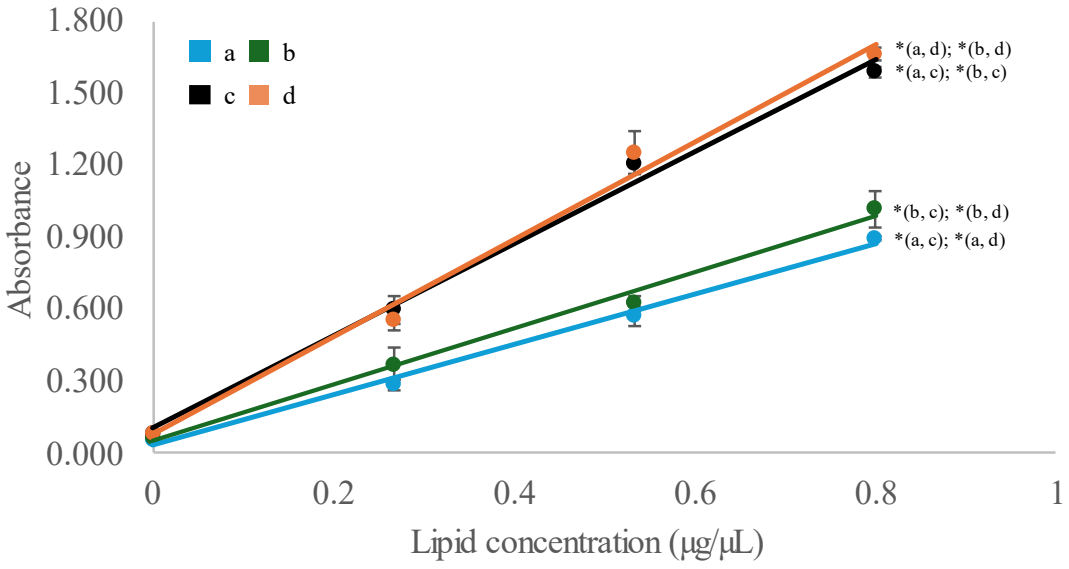

Figure 2.3. Calibration curves under different temperatures and incubation time conditions using oleic acid as a calibrant standard. a) Experiment at room temperature and incubation time of 80 minutes (blue): R2: 0.9945; Equation: Abs= (1.0521±0.0564)x + (0.0319±0.0281); b) Experiment at 40ºC and incubation time of 20 minutes (green): R2: 0.9920; Equation: Abs= (1.1718±0.0745)x + (0.0513±0.0372); c) Experiment at 60ºC and incubation time of 20 minutes (black): R2: 0.9927; Equation: Abs= (1.9218±0.1166)x + (0.1020±0.0582); d) Experiment at 80ºC and incubation time of 20 minutes (orange): R2: 0.9905; Equation: Abs= (2.0355±0.1410)x + (0.0752±0.0703). Significant differences ($p < 0.05$) between the curves are noted by subscript letters

Incubation temperatures between 40 ºC and 80 ºC for 20 minutes resulted in higher slopes than the original room temperature (22 ºC) incubation for 80 minutes. Therefore, heating the samples after adding the phospho-vanillin reagent increases the method's sensitivity. To evaluate if analytical curves were significantly different, the slopes and intercepts of the various conditions were compared using Student t-tests (Supp. Table 2). Significant differences in slope ($p < 0.05$) were observed for the 60 and 80 ºC conditions when compared to the original method. The p-values obtained were less than 0.05, indicating statistically significant differences in the slopes between the high-temperature conditions (60 ºC and 80 ºC) and the original room temperature method (22 ºC). This statistically significant result confirms that heating the samples enhances the sensitivity of the phospho-vanillin assay. The higher slopes at increased temperatures suggest that the method is more responsive to the analyte when the samples are heated, leading to more reliable results. An increased sensitivity means lower limits of detection, which pose an advantage when analytes are present in very low concentrations. However, it's crucial to consider the impact of higher temperatures on the stability of biological samples and reagents[148].

Considering that the highest temperature tested (80 ºC) had the highest sensitivity, it should have been the chosen temperature for incubation. However, this temperature is close to the initial incubation temperature of 90 ºC after adding H_2SO_4. Exposing lipid molecules to elevated temperatures for extended periods may lead to polymerization byproducts[152]. Since no significant differences were observed between 60 and 80 ºC, 60 ºC was chosen as a better incubation temperature after adding the phospho-vanillin reagent.

Different SPV protocols use between 100 and 180 µL of acid, with sample aliquots ranging from 5 to 100 µL. In some cases, this can result in both analytes and standards being diluted over

20-fold, depending on the aliquoted volume, which may cause a significant decrease in sensitivity[148,149]. We opted for reducing the volume of H_2SO_4 to 50 µL (Figure 2.4). When employing a smaller acid volume (50 µL), samples are two-fold less diluted than in the method proposed by Cheng *et al.* (2011), enhancing the method's sensitivity and limit of detection (Table 2.1)[148,149]. Reducing the amount of acid will lower the final dilution of the sample; however, it will also limit the amount of analyte that can be detected since there will be less acid available to react with the lipid molecules. In highly concentrated samples, this could pose an issue; however, in lipidomics, that is hardly ever the case. We often have samples that are too diluted, with only trace amounts of analytes. Additionally, when working with biological samples, the analyst must always be mindful of sample availability, as the amount of sample available might be limited to only a few microliters. Therefore, an analytical method that reduces the volume of required samples and still provides accurate results is typically preferred.

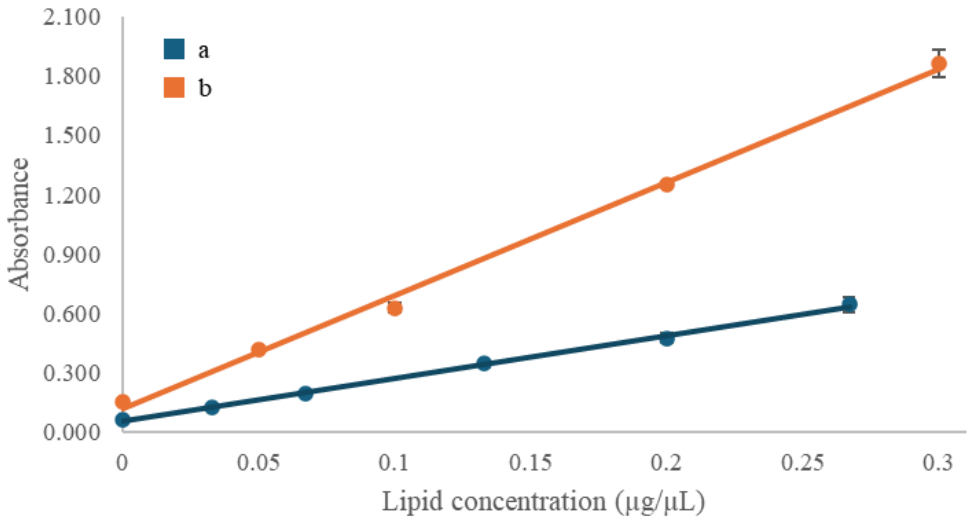

Figure 2.4. Analytical curves for oleic acid (1 mg/mL) comparing the method's sensitivity when using 50 and 100 µL H2SO4 in the SPV method; a) Experiment using 100 µL of H2SO4: R2: 0.9985; Equation: Abs= (2.2021±0.0494) x + (0.01903±0.0081); b) Experiment using 50 µL of H2SO4: R2: 0.9974; Equation: Abs= (5.8788±0.2135) x + (0.0855±0.0403).

We observed a significant difference between the slopes for 100 and 50 µL of H_2SO_4 (p-value < 0.05, shown in Supp. Table 3). The higher slope promoted by the reduced volume of H_2SO_4 resulted in improved LOD, LOQ, and sensitivity (m). The significant changes in the figures of merit make this new condition more suitable for applications in diluted samples. Hence, future experiments employed the volume of 50 µL of H_2SO_4.

Table 2.1. Limits of detection, quantification, and sensitivity for the SPV method using 50 µL and 100 µL of H_2SO_4.

	50 µL	100 µL
LOD (mM)	0.037	0.080
LOQ (mM)	0.122	0.265
Sensitivity (mM)	0.8694	0.2311

After determining the optimum incubation time and temperature after adding the phospho-vanillin reagent and optimizing the amount of H_2SO_4 added, we investigated the solvents used during sample derivatization. Lipids are extracted from the samples before the derivatization procedure. In the original method, Cheng *et al.* (2011) described 2:1 chloroform/MeOH as the best solvent for the lipid extract used in this reaction, which would be advantageous if we could take an aliquot of the organic layer during extraction for derivatization[149]. However, samples are extracted using a high sample/solvent ratio (normally at least 1 part of the sample for 40 parts of solvent), which would mean using a very diluted sample, and in turn, impact our accurate ability to quantify the lipid content[72,108]. Another option would be to resuspend the samples in 2:1 chloroform/MeOH after reconcentration. However, injecting strong solvents, such as chloroform, in the long term could negatively affect the LC system, column, and mass spectrometer. Furthermore, the initial portion of chromatograms would be affected by peak splitting and other effects due to the strong sample composition compared to initial chromatography conditions[78].

Our LC-MS lipidomics protocol requires resuspending samples in 9:1 MPA/MPB before injection. This composition ensures good LC-MS performance and compatibility between the

sample and initial chromatography conditions. However, that would require an additional step if lipid extracts were first resuspended in chloroform/methanol for lipid quantification, then dried to remove this solvent mix and resuspended again in MPA/MPB for injection. Besides increasing sample preparation time, this process would prolong exposure to light and air, which could lead to degradation of the lipids in the sample. It would be advantageous if the same conditions could be used as the solvents for sample derivatization, resulting in fewer drying and resuspending steps, reducing the time required for sample preparation and the possibility of lipid degradation[102]. We compared the performance of the SPV procedure using 2:1 chloroform/MeOH as the sample solvent with 9:1 MPA/MPB with and without ammonium formate (Figure 2.5).

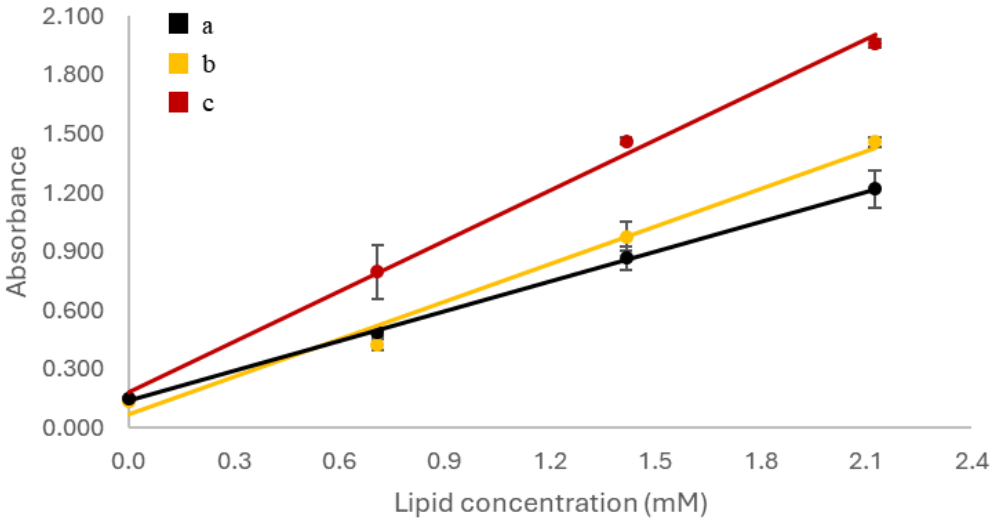

Figure 2.5. Analytical curves for Oleic acid (1 mg/mL) comparing the sensitivity of standard mi in different solvents. a) Experiment using 9:1 MPA/MPB without ammonium formate (black): R2: 0.9995; Equation: Abs= (0.5072±0.0078)x + (0.1422±0.0104).; b) Experiment using 9:1 MPA/MPB with ammonium formate (yellow): R2: 0.9855; Equation: Abs= (0.6388±0.0548)x + (0.0708±0.0726); c) Experiment using 2:1 Chloroform/MeOH (red, initial conditions): R2: 0.9961; Equation: Abs= (0.8596±0.0381)x + (0.1806±0.0505).

Even though the sensitivity of the SPV method is higher when employing a 2:1 mixture of chloroform/MeOH as solvent (curve “c”, red), the sensitivity of the analytical curve is not significantly different (p-value= 0.18, shown in Supp. Table 4) when compared to the curve obtained with 9:1 MPA/MPB with ammonium formate (curve “b”, yellow). The decreased sensitivity comes from lipids being less soluble on our mobile phase mixture than chloroform or DCM. Resuspension of the extract in 9:1 MPA/MPB with ammonium formate allows for an aliquot of our resuspended lipid extract to be analyzed by the SPV method and subsequently by LC-MS without any additional steps, resulting in an optimized timeframe that benefits both the workflow and the samples.

After further optimizing the SPV method for this application, we determined the lower and upper detection limits, as well as aliquot volumes required for reproducible analysis, using the oleic acid standard. The method had the best linearity between 0 and 3.5 mM (total lipid content, Figure 2.6). The detection limit was determined as 0.008 mM.

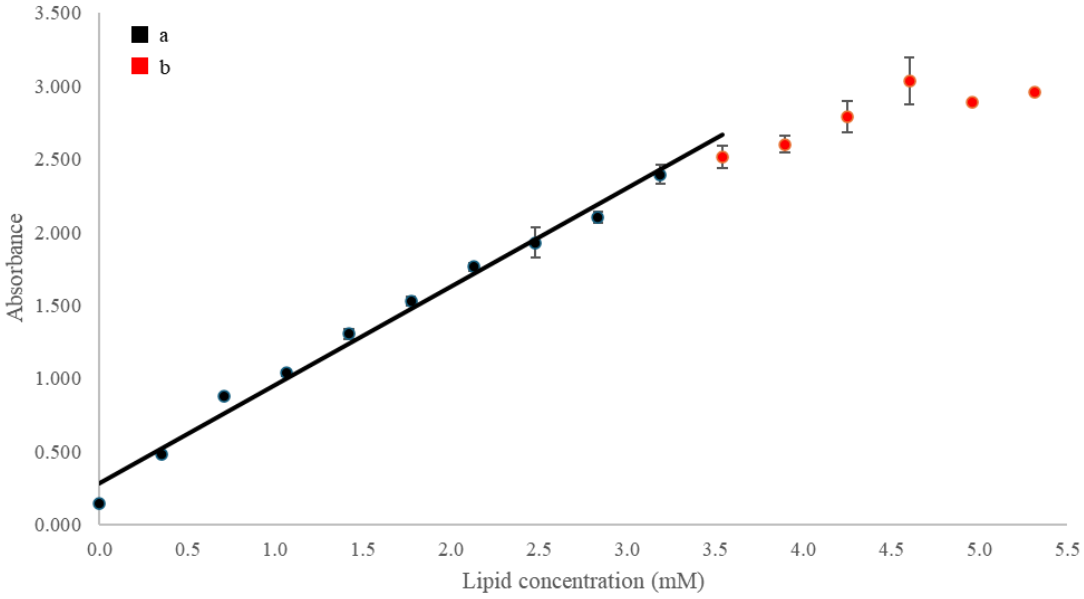

Figure 2.6. Limit of detection and linear range of the optimized SPV calibration curve employing 9:1 MPA/MPB with ammonium formate as solvent. a) Linear range of the calibration curve: R2: 0.9885; Equation: Abs= (0.6716±0.0256) x + (0.2870±0.0484); b) Scatter plot for the region where linearity is lost.

Lastly, we evaluated the ideal sample volume required for best quantification performance using blood serum lipid extract. Serum samples were extracted following a modified Folch liquid-liquid extraction protocol adapted to small sample volumes[72,103]. The obtained extracts were dried down under a gentle nitrogen flow and resuspended in 9:1 MPA/MPB with a 10-fold dilution. For example, the extract obtained from an initial serum aliquot of 1.0 µL was evaporated to dryness and resuspended to 10.0 µL of 9:1 MPA/MPB, always in triplicates. This procedure was repeated for all volumes of serum samples present in Table 2.2. Different volumes of the resuspended extract (0.5 to 5.0 µL) were used to determine the optimum extract volume for quantification (Table 2.2).

Table 2.2. Ideal volume and concentration of lipid extract for SPV using human serum.

Volume of serum (µL)	Volume of extract (µL)	AVG conc. in the original sample (mM)	AVG conc. In aliquot (mM)	AVG abs.	SD	RSD (%)
0.5	5	0.058	0.003	0.212	0.003	2
1.0	10	0.623	0.062	0.292	0.001	0.3
1.5	15	0.491	0.074	0.306	0.018	6
2.0	20	0.453	0.091	0.328	0.013	3
2.5	25	0.522	0.130	0.378	0.013	2
3.0	30	0.530	0.159	0.414	0.047	7
4.0	40	0.572	0.229	0.503	0.013	2
5.0	50	0.557	0.278	0.565	0.047	7
LOD	-	-	0.008	-	-	-
LOQ	-	-	0.028	-	-	-

AVG Original concentration: Lipid concentration in the raw sample before any dilution; AVG concentration: Lipid concentration in the aliquot used in SPV.

All aliquots exhibited relative standard deviations (RSD) lower than 10%. However, when the original concentration was calculated, significant differences were observed between the 5 µL aliquot and the others. We employed Student's t-tests (Supp. Table 5) to evaluate significant differences between 5 µL lipid extract aliquots and all additional extract aliquots, which confirmed there was a significant difference ($p<0.05$) between them. With that in mind, such small samples are unreliable for accurate quantification using the SPV method.

The total lipid concentration obtained for the smallest aliquot (0.5 µL of serum and 5.0 µL of extract) was 0.001 mM, below the LOD of 0.008 mM, which can cause the observed significant differences between this and the other aliquots. The obtained results indicate that the minimum amount of serum for accurate total lipid quantification is 1.0 µL, corresponding to 10 µL of extract, since the smallest volume tested (0.5 µL of the sample) yields concentrations below de LOD. However, if larger amounts of sample are available, 15 µL of lipid extract (1.5 µL of sample) would be the most adequate aliquot volume for quantification. Using higher amounts of sample whenever possible improves the reliability and precision of the measurements by providing a higher concentration of analytes, reducing the relative impact of experimental variability, and ensuring that measurements are well above the LOD.

Hence, the SPV protocol was fully optimized to better suit our applications' needs. The fully optimized version is detailed in Figure 2.7.

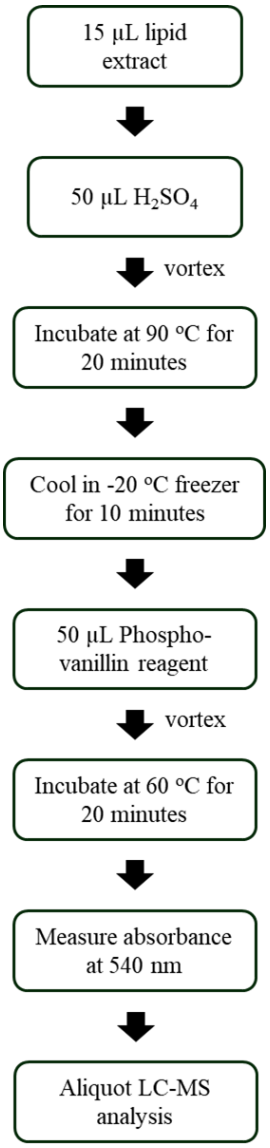

Figure 2.7. Optimized SPV protocol for relative lipid concentration determination followed by LC-MS analyses.

Since the SPV method was first introduced in 1937, many optimizations have been proposed, each applying it to different biological matrices, miniaturizing, and overall improving the limits of detection of the initial method[77,148–150,158,160]. Among those, Vatassery *et al.* (1981) described its use for measuring lipids in cerebral spinal fluid (CSF) using 1 mL of H_2SO_4 and 5 mL of phosphor-vanillin reagent incubated at 37 ºC for 10 minutes[150]. This work used a slightly

elevated temperature to increase reaction efficiency and decrease incubation time, but it required elevated amounts of sample. Cheng *et al.* (2011) proposed a miniaturization of the reaction, using 100 µL of H_2SO_4 and 100 µL of the phospho-vanillin, without any heated incubation after adding the phospho-vanillin reagent[148,149]. The optimizations proposed allow the application of the method when limited amounts of samples are available, though they require longer incubation time. Yet another proposed optimization was described by Anschau *et al.* (2017) using 20 µL of sample, 180 µL of H_2SO_4, and 500 µL of phospho-vanillin, incubated at 37 ºC for 15 minutes to measure lipid concentrations in yeast cells and microalgae. The method used small amounts of sample and a slightly elevated temperature to decrease incubation temperatures. However, the larger amount of H_2SO_4 used caused samples to be too diluted, impacting the method's limit of detection[148,149].

A recent study by Bailey *et al.* (2022) also proposed optimizing the SPV method for lipidomics applications. However, it's important to point out that their focus shifted towards employing higher concentration standards, differing from what is normally seen in our samples, which focus on high-sensitivity analysis of small amounts of biological samples. More specifically, their optimization process involved 10 to 100 µg/mL concentrations. Because of their concentration range, some differences in the optimization outcomes can be observed compared to the method described in this work. One important contract point is the use of lower volumes of H_2SO_4 (50 µL). Lower volumes of H_2SO_4 resulted in decreased sensitivity. However, our study shows that employing such lower volumes can increase sensitivity while still maintaining robustness and linearity ($R^2 > 0.995$) across a satisfactory linear range appropriate to the intended samples (up to 3 mM)[77].

Moreover, Bailey *et al.* (2022) suggested potential reproducibility issues could be associated with dried samples. Drying samples often results in the accumulation of the lipid content at the well's bottom and given the microplate's limitations in aiding thorough sample mixing, concerns regarding reproducibility may arise. Alternatively, we suggest a modification in the procedure by using sterile micropropylene tubes. This modification allows vigorous sample mixing and subsequent transfer of the final-coloured product to a microplate for UV-Vis quantification. At first, this may seem like an unimportant detail; however, it becomes significant when considering the final volume of our solution (100 µL) since even small amounts of solvent (ranging from 10 to 20 µL) can significantly influence the outcomes. Incorporating a drying step within the micropropylene tubes served two purposes: it reduces the final volume, thereby increasing the sensitivity, and effectively addresses potential issues from inadequate sample mixing[77].

Furthermore, differences in the incubation procedure following the addition of the phospho-vanillin reagent are also worthy of attention. Bailey *et al.* (2022) optimized the incubation time and phospho-vanillin concentrations. In contrast, our study optimized incubation time and explored the influence of temperature. Bailey *et al.* (2022) tested a range of incubation temperatures ranging from 10 to 60 minutes and found that 30 minutes yielded a favourable balance between completing the reaction and time efficiency. They also noted that a 60-minute incubation led to a nearly complete reaction. On the other hand, our methodology suggests incubations of 20 minutes at 60 ºC, based on the concept that higher temperatures help expedite reaction kinetics, thus facilitating completion[77,148]. By using elevated temperatures, our study

accelerated the completion of the reaction and increased the linear range compared to other methods[148,149].

In summary, all methods previously cited, including ours, were fine-tuned to align with their respective applications. It is worth noting, however, that the approach outlined in our study benefits from rigorously testing across standards and real-world samples, reinforcing its applicability and leading to a higher confidence in its efficacy for routine lipidomic analyses.

2.3.2. Saliva Sample SPV Normalization for LC-MS Analyses

The fully optimized SPV method (Figure 2.7) was applied to five-fold concentrated saliva samples obtained from a female and a male volunteer at three different time points (morning, afternoon, and evening). Sample normalization was performed by injection of the same number of moles of lipids from each sample, which corresponded to different injection volumes. First, we determined the total lipid content of a pooled saliva sample through the optimized SPV method with oleic acid as the normalization standard (0.578 mmol/L). The ideal injection amount for this pooled sample was determined based on the number of detected features and summed intensities (total intensities for all detected chromatographic peaks), being 3.47×10^{-6} mmol for positive ionization (6 µL injection of the lipid extract with total lipid content of 0.578 mmol/L) and 5.78×10^{-6} mmol for negative ionization (10 µL injection), with injection volumes for pooled samples being 6 and 10 µL for positive and negative ion modes respectively. These ideal injection amounts were then used to determine the optimum injection volume of each individual sample based on their total lipid contents.

The total lipid content of each individual sample was determined using the optimized SPV method (between 0.354 and 1.411 mM). Subsequently, the ideal injection volume was calculated for each sample to match the previously determined optimal injection amounts of 3.47×10^{-6} mmol for positive ionization and 5.78×10^{-6} mmol for negative ionization, *i.e.*, different volumes of each sample were injected to achieve the analysis of the same number of moles of lipids (2 to 17 µL). For example, the sample coded as "F1" had a total lipid concentration of 0.459 mM. To achieve the optimal injection of 3.47×10^{-6} mmol for positive ionization, we injected 7.5 µL of that sample (Table 2.3). Injecting the same amount of analyte (in moles) from each sample ensures consistency and comparability across all samples. This minimizes variations from different concentrations, improving accuracy and reliability. Standardizing the number of moles injected also helps to improve measurement precision and reproducibility, as instrument response and ion suppression will be similar across all samples.

A potential pitfall of injecting different sample volumes is the size of the injection plug in the chromatographic column, which can affect peak shapes and separation. Alternatively, the sample could have been diluted or concentrated to the same concentration before injection. However, this alternative procedure could introduce more variability and potential errors. Dilution might lower concentrations below detection limits, making low-abundance lipids hard to quantify. Concentrating samples could cause lipid degradation, matrix effects, or detector saturation, leading to inaccuracies. Injecting different volumes to achieve the same moles of lipids ensures optimal analysis conditions, maintaining the accuracy and integrity of lipid quantification.

The normalized samples (*i.e.*, injections of different volumes to amount to the same number of moles) were compared to non-normalized samples (same injection volumes for all samples). A

total of 6 µL of the non-normalized samples was used in the positive ion mode and 10 µL in the negative ion mode, while injection volumes ranged from 2 to 17 µL for normalized samples. All injection volumes and lipid concentrations are detailed in Table 2.3.

Table 2.3. The injection volume, total lipid concentration, summed intensity in both polarities, and optimized number of moles were used to inject SPV-normalized saliva samples.

Sample code	Injection volume (µL)		Extract concentration (mM)	Number of moles injected (mmol)	
	Positive ion mode	Negative ion mode		Positive ion mode	Negative ion mode
Pooled sample	6.0	10.0	0.578		
F1 5-fold con.	7.5	12.6	0.459		
F4 5-fold con.	4.7	7.9	0.733		
F6 5-fold con.	3.7	6.2	0.926		
M2 5-fold con.	6.7	11.2	0.515		
M3 5-fold con.	7.2	12.1	0.478		
M5 20-fold con.	5.2	8.7	0.665	3.47×10^{-6}	5.78×10^{-6}
F2 10-fold con.	5.6	9.4	0.615		
F3 5-fold con.	2.5	4.1	1.411		
F5 5-fold con.	7.4	12.4	0.466		
M1 5-fold con.	9.8	16.3	0.354		
M4 5-fold con.	9.6	16.0	0.360		
M6 10-fold con.	8.6	14.3	0.404		

F – Female sample; M- Male sample; con. – concentrated.

We compared the results obtained for normalized samples (injections of the same molar amounts from each sample, resulting in different injection volumes) with LC-MS analyses of non-

normalized samples, which were obtained by injections of the same volumes of each sample (6 µL of the non-for positive ionization and 10 µL for negative ionization). Figure 2.8 compares the number of features and total intensities (the summed intensities for all detected features) between SPV-normalized and non-normalized samples. The observed variation between detected features and summed intensities is reduced for the SPV-normalized saliva samples than for the non-normalized samples, which is also observed for the summed intensities. This indicates that the SPV normalization helps obtain a more similar number of features and summed intensities for all samples, demonstrating the adequacy and validity of this method for lipid normalization before LC-MS analysis.

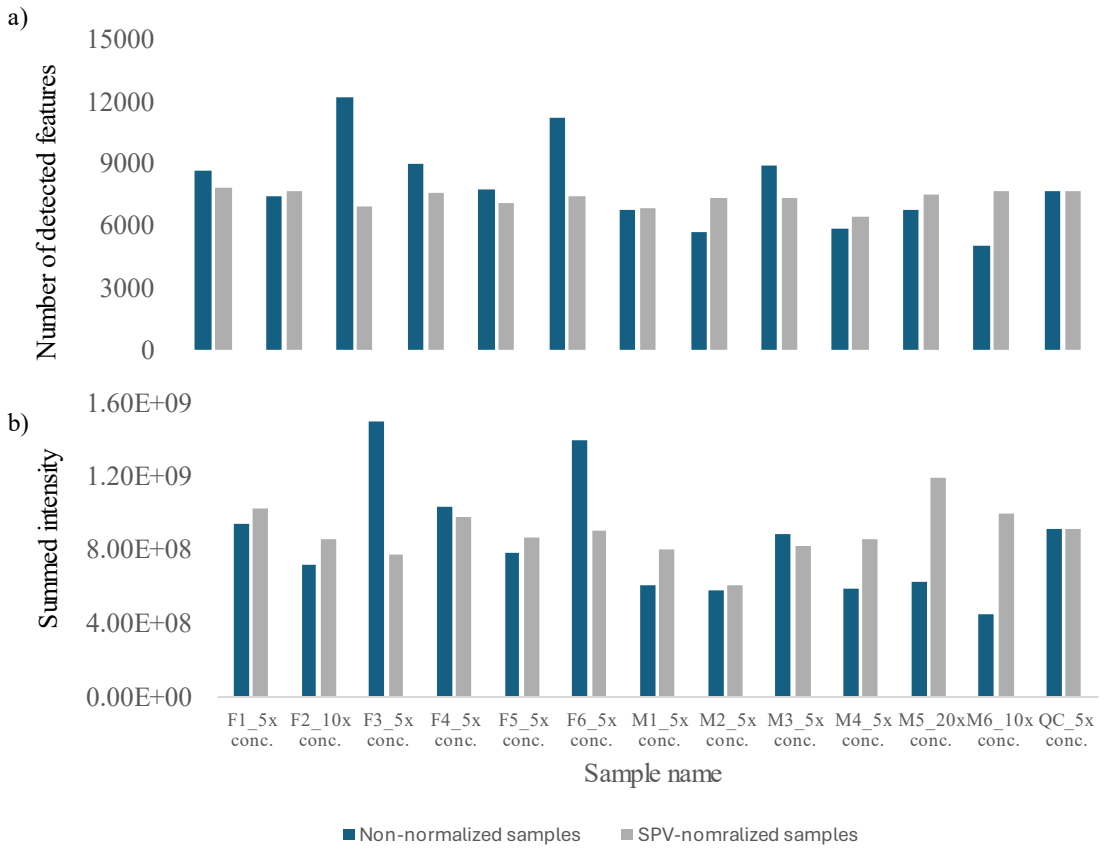

Figure 2.8. Detected features and summed intensities for normalized and non-normalized samples. a) Detected features for non-normalized and normalized saliva samples; b) Summed intensities for non-normalized and normalized saliva samples.

When comparing the number of detected features, a difference greater than 2-fold can be observed among the non-normalized samples (Figure 2.8.a blue), with the number of features ranging from 5,000 to 12,000. In contrast, for normalized samples (Figure 2.8.a gray), it went from 6,000 to 8,000. Similarly, the summed intensities varied significantly for the non-normalized samples (Figure 2.8.b blue), while smaller variations were observed for the normalized samples (Figure 2.8.b gray). Since samples were normalized by the number of injected moles, using the QC as a reference, it was expected that, for the normalized samples, both detected features and

summed intensities would be similar to those observed in the QCs, which indeed happened since variations became more subtle in the normalized samples. Samples that were more concentrated than QCs had fewer detected features after normalization. Furthermore, when comparing inter-sample variability, normalized samples showed a significant reduction in RSDs compared to the non-normalized samples. The RSD for the number of detected features decreased from 26% to 5%, and the RSD for summed intensities dropped from 38% to 16%. These findings show that normalization significantly reduces variability and enhances consistency in lipid analysis. Normalized samples had fewer variations in detected features and summed intensities, making the analysis more reliable.

In biomarker research, we usually opt for maximizing the detection of a higher number of features or more intense signals (higher summed intensities) to ensure the best sensitivity, as that approach means a better chance to identify biomarkers usually present in small concentrations. However, if the samples are too concentrated, the results will be impaired by detector saturation, ion suppression, lipid aggregation, and alterations in the extraction efficiency. For this work, we normalized the samples based on the pooled QC to ensure good analytical performance. Normalization based on the most or the least concentrated sample may be suitable for different applications. In turn, the increased ion suppression will reduce the detected species, reducing the chances of identifying lipids present in lower concentrations and affect quantification performance[102].

Normalized and non-normalized datasets were aligned and processed separately. For non-normalized samples, a total of 12,788 features were detected in positive and negative ionization modes after polarity merging for the saliva samples. These included 9,156 on positive and 3,632

on negative ionization. Regarding lipid annotation, 616 lipid species were annotated by MS/MS match, including 459 lipids in tier 1 (MS/MS score >500) and 152 lipids in tier 2 (MS/MS score <500) for non-normalized saliva samples. The remaining 12,172 features previously not annotated were searched in the LipidMaps database for putative annotations by accurate mass-match (tier 3), which resulted in another 2,008 lipid annotations (with an m/z tolerance of 5.0 mDa). Similarly, 12,580 features were detected in both ionization modes for the normalized dataset, composed of 9,095 on positive and 3,485 on negative ionization. For this dataset, 589 features were annotated by MS/MS match, including 445 in tier 1 and 144 in tier 2. The 11,991 features not annotated by MS/MS match were searched in the LipidMaps database for putative annotations, resulting in 2,315 lipid annotations. All lipid annotations, mass errors, and MS/MS scores for this study can be found in Supp. Table 6 for non-normalized samples and Supp. Table 7 for normalized samples. Some MS/MS-annotated features (tier 1 or 2) were excluded from the statistical analysis since they were not annotated as lipids (medications, other metabolites, and contaminants from sample preparation).

Out of the 14 deuterated lipids contained in the standard mixture, twelve were detected, with a maximum m/z error of 3.5 ppm (Figure A.1). Annotated compounds were matched to one of the internal standards for normalization, according to lipid subclass and retention time range. Since internal standards were added before lipid quantification, all samples had the same amount (number of moles) of internal standards added to them, regardless of total lipid content. However, because different injection volumes were used for each sample, the variation in peak intensities of the internal standards from sample to sample was significant, introducing variability in quantification.

A pooled saliva sample (QC) was used to verify the reproducibility of injections and extractions. Following data processing, the annotated lipids displaying RSDs higher than 30% for the QC experimental replicates were excluded due to low experimental reproducibility.

Multivariate statistical analysis was performed for normalized and non-normalized samples to assess the effects of the two conditions evaluated in this study (sex and sample collection time). Both conditions are known to cause alterations in the lipid profile of samples [134,135]. The PCA plots without (Figure 2.9.a) and with normalization (Figure 2.9.c) show the QC injections tightly clustered, which indicates excellent technical reproducibility. However, differences in sample clustering and statistical analysis can be overcome when both methods are compared. For the non-normalized samples (Figure 2.9.a), the PCA plot shows that the male samples (green) have a slight separation on the first principal component (PC1), and the female samples (red) have a separation on the second principal component (PC2). The same behaviour can be observed for the male samples in the normalized dataset, which have a slightly lower overall variation on the PC1 and marginally higher on the PC2 (Figure 2.9.c). The present findings demonstrate that SPV normalization does not affect the separation between samples with different biological characteristics while ensuring that lipid concentrations remain similar across all samples. The procedure guarantees optimal analytical performance without interfering with the samples' natural biological differences. This finding strongly supports the suitability and potential adoption of the normalization technique in forthcoming biomarker discovery investigations. It is crucial to acknowledge the significance of this approach, as previous research has emphasized the influential role of biological sex in the exploration and interpretation of salivary biomarkers[161,162].

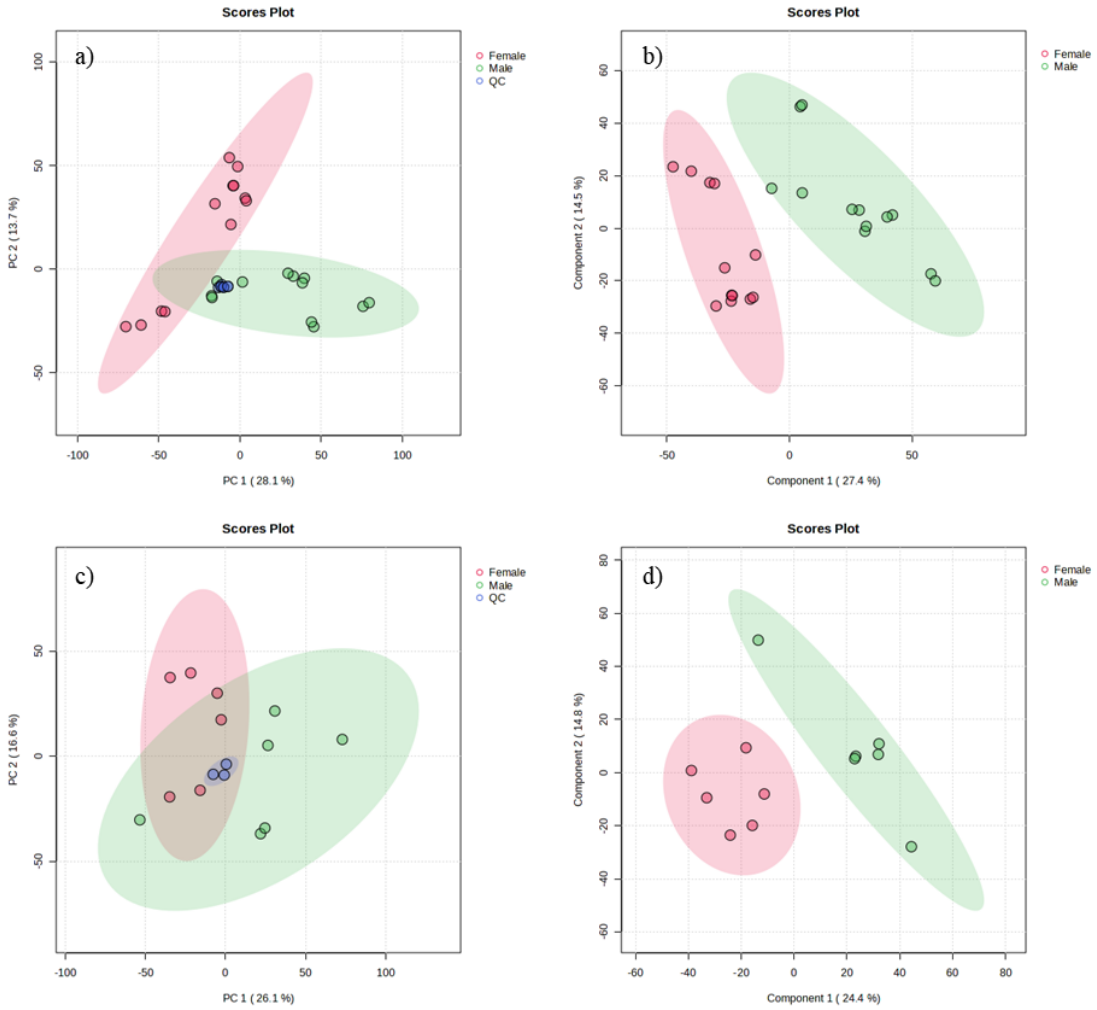

Figure 2.9. Statistical analysis for lipidomics of saliva normalized and non-normalized samples when grouped by sex. a) PCA score plot for non-normalized saliva samples with 3 QCs; b) PLS-DA score plot build for five components for non-normalized samples, resulting in R^2: 0.9995; Q^2: 0.5473 and p= 1 for 1000 permutations; c) PCA score plot for normalized saliva samples with 3 QCs; d) PLS-DA score plot build for five components, for normalized samples, resulting in R^2: 0.9985; Q^2: 0.3994 and p= 1 for 1000 permutations.

The PLS-DA cross-validation results showed relatively low Q^2 values for both the non-normalized and normalized datasets (0.5473 and 0.3994, respectively), indicating overfitting in both statistical models. Despite the overfitting, the PLS-DA plots demonstrate clear and distinct

separation between the groups. However, the low Q^2 values suggest that biological sex alone does not adequately explain the variability in the data. Other factors, such as the time of sample collection or the hydration habits of the volunteers, may have also influenced the lipid profiles observed. This study was intended as a pilot study, focusing on adequate sample handling and analysis to optimize the protocol for saliva samples for future projects. Consequently, a small number of biological replicates (N=1) was used for each collection point, which may reduce the reliability of the statistical models employed in the study.

We also evaluated how the collection period affects the statistical analysis of the lipidome profile in saliva samples. The PCA and PLS-DA score plots in Figure 2.10 differ from those in Figure 2.9 since samples are grouped by collection time instead of sex. When comparing both PCA plots, the morning (dark blue) and evening (green) normalized samples in Figure 2.10.c have a smaller variation on the first principal component (PC1) than their counterparts in the non-normalized dataset in Figure 2.9.a. However, for the morning samples, a greater variation is seen in the second principal component (PC2) for the normalized samples. In contrast, the afternoon samples (red) show a smaller variation in PC2 when comparing normalized and non-normalized samples, respectively.

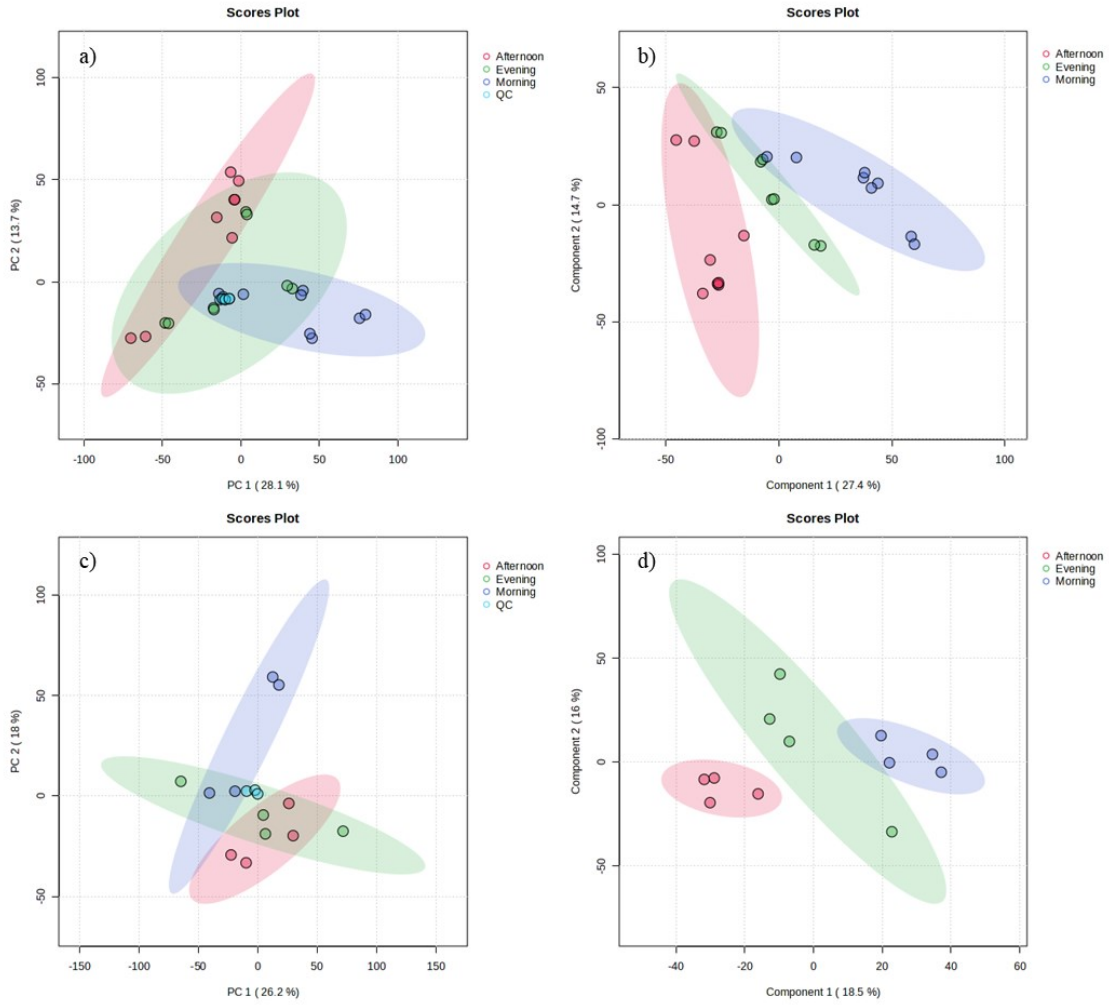

Figure 2.10. Statistical analysis for lipidomics of saliva normalized and non-normalized samples when grouped by sampling time. a) PCA score plot for non-normalized saliva samples with 3 QCs; b) PLS-DA score plot build for five components for non-normalized samples, resulting in R^2: 0.9995; Q^2: 0.6334 and p= 1 for 1000 permutations; c) PCA score plot for normalized saliva samples with 3 QCs; d) PLS-DA score plot build for five components, for normalized samples, resulting in R^2: 0.9999; Q^2: 0.6935 and p= 0.587 for 1000 permutations.

PLS-DA plots have low Q^2 values (0.6334, and 0.6935 for non-normalized and normalized data, respectively). The low Q^2 values suggest the overfitting of the statistical model, which indicates that this model cannot accurately predict the class of the samples when grouped by

collection time. On the other hand, both have R^2>0.995, which indicates that the lipidome variations are highly explained by the sample collection time. Both PLS-DA plots show significant separation between the three collection points. Still, the normalized samples are displayed in tighter groups. Hence, the normalization procedure emphasized the biological differences between the investigated samples without introducing biases. Saliva samples vary significantly in lipid and metabolite concentrations; thus, analyzing it without previous content normalization can introduce bias or complicate biomarker discovery[8].

The small number of biological replicates (N=1) may cause decreased reliability of the statistical models applied herein. Hence, we further performed univariate statistics using Volcano plots. The volcano plot for non-normalized saliva samples, regardless of sex or collection time, (Figure A.2.a) shows that 564 lipid species were significantly changed, with PC, Cer, TG, DG, PE, SM, and HexCer being the lipids classes with the highest numbers of significantly changed lipid species. On the other hand, in the volcano plot for normalized saliva samples (Figure A.2.b), showed 171 altered lipid species, with PE, HexCer, and PC representing the most significant changes.

Figure 2.11 shows a comparison between the number of annotations in each subclass for normalized and non-normalized datasets, as well as highlights the number of statistically different annotations for each method (Figure 2.11.b). These graphs show that the number of annotations for each subclass is similar with and without normalization before LC-MS analysis, corroborating the theory that sample normalization does not add bias to the analysis. However, when looking at the annotated lipid subclasses which were statistically different using the volcano plot analysis, we see that the number of altered lipids is noticeably higher for some subclasses, such as Cer, DG,

PC, SM, and TG. These results show that normalizing the samples reduces the number of significantly altered species compared to non-normalized samples, indicating an inflated number of statistical changes when no normalization is applied. Furthermore, significant changes observed in specific lipid species in this study can be attributed to factors related to sample handling, biological variability, and the physiological roles of these lipids. Proper normalization helps to highlight these changes by reducing technical variability, thereby providing a clearer picture of the biological differences.

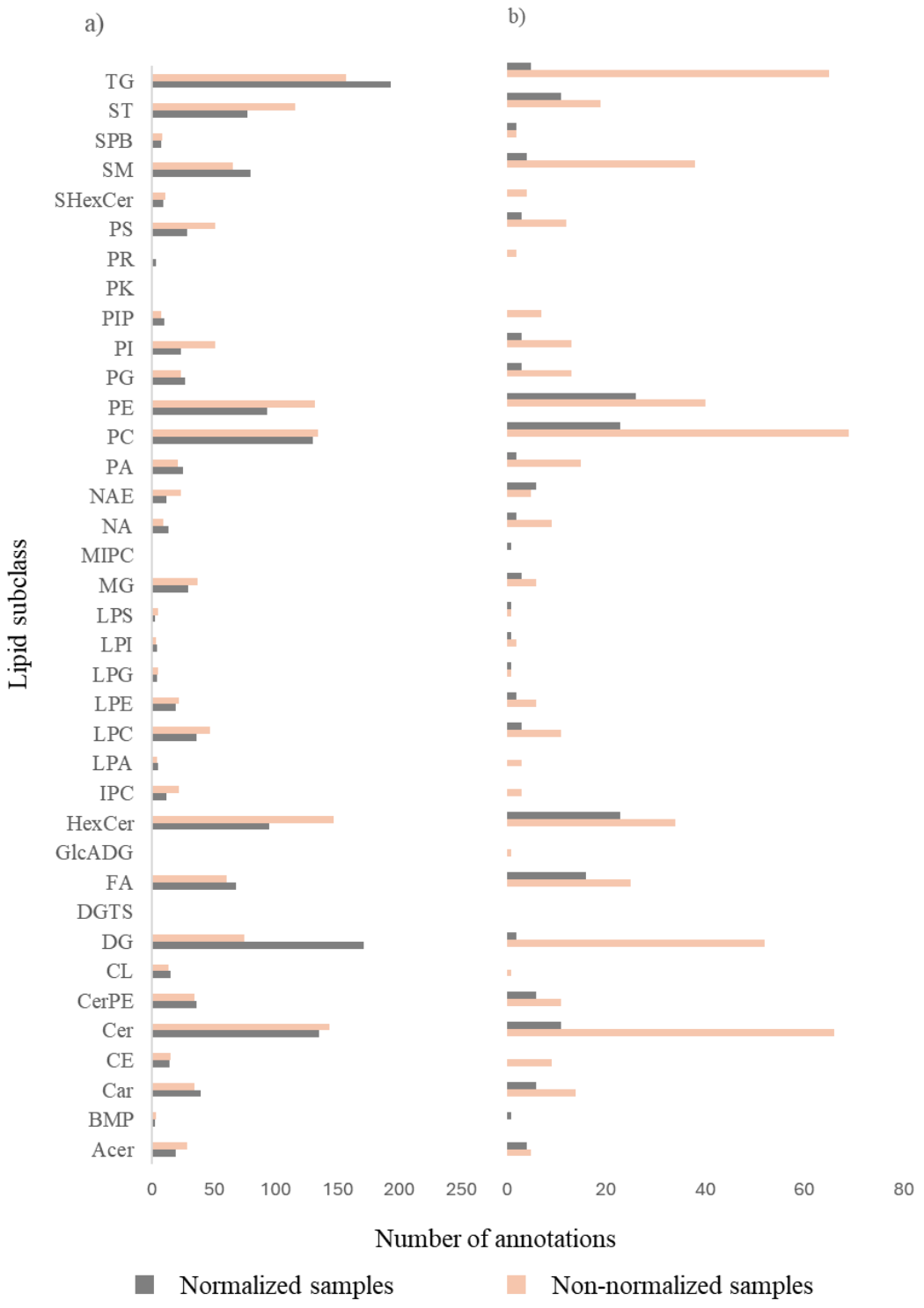

Figure 2.11. Comparison of annotated lipid subclasses present in non-normalized and normalized datasets. a) All subclasses annotated; b) Subclasses that were statistically significant in the Volcano plot ($p<0.05$ and FC <0.67 or FC.> 1.5).

2.3.3. Cell Lysis Optimization

After the pilot study for saliva samples, the SPV method was applied in cell pellets. The main goal was to determine the number of cells in unknown samples when cell counting is not possible or practical to allow normalization to the same concentration (number of cells/µL). First, the sample preparation method was briefly optimized. Three cell lysis methods were evaluated, including bead-assisted lysis, solvent-mediated lysis, and freeze/thaw cycles, based on the number of features, summed intensities, experimental variabilities, and reproducibility. Each lysis method was applied to two MCF-7 cell pellets containing approximately $2x10^6$ cells, and extractions were performed in duplicates. Student's t-test, PCA, and PLS-DA were used to evaluate possible statistical differences among the methods.

Figure 2.12 shows the total number of detected features and total summed intensities (*i.e.*, the summed intensities for all detected features) for each method and Figure 2.13 displays the PCA scores plot. We observed that bead-assisted lysis yields a higher number of features and improved summed intensities, as well as lower variation between experimental replicates. Although the freeze/thaw method is widely used for cell lysis, it resulted in lower reproducibility for untargeted lipidomics, with RSDs of 27% and 48% for the number of detected features and summed intensities, respectively. We found no significant differences when freeze/thaw was compared to both bead-assisted extraction and LLE, but these methods had RSDs of 6% and 7% for the number of detected features and 8% and 16% for summed intensities, respectively (Supp. Table 8). While cost-effective, the freeze/thaw approach can lead to biomolecule degradation and incomplete lysis due to repeated thermal stress, possibly explaining its lower efficiency in feature detection and intensity summation[163]. The high RSDs combined with the reduced number of detected features

and summed intensities indicate that the freeze/thaw method is not ideal for lipidomics, and alternative approaches should be considered if feasible for the intended purposes.

The bead-assisted lysis requires the use of disposable ceramic beads and a bead-beater device, being less cost-effective than the other methods. Still, it provided a higher number of detected features and summed intensities for lipidomics. The mechanical disruption of cellular structures is effective at breaking down membranes and strong protein-lipid and protein-protein interactions, which may not be disrupted by gentler methods such as vortex-assisted LLE without beads[164,165]. LLE can be considered a middle ground between freeze/thaw and bead-assisted extraction since it will not have the drawbacks from thermal stress and the associated cost with beads and bead beater homogenizers. Differences between LLE and bead-assisted extraction are not statistically significant, and they have similar RSD for the number of detected features, although the RSD for summed intensity is slightly higher for LLE. In conclusion, lipid extraction using only solvents yields similar features and summed intensities when compared to bead-assisted extraction, showing the potential of mechanical methods in enhancing lipid recovery[165].

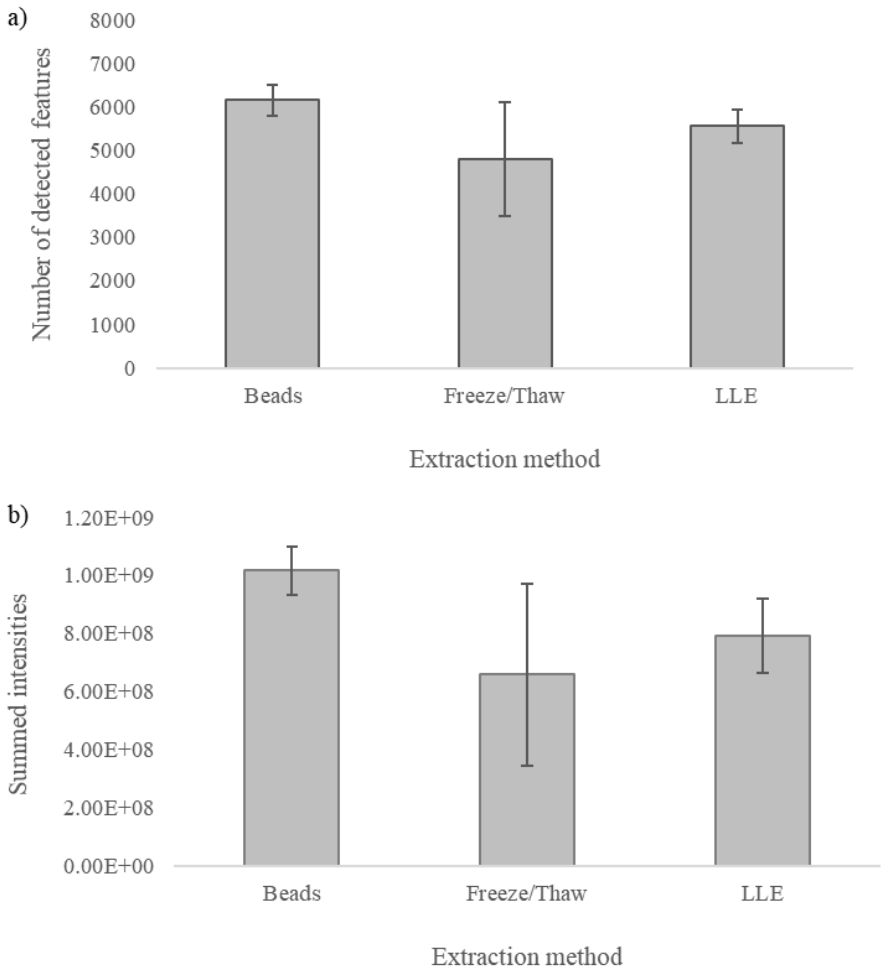

Figure 2.12. Comparison among different cell lysis methods using four cell samples each as of a) Number of detected features for lipid extractions under different conditions; b) Summed intensities for lipid extractions under different conditions.

Since the sample preparation study was only a small part of a larger project, the sample size was limited, resulting in only two biological replicates (with three injections each). The PCA score plot (Figure 2.13) shows that samples extracted using LLE have the lowest variation for both PC1 and PC2. After carefully considering the acquired data, the chosen method for sample preparation was a traditional LLE extraction, using only solvents without any further assistance from freeze/thaw or beads.

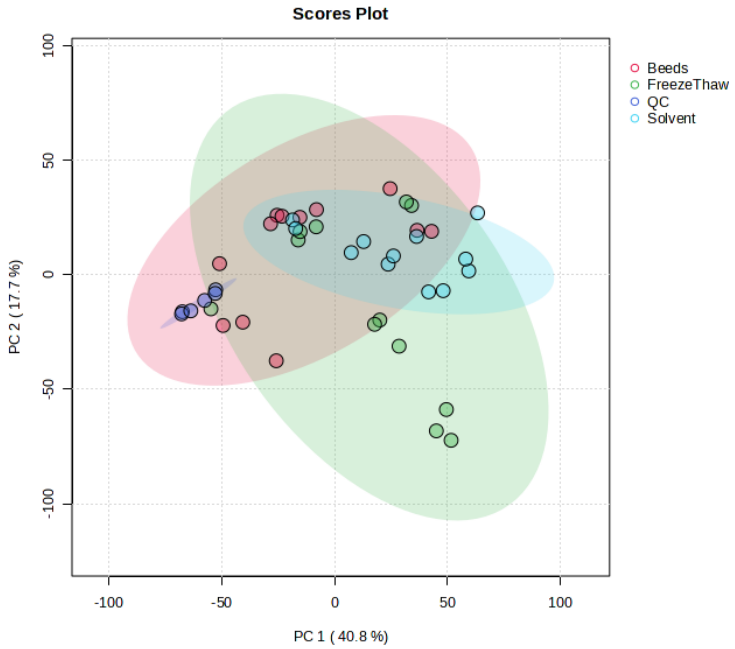

Figure 2.13. PCA score plot for different sample preparation techniques for cellular lipidomics using four biological replicates with three experimental replicates for each condition.

2.3.4. SPV Normalization of Cell Pellet for LC-MS

The SPV method was employed to determine the number of cells in unknown samples from different cell lines (MCF-7 and A549). We first employed the SPV method using MCF-7 pellets to construct a calibration curve correlating the number of cells with lipid concentration (Figure 2.14). All samples were analyzed in triplicates, and the RSD for the estimated cell numbers ranged from 2 to 29%. The number of cells in unknown samples was then calculated based on this analytical curve, and samples were diluted to have the same number of cells per microliter before injection. Samples were analyzed as normalized and non-normalized to evaluate improvements in lipid profile. Figure 2.14.a shows the calibration curve using MCF-7 cells and the concentrations

calculated for each sample. All samples were analyzed in triplicates, and the RSD for the estimated cell numbers ranged from 2 to 19%.

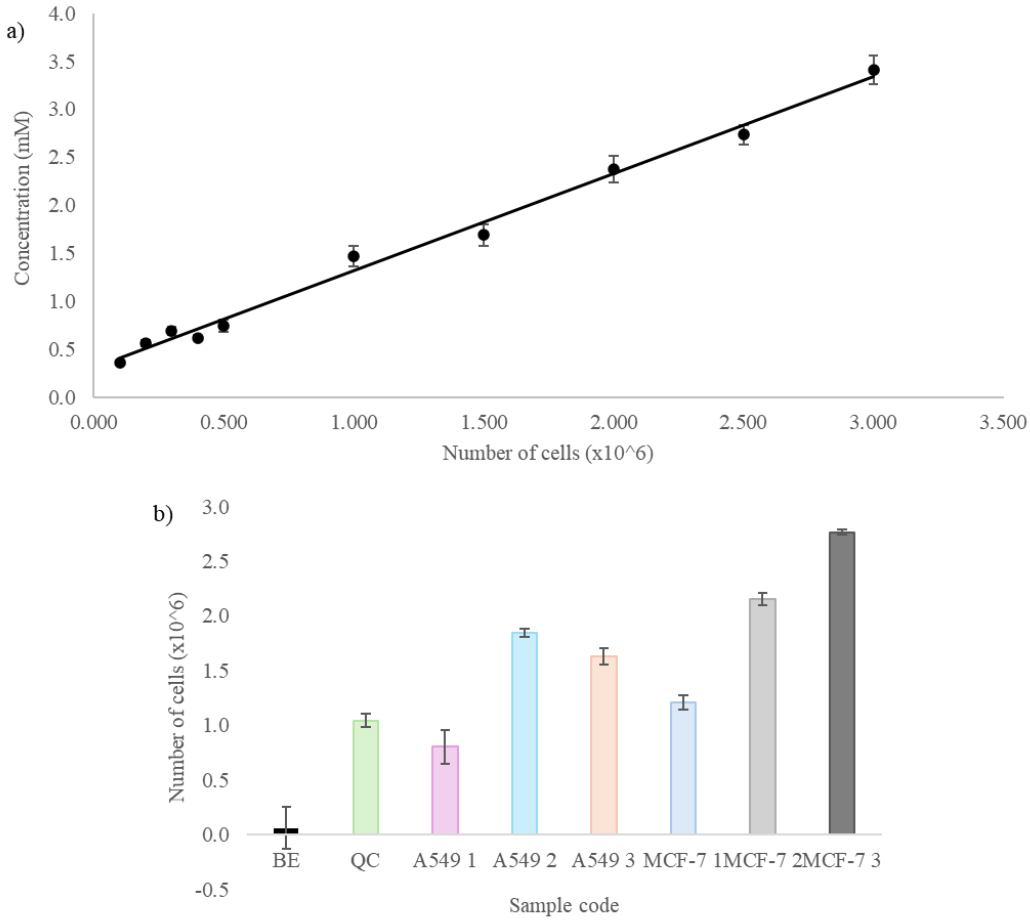

Figure 2.14. The relationship between the number of cells in pellets and lipid concentration is determined by SPV. a) Calibration curve using MCF-7 cell pellets as a calibrant standard ($y=1.00x + 0.3033$ $R^2=0.9919$); b) Average number of cells in each cell pellet.

Following SPV quantification, the analytical curve was employed to determine the number of cells in unknown samples. Unlike what was previously done for saliva samples, the goal was to

inject the same volume of every sample. The approach changed because sometimes a very high (>15 µL) or very low (<2 µL) volume will be needed to achieve the same concentration for all samples, which results in additional sample preparation steps. Additionally, when injecting high volumes, chromatograms are susceptible to peak broadening, splitting, and tailing, which makes data alignment more challenging[157].

Non-normalized cell samples were extracted, resuspended to 9:1 MPA/MPB, and analyzed by LC-MS. Alternatively, normalized samples were diluted to the same concentration (number of cells/µL) before analysis. We injected volumes of 4 and 12 µL for both normalized and non-normalized samples for positive and negative modes. The acquired data was subsequently aligned in MetaboScape 4.0, and lipid annotation was performed as described by Zardini Buzatto *et al.* (2021)[103]. After alignment, 7,938 features were detected after polarity merging, of which 4,847 were detected in positive ion mode, and 3,091 were detected in negative ion mode. MS/MS annotation yielded 1,169 annotations, 1,057 of those tier 1 (MS/MS score > 500) and 112 tier 2 (500 > MSMS score > 100). The remaining features not annotated were searched against the LipidMaps database for accurate mass match annotation (mass error < 5mDa), which resulted in 686 annotations. Figure 2.15 shows the lipid subclass distribution of the annotated species for cell samples, and a list of all annotations can be found in Supp. Table 9.

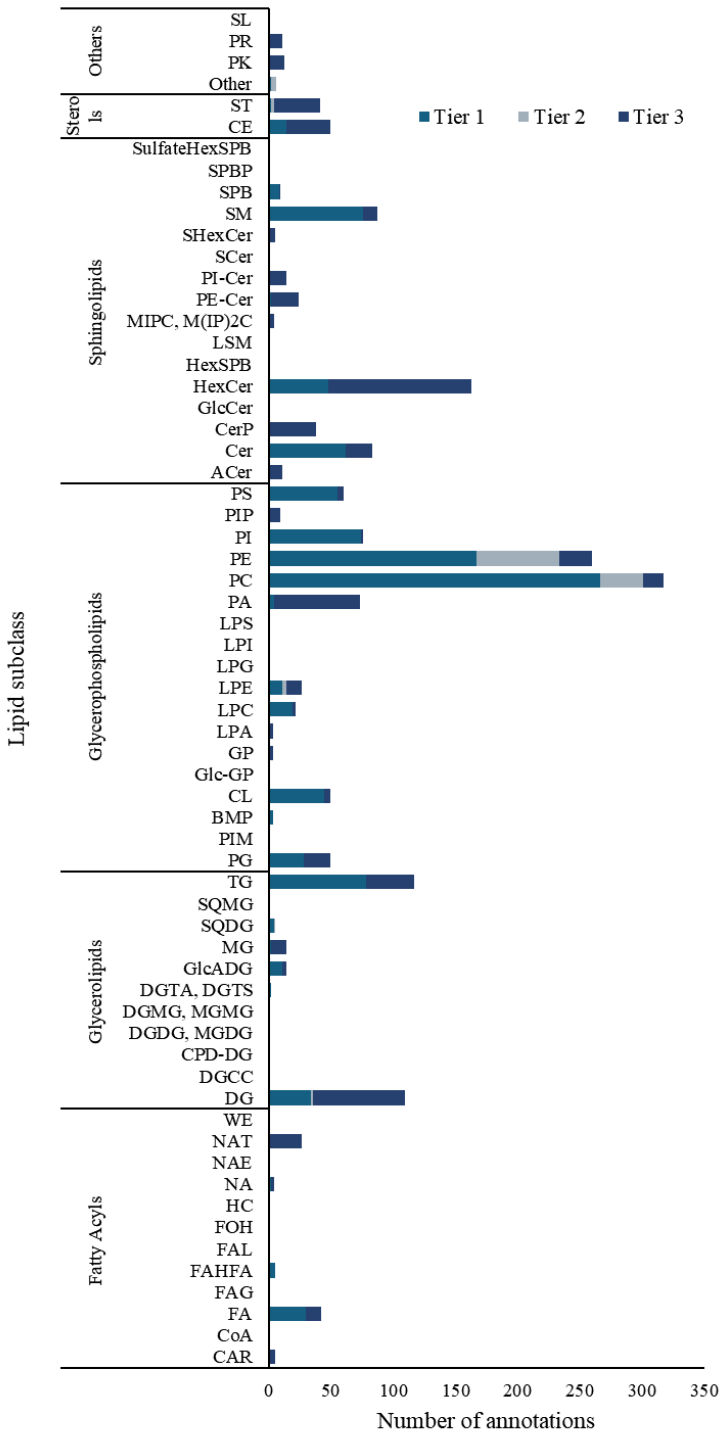

Figure 2.15. Distribution of lipid annotations across lipid subclasses and annotation tiers. Tier 1 annotations were MS/MS matches with scores higher than 500, Tier 2 were MS/MS matches with scores between 100 and 500, and Tier 3 were mass match annotations.

Twelve internal standards (out of 14) were annotated with a maximum m/z error of 1.0 ppm for positive and 1.2 ppm for negative ionization (Figure A-1). Internal standard normalization was performed by matching each annotated lipid to the most similar internal standards, always observing lipid subclass and retention time range. Four annotated features in tiers 1 and 2 (MS/MS) that were not lipids were excluded from the statistical analysis. Quality control was performed by analyzing pooled samples (QC) for every batch of 10 samples to verify the reproducibility of injections and extractions experimental reproducibility. Features with RSD higher than 30% for the QC replicates were excluded before statistics due to low experimental reproducibility. Statistical analysis was performed on the annotated features with RSD lower than 30% in the QC samples.

The PCA scores plots for non-normalized (Figure 2.16.a) and normalized samples (Figure 2.16.c) show tightly clustered QC injections in both datasets, suggesting technical reproducibility. However, sample normalization before LC-MS lipidomics affects sample clustering, as samples appear more clustered in the normalized PCA plot (Figure 2.16.c) than in the non-normalized plot (Figure 2.16.a). Although the QC samples in Figure 2.16.c are somewhat spread out, indicating variability, the overall clustering of the normalized samples shows improved grouping by cell line. Both MCF-7 (green) and A549 samples show lower PC1 and PC2 variations in the normalized dataset, suggesting that normalization can reduce bias regarding lipid concentration (or number of cells) in these samples. Furthermore, cell samples are to be clustered by cell line in both non-normalized and normalized datasets, which indicates that normalization does not add a bias to the samples regarding which cell line they belong to. PLS-DA models for both datasets were also

evaluated (Figure 2.16.b and Figure 2.16.d); however, not much information was obtained, considering both models had high R^2, Q^2, and p>0.05.

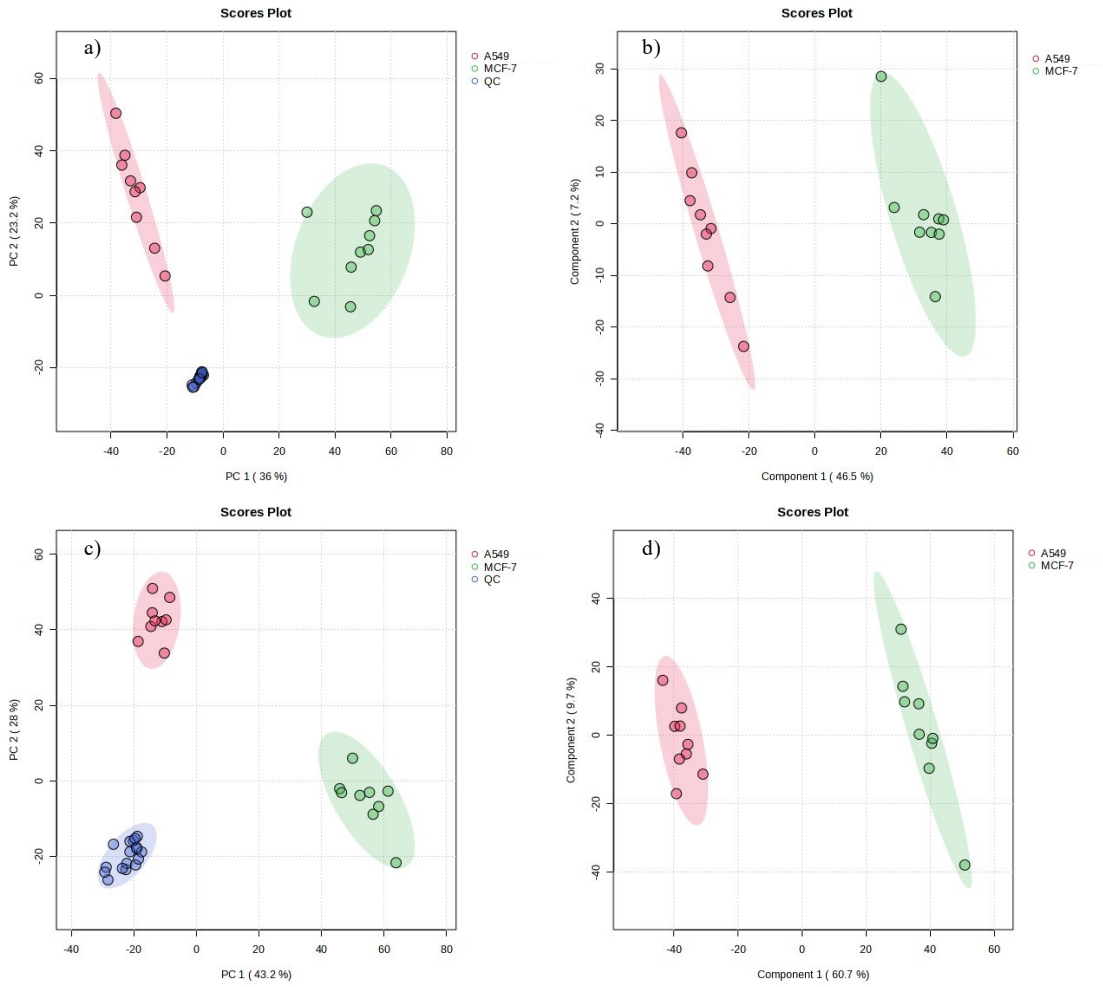

Figure 2.16. Statistical analysis for cellular lipidomics, comparing normalized and non-normalized cell pellets of different cell lines. a) PCA score plot for non-normalized cell samples with 12 QCs; b) PLS-DA score plot build for five components for non-normalized samples, resulting in R^2: 0.9998; Q^2: 0.9585 and p= 1 for 1000 permutations for non-normalized samples; c) PCA score plot for normalized cell samples with 12 QCs; d) PLS-DA score plot build for five components, for non-normalized samples, resulting in R^2: 0.9999; Q^2: 0.9877 and p= 0.001 for 1000 permutations for normalized samples.

We frequently use statistical models to identify significantly altered lipids, which may indicate underlying biological processes. Due to the small number of biological replicates (N=1) in this study, the reliability of these models is limited. However, this project serves as a proof of concept to ensure proper sample handling and analysis for future research. Therefore, we conducted a univariate statistical analysis using volcano plots (Figure A.3) to compare non-normalized and normalized samples for both MCF-7 and A549 cells. Figure 2.17 shows a comparison of the number of significantly different lipid species in normalized and non-normalized datasets. Non-normalized samples had 609 significantly altered lipid species, whereas normalized samples had 632. When looking into the lipid annotation distribution, although Figure 2.17 shows some variations, we can see that most lipid subclasses follow similar profiles. Furthermore, when looking at the individual annotations, only 27 that were present in the non-normalized dataset were not present in the normalized dataset, those belonging to Cer, DG, PC, PE, PG, and PS lipid subclasses. This comparison indicates that both normalized and non-normalized samples have very similar behaviors. While normalization aids us in ensuring robustness and reproducibility from sample to sample, it does not create a bias in the statistical analysis.

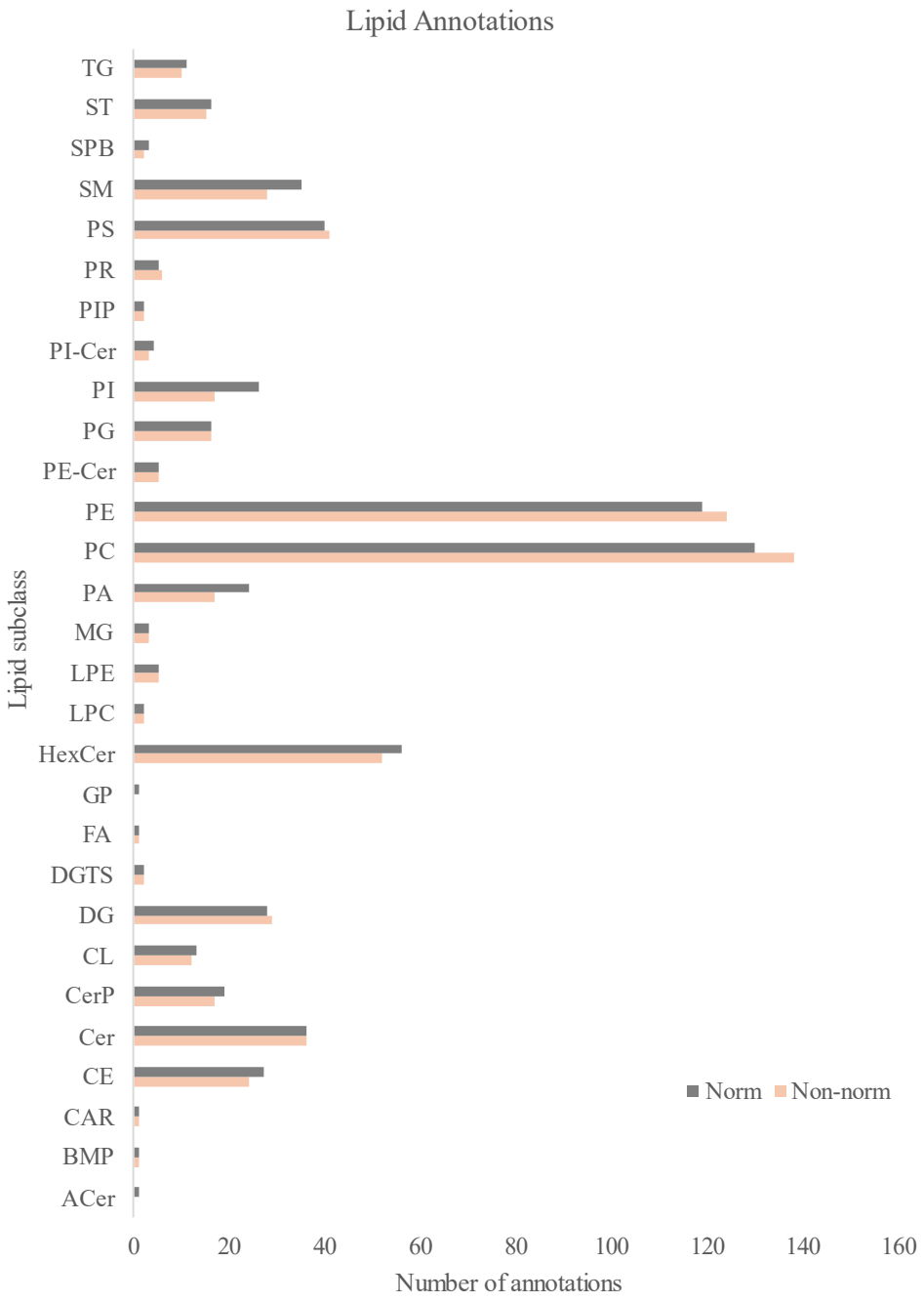

Figure 2.17. Comparison between the number of lipid annotations present in each subclass for MCF-7 and A549 cell lines in normalized and non-normalized conditions.

2.4. Conclusions

This study presents an adaptation of the SPV method, meant to address sample normalization to achieve a uniform concentration of total lipid content in biological samples for lipidomic analysis. Our findings show that our optimized method speeds up normalization, increases sensitivity, and decreases the LOD compared to prior optimizations. By applying this method to real-world samples, we confirmed that this protocol avoids introducing any bias into the analysis and eliminates biases caused by subtle differences within the samples.

Previous studies have also optimized this method for lipidomic workflow. However, this optimization is one of the few to have been employed in a pilot study and have multivariate and univariate statistical analysis performed. Additionally, this optimization allows for a broad concentration range (from 0.009 to 3 mM) without displaying any decrease in reaction efficiency, sensitivity, or reproducibility. To ensure the method's applicability, these studies were conducted and validated using different sample types to provide a comprehensive assessment, ranging from serum for validation and extending to saliva and cell samples for applications. The applications shown in this study corroborate the methods' capability of addressing normalization needs across a diverse range of sample types.

However, this method still presents limitations, one of which is its time-consuming nature. This limitation may restrict its application in some situations, requiring caution. Yet another limitation is that this method may not be suitable for very diluted samples, such as extracellular vesicles, single-cell, or spheroid samples. Although the limit of detection was significantly improved with our modifications, it is still not low enough to accurately quantify samples that are so diluted.

In conclusion, this work presents an optimized version of the Sulfo-phospho-vanillin method, offering an alternative path for sample normalization that uses lipids instead of proteins or metabolites for lipidomic studies. Using the SPV method helps reduce bias and improves the reliability of studies, showing its value in lipidomic studies.

III

Chapter III: Lipidomic Profiling of Human Saliva: Effects of Normalization Methods and Experimental Conditions

3.1. Introduction

Lipidomics is a field that focuses on the role of lipids within biological systems. Over the past two decades, its research importance has increased significantly due to its role in identifying and explaining complex pathways in different health conditions[5,166,167]. Lipidomics studies often use serum or plasma samples; however, saliva offers unique advantages due to its non-invasive and easy collection methods, making it interesting for diagnostic purposes[14,17,70,168].

Saliva is a biofluid that contains a wide range of biomolecules, including proteins, nucleic acids, metabolites, and lipids. It is also known to reflect local and systematic health conditions and is sometimes considered an ultrafiltrate of plasma, highlighting its value as a diagnostic tool. Furthermore, saliva collection can be particularly advantageous in some scenarios, such as longitudinal studies that require frequent sampling. Moreover, people with a fear of needles are more likely to participate in studies if saliva collection is used instead of blood, and children often find blood draws distressing, so using saliva as a sample makes participation more comfortable and less intimidating[17,161,168].

Lipid concentrations in biological fluids are susceptible to change due to a broad range of factors, such as diet, health conditions, biological sex, physical activity, and environmental factors. Ishikawa *et al.* (2014) reported differences in lipid composition found in human blood and that

these were related to the age and biological sex of participants. Moreover, studies by Mielgo-Ayuso *et al.* (2013) showed alterations in lipid compositions due to diet and physical activities. Therefore, although studies have also shown that saliva can be used as a diagnostic biofluid instead of blood, these concentration variations must be addressed for accurate lipid profiling[17,134–136,161,168,169].

When using saliva samples for diagnostic purposes or biomarker discovery, intrasample variations should be minimized, lowering the chance of interference or false positives. One alternative is sample normalization before LC-MS analysis, a common practice for lipidomics and metabolomics, given that different studies have reported significant changes across different samples within the same study[77,136,137]. However, significant discussion has arisen on which normalization method is more suited for lipidomics sample normalization. Studies have normalized sample concentration using various techniques, such as gravimetric normalization and equalizing sample amounts before lipid extraction. Moreover, studies also used protein, DNA, or metabolite concentration, assuming a linear relationship between these and lipids[139,170–172].

Furthermore, Bailey *et al.* (2022) and Wu & Li (2014) highlight the importance of choosing an adequate method for sample normalization[77,137]. One popular way to measure metabolite concentration is by using ninhydrin to detect amino acids. Briefly, the amino group of an amino acid reacts with ninhydrin to form an intermediate (Schiff base). This intermediate reacts with a second ninhydrin molecule, creating an intermediate compound (dihydroxy indene-dione). This compound undergoes rearrangement to form the final product (Ruhemann's purple). The intensity of this colour is directly proportional to the amount of amino acid present, with colours varying from pale yellow for low-concentrated samples to dark purple for high-concentrated samples[137,173,174].

However, some studies suggest that using metabolite or protein concentration methods to infer lipid concentration might lead to data misinterpretation. Phosphatidylcholine (PC) is one of the most abundant lipid subclasses in mammalian samples, a major component of the cell membranes. However, it does not have an amino group in its structure and, therefore, would not react with ninhydrin to form the purple-colored product. Similarly, Phosphatidylinositol (PI), Phosphatidylglycerol (PG), Cardiolipin (CL), Sterol lipids (ST), and Glycerolipids (MG, DG, and TG) are unlikely to undergo reaction with the ninhydrin unless they have structural modifications. Therefore, the ninhydrin reaction may present challenges in properly quantifying lipid content, as it cannot react with some of the most abundant lipid species[1,110,136,175–178].

Alternatively, a quantification method tailored for lipids would mitigate these issues and more accurately describe the lipid composition of the samples. The Sulfo-phospho-vanillin assay (SPV) has been previously used in lipidomic LC-MS studies and yielded lower data variations with higher reproducibility. As proposed by Chabrol & Charonnat (1937), in this assay, a double bond within the lipid backbone reacts with sulfuric acid (H_2SO_4), forming an intermediate that reacts with the phospho-vanillin reagent. The pink-colored compounds indicate the amount of lipid species present in the sample[77,149]. Studies have estimated that the mammalian lipidome comprises around 60% of lipid molecules with at least one double bond. Therefore, the SPV assay reacts with a significant amount of the lipid content of the sample[34,151,154].

The advantages and disadvantages of using total metabolite concentration (TMC) and total lipid concentrations (TLC) to profile saliva sample lipidomics were assessed herein. Furthermore, annotated lipid features were compared, and the effects of normalization before LC-MS analysis on lipid annotation in these samples were evaluated.

3.2. Experimental

3.2.1. Reagents and Equipment

Ascorbic acid (99%) was purchased from Alpha Aesar (Haverhill, Massachusetts, United States), Sodium acetate (Fisher, Waltham, Massachusetts, United States), Acetic acid, LC-MS grade acetonitrile (ACN), methanol (MeOH) and dichloromethane (DCM) were purchased from Honeywell (Charlotte, North Carolina, USA). Ammonium formate (mass spectrometry grade), ethanol (95% v/v, EtOH), LC-MS grade water (H_2O), and isopropanol (IPA) were purchased from Sigma-Aldrich (St. Louis, Missouri, USA). Ninhydrin and LipidRep Internal Standard Basic Mix for Serum/Plasma (NovaMT from Nova Medical Testing, Edmonton, AB, Canada). The composition of LipidRep is shown in Table 3.1.

Table 3.1. List of Lipid Standards present in the NovaMT LipidRep Internal Standard Basic Mix.

Lipid Species	Chemical Formula	Exact Mass	Concentration (mg/mL)
[D5]LPC 18:1	$C_{26}H_{47}D_5NO_7P$	526.37898	1.01
[D5]LPE 18:1	$C_{23}H_{41}D_5NO_7P$	484.33203	2.70
[D5]MG 18:1	$C_{21}H_{35}D_5O_4$	361.32350	3.25
[D3]FA 16:0	$C_{16}H_{29}D_3O_2$	259.25851	3.75
[D5]PI 16:0_18:1	$C_{43}H_{76}D_5O_{13}P$	841.57232	3.37
[D5]PG 16:0_18:1	$C_{40}H_{72}D_5O_{10}P$	753.55627	3.90
[D5]PS 16:0_18:1	$C_{40}H_{71}D_5NO_{10}P$	766.55152	3.15
[D3]ST 27:1;O (cholesterol-d3)	$C_{27}H_{43}D_3O$	389.37315	3.50
[D5]PA 16:0_18:1	$C_{37}H_{66}D_5O_8P$	679.51949	3.50
[D3]Cer 16:0/18:1	$C_{34}H_{64}D_3NO_3$	540.53038	1.95
[D5]PC 16:0_18:1	$C_{42}H_{77}D_5NO_8P$	764.60864	1.65
[D5]PE 16:0_18:1	$C_{39}H_{71}D_5NO_8P$	722.56169	4.00
[D5]DG 16:0_18:1	$C_{37}H_{65}D_5O_5$	599.55316	1.35
[D5]TG 16:0_18:1_16:0	$C_{53}H_{95}D_5O_6$	837.78283	3.75
[D3]CE 18:1	$C_{45}H_{75}D_3O_2$	653.61846	3.50

3.2.2. Study Design and Sample Collection

Saliva samples were collected from six healthy volunteers (three males: MA, MB, MC, and three females: FA, FB, FC) under three conditions: morning (no food or water), morning (after drinking two glasses of water), and evening (two hours after dinner). Morning (no food or water)

samples were collected immediately upon waking, before consuming food or water or brushing teeth. For the morning (after water) condition, participants drank two glasses of water upon waking before collection. Evening samples were collected two hours after dinner. Participants spat into sterile 50 mL polypropylene tubes, stored at -20 °C, and transported to the lab on ice.

Morning (no food or water) samples were diluted with 20% ethanol in 1:1, 1:2, 3:2, and undiluted (raw sample) ratios. Samples were aliquoted and stored at -80 °C for analysis. Two blank samples per condition ensured accuracy and reliability. The dilution with 20% ethanol mimicked commercial saliva collection kits, which stabilize and preserve samples by maintaining pH, preventing bacterial growth, and stabilizing proteins and enzymes. Since these kits are commercially available and well-known to clinicians and researchers, they would be a viable option for collecting saliva samples for future assays. This study aimed to assess how different dilution ratios affect analytical outcomes, providing insights into the impact of commercial kits on sample quality and analysis results[156,179,180].

3.2.3. Sample Preparation

All samples were extracted using a modified Folch liquid-liquid extraction (LLE) method. A 40-fold sample/solvent ratio (saliva/2:1 dichloromethane/methanol) was used for all saliva samples and blanks. A pre-prepared mixture of fifteen deuterated lipid standards in 7:3 (v/v) dichloromethane/methanol (NovaMT LipidRep) was added to each sample before extraction, with concentrations adjusted to match the expected lipid class distribution. The Folch solvent ratios (8:4:3 DCM/MeOH/H2O) were maintained, using dichloromethane instead of chloroform to reduce carcinogenic risk and cost. The original Folch sample/solvent ratio (1:20) was adapted to

1:40 for miniaturized extractions of small sample volumes. The sample (21 µL) and internal standards mixture were vortexed for 20 seconds after the addition of each solvent, starting with 278.7 µL MeOH, followed by 557 µL DCM, and finishing with a clean-up step with 187.9 µL water. The mixture equilibrated at room temperature (20-23 °C) for 10 minutes before centrifugation at 12,000 rpm and 4 °C for 10 minutes. An aliquot of the organic phase was evaporated to dryness under a gentle nitrogen flow at room temperature for 10 minutes. The dried residue was resuspended in a 42 µL of 4:1 MPA/MPB mixture before injection. Samples were stored in polypropylene inserts inside autosampler vials sealed with PTFE/silicone septa at 4 °C for a minimum of 4 hours (to ensure equilibrium) and a maximum of 24 hours (to minimize lipid degradation) before LC-MS analysis[72,103].

3.2.4. Total Metabolite Concentration (TMC) Determination

TMC was carried out using an adapted protocol by Wu & Li (2014). Before quantification, a protein precipitation step was performed: 5 µL of saliva samples were mixed with 25 µL of EtOH in sterile micropropylene tubes. After vortexing the mix, samples were incubated at -20 ºC freezer for 1 hour and then centrifuged at 12,000 rpm for 15 minutes.

After protein precipitation, a 20 µL aliquot of the supernatant was pipetted into a microplate, mixed with 120 µL of the reagent mix, prepared by combining a buffer solution of acetic acid and sodium acetate (pH = 5 and 0.04 M), ascorbic acid (3 mg/mL), and ninhydrin (30 mg/mL) in a 1:2:3 (v/v/v) ratio, and incubated at 90 ºC for 20 minutes. After incubation, samples were cooled in the -20 ºC freezer for 5 minutes before adding 40 µL of cold EtOH. Absorbance was measured at 570 nm using a microplate reader. A mixture of amino acid standards was used

as the external calibration standard, and an analytical curve was constructed by serial dilution of the standard mix solution[137,181].

3.2.5. Total Lipid Concentration (TLC) Determination

TLC was determined using a method previously optimized, described in Chapter II. Briefly, a 20 µL aliquot of lipid extract (organic layer) was dried under a gentle nitrogen stream before the addition of 50 µL of concentrated H_2SO_4, followed by incubation at 90 ºC for 20 minutes and cooling at -20 ºC for 10 minutes. Then, 50 µL of the phospho-vanillin reagent (PV reagent) was added, and the mixture was incubated at 60 ºC for another 20 minutes. After incubation, the absorbances of the samples were determined using a microplate reader at 540 nm. Oleic acid was used as the external calibration standard, and an analytical curve was constructed as previously described in Chapter II[77,149].

3.2.6. LC-MS Analysis

This study was subdivided into three phases. In Phase 1, lipidomic analysis was performed without normalization, using the same sample volumes and dilution factors. In Phase 2, before LC-MS analysis, samples were normalized by TMC, where different volumes of samples were dried and resuspended to the same TMC before extraction, ensuring normalized extraction efficiencies, ion suppression, and aggregation effects. Finally, in Phase 3, normalization by SPV was employed, with samples dried and resuspended to the same lipid concentration before extraction to maintain consistent extraction efficiencies, ion suppression, and aggregation effects.

Injection volumes of 3 and 12 µL were used for positive and negative ion modes, respectively. The same injection volumes were used for non-normalized saliva samples to establish a baseline for comparison. Lipid extracts were then analyzed by reversed-phase (RP) ultra-high-performance liquid chromatography (UHPLC) coupled to a high-resolution quadrupole-time-of-flight (QToF) mass spectrometer with an electrospray ionization (ESI) source. Chromatographic separation was carried out using a Dionex 3000 system and a Waters Acquity CSH Premier C18 column. The mobile phases consisted of MPA (10 mM ammonium formate in 50:40:10 ACN/MeOH/H_2O) and MPB (10 mM ammonium formate in 95:5 IPA/H_2O). A gradient separation of 16 minutes was employed (0 min, 15% MPB; 0.5 min, 15% MPB; 2.3 min, 25% MPB; 9.3 min, 42% MPB; 10.1 min, 78% MPB; 12 min, 90% MPB; 13 min, 98% MPB; 14.5 min, 98% MPB; 15 min, 15% MPB) with a flow rate of 0.300 mL/min from 0 to 9.3 minutes, then decreasing to 0.270 mL/min up to 10.1 minutes, and further reducing to 0.210 mL/min until the end of the run because of increased backpressures when using higher content of 2-propanol in the mobile phase mixture. A re-equilibration segment, with an increasing flow rate from 0.210 mL/min to 0.300 mL/min after 2 minutes, was employed at the end of the separation (0 min, 15% MPB), and the column temperature was maintained at 45 °C throughout[108].

MS/MS qualitative information was obtained for all sample injections using auto-MS/MS mode, with a cycle time of 1.2 seconds and active exclusion of precursors detected for more than three consecutive spectra within 0.50-minute intervals. Injection volumes were adjusted for each polarity and application based on ionization performance and experimental goals. Samples and blanks were prepared and injected randomly, but normalized and non-normalized samples were consistently injected on the same day. A pool of aliquots from all samples was used for quality control (QC) and injected with each batch of 10 samples to ensure consistent quality control[14,110].

3.2.7. Data Processing and Statistical Analysis

Data processing was conducted using LipidScreener, an in-house developed, Python-based software specifically designed for the untargeted lipidomics workflow used by The Metabolomics Innovation Centre (TMIC, Edmonton, Canada). This comprehensive tool includes functionalities for mass recalibration, retention time correction based on internal standards, MS/MS fragmentation patterns, peak picking, alignment, data cleansing, polarity merging, lipid annotation, and normalization. The dataset was recalibrated using a sodium formate segment (1 mM sodium formate solution infused into the mass spectrometer in between the separation gradient and the re-equilibration stage) with a 1 mDa m/z tolerance before data alignment. Peak picking was performed with a minimum intensity threshold of 3,000 counts and a minimum peak length of six spectra for both positive and negative ionization modes. Oligomers and multiple adducts were managed within a 20-ppm m/z tolerance. Aligned features were filtered for detection in at least 80% of injections within one group before merging the data from positive and negative ionization modes.

A three-tier putative annotation approach was used for lipid annotation based on the acquired tandem mass spectrometry (MS/MS) spectra and mass match, following protocols of the Lipidomics Standards Initiative; however, this study did not address the positions of double bonds or the stereospecific configuration of glycerol derivatives[103,182]. Annotated lipids were categorized into subclasses in one of the eight main categories according to standard lipidomics practices previously established by the International Lipid Classification and Nomenclature Committee (ILCNC), the Lipidomics Standards Initiative, and the LipidMaps database[27,36,118,178,182].

Lipid annotations were obtained by comparing MS/MS libraries, such as the MS-Dial LipidBlast library (https://fiehnlab.ucdavis.edu/projects/LipidBlast), the Human Metabolome

Database (https://hmdb.ca), and the MassBank of North America LC−MS/MS libraries (https://mona.fiehnlab.ucdavis.edu) with acquired MS/MS spectra. Annotations had at least a 40% similarity between experimental and library spectra, with a m/z tolerance of 5 mDa for precursor ions and 10 mDa for fragments. Annotated features underwent adducts, m/z error, carbon to double bond ratio, even or odd fatty acyl chains, structural modifications, plasmenyl presence, and expected ionization and detection efficiency for each lipid class filters to ensure accurate and reliable lipid annotation[14,36,183–187].

Variations during sample preparation and ion suppression effects were accounted for using a mixture of 15 deuterated internal lipid standards. Post-acquisition data normalization was performed by class-match by pairing annotated lipids with one of the internal standards from the same or the closest lipid subclass available. Normalized intensities were calculated by dividing the original peak intensity (peak height) of the annotated lipid by the peak intensity of the matched internal standard. The dataset was then normalized by the summed intensity ratios (total intensity) for all annotated features within each sample and auto-scaled before statistical analysis using MetaboAnalyst 6.0. Features with low experimental reproducibility (RSD > 30% for QCs) and unannotated features were excluded before statistical analysis.

Multivariate statistical analysis included Principal Component Analysis (PCA) and Partial Least Square-Discriminant Analysis (PLS-DA), which were validated through leave-one-out cross-validation and permutation tests (1000 permutations). R^2, Q^2, and p-values are provided in the figure captions. Volcano plot analysis was used for univariate statistical analysis.

3.3. Results and Discussions

3.3.1. Sample Normalization

For TMC, samples were subdivided into two batches of 25 and 24 samples. Figure 3.1.a shows the calculated metabolite concentrations for samples and blanks. In contrast, calibration curves for each batch are shown in Figure B.1. The calculated RSD (%) between the method blanks of the two batches was 10.1%, indicating good reproducibility. Supp. Table 10 lists the individual calculated concentrations (in mM) and the amounts aliquoted for each sample to ensure the same molar amount of lipids. Each aliquot was dried and resuspended to 21 µL before lipid extraction, resulting in the same total lipid concentration within each injected sample.

On the other hand, samples were divided into three batches containing 15, 15, and 19 samples for TLC determination, and their calculated lipid concentration for each sample and blank is shown in Figure 3.1.b. The calibration curves for each batch are shown in Figure B.2. Supp. Table 11 lists the individual calculated concentrations (in mM) and the amounts aliquoted for each sample, which was dried and resuspended to 21 µL before lipid extraction.

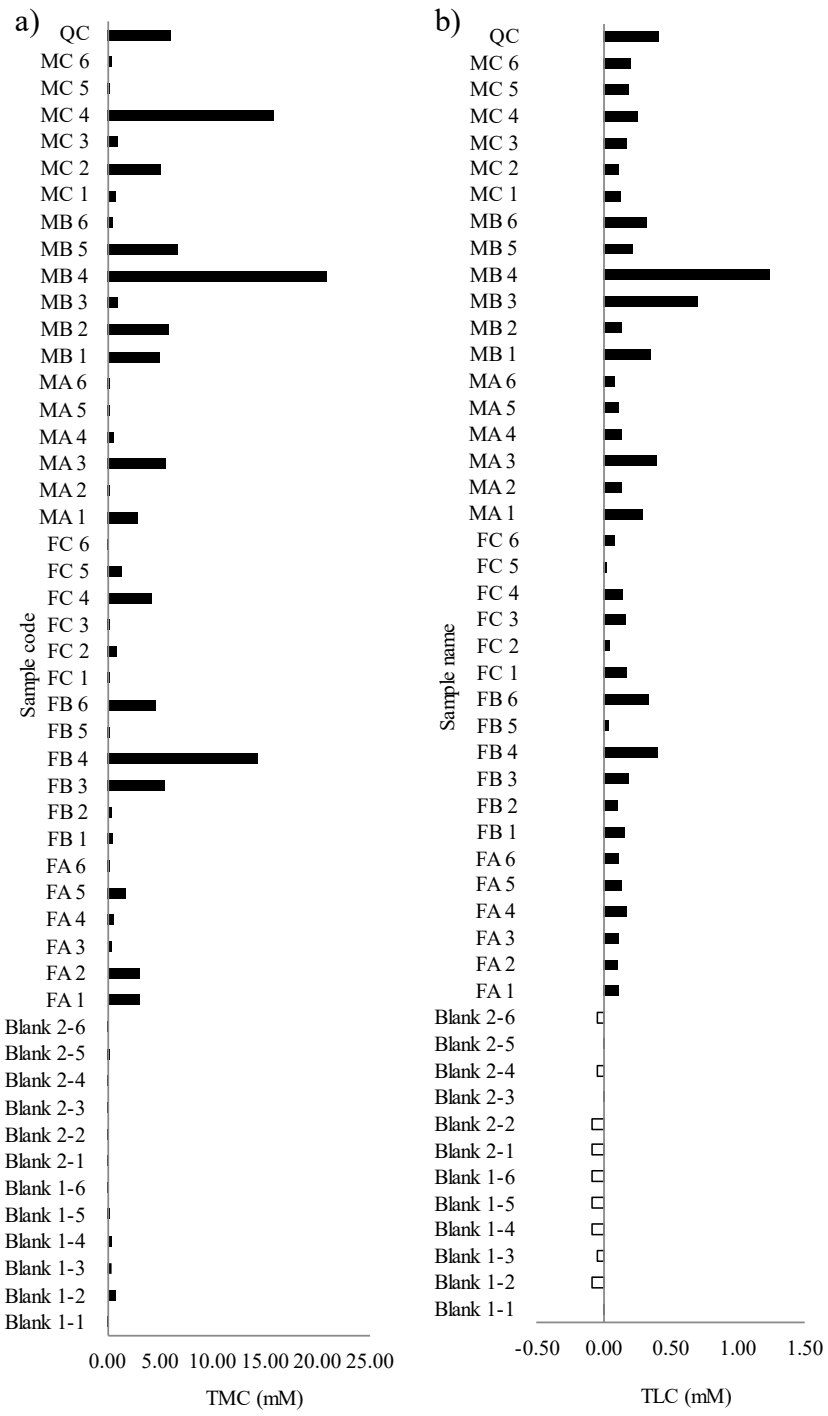

Figure 3.1. Calculated metabolite and lipid concentrations (mM) for saliva, QC, and blank samples. a) Metabolite concentration was determined using the TMC method; b) Lipid concentration was determined using the TLC method.

Figure 3.1 shows the importance of normalizing sample concentration before LC-MS analysis, as concentrations vary significantly among samples. In blank samples, metabolite and lipid concentrations varied significantly and were sometimes higher than in actual samples, resulting in an elevated relative standard deviation (RSD) of 98% and 67%, respectively. This high RSD in blank samples can be due to several factors that impact measurement variability. Blanks serve as controls to provide a baseline for the method's performance without the target analytes. However, residual contaminants, reagents, or background noise from the analytical process can introduce variability. Additionally, the low metabolite concentration in blanks often yields results close to the method's detection limit, making them more prone to fluctuations and measurement errors. Most blank samples yielded negative or near-zero lipid concentrations, likely because the detectable lipids were below the detection limit[77,137].

The literature debates which method is more suitable for sample normalization before LC-MS analysis. Studies have used protein, DNA, and metabolite concentrations to normalize lipid extracts. However, the correlation between those and lipids is unknown and may vary among different sample matrices[170,171,188]. When choosing which method to use for analyte quantification, several factors must be taken into account, such as limit of detection, sensitivity, specificity, sample preparation requirements, reproducibility, precision, and throughput[189,190].

With that in mind, our first comparison regarded each method's detection limit. From the calibration curves generated in our experiments, we calculated that the LOD for the TMC method was 0.05 mM, whereas for the TLC method, it was 0.12 mM. This indicates that TMC is a superior method in terms of sensitivity since its LOD is 2.4-fold lower than the one for TLC. However, extremely low LOD is not often necessary. Therefore, the TLC method could be used in most

situations. Both methods were shown to be reproducible, as multiple batch analyses were performed, and all of them had similar results and low RSDs for the method blanks, 4.3% and 10% for TLC and TMC, respectively, indicating a slightly higher reproducibility to TLC method since its RSD is 2.3-fold lower than for TMC.

Regarding sample preparation requirements, the TMC only needs a protein precipitation step before sample analysis. In contrast, TLC samples need to undergo LLE to extract lipids before quantification. That means that for TLC, in this proposed workflow, we would need two extractions, one for quantification and another for LC-MS analysis after sample normalization. In contrast, for TMC, we would only need to perform one extraction after sample normalization. Nevertheless, low throughput workflows should not significantly impact performance, as parallel LLE is possible, and four or five batches can be extracted in a day. However, when considering high throughput workflows, this would decrease efficiency.

When evaluating specificity and selectivity, TMC is based on the reaction of ninhydrin with amino acids. It can react with other compounds that have an amino group present, including lipids. Considering the sample preparation before sample normalization by TMC, it is possible other compounds would react with the ninhydrin and thus generate an increased signal [174]. On the other hand, the TLC method is based on the reaction between the phospho-vanillin reagent and a double bond within the analyte. Since it is performed after an LLE, the labeling is more specific to hydrophobic compounds, including lipids. It excludes most metabolites, proteins, and other potential interferents, making this approach more specific[151].

As outlined herein, each of these methods presents advantages and disadvantages; therefore, another factor to evaluate is how well they correlate. Ideally, using a lipid-specific

quantification method would be best. However, in a scenario where another method has similar performance and is less time-consuming or allows for high throughput if the correlation between the quantification results between both methods is high, this other method might be a suitable alternative[77,137,138]. Figure 3.2 displays the relationship between the quantification results for TLC and TMC.

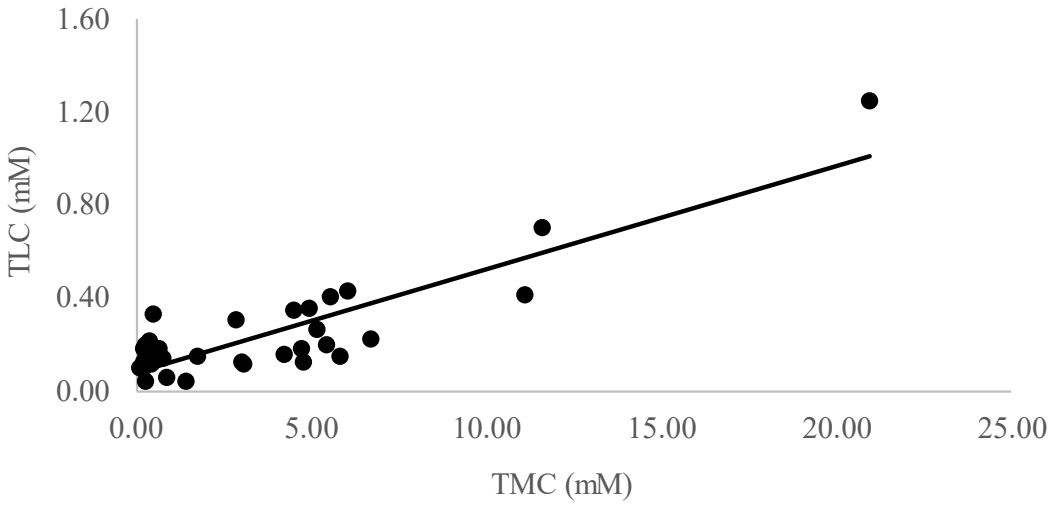

Figure 3.2. Relationship between metabolite concentration and lipid concentration in saliva samples ($R^2 = 0.7620$).

The linear regression in Figure 3.2 demonstrates a significant direct correlation between these two measurement methods in these saliva samples. An R^2 value of 0.7620 indicates that the TMC measurements can explain approximately 76.20% of the TLC variance. This correlation implies that TMC can reliably predict TLC results, supporting the potential use of TLC as an alternative method for lipid quantification, at least in saliva samples. This linear correlation

indicates that TMC can be used alternatively when TLC is considered too time-consuming or impractical, especially when high-throughput quantification may be necessary [191].

3.3.2. Lipidomics profile of saliva samples generated by UHPLC-QToF-MS

Fourteen internal standards were detected in positive and negative ionization, with absolute values for m/z error inferior to 2.3 ppm (Figure B.3). The only standard not detected in the positive ionization mode was [D5]FA 16:0, while cholesterol was not detected in the negative ionization mode due to poor ionization. Because of their structural and chemical properties, FA and cholesterol were not expected to be detected in the respective polarities.

The LC-MS analysis of saliva samples resulted in 9,055 detected features, including 4,594 detected in positive ionization and 4,461 in negative ionization. Lipid annotation yielded 2,829 annotations, including 1,162 in Tier 1 (MSMS score ≥ 500), 170 in Tier 2 (100 ≤ MSMS score < 500), and 1,497 in Tier 3 (mass matched annotations), all with m/z error up to 6 ppm (Supp. Table 12). The most abundant lipid category was Sphingolipids, with 34.3% of annotated species (968 lipids) belonging to this category, followed by Glycerophospholipids with 30.1% of annotation (852 lipid species) and Glycerolipids with 24.1% of annotations (682 lipids, Figure B.4). Figure 3.3 illustrated the lipid annotation distribution among the different lipid subclasses and annotation tiers.

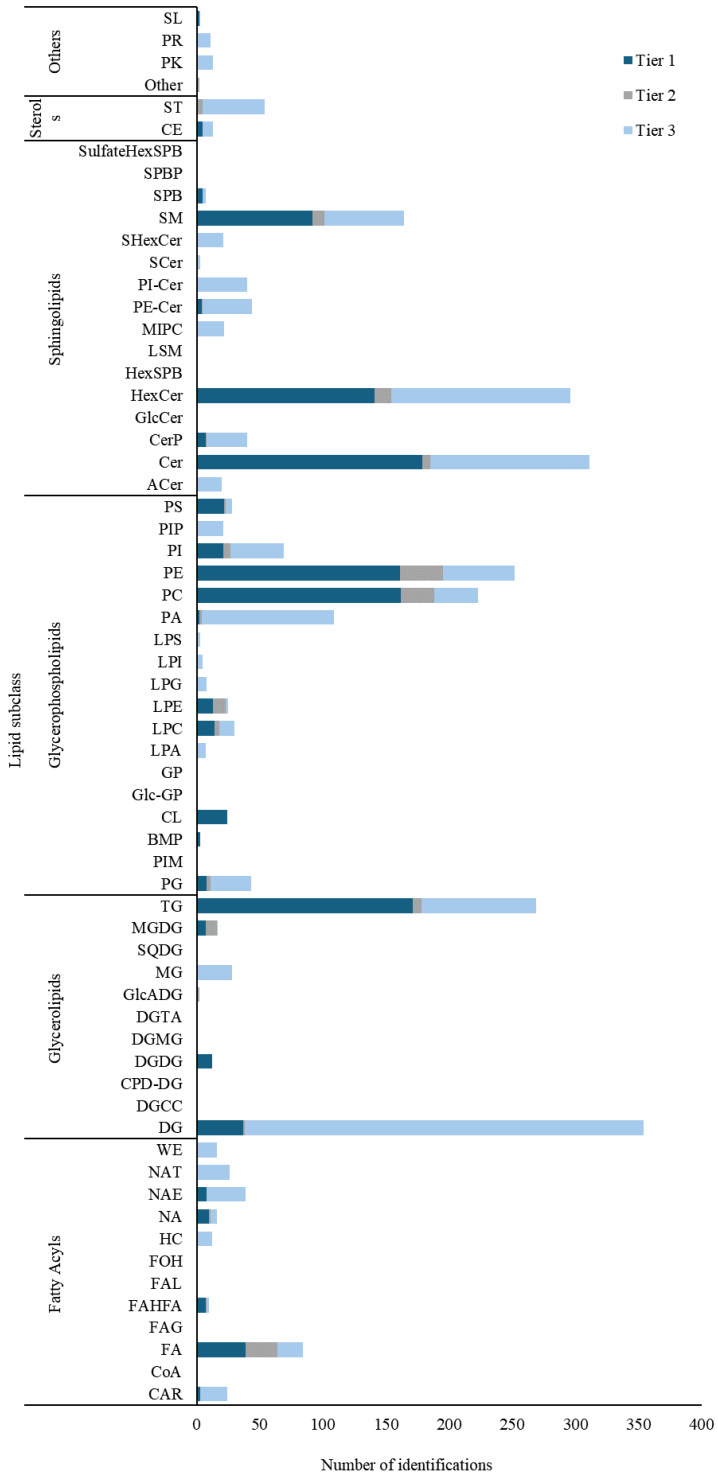

Figure 3.3. Distribution of lipid annotations across lipid subclasses and annotation tiers. Tier 1 annotations were MS/MS matches with scores higher than 500, Tier 2 were MS/MS matches with scores between 100 and 500, and Tier 3 were mass match annotations.

Saliva can be considered an ultrafiltrate of plasma samples. However, we observed some differences in their lipid composition. In plasma, the most abundant lipid species are often TGs, CEs, PCs, and PEs, whereas, in saliva, we observed DG, Cer, HexCer, TG, PE, and PC as the most abundant. One of the possible reasons for the observed difference in lipid distribution is that saliva's lipid composition is known to reflect the health of the oral cavity. In situations where the conditions in the oral cavity have suffered any alterations (hygiene, disease-related, or gut microbiome), the lipidome will reflect those[17,168,177,192,193].

The peak intensities (*i.e.*, peak heights) of annotated lipids were normalized using the most similar internal standards (peak intensity of the annotated lipid/peak intensity of the most similar internal standards). Those annotations that belonged to a subclass we did not have standards for were normalized by matching to the most similar lipid class, considering molecular structure, properties, and chromatographic retention times. Normalized features were filtered by RSD < 30% to remove non-reproducible lipids. The remaining features were auto-scaled and normalized by sum (*i.e.*, total peak intensities for all annotated lipids) before statistical analysis. The PCA score plot (Figure 3.3 Figure 3.4.a) shows tightly clustered QC injections, indicating the reproducibility and suitability of the methods used. In the PCA plot without the QC replicates (Figure 3.4.b), we see samples normalized by TLC slightly more clustered than Controls and TMC samples. The PLS-DA score plot (Figure 3.4.c) suggests separating the normalized (TMC and TLC) samples from the control group, indicating that sample normalization before LC-MS analysis may lead to different biochemical states.

Unfortunately, the limited number of samples and the complexity of the dataset resulted in an overfitted PLS-DA model, as indicated by the low Q^2 value. The model passed a permutation

test and showed good linearity (R^2 of 0.8167) but poor predictive ability (Q^2 of 0.5634). This work does not intend to employ PLS-DA models to predict sample groups but to evaluate each normalization method's applicability. Hence, the model is appropriate for the intended purpose. Still, expanding the number of samples when building PLS-DA models for predictive purposes based on highly complex datasets is recommended to prevent overfitting. However, the results indicate that large-scale studies of the effect of normalization on samples before LC-MS are reasonable.

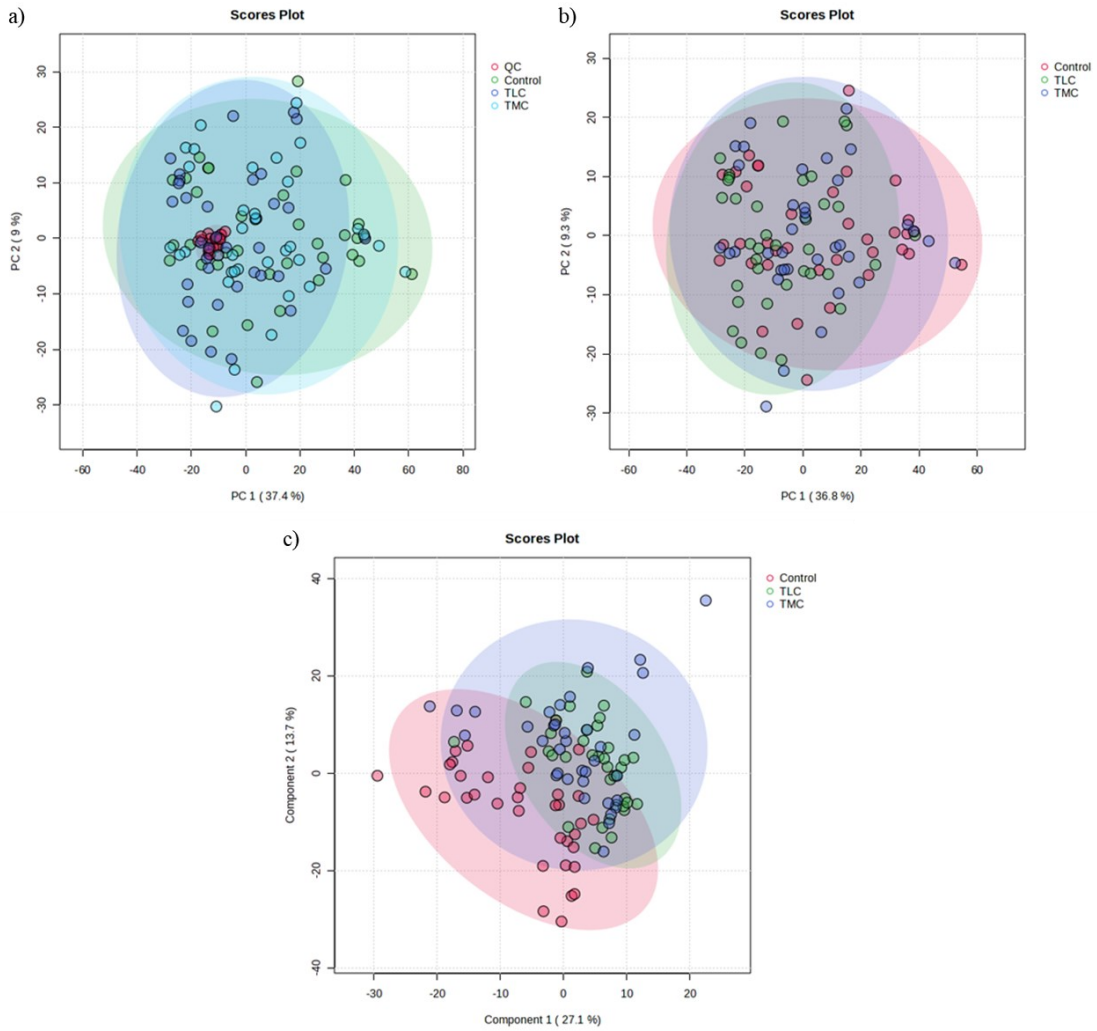

Figure 3.4. Statistical analysis for lipidome of saliva samples using different normalization methods before lipid extraction (control – samples which were not normalized; TMC – samples normalized by total metabolite concentration; TLC – samples normalized by total lipid concentration). a) PCA score plot with 24 QC replicates (pooled from individual saliva samples); b) PCA score plot without QCs; c) PLS-DA score plot with 5 components (R^2: 0.8167; Q^2: 0.5634; p 0.001).

The small number of biological replicates (N=1) may decrease the reliability of the statistical models applied herein to find significantly altered lipids that may relate to sample normalization before LC-MS analysis. However, the project was a pilot study to ensure adequate

sample handling and analysis for future research. Hence, we performed univariate statistics using Volcano plots (Figure B.5). Comparisons were made by analyzing Controls and TLC-normalized samples (Figure B.5.a), Controls with TMC-normalized samples (Figure B.5.b), and lastly, TMC-normalized and TLC-normalized samples (Figure B.5.c), and the number of significantly altered species is shown in Figure 3.*5*. When comparing Control and TLC-normalized samples, 304 features (27%, Supp. Table 13) were significantly altered, with PE contributing 51% of the altered species, with most being unsaturated PEs. Furthermore, 74% of significantly altered features were high-confidence annotations as they were Tier 1 or Tier 2 annotations. The most significant fold changes observed were PE 18:0_20:3 (Tier 1, FC 3.9404 and $p < 0.05$) and DG 43:8 (Tier 3, FC 3.9841 and p 0.005).

Second, we compared Control and TMC-normalized samples, which resulted in 39 altered lipid annotations, or 3% of all annotations (Supp. Table 14). Of those, 74% were Tier 1 or Tier 2 annotations, and FA was the lipid subclass with more altered lipids (11 or 28%), which were Tier 1 or Tier 2 annotations. PE was the subclass with the second-highest number of altered lipids (13%), and its annotations were 40% in Tier 1 and 60% in Tier 3. The highest fold change was observed for DGDG 16:0_17:1 (Tier 1, FC 1.9231 and p 0.03718).

Last, we compared the lipidome of TMC-normalized and TLC-normalized samples, which yielded 197 significantly altered lipids (18%, Supp. Table 15), and among those, 69% were Tier 1 and Tier 2 annotation. Similar to what was noted when comparing Control and TLC-normalized samples, 63% were PE lipids, annotated mostly in Tiers 1 and 2. PE 14:0_16:1 showed the highest fold change (Tier 1, FC 2.5685, and p 0.00022).

Only one lipid, PE 54:3, was affected in all three comparisons. In addition, another 27 lipid species were simultaneously altered in Control/TLC-normalized samples and Control/TMC-normalized samples (PE 50:1, CerP 43:5;O2, PI 36:2, FA 17:0, FA 17:0, CerP 19:0;O2/2:0, FA 22:1, FA 19:1, FA 24:2, CE 33:6;O2, PC 22:0_22:0, NAGlySer 15:0/16:0, NAGlySer 15:0/17:0, PE O-52:4, FA 20:4;O, MG 18:1, ACer 42:6;O3, LPE O-18:2, HexCer 18:1;O2/38:9, FA 18:2;O, LPC 20:4, SPB 32:3;O5;S, LPC O-16:0, LPC 18:2, PE 18:0_20:3, PE 16:0_20:3, and DGDG 16:0_17:1). Furthermore, another 28 lipid species were simultaneously altered in Control/TLC-normalized samples and TMC-normalized/TMC-normalized samples (PIP2 35:5;O, FA 20:4, TG 59:7;O2, HexCer 41:2;O4, FA 20:3, TG 49:0;O3, GlcADG 19:0_18:1, HexCer 18:0;O2/18:1, TG 50:5;O2, TG 55:3;O2, HexCer 20:1;O2/34:4, TG 64:10, Cer 17:0;O3/36:2, SM 46:0;O4, PE 54:1, PE 54:2, PE 26:1_26:2, SM 45:5;O6, TG 59:8;O2, PE 42:0;O, Cer 18:0;O2/32:2;O, Cer 20:0;O3/32:1, HexCer 37:1;O4, TG 55:6;O2, LPC 34:3, HexCer 43:3;O5, and PC O-18:0_26:4).

Moreover, in Figure 3.5 PE is the most altered species when comparing Control vs. TLC and TMC vs. TLC. Alterations in PE levels may indicate changes in cellular processes, potentially driven by physiological changes in the oral cavity, inflammation, or overall health of the participants. These findings suggest that PE lipids are sensitive to experimental conditions or the normalization methods employed in this study. Additionally, since PEs contain a free amine group that can react with ninhydrin, their increased reactivity might contribute to the observed alterations.

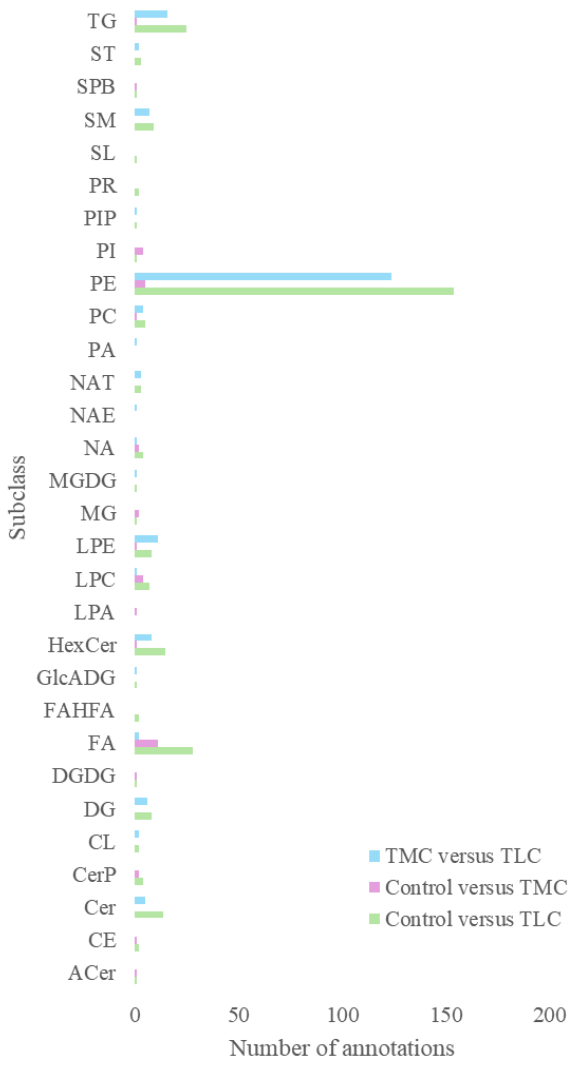

Figure 3.5. Number of annotations that were significantly different ($p < 0.05$ and $FC < 0.67$ or > 1.5) in the Volcano Plot analysis for TMC versus TLC (blue), Control versus TMC (pink), and Control versus TLC (green).

3.3.3. Implications and Considerations for Choosing a Normalization Method for Lipidomic Profiling of Saliva

In this study, we performed a comprehensive lipidomic analysis of human saliva samples collected under different conditions. The results show the importance of sample normalization and

how normalization methods can impact lipidomic data. Understanding the biological implications of our findings is essential, not just for guiding future studies but for making lipid annotation more reliable and improving knowledge of the lipid roles in physiological and pathological processes[77,110,120,184].

Previous studies have demonstrated the importance of sample normalization in lipidomic analyses. For example, Bailey *et al.* (2022) reported that normalization by TLC improves the reproducibility of lipidomic data. Similarly, our results indicate that TLC normalization provides higher reproducibility than TMC normalization in saliva samples. However, our study highlights significant variations in lipid profiles depending on the normalization method used. These differences could be attributed to saliva's unique composition and complexity as a biological fluid[77].

LC-MS analysis often requires sample normalization before injection to ensure accurate and reproducible quantification. In this study, we compared two different methods for sample normalization: TMC and TLC). Each method offers advantages and disadvantages to our workflow and has the potential to influence the interpretation and reliability of the data.

The TMC method has a higher sensitivity, emphasized by a lower LOD when compared to TLC. This increased sensitivity can be beneficial when working with samples containing low concentrations of metabolites, such as saliva, which also displays a low concentration of lipids[8,121,168]. Additionally, TMC involves a simpler sample preparation process, requiring only a protein precipitation step before derivatization and analysis. It fits almost effortlessly in our workflow and is more suited for high-throughput studies. Furthermore, in studies regarding both metabolomics and lipidomics, TMC has shown a high correlation with total lipid content. Thus, it

can be used to normalize samples for both analyses. However, using TMC to normalize lipid samples can also lead to specificity issues, as the method is based on the reaction of ninhydrin with compounds containing amino groups. Some common lipid subclasses are not expected to have an amino group in their structure (*e.g.*, PC, FA, MG, TG, DG, and ST) and, therefore, would not react with ninhydrin. PC is often the most abundant lipid subclass in mammalian samples; thus, using a method that would not account for the content of PC in the samples can generate bias[17,36,77,136,137,168,175,192,194].

On the other hand, although TLC can be more time-consuming since it requires a longer sample preparation workflow, using a method targeted to lipid quantification can increase specificity and reduce interferences. The phospho-vanillin reagent used in TLC reacts with double bonds, which, although they can be present in any molecule, are known to be present in most lipid structures. However, since lipid quantification is performed after LLE, the likelihood of interference from metabolites or other molecules is lower. Furthermore, the TLC method shows higher reproducibility, with lower relative standard deviations (RSDs), which is essential to ensure consistency[13,33,34,153,195].

Furthermore, data interpretation and statistical analysis show that the implications of choosing a normalization method go beyond just which one is more reproducible or sensitive. PCA and PLS-DA analyses show that both methods behave similarly. However, when analyzing the volcano plots, we see a higher number of features being significantly different from controls when samples are normalized by TLC. In contrast, the opposite is seen when samples are normalized by TMC.

Although this might indicate that TMC is more suitable for LC-MS lipidomics sample normalization, another possibility exists. Because TMC lacks specificity and fails to account for some of the most abundant lipid classes, bias in the analyses is created, which can mask the significance of some features. Therefore, when comparing TMC and control samples using the Volcano plot analysis, a very small number of features are shown to have a significant difference.

In summary, comparing TMC and TLC normalization methods highlights the importance of carefully selecting the appropriate normalization strategy based on the study's goals and the specific characteristics of the sample matrix and analytes of interest. While TMC offers greater sensitivity and simplicity, it may introduce bias by failing to capture significant alterations in lipid subclasses that lack amino groups. This limitation could mask biologically relevant differences, as reflected in the smaller number of significantly altered features. On the other hand, despite being more time-consuming, TLC provides higher specificity and reproducibility by directly targeting lipid quantification. The increased number of significantly altered features in TLC-normalized samples suggests it may be a more reliable choice for detailed lipidomic studies.

3.4. Conclusions

TMC and TLC normalization methods displayed both advantages and disadvantages for lipidomics sample normalization. Therefore, the choice of which method to use depends on the specific goals of the study. TLC is preferred for detailed, lipid-focused studies due to its specificity and reliability. However, despite its lower specificity, TMC can be valuable for larger metabolic profiling studies.

Furthermore, the choice of normalization method can have implications for the accuracy and reliability of lipidomic data. Precise lipid quantification is essential for developing diagnostic tests and biomarker discovery in clinical settings. Our study suggests that TLC normalization is more suitable for detailed lipid-focused studies due to its specificity and lower variability. Our findings suggest the potential of salivary lipidomics as a diagnostic tool and provide grounds for future large-scale studies to explore lipid biomarkers for various health conditions and how sample normalization affects these results.

However, the small sample size used in this study and the fact that only two normalization methods were evaluated may limit the correlation of our findings with those from large-scale works. Additionally, the heterogeneity of saliva samples and potential biases introduced during sample collection and storage could also influence the results. To address these limitations, future studies should aim to include a larger and more diverse cohort of participants to validate the results. Additional studies involving other biological fluids, such as blood or urine, would also aid in determining whether the effects observed herein are specific to saliva.

IV

Chapter IV: Enhancing untargeted lipidomics through offline 2DLC: method development and evaluation of data processing tools.

4.1. Introduction

Lipidomics is a rapidly growing research area characterized by analyzing lipid species in biological samples and their relationship to physiological or pathological processes[77,108]. Given the importance of lipids in structural composition, cell signaling, energy storage, health and environmental changes can cause significant alterations in the lipidome. Therefore, the study of these hydrophobic biomolecules can help in biomarker discovery, the elucidation of biochemical pathways, and the characterization of organisms and cell lines, amongst other applications[17,77,108]. Still, comprehensive lipid analysis remains a field that needs research due to challenges in lipid separation, annotation, and data processing routines.

The Lipid Maps Structure Database (https://www.lipidmaps.org/) includes over 48,000 unique lipid structures, subdivided into eight categories: Fatty acyls (FA), Glycerolipids (GL), Glycerophospholipids (GP), Sphingolipids (SP), Sterol lipids (ST), Prenol lipids (PR), Saccharolipids (SL) and Polyketides (PK)[36,178]. Considering the diversity of lipid structures, defined mainly by different headgroups (*i.e.*, phosphocholines, glycerol, and phosphoethanolamines) and fatty acyl compositions, untargeted lipidomic analysis requires precise analytical methods capable of annotating and quantifying a wide array of species. Reversed-phase liquid chromatography (RPLC) is often used in untargeted lipidomics approaches to separate lipids according to their hydrophobicity. However, it suffers from drawbacks such as ion suppression and

coelutions since many species can have similar overall molecule polarities, affecting sensitivity, quantification performance, and annotation accuracies[83,110,196]. Alternatively, Hydrophilic Interaction Liquid Chromatography (HILIC) separates lipids based on their head group polarity. Furthermore, it offers enhanced retention for analytes poorly retained in RPLC, such as lysophospholipids (LGPs), emerging as an orthogonal method to complement RPLC[78,196,197]. Hence, combining HILIC and RPLC into a two-dimensional liquid chromatographic method (2DLC) could help improve lipid class separation and reduce ion suppression and coelutions, further improving untargeted lipidomics studies[63,198].

Although 2DLC can significantly enhance lipid class separation and address common analytical challenges, selecting and evaluating processing software tools becomes crucial. LC-MS data's peak picking, and alignment algorithms are vital for reliable quantifications or relative comparisons[199,200]. The annotation of lipid species typically depends on tandem mass spectrometry (MS/MS), which provides information on headgroups and fatty acyl chains. The obtained spectra are compared to in silico databases through various algorithms, (*e.g.*, dot-product or cosine similarity scores), and the accuracy of annotations is impacted by factors such as low spectral resolution, alterations of fragmentation patterns for different instruments, lack of standards, and low-quality library data[75,201,202]. Considering the importance of data analysis for lipidomics, it is vital to choose appropriately which platform to use[11,178,201].

One of the most common 2DLC challenges, specifically online versions, is sample dilution in the first dimension. This makes analysis more challenging since analytes are now present in a lower concentration (m/v), making them harder to detected[78,203]. Furthermore, offline methodologies offer more possibilities for mobile phase resuspension solvents and ratios, reducing

possible problems from incompatibility between solvents and initial conditions from both dimensions. Considering the challenges mentioned above in separating and annotating lipids, we describe the development of an offline two-dimensional liquid chromatography-mass spectrometry (2DLC-MS) method, combining HILIC with reverse-phase liquid chromatography (RPLC-MS) to improve lipidomics data acquisition. However, even when 2DLC methods are used, some challenges regarding data processing will still be present, such as peak picking, alignment, and MS/MS matching routines. With that in mind, we compared different data processing tools for lipidomic analysis to decide which software performs best for our approach.

4.2. Experimental

4.2.1. Reagents and Equipment

LC-MS grade acetonitrile (ACN), methanol (MeOH), and dichloromethane (DCM) were sourced from Honeywell (Charlotte, North Carolina, USA). Ammonium formate (mass spectrometry grade) and LC-MS grade water (H_2O) and isopropanol (IPA) were obtained from Sigma-Aldrich (St. Louis, Missouri, USA). A mixture of 15 deuterated lipids was used for internal standardization, including standards for different subclasses (NovaMT LipidRep Internal Standard Basic Mixes for Tissue/Cells and Serum/Plasma, Nova Medical Testing, Edmonton, AB, Canada). Supp. Table 16 lists all standards used for method validation.

Table 4.1 List of Lipid Standards present in NovaMT LipidRep Internal Standard Basic Mix.

Lipid species	Chemical formula	Exact mass
[D5]LPC 18:1	$C_{26}H_{47}D_5NO_7P$	526.37898
[D5]LPE 18:1	$C_{23}H_{41}D_5NO_7P$	484.33203
[D5]MG 18:1	$C_{21}H_{35}D_5O_4$	361.32350
[D3]FA 16:0	$C_{16}H_{29}D_3O_2$	259.25851
[D5]PI 16:0_18:1	$C_{43}H_{76}D_5O_{13}P$	841.57232
[D5]PG 16:0_18:1	$C_{40}H_{72}D_5O_{10}P$	753.55627
[D5]PS 16:0_18:1	$C_{40}H_{71}D_5NO_{10}P$	766.55152
[D3]ST 27:1;O (cholesterol-d3)	$C_{27}H_{43}D_3O$	389.37315
[D5]PA 16:0_18:1	$C_{37}H_{66}D_5O_8P$	679.51949
[D3]Cer 16:0/18:1	$C_{34}H_{64}D_3NO_3$	540.53038
[D5]PC 16:0_18:1	$C_{42}H_{77}D_5NO_8P$	764.60864
[D5]PE 16:0_18:1	$C_{39}H_{71}D_5NO_8P$	722.56169
[D5]DG 16:0_18:1	$C_{37}H_{65}D_5O_5$	599.55316
[D5]TG 16:0_18:1_16:0	$C_{53}H_{95}D_5O_6$	837.78283
[D3]CE 18:1	$C_{45}H_{75}D_3O_2$	653.61846

4.2.2. Sample Preparation

The analyses were performed with chicken liver tissue, human serum, and MCF-7 cells (human breast cancer). Chicken liver was purchased from the local supermarket, subdivided into small aliquots, and stored in 2 mL sterile polypropylene tubes in the -20 ºC freezer until analysis.

Tissue sample homogenization was performed using the Bioprep-24 Homogenizer (Bio-Equip) and ceramic beads. Human serum samples were purchased from Sigma-Aldrich (St. Louis, Missouri, USA), aliquoted and freeze-dried. Aliquots were then stored in the -20 ºC freezer until resuspension in 1 mL of LC-MS grade water and analysis. MCF-7 (ATCC HTB-22) cells were cultured individually in T-75 flasks under optimum conditions using Dulbecco's Modified Eagle Medium (DMEM), supplemented with 10% fetal bovine serum (FBS). Cultures were incubated at 37 ºC in a humidified 5% CO_2 atmosphere and renewed every two to three days. When 80% confluency was reached, cell samples were harvested by trypsinization. Briefly, after washing the cells with phosphate buffer saline (PBS), 3.0 mL of 0.25% trypsin/EDTA (Hyclone, Logan, Utah) was added, and samples were incubated at 37 ºC for 5 minutes. Quenching was performed by adding 8 mL of growth medium. Samples were transferred into 15 mL sterile polypropylene tubes and centrifuged for 7 minutes at 900 rpm before the supernatant was gently aspirated to separate it from the cell pellet.

All samples were extracted using a modified Folch liquid-liquid extraction (LLE) method[72,103]. To this end, a 40-sample/solvent ratio (µL/mL) was used for serum samples, whereas a 200-sample/solvent ratio (mg/mL) was used for tissue and cell samples; extraction volumes and masses can be found in Supp. Table 17 A mixture of 15 deuterated lipid standards (NovaMT LipidRep) was added to each sample before extraction, and the standard concentrations were adapted to match the expected lipid class distribution in each sample type. The classical Folch solvent ratios (8:4:3 DCM/MeOH/H_2O) were maintained for all extractions, although DCM replaced chloroform due to lower carcinogenic risk and costs. The mixture of sample and internal standards was sequentially vortexed for 20 second intervals with each solvent, starting with MeOH, followed by DCM, and finalizing with a clean-up step with water. The mixture was then

equilibrated at room temperature (20-23ºC) for 10 minutes before centrifugation at 12,000 rpm and 4 ºC for 10 minutes. An aliquot of the organic phase was evaporated to dryness under a gentle nitrogen flow and at room temperature for 10 minutes. The dried residue was resuspended in 30:15:4:1 ACN/IPA/MeOH/H_2O before injection.

To prevent sample degradation, samples were stored in polypropylene inserts placed inside autosampler vials sealed with PTFE/silicone septa at 4 ºC for a minimum of 4 hours (equilibration period) and a maximum of 24 hours (to prevent lipid degradation) before the LC-MS analysis.

4.2.3. Hydrophilic Interaction Liquid Chromatography (HILIC) Method Optimization

A previously published HILIC-MS method employed for the comprehensive annotation of lipids species was used as the foundation for this study. The original method described by Xu *et al.* (2020) employed a 25-minute gradient slope at a 0.2 mL/min flow rate with MPA - 10mM ammonium formate and 0.1% formic acid in 50:50 ACN/H_2O and MPB - 10mM ammonium formate and 0.1% formic acid in 95:5 ACN/H_2O. The lipid extract was resuspended in 5:4:1 IPA/ACN/H_2O before injection[83]. After obtaining preliminary results using this method, modifications were proposed to make it more suitable for this application, including resuspension solvents, mobile phase compositions, and gradient slopes. The optimized HILIC-MS methodology employed mobile phases composed of MPA - 10 mM ammonium formate in 60:40 ACN/H_2O (v/v) and MPB - 10 mM ammonium formate in 95:3:2 ACN/MeOH/H_2O (v/v/v). Additionally, a 26-minute gradient separation was employed (0 min 100% MPB; 0-2 min 100% MPB; 2-4 min 98% MPB; 4-4.5 min 98% MPB; 4.5-6 min 96% MPB; 6-8.5 min 93% MPB; 8.5-9.5 min 93% MPB; 9.5-12 min 91% MPB; 12-17 min 86% MPB; 17–25min 80% MPB; 25-26 min 20% MPB),

followed by 4 min re-equilibration (0 min, 20% MPB; 0.5 min, 100 % MPB; 6 min, 100% MPB) at a 0.250 mL/min flow rate and column temperature of 45 °C. Dried lipid extracts were resuspended in 30:15:4:1 ACN/IPA/MeOH/H_2O for injection.

To perform the offline 2DLC experiments, lipid extracts were fractionated into five fractions using an Agilent Infinity 1220 LC coupled to a 1260 Infinity II Analytical-Scale Fraction Collector and a Waters Acquity Premier BEH Amide column (1.7 µm, 2.1×100mm, Waters Corporation, Milford, MA, USA). All fractions were collected into sterile polypropylene 1.5 mL tubes and evaporated to dryness under a gentle nitrogen flow and at room temperature for 1 hour. The method was tested using 85 commercial lipid standards from different subclasses (Supp. Table 16) with variable fatty acid chain lengths, number of double bonds, and modifications.

4.2.4. HILIC-RPLC-MS analysis

For the second LC dimension, the dried fractions obtained from the HILIC separations in the fraction collector were resuspended in 8 µL of MPA and 2 µL of MPB (MPA - 10 mM ammonium formate in 50:40:10 MeOH/ACN/H_2O and MPB - 10 mM ammonium formate in 95:5 IPA/H_2O) and analyzed by reverse-phase ultra-high-performance liquid chromatography (RP-UHPLC) coupled to mass spectrometry. Chromatographic separation was achieved with a Dionex 3000 system (Thermo Fisher Scientific, Waltham, MA, USA) and a Waters Acquity CSH Premier C18 column (1.7 µm, 2.1×100mm, Waters Corporation, Milford, MA, USA). A 16-min gradient was used for separation (0 min, 15% MPB; 0.5 min, 15% MPB; 2.3 min, 25% MPB; 9.3 min, 42% MPB, 10.1 min, 78% MPB; 12 min, 90% MPB; 13 min, 98% MPB; 14.5 min, 98% MPB; 15 min, 15% MPB) using a 0.300 mL/min flow rate from 0 to 9.3 minutes, decreasing to 0.270 mL/min up

to 10.1 minutes, and subsequently reducing further to 0.210 mL/min until the end of the run due to backpressure constraints. Separation was followed by 4 min re-equilibration (0 min, 15% MPB, with flow rate increasing from 0.210 mL/min to 0.300 mL/min after 2 minutes), and the column temperature was kept at 45 °C throughout. The UHPLC instrument was coupled to an ultra-high-resolution quadrupole-time-of-flight (QToF) mass spectrometer (Maxis II, Bruker Daltonics, Billerica, MA, USA) with an electrospray ionization (ESI) source (capillary voltage of 4500 V, endplate offset of 500 V; nebulizer gas pressure of 1.0 bar, dry gas flow rate of 4.0 L min-1; dry temperature of 220 °C, spectra acquisition rate of 1.0 Hz; and m/z range from 150 to 1500 Da). A 0.40 min mass re-calibration segment was inserted at the end of each chromatogram, during which 1.0 mM sodium formate calibrant solution in 1:1 IPA/H_2O (v/v) was infused with a peristaltic pump to ensure high mass accuracy.

MS/MS qualitative data were acquired for all sample injections using the auto-MS/MS feature (oToF Control, Bruker Daltonics). A cycle time of 1.2 s was used, during which one MS1 spectrum was acquired at 1.44 Hz, followed by multiple MS/MS collision-induced dissociation (CID) spectra at a variable acquisition rate of 0.5-2.0 Hz, depending on the precursor intensity (500 – 500,000 counts, respectively). Active exclusion of precursors was employed for compounds detected for more than three consecutive spectra within 0.50 min intervals. Collision energies varied according to the precursor m/z values between 20 and 30 eV. Samples were analyzed separately in positive and negative ionization modes, using 3 and 12 µL of the lipid extracts, respectively.

4.2.5. Data Processing and Lipid Annotation

Three data processing software tools (MetaboScape, MS-Dial, and LipidScreener) were used for alignment and lipid annotation. Results were then compared to ensure consistency among these software options so that we could make the best choice regarding which software is better for processing our 2DLC-MS datasets. A two-tier putative annotation approach was used for lipid annotation based on the acquired tandem mass spectrometry (MS/MS) spectra, following the previously established protocols by the Lipidomics Standards Initiative and approaches developed by previous research group members and previously described in Chapter II[103,182].

For each software, annotations were filtered based on expected adducts and retention times for each lipid class and fatty acid composition to filter out potentially incorrect matches. All lipid annotations were then converted to a shorthand notation at the species level (definition of lipid class or subclass and the summed composition of side fatty acyl chains, PC 36:1), and duplicated annotations were filtered out based on MS/MS score and mass error.

The annotation performance from each software was evaluated based on the expected subclasses within each HILIC fraction. Lipid standards from different subclasses were used to determine their elution patterns amongst the five fractions collected after the HILIC separation. The obtained annotations were compared against the expected patterns. Subclasses without suitable representative standards were assumed to elute in the fraction that contained lipid standards with the most similar headgroups but were not considered when discussing annotation accuracy.

4.2.5.1.MetaboScape Annotation Procedure

We first employed MetaboScape 2023b for data processing (Bruker Daltonics, Billerica, MA, USA) with a minimum intensity cut-off of 5,000 counts for positive and 3,000 counts for negative ionization, a minimum peak length of six spectra, and retention time tolerance of 10 s. The detected m/z were re-calibrated based on the sodium formate segment with a m/z tolerance of 5.0 mDa and lock mass (ESI+ m/z 338.341741 and ESI- m/z 283.264254). We further applied the removal of isotopes and adducts within a correlation threshold of 0.8 and recursive extraction (*i.e.*, features with missing values found in over 80% of the injections in at least one group were searched again within the raw data without applying the minimum intensity limit). The aligned features were filtered by detection in over 80% of injections in at least one group. Positive and negative ionization features were merged using a 10 ppm and 15-second tolerance before lipid annotation.

For the MS/MS annotations, we employed the MS-Dial LipidBlast library (https://fiehnlab.ucdavis.edu/projects/LipidBlast), the Human Metabolome Database (https://hmdb.ca), and the MassBank of North America LC−MS/MS libraries (https://mona.fiehnlab.ucdavis.edu). The annotations were split into two confidence tiers: tier 1 includes lipids annotated within an m/z tolerance of 5.0 mDa for precursors and an MS/MS score threshold of at least 500. In tier 2, an MS/MS score between 100 and 500 was used with the same m/z tolerance used for tier 1[27,36,103,119,178,184,187,204].

4.2.5.2.MS-Dial Annotation Procedure

Second, we tested the annotation performance of MS-Dial (version 5.1.230719), a popular open-source software for lipidomics data processing. Peak picking and alignment were performed

with a minimum intensity cut-off of 5,000 counts for positive and 3,000 counts for negative ionization, mass tolerance of 5 mDa, and retention time tolerance of 15s. The aligned features were kept if present in at least 80% of injections in at least one group.

The default MS-Dial Lipidomics library was used for MS/MS annotations, with a m/z tolerance of 5.0 mDa and a minimum fragment intensity of 300 counts. Furthermore, the annotation cut-off for the dot product score, weighted dot product score, and reversed dot product score was set at 500. The similarity between library and experimental spectra was set to a minimum of 51%[119].

Initial tests with the MSDial software resulted in poor performance. Hence, following alignment and annotation using the MS-Dial software, a few in-house Python scripts were developed to further improve the software output, using specific parameters to ensure data accuracy and reliability. The first step involved removing duplicate entries and a signal-to-noise ratio (S/N) filter with a threshold of at least 3. Second, annotations were filtered by RSD and match score. Lastly, positive and negative ionization output features were merged using a 5 ppm and 15-second tolerance, retaining only high-confidence annotations.

4.2.5.3.LipidScreener as a Tool for Lipidomics Data Processing

Lastly, we evaluated the performance of an in-house developed, Python-based software explicitly designed for the untargeted lipidomics routine employed by The Metabolomics Innovation Centre (TMIC, Edmonton, Canada), named LipidScreener. This comprehensive tool includes mass recalibration, retention time correction based on internal standards and MS/MS fragmentation patterns, peak picking, alignment, data cleansing, polarity merging, lipid annotation, normalization, and biostatistics. The dataset was first recalibrated based on the sodium formate

segment with a 1 mDa m/z tolerance. The chromatograms obtained under positive and negative ionization were aligned using a minimum intensity cut-off of 3,000 counts and a minimum peak length of six spectra. Oligomers and multiple adducts were handled within a 20-ppm m/z tolerance. Aligned features were filtered by detection in at least 80% of injections in one group before positive and negative ionization merging.

MS/MS annotations were obtained through spectral comparisons with the MS-Dial LipidBlast library (https://fiehnlab.ucdavis.edu/projects/ LipidBlast), the Human Metabolome Database (https:// hmdb.ca), and the MassBank of North America LC−MS/MS libraries (https://mona.fiehnlab.ucdavis.edu). We employed a m/z tolerance of 5 mDa for the precursor ion and 10 mDa for fragments, combined with minimum similarity between library spectra and experimental spectra of 40%. All annotated features underwent several filtering parameters to ensure accurate and reliable lipid annotation. These parameters include possible adducts, m/z error, the ratio of carbon to double bond present in the molecule, even or odd fatty acyl chains, structural modifications, presence of plasmenyl, and expected ionization and detection efficiency for each lipid class, which had been previously calculated based on ionization efficiency and biological properties for each subclass. Additional parameters include MS/MS similarity between library and experimental spectra, fragmentation patterns, and expected fatty acyl composition. These weights help in scoring and annotating lipid species by balancing different factors such as ion scores, modifications, and library matches, ensuring high-confidence annotations and accurate lipid profiles[14,36,103,183–187].

4.3. Results and Discussions

4.3.1. HILIC Method Development

We began this study by reproducing the HILIC-MS method previously published by Xu *et al.* (2020), which uses a 25-minute gradient for comprehensive lipid annotation (Figure 4.1)[83]. For this, serum samples were extracted using an adaptation of the Folch method[72,108] to extract small sample amounts as described in Chapter II (Supp. Table 17). Samples were mixed with 15 deuterated lipid standards before extraction (NovaMT LipidRep), and lipid extracts were resuspended in a 5:4:1 IPA/ACN/H_2O (v/v/v) mixture.

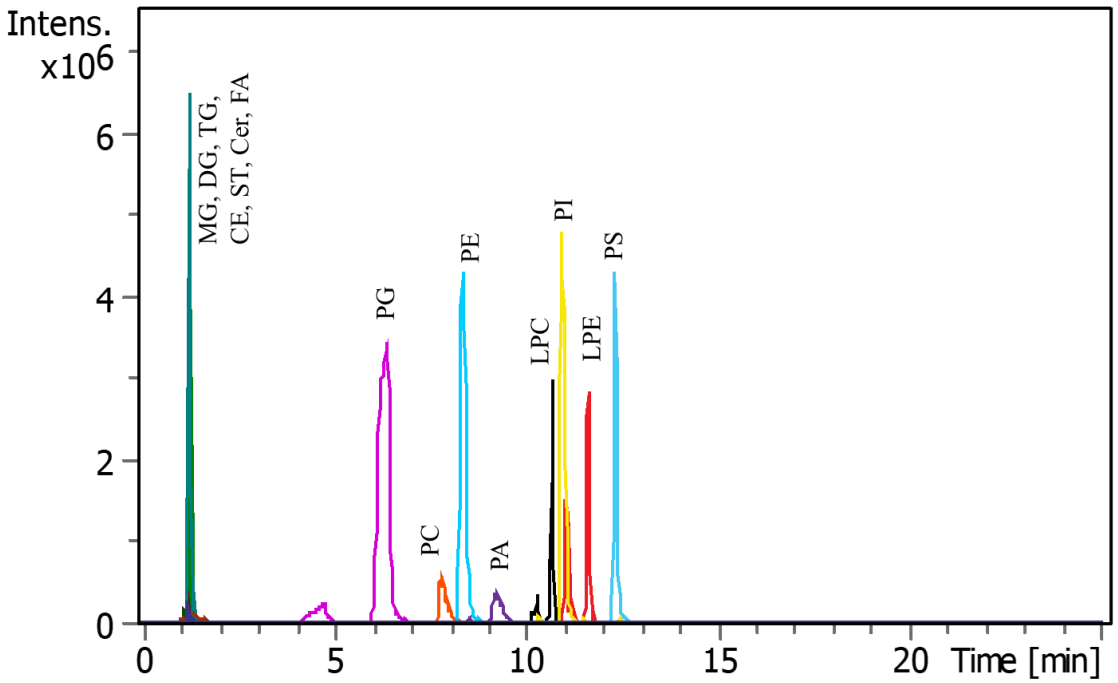

Figure 4.1. Base Peak Chromatogram (BPC) for Human Serum samples extracted with NovaMT LipidRep Internal Standard mix and analyzed using a Bruker Impact I under positive ionization conditions, reproducing Xu *et al.* (2020). Results for the HILIC-MS method with MPA: 10 mM NH_4COOH 50:50 ACN/H_2O; MPB: 10 mM NH_4COOH 95:5 ACN/H_2O; 0.200 mL/min; 45ºC; 25 min gradient (0 min – 100% MPB, 10 min – 80% MPB, 25 min – 20% MPB); 13 min equilibration (100% MPB).

Chromatographic results obtained using the original gradient indicate that all 15 deuterated internal standards in the mix and all other lipid compounds extracted from serum samples eluted before the 13-minute mark, even though the proposed gradient was 25 minutes long. Furthermore, some lipid species, such as [D5]PG 16:0_18:1, exhibited broadened and split peaks. The composition of the resuspension solvent had a high water content (10%), which likely contributed to the observed band broadening and peak splitting. Considering water is a highly polar solvent, its presence increases the mobile phase's overall polarity, affecting the solute's interaction with the stationary phase and retention times and elution profiles. Additionally, the interaction between the polar mobile phase and the stationary phase designed for HILIC, which typically favors polar interactions, might not be optimal with excessive water, leading to decreased efficiency. Furthermore, it can also influence the viscosity and diffusion rates of analytes within the column, further exacerbating band broadening and leading to atypical peak shapes[78].

Given the amphiphilic nature of lipids, there is a need to ensure the complete dissolution of species within a wide range of polarities and, simultaneously, chromatography requirements to ensure suitable peak shapes and reliable injections. With that in mind, we optimized the resuspension solvent composition to be more like the initial mobile phase conditions while still solubilizing a broad range of lipid structures[38,102,205,206]. Chromatograms for all resuspension solvent tests can be found in Figure C.1. From our optimizations, the optimized resuspension solvent composition is 30:15:4:1 ACN/IPA/MeOH/H_2O (Figure 4.2).

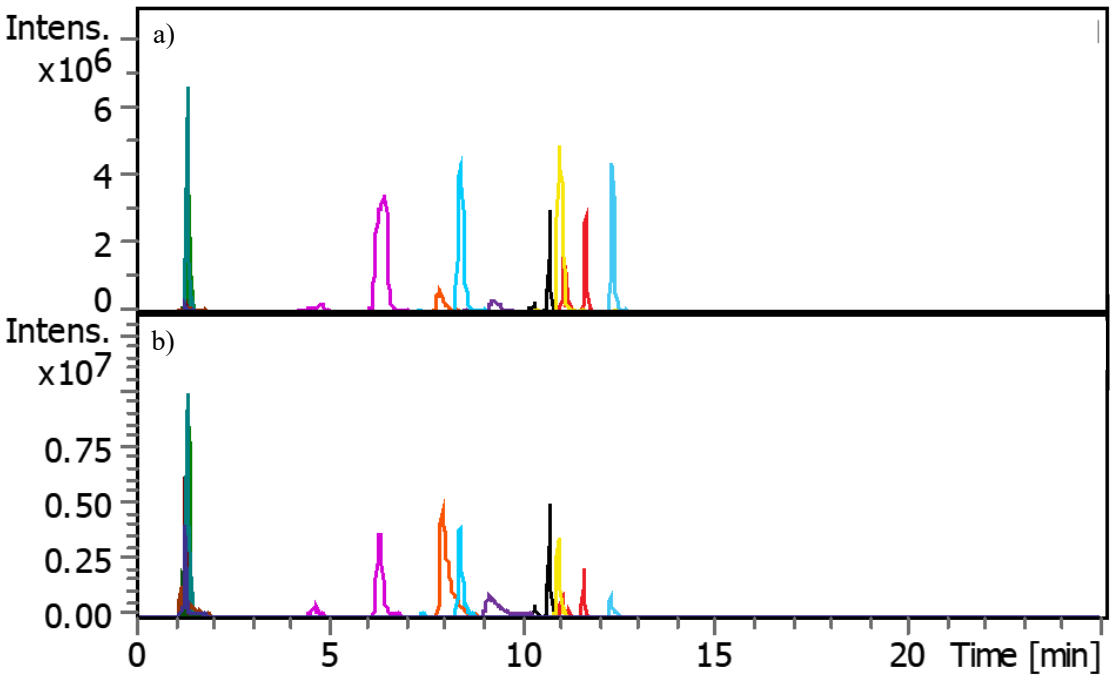

Figure 4.2. Extracted Ion Chromatogram (EIC) of NovaMT LipidRep Internal Standard Serum analyzed using a Bruker Impact I under positive ionization conditions; MPA: 10 mM NH_4COOH 50:50 ACN/H_2O; MPB: 10 mM NH_4COOH 95:5 ACN/H_2O; 0.200 mL/min; 45ºC; 25 min gradient (0 min – 100% MPB, 10 min – 80% MPB, 25 min – 20% MPB); 13 min equilibration (100% MPB). a) Original resuspension solvent (5:4:1 IPA/ACN/H_2O); b) Optimized resuspension solvent (30:15:4:1 ACN/IPA/MeOH/H_2O).

The resuspension solvent adjustments led to improvements in peak sharpness and higher intensities. For example, peak intensities in the 5 to 15-minute elution window improved from approximately 3×10^6 (Figure 4.2.a) to 4×10^6 counts (Figure 4.2.b). This improvement represents a 1.3-fold peak intensity increase alongside a notable band-broadening reduction.

Next, we evaluated the composition of our mobile phases. The original MPB composition was 10 mM ammonium formate and 0.1% formic acid in a 95:5 ACN/H_2O (v/v). However, all lipids eluted within one-half of the total gradient time, indicating a stronger-than-needed composition. To improve the separation within the proposed run time, we proposed a slightly

weaker MPB composition to 10 mM ammonium formate in 95:2:3 ACN/MeOH/H_2O (Figure 4.3.b), which mitigated the excessive mobile phase strength through the decrease of water content, which was replaced with IPA[19,78,83,197].

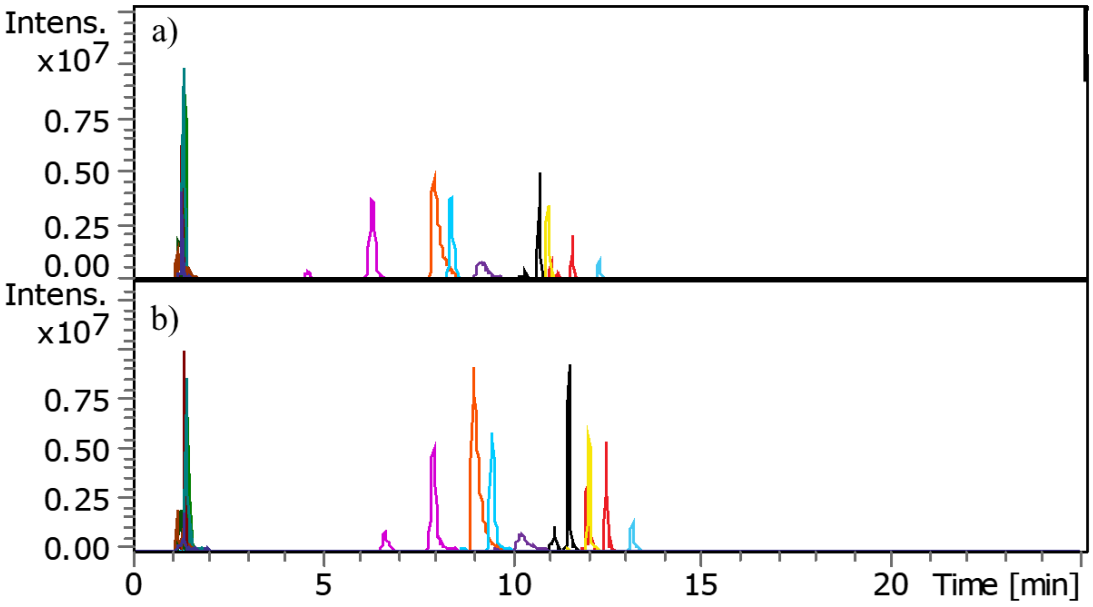

Figure 4.3. Extracted Ion Chromatogram (EIC) of NovaMT LipidRep Internal Standard analyzed using a Bruker Impact I under positive ionization conditions; MPA: 10 mM NH_4COOH 50:50 ACN/H_2O; 0.200 mL/min; 45ºC; 25 min gradient (0 min – 100% MPB, 10 min – 80% MPB, 25 min – 20% MPB); 13 min equilibration (100% MPB). a) Original MPB composition - 10mM ammonium formate and 0.1% formic acid in a 95:5 ACN/H_2O (v/v); b) Optimized MPB composition - 10 mM ammonium formate in 95:2:3 ACN/MeOH/H_2O.

These MPB modifications led to a modest increase in retention times and visually improved the chromatographic separation, with the last peak delayed from 12.5 to 13.2 minutes while maintaining peak shape integrity. Moreover, we observed a 1.5-fold increase in peak intensities. Specifically, focusing on the elution window from 5 to 15 minutes, peak intensities increased

between 1.2 and 1.6-fold when comparing pre-MPB optimization (Figure 4.3.a) and post-MPB optimization (Figure 4.3.b), indicating a notable signal strength enhancement. This result also encouraged us to optimize the MPA composition, initially set at 10 mM ammonium formate and 0.1% formic acid in a 50:50 ACN/H_2O (v/v, Figure 4.4.a). We hypothesized that higher ACN contents could improve analyte retention and separation since, in HILIC separation, water is considered the strongest solvent, whereas ACN is the weaker[78,83]. Hence, we tested different ACN/H_2O ratios, including 60:40 (Figure 4.4.b) and 70:30 (Figure 4.4.c) (v/v).

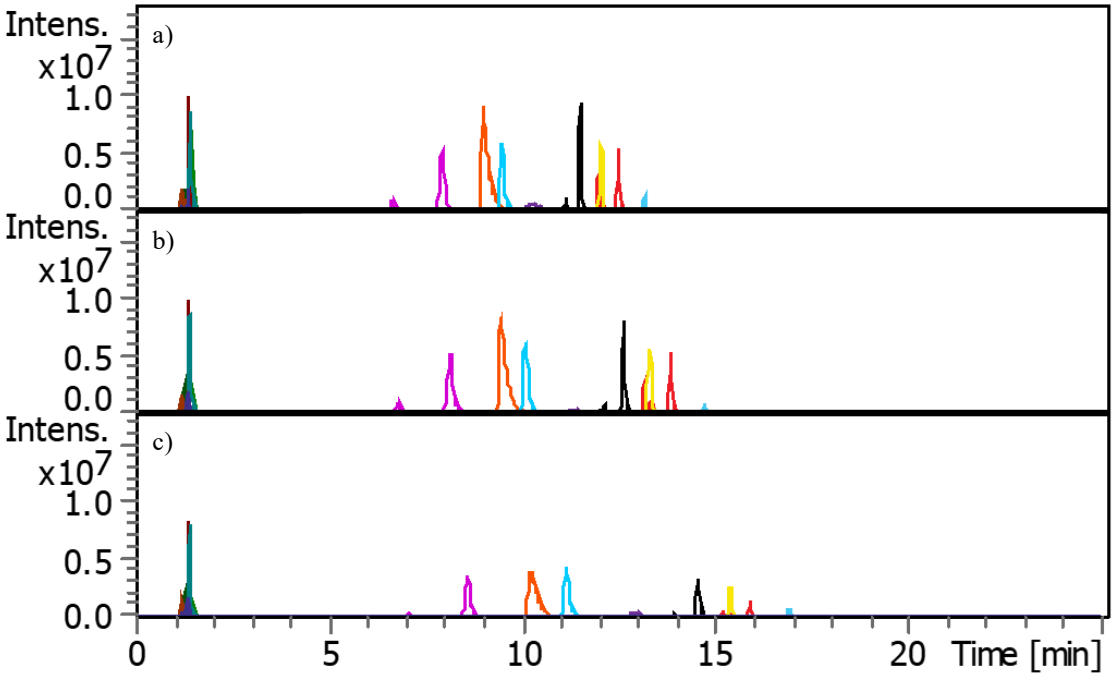

Figure 4.4. Extracted Ion Chromatogram (EIC) of NovaMT LipidRep Internal Standard was analyzed using a Bruker Impact I under positive ionization conditions; MPB: 10 mM NH_4COOH 95:2:3 ACN/MeOH/H_2O; 0.200 mL/min; 45ºC; 25 min gradient (0 min – 100% MPB, 10 min – 80% MPB, 25 min – 20% MPB); 13 min equilibration (100% MPB). a) Original MPA composition - 10mM ammonium formate and 0.1% formic acid in a 50:50 ACN/H_2O (v/v); b) MPA composition 10mM ammonium formate in 60:40 ACN/H_2O (v/v); c) MPA composition 10mM ammonium formate in 70:30 ACN/H_2O (v/v).

Reducing the water content significantly increased analyte retention by enhancing interactions with the stationary phase. Although the 70:30 mix provided the best separation, it also introduced some peak broadening and slightly reduced peak intensities (Fig. 4.4c). The 60:40 ACN/H_2O ratio was considered a reasonable compromise (Fig. 4.4b), balancing peak shape, separation quality, overall peak intensities, and analysis time. This configuration achieved clear analyte separation while preserving peak shapes and avoiding unnecessarily long chromatographic runs.

Last, we evaluated the chromatographic gradient, aiming for higher efficiency with improved analyte separation. After our modifications, the initial gradient lasted 25 minutes (Figure 4.5.a), with the last analytes eluting around the 15-minute mark, leaving 10 minutes, or 40% of the runtime, unused.

We proposed different gradient elution and flow rates to try to improve separation. For the optimization, we subdivided our chromatogram into three areas: the first 2 minutes of the run (where six different subclasses with no chromatographic retention eluted in less than 0.5 minutes), the middle area where phospholipids eluted, and the end area where we had the more hydrophilic lysophospholipids. After a few tests, we noticed that MPB was too strong to ensure proper separation, and those lipid classes were not retained enough in HILIC for it to make significant changes in separation (Figure C.2).

After several tests changing the gradient slope throughout the run, we proposed a new gradient elution within 26 minutes (Figure 4.5). This proposed gradient separation aims to maintain an appropriate run time while improving peak efficiency and separation[78].

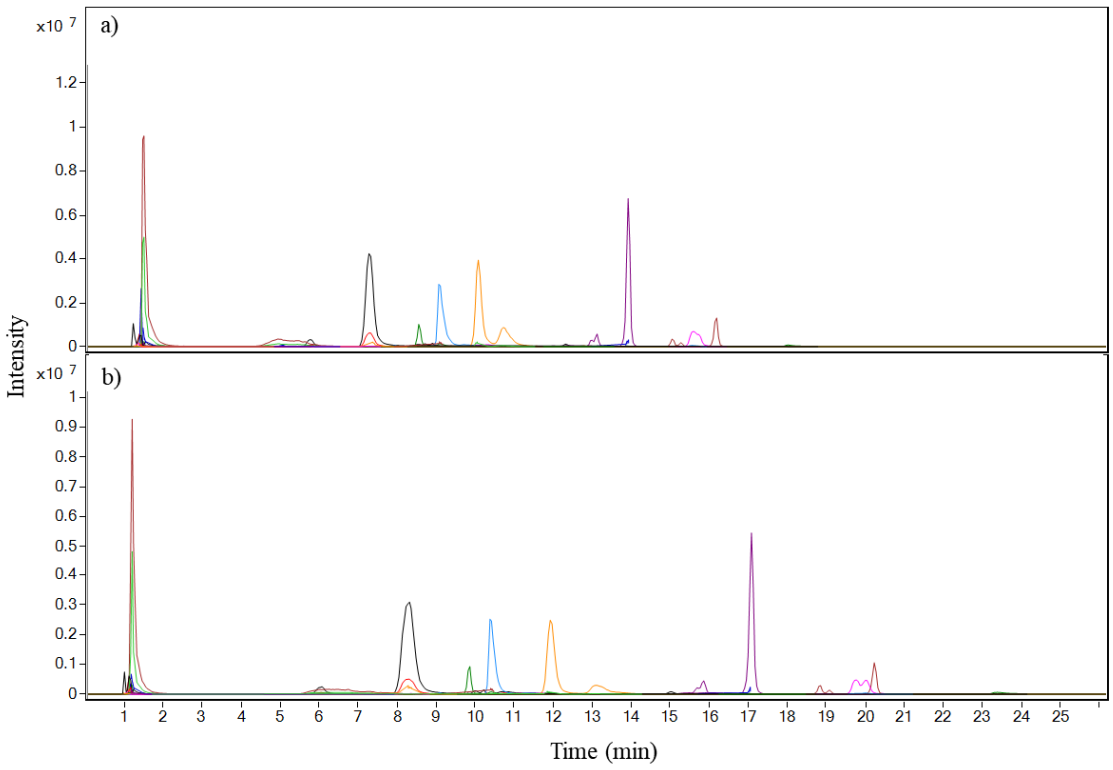

Figure 4.5. Extracted Ion Chromatogram (EIC) of NovaMT LipidRep Internal Standard analyzed using an Agilent QTOF under positive ionization conditions. A) Initial conditions, including MPA: 10 mM NH_4COOH 50:50 ACN/H_2O; MPB: 10 mM NH_4COOH 95:5 ACN/H_2O; 0.200 mL/min; 45ºC; 25 min gradient (0 min – 100% MPB, 10 min – 80% MPB, 25 min – 20% MPB); 13 min equilibration (100% MPB); B) Optimized gradient, including MPA: 10 mM NH_4COOH 60:40 ACN/H_2O; MPB: 10 mM NH4COOH 95:2:3 ACN/MeOH/H_2O; 0.250 mL/min; 45ºC, 26 min gradient elution (0 min 100% MPB, 2 min 100% MPB, 2-4 min 98% MPB, 4.5 min 98% MPB, 6 min 96% MPB, 8.5 min 93% MPB, 9.5 min 93% MPB, 12 min 91% MPB, 17 min 86% MPB, 25min 80% MPB, 26 min 20% MPB); 4 min equilibration (100% MPB).

After the gradient optimization, better use of the total run time and improved peak separation can be observed, with the last analytes eluting around 21 minutes (Figure 4.5.b). However, we can also observe increased peak broadening and lower intensities for specific standards. Nonetheless, our primary goal in optimizing a HILIC method was that it would serve as the first dimension in a two-dimensional liquid chromatography-mass spectrometry (2DLC-MS)

framework. Therefore, its main purpose is to effectively separate lipids based on headgroup polarity before they undergo RPLC-MS analysis.

Given that fractions from the first dimension will be further analyzed using RPLC-MS, the observed peak broadening was considered not as significant for the overall goal of this work. Regardless, the observed peak broadening was considered when planning each collected fraction, mitigating further issues.

The improvement in lipid class separation achieved with this revised gradient was considered sufficient for a first-dimension separation. Therefore, it would allow for the collection of well-defined fractions and lay the groundwork for developing our offline 2DLC method.

4.3.2. 2DLC-MS Method Development

4.3.2.1.Development of the Fractionation Method and Injection Of Standards

After optimizing the HILIC-MS method, we started its integration with our already established RPLC-MS methodology to reduce sample complexity and the co-elution of lipid species [78,83,103]. Lipid extracts were initially prepared for HILIC separation, followed by the collection of fractions. These fractions were dried under gentle nitrogen flow and resuspended for RPLC-MS analysis.

In our first attempt, we tried to collect eight fractions (Figure C.3), targeting separating lipid classes that typically co-elute in RPLC-MS, such as PCs and PEs. However, this task proved not viable with our current HILIC method, as the resolution between PC and PE is insufficient for them to be fully separated. Additionally, having eight fractions was considered excessively time-

consuming since all of them will have to be analyzed on RPLC-MS, increasing the length of our workflow 8-fold.

After conducting additional tests, we opted for a more efficient approach, settling on a five-fraction collection strategy. The specific time collection intervals for each fraction are outlined in Table 4.2, along with the lipid classes expected in each fraction.

Table 4.2. Time Intervals and Expected Lipid Classes for Fraction Collection

Fraction Code	Time Interval (min)	Expected Lipid Subclasses
F1	0 – 5	CE, Cer, DG FA, HexCer, MG, PR, ST, TG
F2	5 – 10	PG
F3	10 – 15	PA, PC, PE, SM, SPB
F4	15 – 20	LPC
F5	20 – 25	LPE, PI, PS

We separated our samples into five fractions to improve the analytical resolution and specificity, minimize ion suppression, and reduce co-elution among different lipid classes. These steps are crucial for precisely annotating and quantifying lipids[9,83].

A recognized challenge concerning 2DLC methods, particularly online versions, is the dilution of samples in the first dimension, which complicates the analysis and often decreases the limit of detection[78,203]. This prompted us to adopt an offline approach, allowing us to concentrate

each fraction by evaporation before reconstituting it in a smaller volume of solvent mixture fully compatible with our RPLC-MS conditions. This decreased the chance of clogging and peak broadening. We opted to resuspend each fraction to the original injection volume (10 μL for this study) to aid the performance evaluation.

We used a mixture of 15 deuterated lipids (NovaMT LipidRep) to evaluate the performance of the developed offline 2DLC-MS protocol (Figure 4.6). This experiment addressed two primary concerns: assessing potential sample loss throughout the process and determining each standard's fractionation pattern and separation improvement.

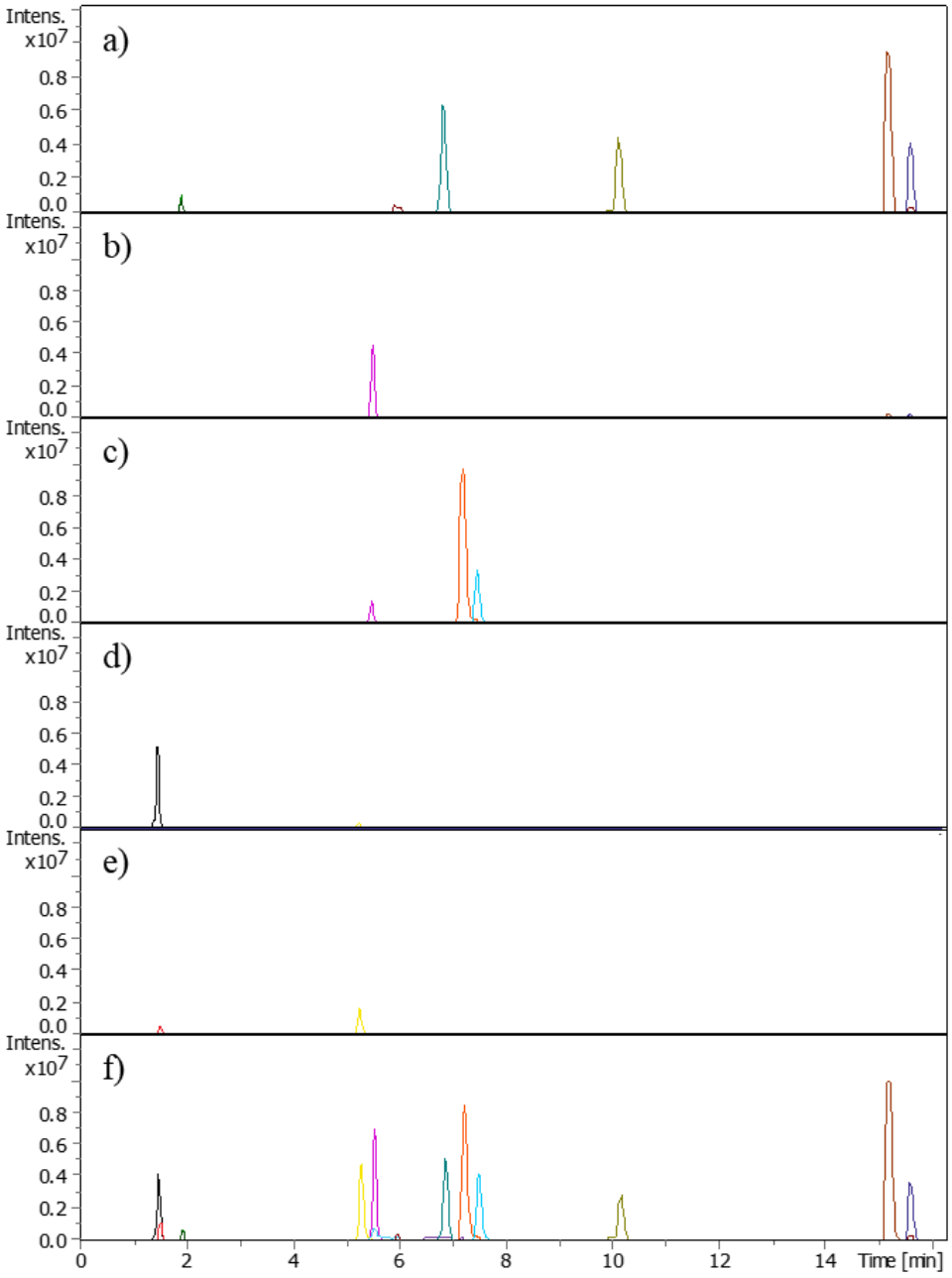

Figure 4.6. Extracted Ion Chromatogram (EIC) for NovaMT LipidRep Internal Standard Serum mix acquired on Bruker Maxis Impact II, MPA: 10 mM NH_4COOH 60:40 ACN/H_2O; MPB: 10 mM NH4COOH 95:2:3 ACN/MeOH/H_2O; 0.250 mL/min; 45ºC, 26 min gradient elution (0 min 100% MPB, 2 min 100% MPB, 2-4 min 98% MPB, 4.5 min 98% MPB, 6 min 96% MPB, 8.5 min 93% MPB, 9.5 min 93% MPB, 12 min 91% MPB, 17 min 86% MPB, 25min 80% MPB, 26 min 20% MPB); 4 min equilibration (100% MPB), diluted 8-fold. a) Standards eluted in F1; b) Standard eluted in F2; c) Standard eluted in F3; d) Standard eluted in F4; e) Standard eluted in F5; f) Non-Fractionated standard mix.

Figure 4.6 highlights that fraction 1 contains seven of the 15 lipid classes initially present in our internal standard mix (MG, DG, TG, CE, Cer, FA, and ST), which correspond to those with limited HILIC retention (retention times smaller than 2 min). Yet, when subjected to HILIC fractionation followed by RPLC-MS (Figure 4.6.a), these previously coeluting standards are well separated in the second dimension, which can be attributed to their different polarities. Additionally, certain classes often co-elute by RPLC, such as PG and PI, can be observed eluting in distinct fractions when using our 2DLC method. PG is found in fraction 2 (Figure 4.6.b), whereas PI is in fraction 5 (Figure 4.6.e).

Moreover, we compared the average peak intensities obtained for RPLC-MS internal standards to those obtained when using 2DLC-MS. The results shown in Supp. Table 18 displays recoveries ranging from 81% to 127%, indicating no substantial sample loss during the fractionation process. These findings confirm the efficiency of our fractionation and reconstitution strategy in preserving sample integrity throughout the 2DLC workflow.

One of the goals of our study was to improve lipid separation and enhance annotation confidence. Hence, we tested several commercially available standards incorporated into pre-defined mixtures, analyzing them by HILIC-MS alone and subsequently by 2DLC-MS (Figure C.4). This way, we were able to determine the fractionation profiles of different lipid subclasses with variable fatty acyl composition, which has been previously highlighted in Table 4.2. With that information, we determined which fraction of the most common lipid subclasses was more likely to appear and used that information to develop our annotation confidence procedure.

Injecting our standards in the stand-alone HILIC-MS method allowed us to assess specific characteristics, such as different fatty acyl chain lengths, number of double bonds, and

modifications of those molecules, and draw comparisons between the lipid classes involved in our study. We were able to establish a relationship between the retention times and the carbon chain lengths of our analytes in HILIC-MS (Figure C.5). Within the same subclass, most standards eluted within a 2-minute interval, regardless of any structure differences. These results corroborate that the fatty acyl chain length has a minor influence on the retention times in HILIC separations, so HILIC focuses on separating analytes mostly based on their headgroup polarity[78,83]. For instance, sterols (ST) with the same number of carbons but varying structural modifications (number of oxygens or unique configurations) demonstrated elution times ranging between 1 and 2 minutes in HILIC separation. In contrast, in RPLC-MS, those would elute throughout the chromatogram.

Analyzing the elution patterns of the commercial standards accomplished two objectives: first, it demonstrated the efficiency of our fractionation technique, and second, it improved our understanding of the post-fractionation distribution of lipid subclasses. The insights this experiment gave us were crucial for recognizing potential misannotations in future analyses of biological samples and, therefore, in determining our annotation accuracy.

4.3.2.2.Application of 2DLC-MS Method on Biological Samples

After optimizing the 2DLC method and validating its performance using commercial standards, our next objective was to assess its efficiency on complex biological matrices, such as tissue or cell samples, showcasing its potential for real-world applications. Chicken liver extracts were prepared by homogenization with a bead-beater and ceramic beads after adding internal standards, followed by LLE, following the procedure previously described and the volumes shown in Supp. Table 17. A portion of the organic phase was evaporated to dryness and resuspended to a

75-fold dilution (mg/mL of resuspended extract). In Figure 4.7, we have a lipidomic profile across all five fractions obtained from the chicken liver tissue extracts and a comparison with a non-fractionated sample.

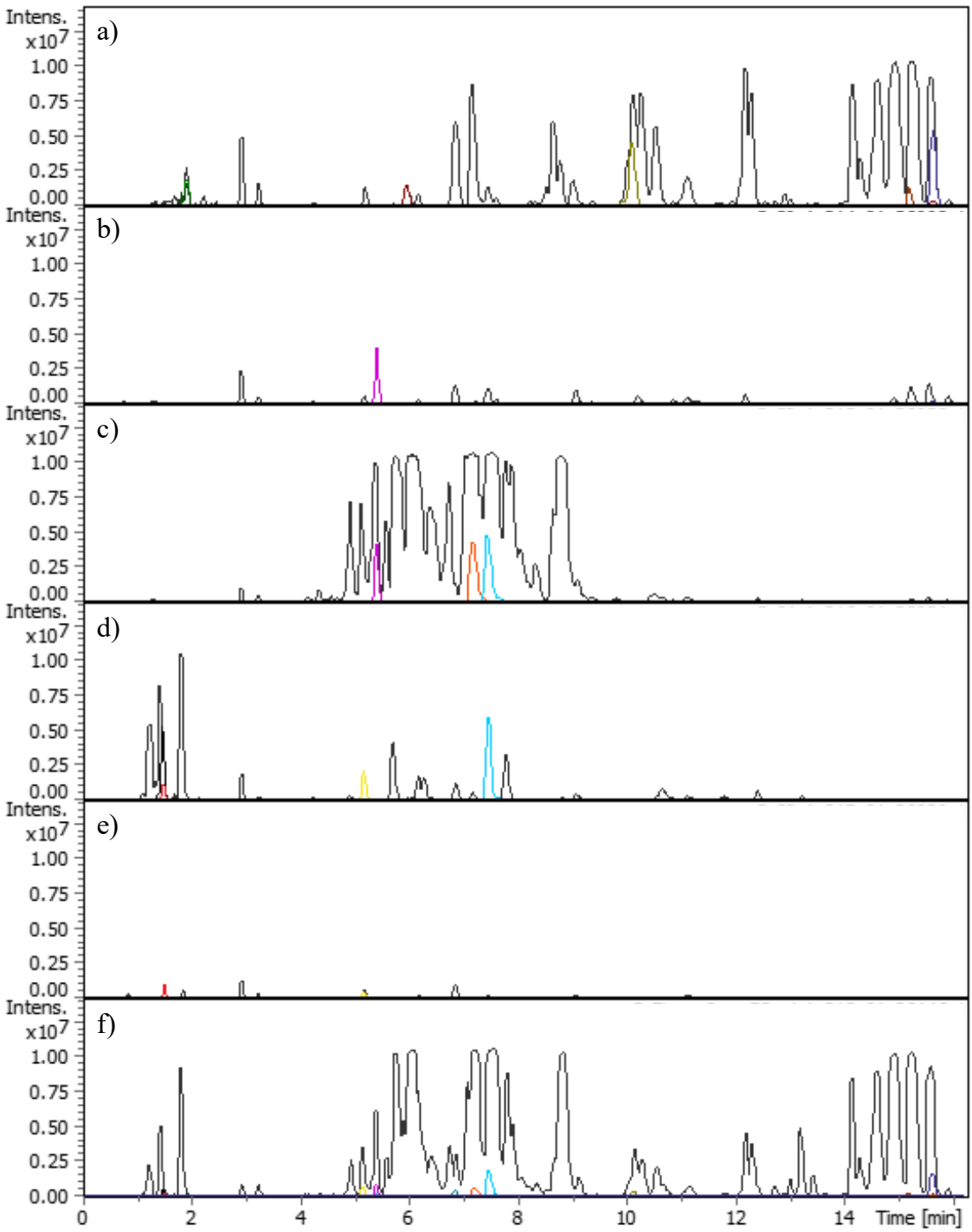

Figure 4.7. Base Peak Chromatogram (BPC) for chicken liver tissue diluted 75x and NovaMT LipidRep Internal Standard Tissue mix; a) Fraction 1; b) Fraction 2; c) Fraction 3; d) Fraction 4; e) Fraction 5; and f) Non-fractionated sample.

From Figure 4.7, we observe that, for tissue samples, most detected features elute in fractions 1 and 3, representing 38% and 23% of the features, respectively (Figure C.6.a). The 2DLC-MS method reveals a 2.1-fold increase in detected features compared to RPLC-MS. The summed intensity shows a similar trend, with fractions 1 and 3 corresponding to 46% and 37% of peak intensities, reflecting a 1.3-fold increase over RPLC-MS data (Figure C.6.b).

Similar behaviors are observed in serum and cell samples (Figure C.7 and Figure C.8, respectively). Serum samples follow a trend similar to tissue samples, with most detected features in fractions 1 and 3, representing 36% and 24% of the total, respectively. This represents a 2.2-fold increase compared to RPLC-MS (Figure C.5.a). Summed intensities for fractions 1 and 3 correspond to 44% and 30% of the total, showing a 1.2-fold increase over RPLC-MS (Figure C.5.b). Cell samples show slight differences, with fractions 1 and 3 having the highest number of detected features at 29% and 25%, representing a 2.3-fold increase (Figure C.5.a). However, 75% of the total summed intensities come from fractions 1 and 3, at 23% and 50%, indicating a 1.2-fold increase compared to RPLC-MS (Figure C.5.b). These results indicate that our 2DLC method simplifies sample complexity and provides a more detailed and comprehensive view of the lipidome across different sample types.

Drawing from our earlier findings (shown in Figure 4.6), fraction 1 (Figure 4.7.a) predominantly contains lipids with hydrophobic headgroups (MG, DG, TG, CE), fatty acids, ceramides, and sterols. In contrast, fraction 3 (Figure 4.7.c) mainly comprises glycerophospholipids, such as PCs and PEs. The high feature counts and summed intensities in these fractions suggest that the lipidome of the analyzed samples is predominantly composed of

those species, which aligns with previous studies that say those are the most abundant subclasses in tissue samples[1,15,110,136,175].

Lastly, we evaluated the annotation capabilities of our software by comparing the 2DLC-MS and RPLC-MS methods and examining how many annotations were common to both datasets. This comparison allowed us to assess the consistency and coverage of lipid annotations provided by each technique, highlighting the strengths and limitations of each approach in annotating lipid species displayed in Figure 4.8.

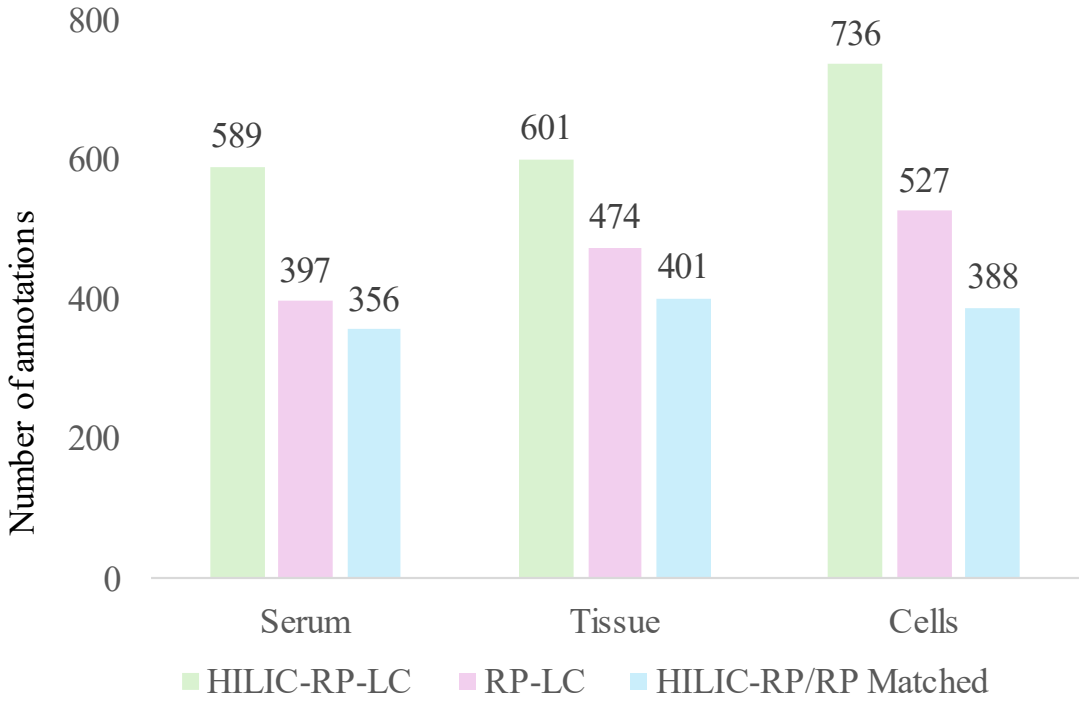

Figure 4.8. Comparison of lipid annotations annotated by the software using 2DLC-MS and RPLC-MS methods. The figure shows the number of lipids successfully annotated in the 2DLC-MS and RPLC-MS methods separately and those consistent across both methods.

The 2DLC-MS method resulted in more lipid annotations across all matrices. Figure 4.7 and Figure 4.8 show that this method's advantages include reduced sample complexity, fewer coelutions, and lower ion suppression. These effects increase summed intensities and the number of detected features, which facilitate potentially uncovering low-abundance peaks.

The 2DLC-MS method reduces sample complexity and reveals more details of the lipidome. However, some annotations using only RP may be incorrect due to poor library and low-quality experimental spectra caused by ion suppression or matrix effects. Since 2DLC minimizes these issues, previously misannotated structures can be correctly reannotated, leading to mismatches between 2DLC and RP methods. Additionally, incomplete fragmentation, isobaric interference, and ion suppression in RPLC further complicate accurate annotation. Lipid species like ACer, MGDG, and DGDG are typically found in plants and are rare in other sample types, explaining their absence in 2DLC analysis[175,202,207].

Supp. Table 19 to Supp. Table 24 lists all annotated lipids for each method, sample type, and Supp. Table 25 lists all features present in RPLC-MS that were not present in 2DLC-MS for all sample types. These factors highlight the complexity of lipidomics and the importance of using complementary techniques for accurate lipid profiling. By considering these aspects and improving sample preparation, instrumental settings, and database quality, the accuracy of MS/MS matching can be significantly enhanced.

The development and proof-of-concept application of our 2DLC-MS method provided an overview of its potential for reducing sample complexity and increasing the number of detected features. The next step was to evaluate its benefits in other biological samples, including human serum and MCF-7 cells (human breast cancer), based on the total number of annotated lipid species

and the proportion of annotations assigned to the expected HILIC fraction. Moreover, we compared annotation results from fractionated samples against those from non-fractionated samples to identify the overlap in annotated lipid species.

These factors highlight the complexity of lipidomics and the importance of using complementary chromatographic techniques, such as HILIC and RP, for accurate lipid profiling. The development and proof of concept application of our 2DLC-MS method gave us an overview of its potential for reducing sample complexity and increasing the number of detected features.

4.3.3. Lipid Annotation Confidence

Next, we evaluated our method's ability to determine lipid annotation confidence across different biological matrices, including human serum, MCF-7 cells (human breast cancer), and chicken heart tissue samples. For this, we evaluated the total number of annotated lipid species and how many of those annotations were assigned to their expected HILIC fraction.

We first evaluated the annotation performance of lipids detected in human serum using LipidScreener (Figure 4.9). Of all annotated lipid species, 93% (548 lipids) belonged to a subclass represented in our standard set, indicating whether they were annotated within their expected fraction. Among the subclasses with known expected fractions, 79% of them eluted in their anticipated fraction (Figure 4.9). This observation further indicates that our offline 2DLC approach can be a reliable tool for determining annotation accuracy since most annotations were present in their expected fraction, even though some unexpected annotations were present in every fraction.

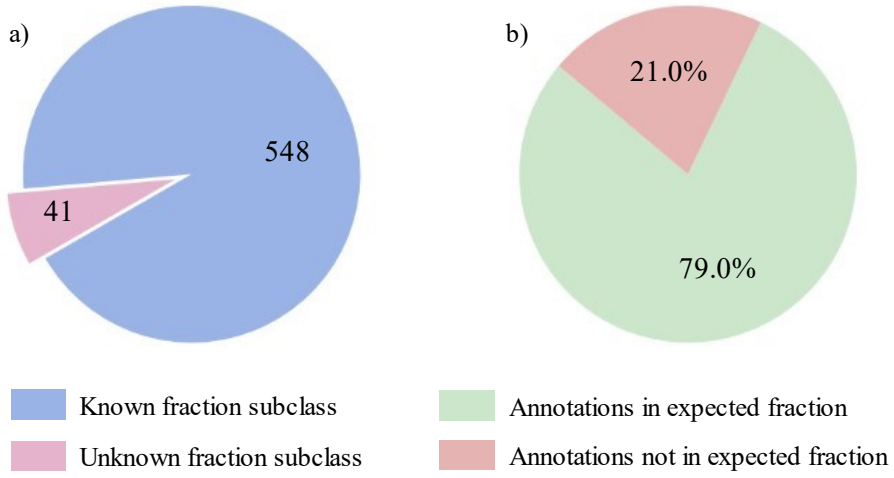

Figure 4.9. Comparative Analysis of Lipid Annotations by Fraction Association for Serum Samples. a) Distribution of lipid annotations, which belong to subclasses with a known fraction, and annotations with subclasses with an unknown fraction. b) Annotations assigned to a feature in their expected fraction.

Individually analyzing each fraction (Figure 4.10), we can see the percentage of annotations that eluted in their expected fraction. Out of the 155 annotations in fraction 1, 85.2% were expected, whereas 14.8% were not. Most unexpected annotations in this fraction were assigned to PE, PG, and SM. In fraction 2, out of 72 annotations, 91.7% were in their expected fraction, and 8.3% were not, with the most unexpected annotations being PI. For fraction 3, out of 164 annotations, 68.9% were in their expected fraction, while 31.1% were not, most of these being Cer. Fraction 4 had 120 annotations, with 81.7% in their expected fraction and 18.3% not, with the most unexpected annotations being TG. Lastly, fraction 5 had 36 annotations, with 63.9% in their expected fraction and 36.1% not, most being TG.

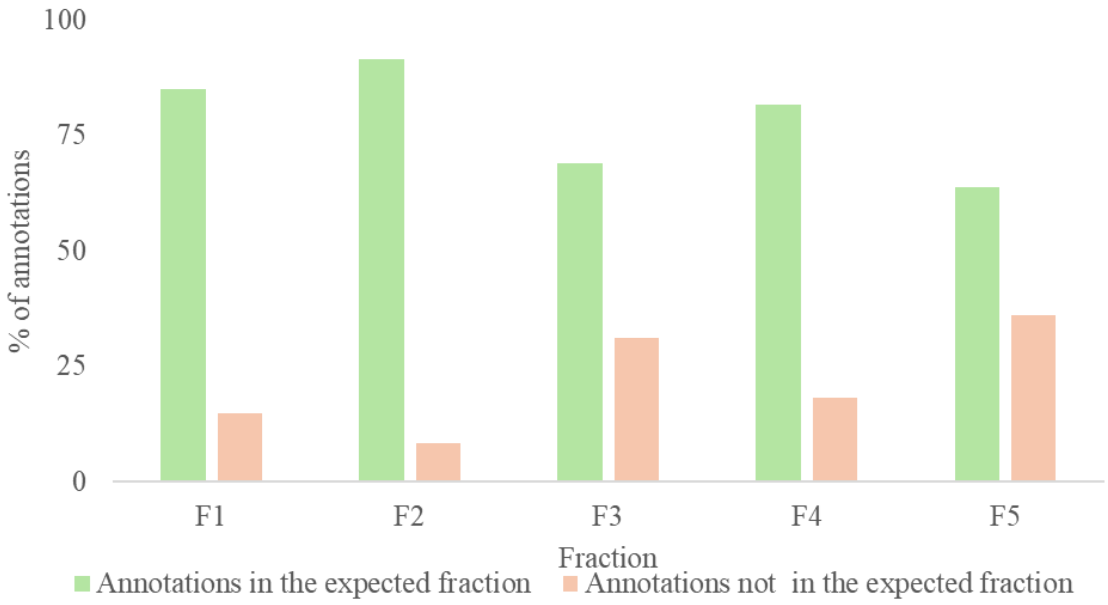

Figure 4.10. Distribution of lipid annotations in their expected fractions (green) versus those not in their expected fractions (orange) across five serum sample fractions. The x-axis represents the five fractions, while the y-axis indicates the percentage of annotations.

The annotation performance for fractions 3 and 5 is generally lower than for other fractions. Fraction 3 mainly contains phospholipids (PC, PE, and PA), which often coelute in RPLC-MS, making accurate annotation difficult because of ion suppression and matrix effects. This can lower MS/MS spectra quality and lead to misannotations[80,120]. Fraction 5 has additional challenges due to low-abundant lipid species like LPC, LPE, and PI. The low abundance results in lower signal intensities, poorer-quality spectra, and more complicated annotation. Mismatch annotation could also occur due to suboptimal fraction collection intervals or unsuitable MS/MS matching procedures influenced by data quality from libraries, spectral acquisitions, and algorithms.

Furthermore, mismatch annotation can happen due to a poor fraction collection interval or unsuitable MS/MS matching procedures. These issues may be influenced by the quality of data

from existing libraries, our spectral acquisitions, and the matching algorithms used. This points to areas for improvement in future work. Additionally, the injection volume of 10 µL in the first LC dimension might be causing broader peaks, leading to some lipid classes eluting in multiple fractions. Some subclasses have tailing profiles, resulting in multiple fraction elution. Also, a few species elute in the last fraction, so even a few false positives can significantly affect the expected versus unexpected annotation ratio[208].

To evaluate the versatility and consistency of our method across different sample matrices, we repeated this assessment with MCF-7 cell samples and chicken liver samples. Figure 4.11 shows a consistent trend, following the pattern previously observed for serum samples. In chicken liver samples (Figure 4.11.a), 93% of annotated lipids matched the standard subclasses, with 79% assigned to the correct fractions (Figure 4.11.b). For cell samples (Figure 4.11.c), 92% of annotated lipids aligned with the subclasses represented by our standards, with 78% of lipid annotations assigned to the correct fractions (Figure 4.11.d).

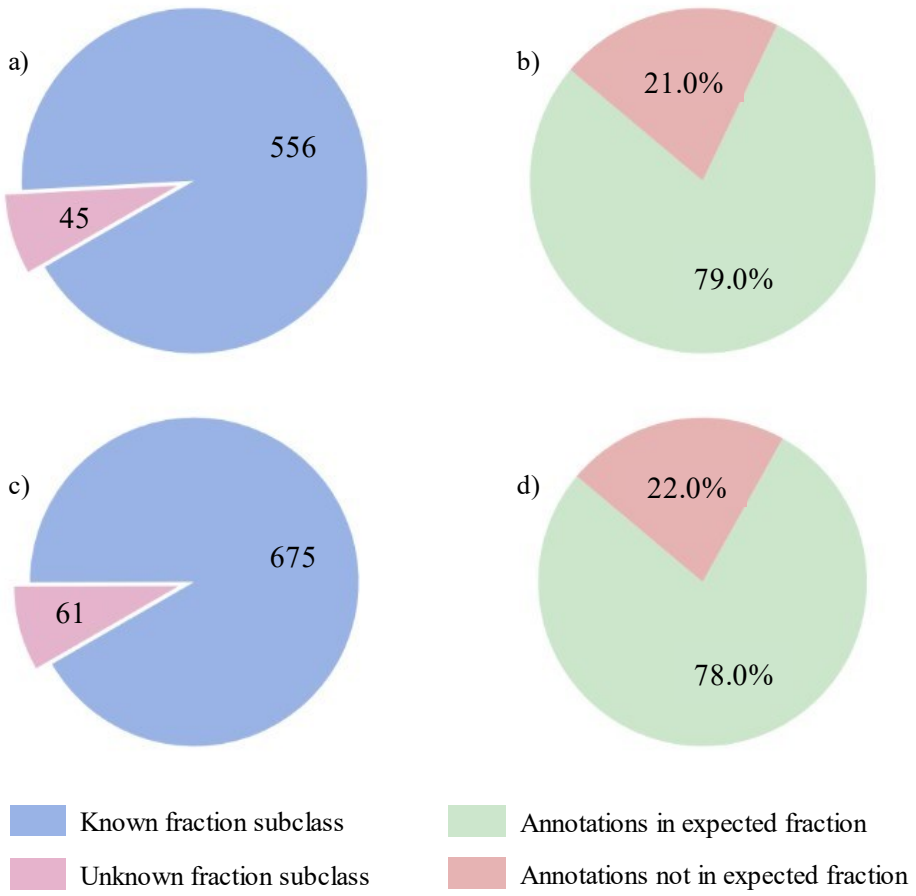

Figure 4.11. Comparative Analysis of Lipid Annotations by Fraction Association for tissue and cell samples. a) Distribution of lipid annotations for tissue samples, which belong to subclasses with a known fraction, and annotations with subclasses with an unknown fraction. b) Annotations for tissue samples assigned to a feature in their expected fraction. c) Distribution of lipid annotations for cell samples, which belong to subclasses with a known fraction, and annotations, which belong to subclasses with an unknown fraction. d) Annotations for cell samples assigned to a feature in their expected fraction.

A similar analysis was conducted for tissue and cell samples to evaluate annotation performance for each fraction (Figure C.9), paralleling the findings from serum samples. In both tissue and cell samples, fraction 5 showed a significantly lower percentage of expected annotations (38.8% for tissue and 26.8% for cells). Most of the unexpected matches in tissue samples were TG,

while cell samples were primarily SM. This pattern mirrors the trend observed in serum samples, where fraction 5 also had lower annotation performance, primarily due to the complexities of lipid elution and the quality of MS/MS matching procedures. Overall, this consistency highlights areas for potential improvement in fraction collection intervals and MS/MS matching algorithms.

4.3.4. Performance of Different Software for Lipidomics Data Processing

We compared the lipid annotation results obtained from three software tools: Metaboscape (Bruker Daltonics, Billerica, MA, USA), MS-Dial, and LipidScreener. The first two options are well-known and often used in the lipidomics community. However, LipidScreener is an in-house software developed for our RPLC-MS/MS untargeted lipidomics approach. Thus, it may present superior results than software that analyzes datasets acquired using other methodologies. For each software, we evaluated the accuracy of subclass attributions to the expected fractions and the consistency of annotations across the software platforms.

Figure 4.12 displays the total number of annotations obtained using each software for our 2DLC-MS/MS data. LipidScreener annotated the highest number of features for all sample types, initially suggesting it may be more suitable for processing our datasets. Metaboscape and MS-Dial were superior when comparing the percentage of annotated features that eluted within their expected fraction (92% average across the different sample types), suggesting their matching algorithms might be superior to the ones used by LipidScreener. However, LipidSceener provided a higher absolute number of correct annotations (*i.e.*, that eluted within the expected fractions).

Figure 4.12. Comparative Analysis of Lipidomics Software Performance. The bar graph displays the total MS/MS annotation features obtained by Lipid Screener, MS-Dial, and MetaboScape in the 2DLC-MS analysis across various sample types. It illustrates the number of lipid annotations by each software and the proportion of these annotations that coincided with their expected fractionation, highlighting the accuracy and efficiency of each software in predicting lipid elution profiles.

While LipidScreener stands out in detecting many features, MetaboScape and MS-Dial show a higher annotation accuracy for MS/MS matches. While MetaboScape and MS-Dial show similar performance percentage-wise, if we look at the absolute numbers, MetaboScape shows its superiority by annotating 1.6-fold more features within their expected fraction than MS-Dial. Furthermore, although MS-Dial and MetaboScape have similar performances in annotating features in their expected fraction, MetaboScape annotates more lipid species correctly.

The balance between annotation quantity and accuracy highlights the importance of selecting the appropriate software based on the analysis's specific needs. Despite MetaboScape and MS-Dial's superior performance in accurately matching features, there are still advantages of using LipidScreener for lipidomics analysis, as it annotates the most features across all sample types, capturing a wide range of lipid species, including low-abundance lipids. Furthermore, like the other software, its consistent performance across different samples suggests robustness and adaptability. While MetaboScape and MS-Dial offer precise matching, LipidScreener’s extensive detection capabilities and customization for our needs may make it more suitable for our workflow.

To extend the comparison between the three software options, we generated Venn diagrams (Figure 18), which highlighted the similarities and differences in annotated species (only those found in their specific fraction) from serum, cell, and tissue samples among the software used.

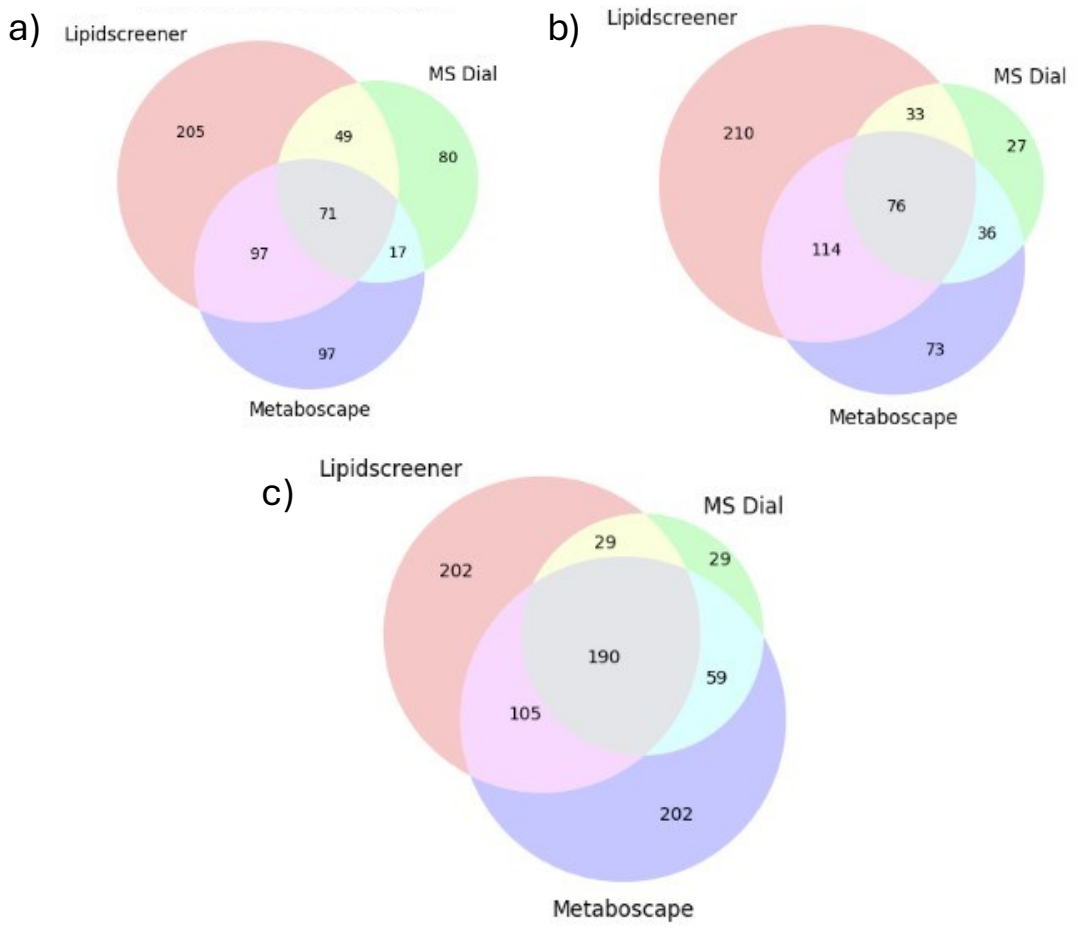

Figure 4.13. Venn diagram displaying unique and shared lipid species annotated by LipidScreener, MS-Dial, and MetaboScape. The central intersection represents lipids annotated by all three software. At the same time, the outer sections denote the number of unique annotations made by each software in a) Serum samples, b) Chicken liver samples, and c) Cell samples.

The Venn diagram analysis (Figure 4.13), showed that LipidScreener exhibits a significant number of unique annotations that eluted within their expected fractions. For example, for serum samples (Figure 4.13.a) 205 species were only annotated by LipidScreener, 97 were only found by Metaboscape, and 80 were seen only on MS-Dial data. Considering LipidScreener detects and annotates more features (in absolute numbers) than the other two software, it was expected to have

more unique annotations. Furthermore, although MS-Dial and MetaboScape perform similarly, a third of their annotations are unique to each software.

LipidScreener displays similar results for tissue and cell samples (Figure 4.13.b and Figure 4.13.b, respectively); however, MetaboScape shows the same number of uniquely annotated lipids as LipidScreener for cell samples. In both cases, the number of uniquely annotated species by MS-Dial is smaller than for serum samples. This could indicate that MS-Dial's capability to annotate some lipid species in complex sample types may be compromised, possibly due to the nuanced interpretation of mass spectrometry data or lack of a more comprehensive reference database.

This comparison further exemplifies the need for further research and standardization within the lipidomics community. MS Dial and Metaboscape, two popular software platforms for lipidomics data processing, provided significantly different results. Only 41% of the MS-Dial annotated species were also annotated by Metaboscape, while 55% were annotated by LipidScreener (33% of those annotated in the three software) for serum samples. Still, the 71 annotations all software platforms share highlight their power to annotate lipid species accurately, even with their differences. We looked for similarities and patterns in the shared annotations but found none.

In the qualitative analysis, PC had the highest number of annotations, with 27 in serum, 21 in tissue, and 54 in cells. Other notable lipid classes include DG, which had 4 in serum, 10 in tissue, and 15 in cells, and PE, with 1 in serum, 12 in tissue, and 53 in cells. The lipid classes TG and HexCer also showed varied concentrations across the sample types, emphasizing the complexity and diversity of lipid distributions in different biological matrices. All annotated features in the three software for each sample type were summarized into Supp. Table 26.

Patterns among the shared and unique annotations were examined to discern any underlying trends. For instance, the high abundance of PC across all sample types suggests its critical role in cellular structure and function. PCs are known to be significant components of cell membranes, contributing to membrane fluidity and signaling pathways, which highlight their biological importance. In contrast, the presence of SM in tissue and cell samples but not in serum may indicate tissue-specific roles, possibly related to sphingolipid metabolism and cellular stress responses. This specificity suggests the biological significance of lipid class distribution and composition in different sample types. FA, another lipid class, exhibited minimal variation, suggesting it may not be as biologically distinctive in this context as other classes[1,110,209,210].

Carefully looking at our annotation list for each software shows that PCs, SMs, and TGs are some of the most abundant subclasses annotated. However, none of the SMs annotated were present in the correct fraction and all software simultaneously. Further analyzing these annotations, most had different modifications in their structure (*i.e.*, SM 36:0;O2 and SM 36:0;O3 for MS-Dial and LipidScreener, respectively). On the other hand, TG, which had the least annotations in MetaboScape, was present in all software and in its expected fraction 78% of the time. No specific trends were observed for the shared or unique annotations, suggesting that 1) software tailored for this specific dataset might detect more peaks and, therefore, have more peaks to annotate possibly; 2) potential issues in the theoretical libraries or dataset may lead to spectra with a lot of noise, causing potential confusion to the software during the annotation step.

While all platforms can reliably annotate many lipid species, exclusive reliance on a singular software may lead to missed or incorrect annotations. Implementing a multi-software approach could significantly broaden the scope of lipidomic analysis, although practical limitations

such as processing time and resource allocation must be considered. Critical factors for selecting optimal software include user-friendliness, customizability to project-specific requirements, potent annotation capabilities, and overall performance. Regarding our needs, LipidScreener emerges as a promising option, especially given its design for customization and adaptation to our specialized methods and analytical needs.

LipidScreener, despite being an in-house tool, demonstrated the highest number of annotations, making it highly effective for comprehensive lipid detection, suggesting its design, tailored for our RPLC-MS/MS workflow, may offer better coverage, especially for low-abundance lipids. On the other hand, Metaboscape and MS-Dial, showed higher accuracy in annotating species to their expected fractions, indicating they may be more suitable for studies requiring highly precise lipid matching.

A balance between annotation accuracy and quantity is vital in lipidomics studies, emphasizing the importance of choosing the right tool based on the study's objectives. While Metaboscape and MS-Dial provide precise matching, LipidScreener offers broader detection and is customizable for specific workflows. With that in mind, LipidScreener may be the most suitable option for our lipidomics research due to its adaptability and ability to capture a broader range of lipid species.

4.3.5. Proof-of-Concept Study on Integrating 2DLC Method with LipidScreener Software

After demonstrating the value of our 2DLC method and comparing our in-house software against more established alternatives, we conducted a small proof-of-concept study. This study aimed to modify our workflow and data processing routine to incorporate this method.

In this study, tissue and serum samples were used. Each sample was extracted as described in Supp. Table 17 and injected into RPLC-MS. Pooled tissue and serum samples were used for quality control and fractionation. The pooled samples used for fractionation were subsequently injected in RPLC-MS along with the other samples.

We chose LipidScreener as the most suitable software for processing the 2DLC-MS datasets because of its adaptability. Minor modifications were made to the original software to allow the alignment of fractionated and non-fractionated samples. These modifications included adjustments to feature filtering and missing value substitution. Usually, we filter out features that are not present in at least 80% of injections in at least one group; this condition was maintained. However, features assigned to a fraction group (*i.e.*, F1, F2, F3, F4, or F5) were only kept if they satisfied the condition in a non-fractionated group. Additionally, features were only considered present in a fraction if present in at least 50% of injections. Furthermore, if a feature was present in multiple fractions simultaneously, it was assigned to the fraction with the highest intensity. Notably, no missing value substitution was performed for fractionated samples to get the raw highest intensity for each fraction.

After that, data processing followed the previously outlined steps of merging and MS/MS annotation. Annotations were then exported to an Excel file, where duplicated annotations were sorted by MS/MS score (highest to smallest) and mass error (lowest to largest). Figure 4.14 shows a summary of all maintained annotations, which were further evaluated based on their assigned fraction. Annotation confidence was assigned as previously described.

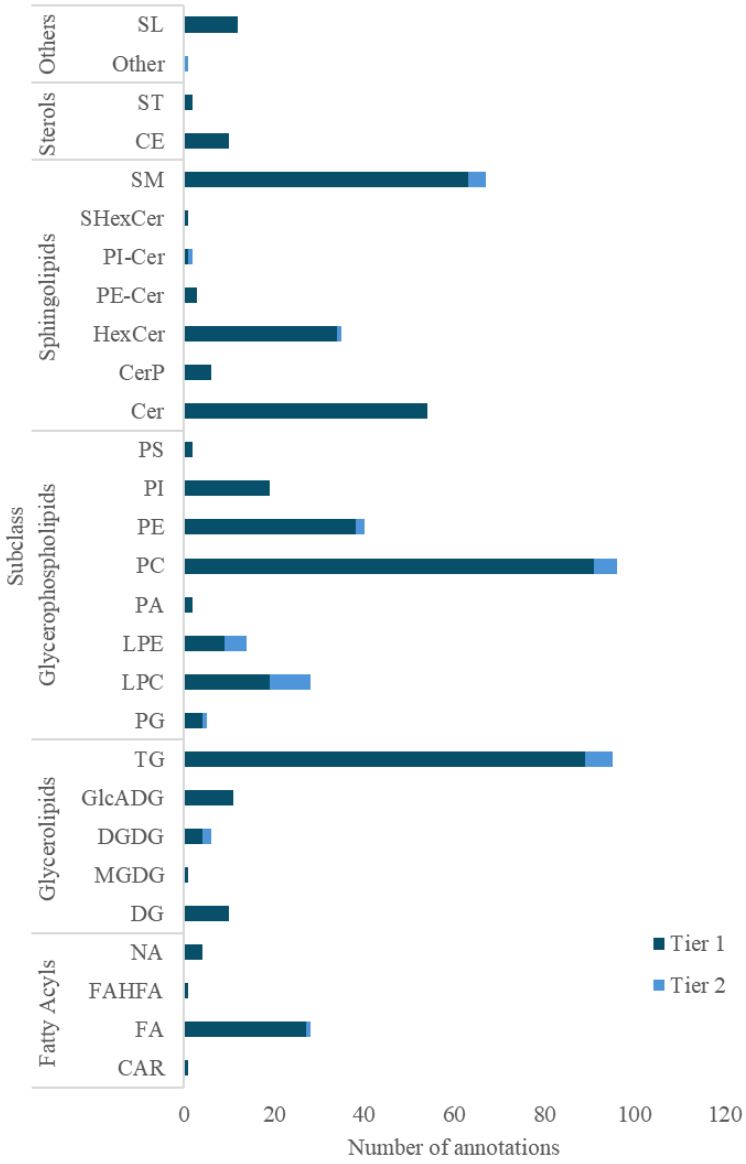

Figure 4.14. Distribution of lipid annotations across lipid subclasses and annotation tiers. Tier 1 annotations were MS/MS matches with scores higher than 500, Tier 2 were MS/MS matches with scores between 100 and 500.

After alignment, 17,474 features were detected following polarity merging, with 11,032 features detected in positive ion mode and 6,442 in negative ion mode. MS/MS annotation yielded a total of 996 annotations. Among these, 179 annotations were duplicated, meaning they appeared

at least twice in our dataset. After filtering out these duplicates and ten contaminant annotations, we were left with 555 MS/MS annotations. Of these, 518 were classified as Tier 1 (MS/MS score > 500), and 37 were classified as Tier 2 (500 > MS/MS score > 100). Of the 15 internal standards in our mix, 14 were detected in at least one ionization mode, with a mass error lower than 3 ppm for positive and 2 ppm for negative ionization. A list of annotations that have been kept can be found in Supp. Table 27.

Figure 4.14 the most common lipid classes detected are TGs, PCs, PEs, and SMs. These findings align with what is typically expected in tissue and serum samples due to their roles in energy storage, transport, and cellular structure [110,175,211,212].

Out of the 555 MS/MS annotations, only eight did not have a fraction assigned to them. This indicates that our samples did not detect these features after fraction collection. One possible reason for this is that, even before fractionation, these peaks were present in low abundance (average intensity of $2x10^4$ or lower, after missing value substitution). Thus, these low-intensity peaks might not have been present enough to be detected because of sample losses after fractionation.

After assigning fractions (F1, F2, F3, F4, F5, or RP for those whose peak was not detected in the fractionated samples) to our MS/MS annotations, we cross-referenced it with our database to correlate lipid subclass to its respective fraction. We used that to determine the annotation confidence for this study. From these 555 annotations, 500, or 90.1%, belonged to a subclass we had previously profiled, which meant we knew which fraction it was expected to elute, and from these 500, 84%, or 418 annotations, were present in the predicted fraction. Figure 4.15 shows how these annotations are distributed across the five fractions.

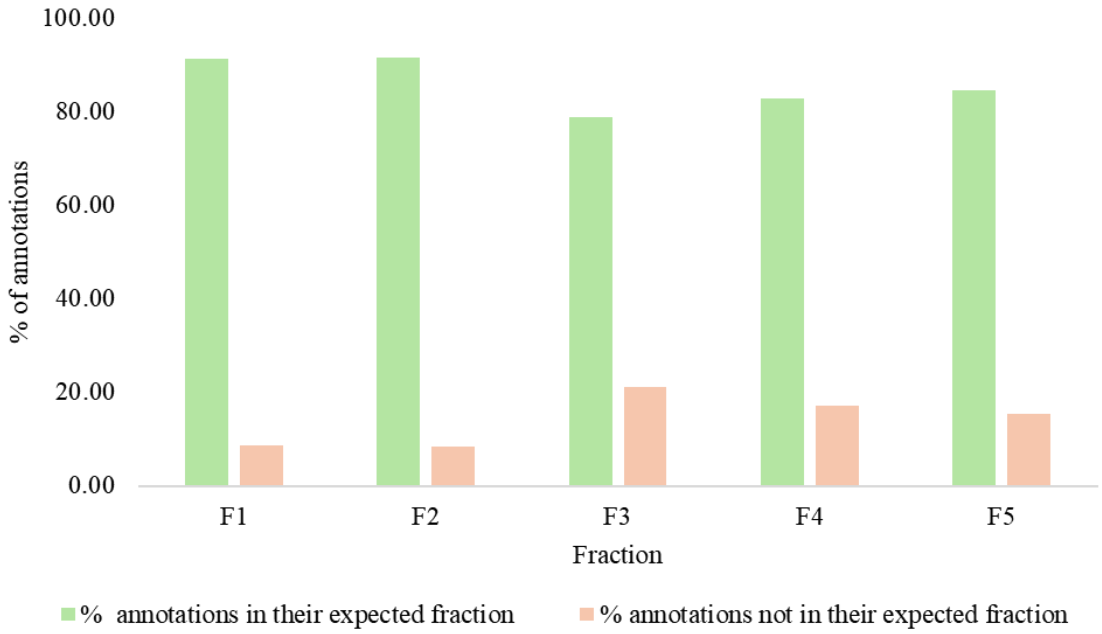

Figure 4.15. Distribution of lipid annotations in their expected fractions (green) versus those not in their expected fractions (orange) across five serum sample fractions. The x-axis represents the five fractions, while the y-axis indicates the percentage of annotations.

Previously, when evaluating our 2DLC method, fractions would be aligned and annotated individually and then combined for annotation accuracy assessment. If we compare the results in Figure 4.10 and Figure 4.15, we can see improvements, especially in fractions 3 and 5. The overall improvement in annotation confidence went from 79% to 84%. However, the improvement is more significant when we evaluate individual fractions. Fractions 2 and 4 had very similar performance in both data processing scenarios, having about the same percentage of annotations not in their expected fraction. However, fraction 1 showed a reduction of 1.7-fold in the annotations, not in their expected fraction, going from 14.8% to 8.6%. Similarly, fraction 3 showed a reduction of 1.5-fold (going from 31.1% to 21.2%), and fraction 5 showed a 2.3-fold (36.1% to 15.4%) reduction. These results indicate that aligning and processing fractionated, and non-fractionation injections

together aid in annotation accuracy since fractions are less susceptible to ion suppression and, therefore, might generate a better fragmentation spectrum for our peaks, improving MS/MS annotation[83,102].

4.4. Conclusions

We developed and optimized herein an offline two-dimensional liquid chromatography-mass spectrometry (2DLC-MS) method for untargeted lipidomics of biological samples. By fine-tuning the HILIC separation method and integrating it with RPLC-MS, we established a robust analytical framework that enhances lipid detection and addresses inherent challenges posed by the complexity of biological samples, such as coelutions and ion suppression. The offline 2DLC fractionation approach successfully reduced ion suppression and co-elution among lipid classes, simplifying sample complexity and significantly improving the accuracy of lipid subclass determination.

The comparative analysis of lipid annotation across different data processing software - Metaboscape, MS-Dial, and LipidScreener – confirms the role of data processing and annotation tools in enhancing annotation reliability in lipidomic studies. More importantly, it shows the importance of future research about annotation algorithms to generate more reliable results across different laboratories and data processing routines; this highlights that lipidomics is an evolving research field, indicating a need for further research.

Developing and optimizing the method herein is an important step in lipidomic analyses to evaluate and improve annotation accuracy. By addressing previous challenges, such as sample dilution, ion suppression, and broad peak shapes, our study may guide future research to unravel

the complexity of lipids in biological systems, such as disease biomarkers. However, it would be significantly more time-consuming, considering all the involved steps (first-dimension separation, drying, and second-dimension separation) to perform this method for all samples. Therefore, instead of making every sample go through the whole process, we perform the 2DLC analysis only on the extra pooled samples. This would give us all the RPLC-MS peaks and fragmentation patterns, in addition to the ones unveiled by 2DLC-MS.

Previous studies have explored the improvement in lipid annotation by reducing sample complexity using a 2DLC method. Although our study shares some similarities with other previously conducted assessments, ours focuses less on increasing lipid detectability and more on annotation accuracy. Although increasing detectability is important, as shown herein, improving lipidomics methods to generate consistent and accurate results should be the priority, as both higher detectability and accuracy are required for future biomarker and therapeutical studies.

V

Chapter V: Instrument and Column Inner Diameter Effects on LC-MS Lipidomics: Quadrupole Time-of-Flight MS vs. Orbitrap MS

5.1. Introduction

Lipidomics aims to study lipids in biological systems to understand cellular functions and disease pathways, as well as aid in biomarker discovery[2,38]. Lipid molecules maintain cell membrane integrity, mediate signaling processes, and serve as energy reservoirs. Because of their diverse roles in biological systems, accurate and sensitive lipid profiling is vital for advancing knowledge on health and disease[1,103,213]. However, lipid profiling can be challenging due to the low abundance and diverse chemical structures, requiring more sensitive techniques[9,24,70,102,132].

Advances in Mass Spectrometry (MS) and Liquid Chromatography (LC) technologies, particularly high-resolution instruments such as Orbitrap-MS and Quadruple time-of-flight (QToF-MS) and smaller inner diameter (ID) LC columns, have shown a significant potential for enhanced analyses of small molecules[71,81,213–217]. QToF-MS has been extensively used for targeted and untargeted lipidomics and metabolomic studies due to its sensitivity and data acquisition rates, which make it suitable for high-throughput analyses. Furthermore, QToFs are known to be robust and cost-effective instruments, with resolutions ranging from 30,000 to 60,000, making them appropriate for most applications[14,102,106].

On the other hand, Orbitrap-MS can provide superior sensitivity and resolution; depending on the instrument of choice, the resolution can reach 360,000, which is essential for accurately

profiling lipids. These features allow the detection of low-abundance lipid species and the differentiation of isomeric and isobaric species, which are common in lipid sampels[102,106,108]. The high mass accuracy displayed by Orbitrap instruments also improves the reliability of the data, reducing the chances of missannotation. Additionally, Orbitrap's high dynamic range allows the detection of a wide range of lipid molecules, from very low to very high abundant species, which is essential for comprehensive lipidomics studies and a better understanding of lipid pathways in diseases[71,102,106,107].

Another challenge in lipidomic studies comprises lipid separation. Finding a suitable balance between analysis time and separation remains challenging in LC-MS-based lipidomics. Different studies have proposed separation gradients lasting from 20 to 60 minutes to achieve optimum separation[5,102,108,218]. However, extended runs are not practical for high-throughput analysis. A significant part of the lipidomics work has been conducted using at least a 2.1 mm ID column[69,78,108,219]. However, studies have shown the advantages of using columns with smaller IDs, such as 1 mm ID or even nanoLC columns, making them a promising alternative for improvement[102,220–222].

Smaller ID columns, such as 1 mm, enhance the sensitivity and resolution of the analysis by reducing band broadening. This leads to sharper peaks and better separation than their 2.1 mm counterparts[221,222]. These improvements can be significant in studies aiming to detect subtle changes in the lipidome or low-abundant species. Additionally, 1 mm ID columns require less solvent, making the method more cost-effective and environmentally friendly. However, some disadvantages are also noted. Smaller columns are more likely to clog and often have lower sample loading capacity, which might limit their use in applications requiring larger sample volumes.

Despite these challenges, the benefits of increased sensitivity and resolution make 1 mm ID columns a valuable tool in advancing lipidomic analyses, particularly in high-throughput settings where quick and efficient separation is crucial[215–217,221–224].

With this in mind, this study aims to improve lipidomic analysis and workflows. First, a UHPLC method for the Orbitrap-MS was adapted, and its performance compared with the QToF-MS. This involves optimizing ion source parameters and evaluating the performance in terms of sensitivity, resolution, and the ability to detect and quantify lipid species. Second, develop and optimize a UHPLC method using a 1 mm ID column and compare it with the traditional 2.1 mm ID column. This comparison will assess how the smaller column affects lipid separation, sensitivity, and resolution. These efforts aim to improve lipid detection and quantification accuracy, a crucial step for better understanding the role of lipid molecules in biological processes and disease states.

5.2. Experimental

5.2.1. Reagents and Equipment

A standard mixture containing 15 deuterated lipids from various subclasses was purchased from NovaMT (LipidRep Internal Standard Basic Mix Serum/Plasma, Nova Medical Testing, Edmonton, AB, Canada. Human serum samples, LC-MS-grade water (H2O), and isopropanol (IPA) were purchased from Sigma-Aldrich (St. Louis, Missouri, USA). LC-MS-grade acetonitrile (ACN), methanol (MeOH), dichloromethane (DCM), and ammonium formate (mass spectrometry grade) were obtained from Honeywell (Charlotte, North Carolina, USA).

Chicken liver tissue samples were bought from a local supermarket, subdivided into aliquots, and placed into 2 mL sterile polypropylene tubes for long-term storage at -80 ºC. Sample homogenization was performed using a Bioprep-24 Homogenizer (Bio-Equip) with ceramic beads.

5.2.2. Instrumentation

The UHPLC experiments described herein were performed under three different settings: (1) a Dionex 3000 system (Thermo Fisher Scientific, Waltham, MA, USA) with a Waters Acquity CSH Premier C18 column (1.7 µm, 2.1×100mm, Waters Corporation, Milford, MA, USA) coupled to a MaXis II ESI QqToF (Bruker Daltonics, Billerica, MA, USA); (2) a Vanquish Duo system (Thermo Fisher Scientific, Waltham, MA, USA) with a Waters Acquity CSH Premier C18 column coupled to a H-ESI Orbitrap Exploris 240 (Thermo Fisher Scientific, Waltham, MA, USA); and (3) a Vanquish Neo system (Thermo Fisher Scientific, Waltham, MA, USA) with a Waters Acquity CSH C18 column (1.7 µm, 1.0×100mm, Waters Corporation, Milford, MA, USA) coupled to a H-ESI Orbitrap Exploris 240.

5.2.3. Orbitrap Method Optimization

An Orbitrap mass spectrometer initially operated with the manufacturer's default ion source parameters, outlined in

Table 5.1. LC conditions followed those from previous works with a 16-minute gradient separation followed by a 4-minute re-equilibration. The separation flow rate was 0.300 mL/min from 0 to 9.3 minutes, reduced to 0.270 mL/min from 9.3 to 10.1 minutes, and kept at 0.210 mL/min

from 10.1 min to the end of the run, with column temperature at 45 °C throughout. The initial conditions were 15% MPB, and the gradient progressed as follows: 0.5 min at 15% MPB, 2.3 min at 25% MPB, 9.3 min at 42% MPB, 10.1 min at 78% MPB, 12 min at 90% MPB, 13 min at 98% MPB, and held at 98% MPB until 14.5 min, then returned to 15% MPB by 15 min. The mobile phase composition used in this work was MPA - 10 mM ammonium formate in 50:40:10 MeOH/ACN/H_2O and MPB - 10 mM ammonium formate in 95:5 IPA/H_2O[108]. After obtaining preliminary results, optimizing the ion source parameters was proposed to enhance the signal intensity and improve peak shape (

Table 5.1). We compared our optimized ion source parameters with those used in the QToF and other published works using Orbitrap[103,225].

Table 5.1. Ion source parameters used for the H-ESI Orbitrap Exploris 240, using manufacturers' default and optimized parameters.

	Default parameters	Optimized parameters
Positive ion voltage (V)	3400	4000
Negative Ion voltage (V)	2300	3500
Sheath Gas (Arb)	3	60
Aux Gas (Arb)	2	15
Sweep Gas (Arb)	0	1
Ion Transfer Tuber Temp. (ºC)	320	300

Vaporizer Temp. (ºC)	0	250

5.2.4. Sample Preparation

Serum and tissue samples were extracted using a modified Folch liquid-liquid extraction (LLE) method[72,110]. A 40-sample/solvent ratio (µL/mL) was used for serum samples, and a 200-sample/solvent ratio (mg/mL) was used for tissue samples. Solvent ratios used in the Folch method were maintained (8:4:3 DCM/MeOH/H_2O). However, chloroform was replaced by DCM to reduce carcinogenic risks and costs. The sample and internal standards mixture was vortexed sequentially for 20 seconds with each solvent (MeOH, DCM, H_2O) before equilibration at room temperature (20-23ºC) for 10 minutes and centrifugation at 12,000 pm and 4 ºC for 10 minutes. An aliquot of the organic phase was dried under a gentle nitrogen flow (10 minutes at room temperature) before the lipid extract was resuspended in 8:2 MPA/MPB. Serum samples used a 40-sample/solvent ratio (µL/mL), and tissue samples used a 200-sample/solvent ratio (mg/mL).

To avoid lipid degradation, samples were stored inside the autosampler at 8ºC for at least 4 hours (to allow equilibration) and 24 hours before LC-MS analysis. All samples were placed in polypropylene inserts inside with PTFE/silicone septa.

5.2.5. LC-MS Analysis and Data Processing

To compare LC-QTOF-MS and LC-Orbitrap-MS for lipidomics, we evaluated the acquired data based on 1) the number of detected features and 2) the number of MS/MS annotations. Moreover, comparisons regarding sensitivity, resolution, and overall analytical capabilities aimed

to identify the strengths and weaknesses of each instrument in the context of our specific experimental requirements.

In both cases, LC separation followed the gradient mentioned herein. The ion source parameters used for the LC-Orbitrap-MS were optimized, as shown in Table 5.1. For Orbitrap-MS, in addition to the ion source parameters, full scans were performed with an orbitrap resolution of 240,000, an m/z range of 150 to 1500 Da, and an RF lens set to 90%, with a maximum injection time of 60 ms and micro scans set to 2.

MS/MS data acquisition employed a resolution of 45000, an isolation window of 1.5 m/z, and a cycle of 5 scans. Dynamic exclusion was used for acquisition, excluding precursors after being detected three consecutive times, with a duration of 5 seconds and a mass tolerance of 10 ppm. Collision energies varied according to the precursor m/z values between 20 and 35 eV.

For the QTOF-MS, ion source parameters were set at 4000 V and 4500 V for positive and negative ion modes, respectively, with an endplate offset of 500 V; nebulizer gas pressure of 1.2 bar, dry gas flow rate of 5.0 L min-1; dry temperature of 240 °C, spectra acquisition rate of 1.44 Hz; and m/z range from 150 to 1500 Da. A 1.0 mM sodium formate calibrant solution in 1:1 IPA/H2O (v/v) was infused at the end of each chromatogram to ensure mass re-calibration and mass accuracy.

For MS/MS data acquisition, the auto-MS/MS feature (oToF Control, Bruker Daltonics) was utilized. The cycle time was set to 1.2 seconds, with active exclusion of precursors detected for more than three consecutive spectra within 0.50-minute intervals. For low-intensity precursor ions (below 500 counts), an acquisition rate of 0.5 Hz was used, whereas 2.0 Hz was used for high-

intensity precursor ions (above 500,000 counts). Collision energies ranged between 20 and 30 eV depending on the precursor m/z values.

For both instruments, samples were analyzed separately in the positive and negative ionization modes, using 3 µL and 12 µL of the lipid extracts, respectively.

The acquired data was processed using an in-house-developed Python-based software called LipidScreener, designed explicitly for lipidomics workflows used by The Metabolomics Innovation Centre (TMIC, Edmonton, Canada). QTOF-MS chromatograms from positive and negative ionization were aligned using a minimum intensity cut-off of 3,000 counts. In contrast, Orbitrap-MS chromatograms were aligned using a minimum intensity of 150,000 counts. The minimum peak length for both datasets was six spectra, and oligomers and multiple adducts were managed within a 20-ppm m/z tolerance. After alignment, features were filtered out if they were not present in at least 80% of injections in one group before merging the positive and negative ionization data.

LipidScreener can perform MS/MS annotations by comparing acquired MS/MS spectra with established libraries, such as MS-Dial LipidBlast library (https://fiehnlab.ucdavis.edu/projects/LipidBlast), the Human Metabolome Database (https://hmdb.ca), and the MassBank of North America LC−MS/MS (https://mona.fiehnlab.ucdavis.edu). For matching, I used a 5 and 10 mDa m/z tolerance for the precursor ion and fragments, respectively, along with a minimum similarity spectra of 40%. After annotation, filtering parameters (possible adducts, m/z error, the ratio of carbon to double bond present in the molecule, even or odd fatty acyl chains, structural modifications, and presence of plasmenyl) were applied to

all annotated features to ensure accurate and reliable lipid annotation[14,36,110,183–187]. Mass match annotations were not assessed for the practices described in this chapter.

5.2.6. Optimization of a Micro LC-MS Method Using a 1mm Inner Diameter Column

Next, the effect of the column's inner diameter on lipidomics assessments was verified by adapting the LC-MS gradient separation to a 1 mm I.D. column. The initial method was adapted from the previously described procedure, although employing lower flow rates due to backpressure constraints. Briefly, A 37-minute gradient was used for separation (0 min, 10% MPB; 1 min, 10% MPB; 4 min, 30% MPB; 15 min, 40% MPB; 20 min, 60% MPB; 24.8 min, 60% MPB; 25.8 min, 93% MPB; 32.8 min, 98% MPB; 35.8 min, 98% MPB; 37 min, 15% MPB), starting with a flow rate of 90 µL/min, decreasing to 30 µL/min throughout the run. The column was maintained at 45 ºC, and separation was followed by a 5-minute re-equilibration segment at 15% MPB, with a 90 µL/min flow rate. Mobile phase compositions were MPA - 10 mM ammonium formate in 50:40:10 MeOH/ACN/H_2O and MPB - 10 mM ammonium formate in 95:5 IPA/H_2O.

Mobile phase compositions, flow rates, column temperature, and gradient separation were fully optimized. Optimal conditions were selected based on peak intensity, visual chromatographic separation, and run time, which resulted in a 21.6-minute gradient separation (0 min, 15% MPB; 2 min, 30% MPB; 4.5 min, 37% MPB; 8.8 min, 48% MPB; 12.7 min, 53% MPB; 12.8 min, 53% MPB; 14.8 min, 75% MPB; 17.8 min, 93% MPB; 19.3 min, 98% MPB; 20.4 min, 98% MPB; 21.6 min, 15% MPB), using a flow rate of 50 µL/min, decreasing to 30 µL/min at 12.8 minutes until the end of the run. Separation was followed by a 2.4-minute re-equilibration segment at 15% MPB, with a 50 µL/min flow rate, and the column was kept at 55 ºC. Mobile phase compositions were

MPA - 10 mM ammonium formate in 40:40:20 MeOH/ACN/H_2O and MPB - 10 mM ammonium formate in 95:5 IPA/H_2O. After optimization, the 1 mm ID LC-MS method was compared to the 2.1 mm ID LC-MS method described in the previous section.

5.3. Results and Discussions

5.3.1. Ion Source Parameter Optimization for Orbitrap Exploris 240

To test ion source parameters for the Orbitrap, the LipidRep IS mix was prepared in the same way it was analyzed in the Bruker QToF. The IS mix injection resulted in low-intensity and poorly defined peak shapes (Figure 5.1.a). To optimize these parameters, Orbitrap's ion source default parameters were compared with those from the QToF and some lipidomics studies using the Orbitrap instrument[110,225]. Different conditions (Figure D.1) were tested before choosing the optimum ion source conditions for these experiments, which were selected based on signal intensity, visual peak separation, and peak shapes displayed in Figure 5.1.b.

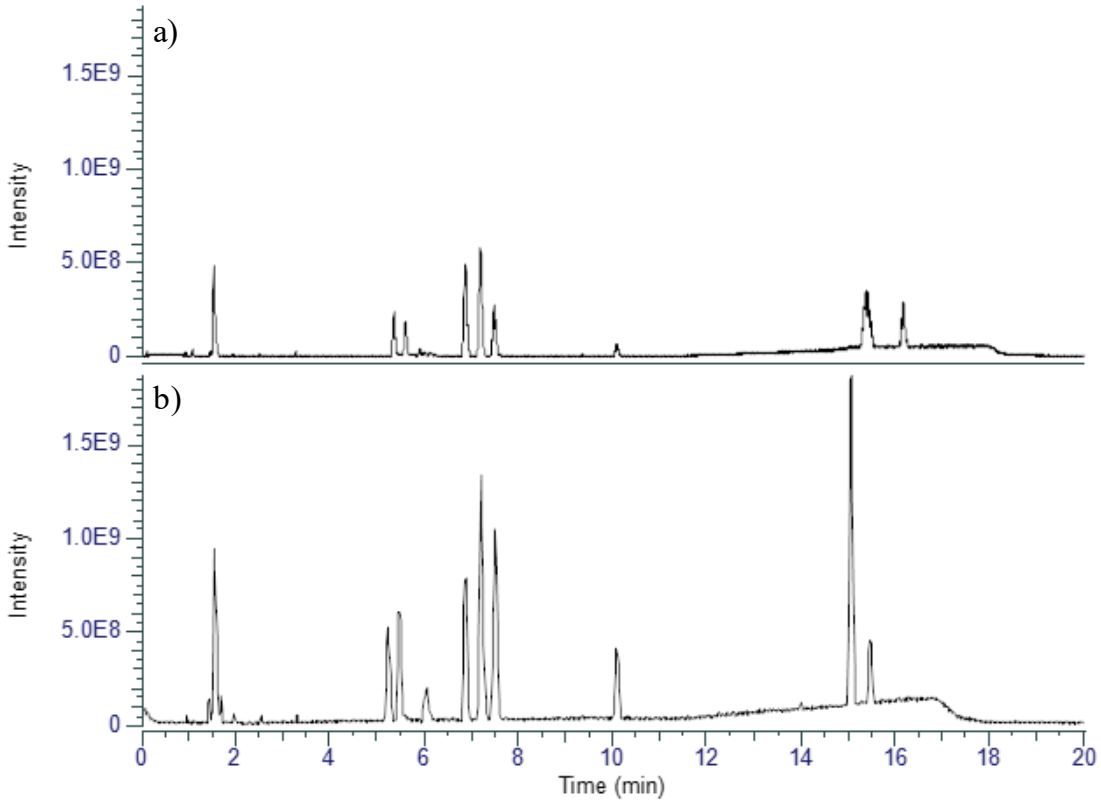

Figure 5.1. Base Peak Chromatograms (BPC) for LipidRep Basic Standard Mix for Tissue used to optimize the ion source parameter optimization a) Orbitrap's default ion source parameters (Spray Voltage: 3400 V on positive and 2300 on negative; Sheath Gas: 3 Arb; Aux Gas: 2 Arb; Sweep Gas: 0 Arb; Ion Transfer Tube Temp.: 320 ºC; Vaporizer Temp.: 0 ºC); b) Optimized parameters (Spray Voltage: 4000 V on positive and 4500 on negative; Sheath Gas: 60 Arb; Aux Gas: 15 Arb; Sweep Gas: 1 Arb; Ion Transfer Tube Temp.: 300 ºC; Vaporizer Temp.: 250 ºC).

As shown in Figure 5.1, optimizing the Orbitrap's ion source parameters led to significant improvement. When comparing Figure 5.1.a and Figure 5.1.b, the signal intensity significantly improved, with increases ranging from 2 to 9 fold. For example, the intensities of the LPC and PC peaks increased from 4.5E8 to 9.0E8 and 5.85E8 to 1.34E9, respectively, representing a 2-fold increase. The peak for TG displayed a 5-fold intensity increase from 3.5E8 to 1.88E9. The

improvement was even more significant for low-abundance peaks, with the intensity of PA increasing from 2.21E7 to 2.04E8, representing a 9.2-fold increase in intensity.

Furthermore, the optimization also yielded an improved signal-to-noise (s/n) ratio, resulting in more well-defined chromatographic peaks. This enhancement in the s/n ratio facilitates more accurate and reliable annotation of lipid species by reducing the background noise that can obscure small peaks. Thirdly, the optimization reduced in-source fragmentation, as indicated by the chromatogram's sharper and more well-defined peaks. Moreover, the CE standard in our mix is subjected to in-source fragmentation, shown by the m/z 372.37 (m/z for ST) being detected at the same retention time as m/z 671.65 (CE main m/z). By optimizing the ion source parameters, in-source fragmentation was reduced to similar levels as previously observed in the QToF (Figure D.2).

The improved detectability of low-abundance internal standards (*i.e.*, PA, PS, and ST) showcases that optimizing the ion source's parameters is crucial for accurate lipidomic analysis. The improved intensity and better-defined peak shapes enhance the robustness of the analytical method, ensuring consistent and reliable results across different samples. These low-abundance lipid classes play roles in cellular membrane function, signaling, and energy storage; therefore, detecting them can be crucial for understanding biological changes in the organism and profiling health and disease. These optimizations contribute to more sensitive and accurate lipidomic profiling, paving the way for future studies that require high-quality data, such as biomarker discovery and the understanding of lipid-related biological processes[9,78,81,125,213].

Orbitrap source parameters vary widely across lipidomics studies depending on the specific lipid class being analyzed and the experimental conditions. For instance, some studies may favor

higher sheath and auxiliary gas flow rates to enhance ionization efficiency for certain lipid species. In contrast, others may optimize ion transfer temperatures or spray voltages to improve the detection of low-abundance lipids. These variations highlight the need for customized optimization to achieve the most accurate and sensitive results for specific lipidomic applications[79,107,226,227].

After optimizing the Orbitrap's ion source parameters, its performance was compared to that of the QToF for lipidomic analysis of biological samples. For both instruments, 3 µL and 12 µL of serum and tissue extracts were injected on positive and negative ionization, respectively. Both instruments were coupled to the same column, following the same gradient separation. A pooled sample of serum and tissue was prepared by mixing equal volumes of all samples, and it was used for quality control (QC samples). Figure 5.2 shows the acquired chromatograms for the MaXis QToF, and Figure 5.3 shows the chromatograms acquired for the Orbitrap Exploris 240.

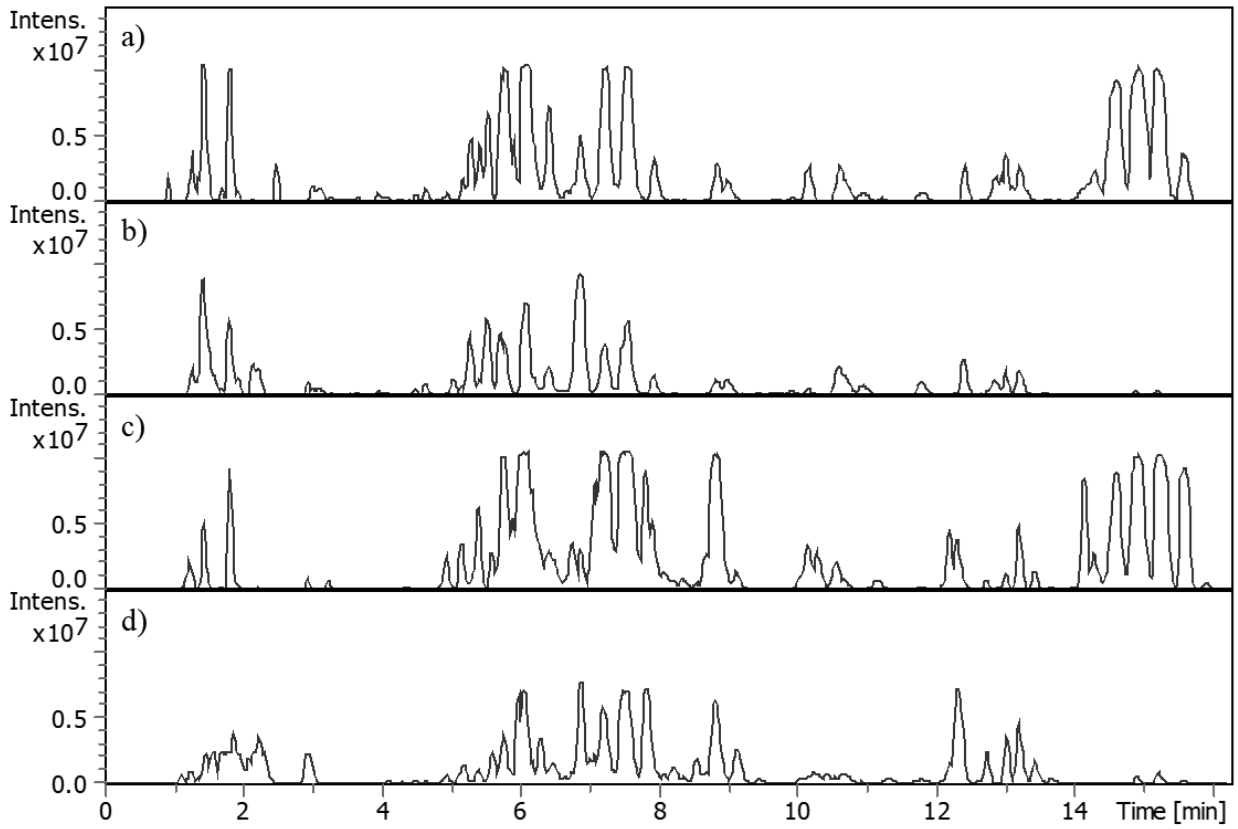

Figure 5.2. Base Peak Chromatograms (BPC) for serum and tissue samples was injected on a Dionex 3000 system with a Waters Acquity CSH Premier C18 column coupled to a MaXis II ESI QToF-MS, with injection volumes of 3 and 12 µL for positive and negative ionization, respectively. A) Positive ionization chromatogram for serum samples; b) Negative ionization chromatogram serum samples; c) positive ionization chromatogram tissue samples; d) negative ionization chromatogram tissue

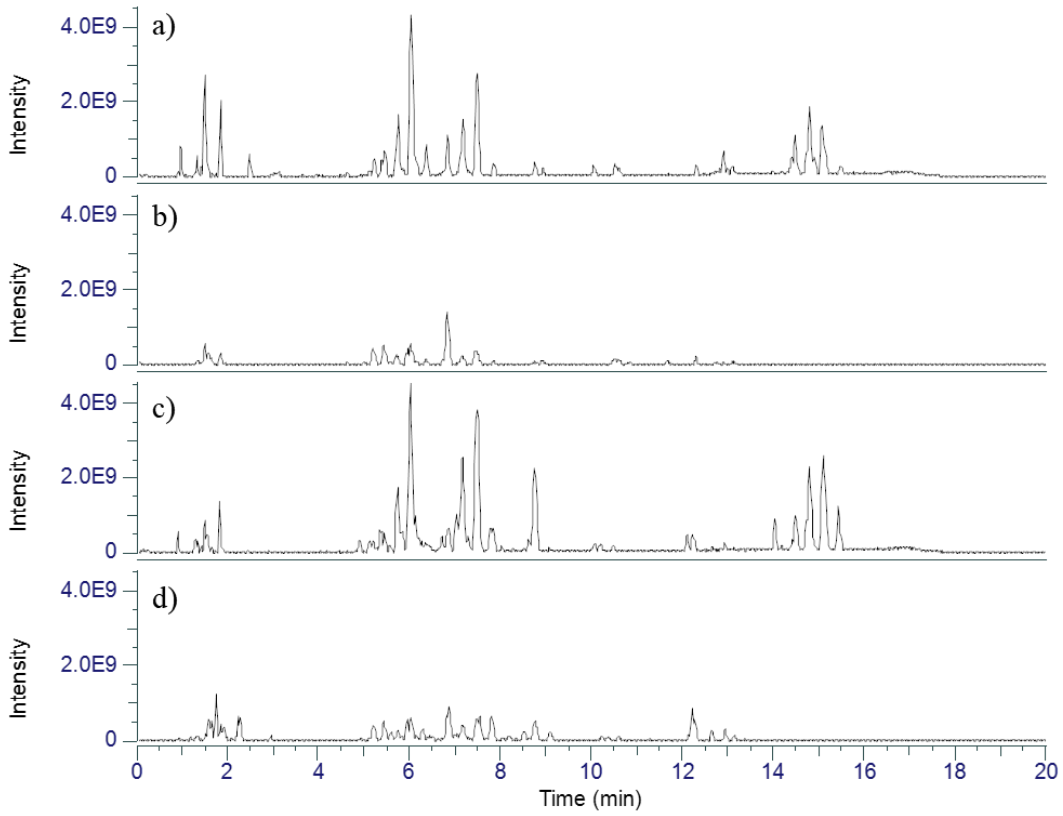

Figure 5.3. Base Peak Chromatograms (BPC) for serum and tissue samples injected on Vanquish Duo with a Waters Acquity CSH Premier C18 column coupled to an H-ESI Orbitrap Exploris 240, with injection volumes of 4 and 12 µL for positive and negative ionization, respectively. a) Positive ionization chromatogram for serum samples; b) negative ionization chromatogram for serum samples; c) positive ionization chromatogram for tissue samples; d) negative ionization chromatogram for tissue samples.

Some key points should be highlighted when comparing the data acquired by both instruments. The baseline for QToF is around 1 x10^4 in positive ionization, whereas in the Orbitrap, it is 4x10^7. One reason for this observed difference is the distinct detection methods used. Orbitrap uses image current detection, which is inherently more sensitive and thus more prone to higher baseline noise. In contrast, the QToF uses a microchannel plate detector, typically resulting in lower baseline levels[107,228].

The detectors in the Bruker QToF saturate at 1 x10^7 when peaks start to plateau and lose their Gaussian shape, as shown in Figure 5.2. On the other hand, Orbitrap instruments do not show the same saturation profile, partially because of their detection system; however, peaks are considered saturated at 1 x10^{10} [107,228]. Moreover, because Orbitrap peaks are sharper and narrower, it helps in peak picking and data alignment[119,120]. Both instruments detected similar features, with QToF data yielding 14,373 and Orbitrap 15,487 features. Considering the same injection volume was used for analysis in both instruments, the ratio between the number of detected features and the amount (in µL) injected is 7% (Figure 5.4). At first, this might not seem significant, although it highlights the higher sensitivity of Orbitrap systems[106].

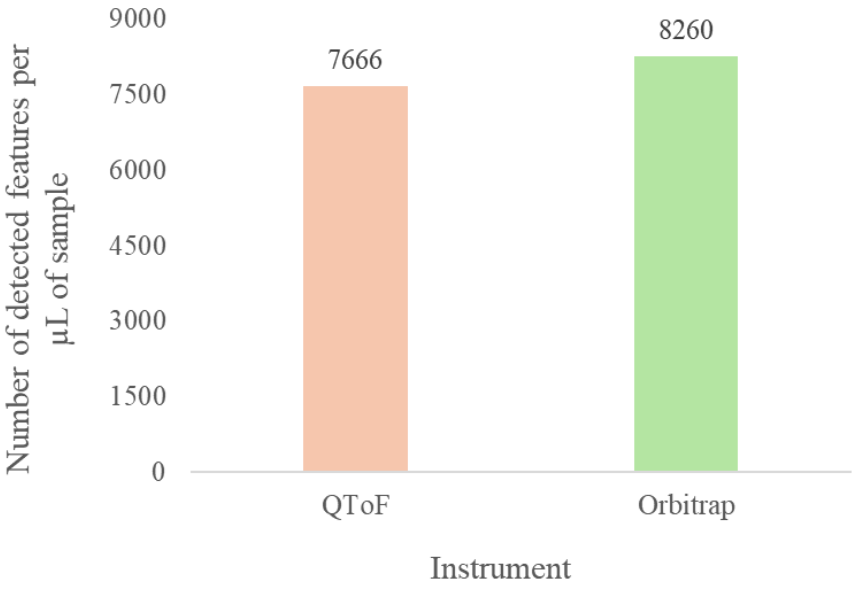

Figure 5.4. The number of detected features detected in QToF and Orbitrap normalized by the amount of raw samples injected (*i.e.*, 2 µL for Orbitrap samples and 1.88 µL for QToF samples).

Evaluating how many of the detected features were MS/MS and how many are MS features can bring further insights into instrument performance, which can help select the instrument that might be more suitable for our applications. Of the 15487 features detected for Orbitrap data, 11983 were MS/MS features, meaning 77% of the detected features can be used for MS/MS annotation. On the other hand, out of the 14373 features detected for QToF, only 18% (or 2790 features) were MS/MS features (Figure D.3). This indicates that, although both instruments yield a similar number of features, Orbitrap can be more suited for studies that require higher annotation confidence results, such as biomarker discovery[102,117,120]. Furthermore, since the Orbitrap was operating at a superior resolution (240k) than QToF (60K), this may have contributed to detecting and distinguishing between closely related ion peaks[106].

After observing the difference in the number of detected MS/MS features, the next step of the data evaluation involved looking at the annotated features. For the QToF dataset, 823 lipid species were annotated by MS/MS match. At the same time, 1,252 annotations were found for the Orbitrap MS/MS features, representing a 1.5-fold increase in both cases with m/z errors lower than 5 ppm (Figure D.*4.* Figure D.4). All annotated features for QToF and Orbitrap can be found in Supp. Table 28 and Supp. Table 29, respectively. Moreover, of all QToF annotations, only 527, or 64%, were also present in the Orbitrap dataset. In contrast, the remaining 296 annotations were uniquely annotated in QToF, as shown in the Venn diagram in Figure 5.5. One possible reason for this discrepancy is that in the QToF data, some peaks, especially in the middle region of the chromatogram, were broad and saturated (Figure 5.2), whereas this was not the case for Orbitrap data (Figure 5.3), resulting in less ion suppression and, consequently, not only more but different annotations[11,184,229]. Furthermore, since Orbitrap-MS was being operated in a higher resolution than

the QToF, it could differentiate between some peaks with similar m/z[106]. The subclass lipid distribution of all annotated features for both QToF and Orbitrap-MS are shown in Figure D.5.

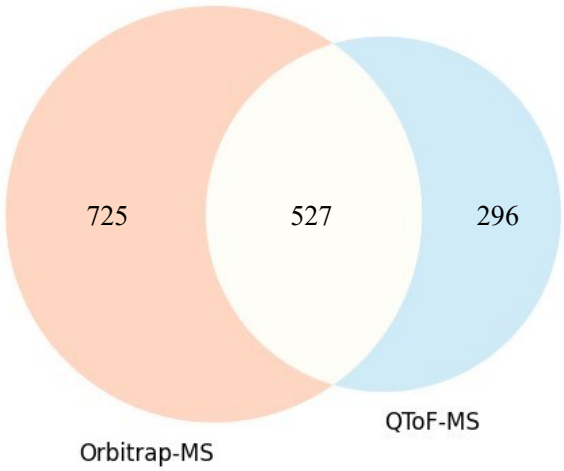

Figure 5.5. Venn diagram displaying unique and shared MS/MS annotated lipid species in Orbitrap-MS and QToF-MS. The central intersection represents lipids annotated by both instruments, and the outer sections denote the number of unique annotations made by each instrument.

The choice of instrument significantly impacts study outcomes in lipidomics. Orbitrap's higher sensitivity and resolution make it more suitable for comprehensive lipidomics studies, offering a more detailed lipid profile. However, QToF remains more accessible and cost-effective for some applications. As demonstrated in this study, the choice of instrument can lead to different outcomes, with Orbitrap providing more in-depth insights into the lipid profile of the samples.

The comparison between QToF and Orbitrap instruments demonstrates each platform's advantages and trade-offs for lipidomic analysis. While QToF provides faster data acquisition rates and is more cost-effective, Orbitrap's higher sensitivity and resolution make it more suitable for comprehensive lipidomics, particularly for detecting low-abundance lipids. In this study, the

Orbitrap's enhanced performance resulted in improved peak shapes, higher intensities, and a greater number of MS/MS features, contributing to annotating a broader range of lipid species. Moreover, Orbitrap's superior resolution allows for better separation of isobaric and closely related ion species, making it a powerful tool for untargeted lipidomics where precision is important.

5.3.2. Effect of Column Inner Diameter in Lipidomic Analysis

Considering the higher number of annotated features yielded by Orbitrap-MS, future studies were conducted using it instead of QToF-MS, aiming to increase the number of detected features, mass accuracy, and annotated species. However, aiming to improve separation efficiency and increase sensitivity, I decided to adapt the UHPLC method described herein to an LC column with a smaller inner diameter[222].

To successfully adapt the UHPLC previously described to the column with a smaller inner diameter, some separation conditions, besides the gradient, had to be optimized. The original method described herein employed a column oven temperature of 45 ºC. However, as it can be observed in Figure 5.6.a this leads to broad peaks. Lipidomic studies have used temperatures ranging from 40 ºC to 65 ºC. Therefore, different temperatures were tested to see how this would affect peak shape and separation. Figure 5.6 displays the chromatograms acquired for each tested temperature.

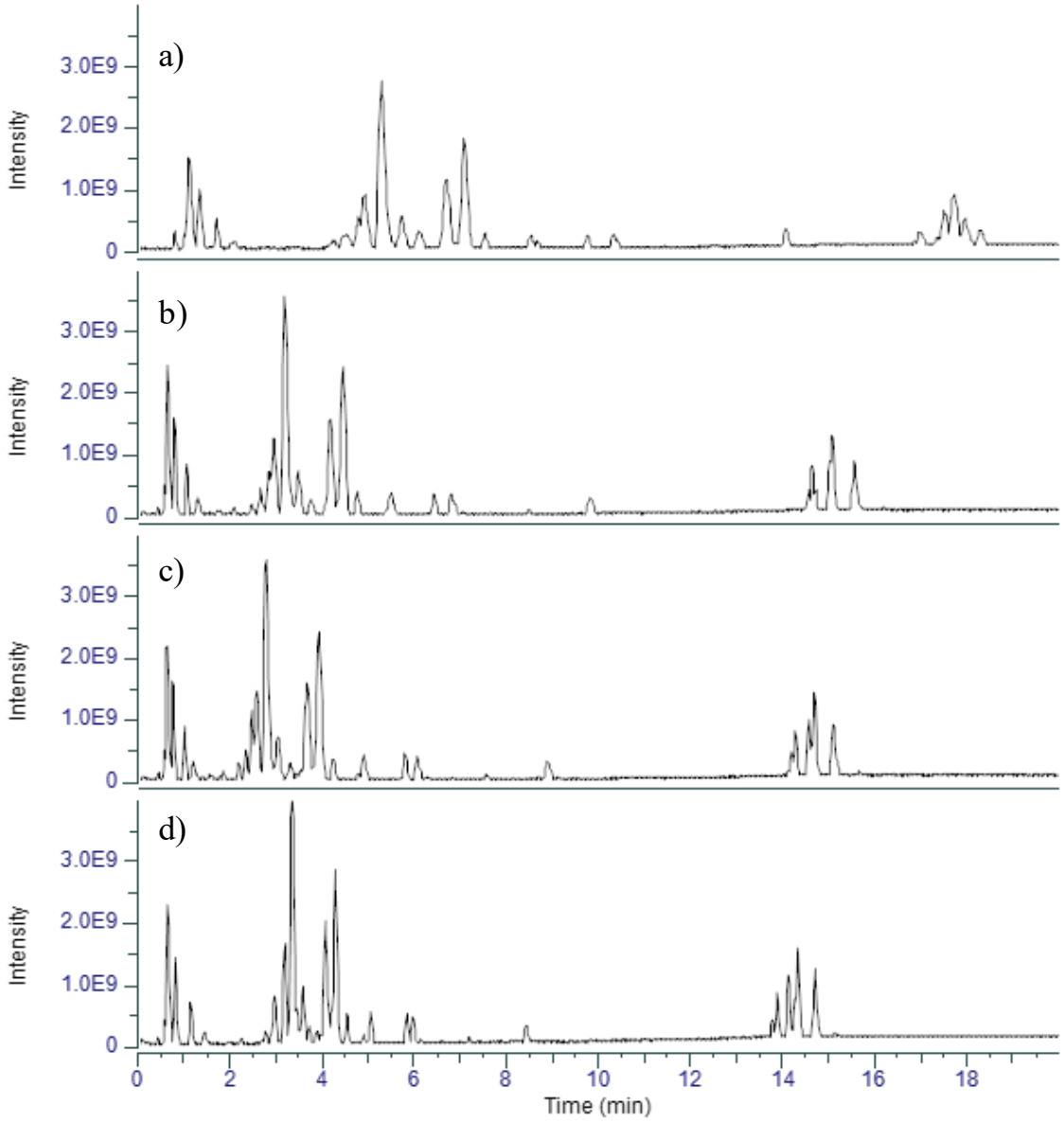

Figure 5.6. Base Peak Chromatograms (BPC) for Serum samples acquired using MPA - 10mM ammonium formate in 50:40:10 MeOH/ACN/H_2O and MPB - 10mM ammonium formate in 95:5 IPA/H_2O; 16-minute gradient (0 min – 15% MPB, 0.5 min – 15% MPB, 2.3 min – 25% MPB, 9.3 min – 42% MPB, 10.1 min – 78% MPB, 12 min – 90% MPB, 13 min – 98% MPB, 14.5 min – 98% MPB, 15 min – 15% MPB); 4 min equilibration (15% MPB); with flow rate starting at 100 µL/min until 10.1 min, reducing it to 80 µL/min from 10.1 to 14.5 µL/min and further reducing it to 50 µL/min until the end of the run. a) Column oven at 45 ºC; b) Column oven at 50 ºC; c) Column oven at 55 ºC; d) Column oven at 60 ºC.

Figure 5.6 indicates that the increase in temperature led to peak shape improvement, as all conditions show narrower and sharper peaks than the starting condition. Analyzing the chromatograms, the optimum column temperature of 55 ºC was selected based on peak shape and separation (Figure 5.6.e). However, lipid molecules are prone to degradation under increased temperatures. Therefore, potential oxidation or sample degradation would be a concern[78,102]. Although there are some differences in chromatographic separation between Figure 5.6.c and Figure 5.6.d, a column oven temperature of 55 ºC still significantly improves separation while being softer, reducing the risk of sample degradation. This careful consideration of potential issues ensures that the proposed modifications are not only beneficial but also reliable.

With the change in column oven temperature, analytes displayed a reduced retention time, causing hydrophilic lipid species, such as LPC, LPE, FA, and MG, to elute between 0.5 and 2 minutes. Although there was a separation among peaks, most eluted before 6 minutes, indicating that the separation conditions were not optimum. To improve analyte retention and interaction with the stationary phase, we proposed modifying MPA from 10mM ammonium formate in 50:40:10 MeOH/ACN/H2O to 10mM ammonium formate in 40:40:20 MeOH/ACN/H2O, making it more hydrophilic (Figure D.6). This modification increased peak intensities and improved the separation of hydrophilic and phospholipid peaks, which eluted in longer retention times. Hydrophobic lipids (TGs and CEs) also showed improved separation, higher intensities, and peak shapes. Although this increased the run time from 16 to 20 minutes, the overall improvement in separation, peak shapes, and reduced ion suppression made this a valuable optimization[230].

Different studies have demonstrated the effects of temperature on chromatographic separation and LC-MS analysis, such as Lenčo *et al.* (2021). Using slightly more elevated column

oven temperatures improves lipid separation, leading to more accurate lipidomic profiling and more reliable applications in clinical diagnostics and biomarker discovery[108,230,231]. Comparing these results with the existing literature, our modified method showed superior separation and sensitivity, aligning with findings by Lenčo *et al.* (2021)[230]. Potential limitations include an extended run time, which may affect sample throughput. Future directions could involve testing alternative buffers or gradient profiles to enhance separation efficiency further. As shown in Figure 5.*6*, the chromatogram illustrates the improved separation and increased peak intensity post-modification, with sharper and more distinct peaks, particularly for hydrophilic lipids.

Therefore, we optimized the separation gradient since, until this point, I had been using the adapted UHPLC gradient optimized initially for a 2.1 mm ID column. A total of 15 gradients were tested (Figure D.7, Figure D.8, and Figure D.9), and the best separation was obtained with a 21 min gradient (0 min – 15% MPB, 2.5 min – 31% MPB, 6.4 min – 37% MPB, 9.3 min – 53% MPB, 9.4 min – 53% MPB, 10.8 min – 65% MPB, 14.8 min – 75% MPB, 16.4 min – 93% MPB, 17.5 min – 98% MPB, 20 min – 98% MPB, 21 min – 15% MPB); 4 min equilibration (15% MPB); with flow rate starting at 50 µL/min until 9.3 min, reducing it to 35 µL/min from 9.3 to 9.4 min and maintaining it until the end of the run. The Vanquish Neo LC system has a solvent calibration feature, in which all solvents used in the instrument have to be pre-programmed for the system to adjust to its viscosity and determine maximum flow rates[232]. The maximum allowed flow rate for MPA was 100 µL/min; however, due to MPB's high viscosity, even at a slightly elevated temperature, the maximum allowed flow rate was 35 µL/min.

In RPLC-MS runs, pressures are usually lower at the start and increase towards the end due to the gradient elution of more viscous solvents. However, when running the gradient separations

with starting flow rates of 100 µL/min experiments, pressures were higher at the start compared to the end (Figure D.10). This atypical behavior led to reducing the starting flow rate to 50 µL/min to maintain consistent and optimal system performance. At 12.8 minutes, the flow rate was further reduced to 35 µL/min because of backpressure and viscosity constraints. Figure 5.7 shows a comparison between the original gradient (with the optimized temperature and MPA) and the fully optimized gradient. The chromatogram in Figure 5.7.b has more peaks and an overall higher intensity, especially in the middle region, where the phospholipids elute. However, this same region looks more crowded because previously coeluted peaks are now being separated after optimizing the separation.

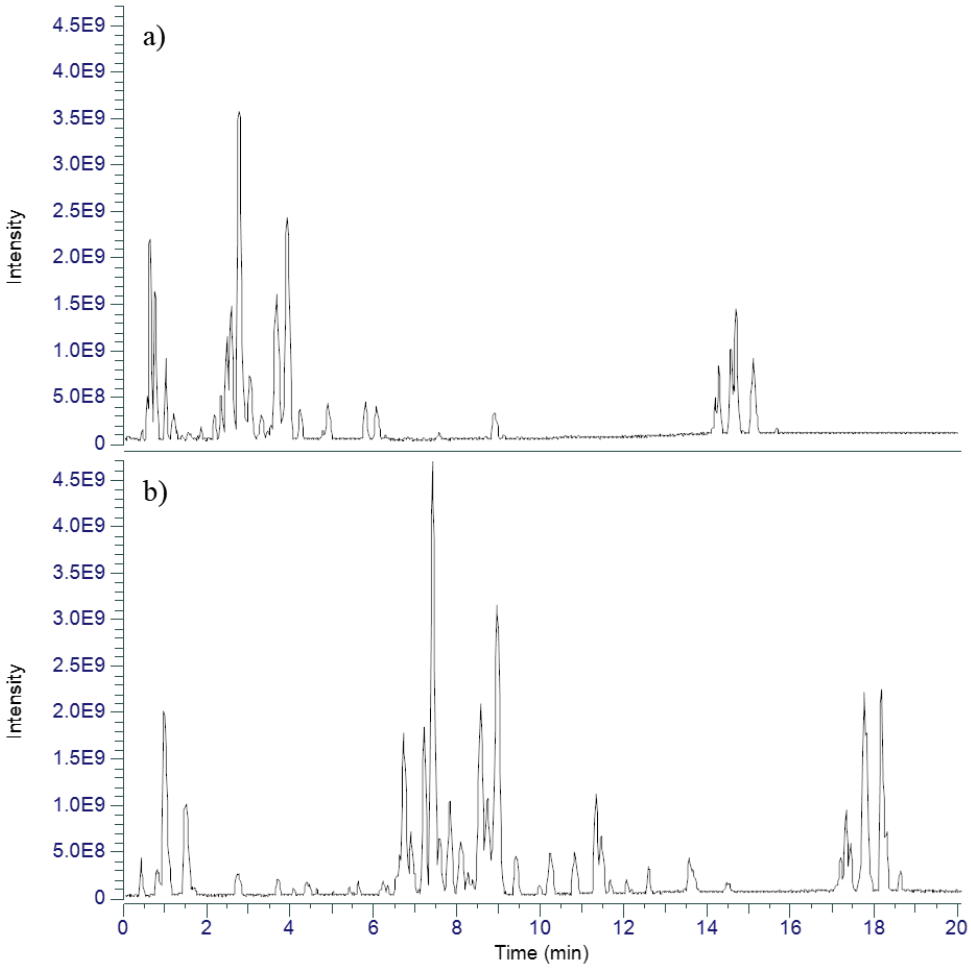

Figure 5.7. BPC for human serum samples extracted with NovaMT LipidRep Internal Standard mix and analyzed using an H-ESI Orbitrap-MS under positive ionization conditions. a) Chromatogram for the original gradient, using MPA - 10mM ammonium formate in 50:40:10 MeOH/ACN/H_2O and MPB - 10mM ammonium formate in 95:5 IPA/H_2O; 16-minute gradient (0 min – 15% MPB, 0.5 min – 15% MPB, 2.3 min – 25% MPB, 9.3 min – 42% MPB, 10.1 min – 78% MPB, 12 min – 90% MPB, 13 min – 98% MPB, 14.5 min – 98% MPB, 15 min – 15% MPB); 4 min equilibration (15% MPB); with flow rate starting at 100 µL/min until 10.1 min, reducing it to 80 µL/min from 10.1 to 14.5 µL/min and further reducing it to 50 µL/min until the end of the run; and b) Chromatogram for the optimized gradient, using MPA - 10mM ammonium formate in 40:40:20 MeOH/ACN/H_2O and MPB - 10mM ammonium formate in 95:5 IPA/H_2O; 21.6-minute gradient (0 min, 15% MPB; 2 min, 30% MPB; 4.5 min, 37% MPB; 8.8 min, 48% MPB; 12.7 min, 53% MPB; 12.8 min, 53% MPB; 14.8 min, 75% MPB; 17.8 min, 93% MPB; 19.3 min, 98% MPB; 20.4 min, 98% MPB; 21.6 min, 15% MPB) with flow rate starting at 50 µL/min until 12.7 min, reducing it to 35 µL/min from 12.7 to 12.8 µL/min and maintaining it at 35 µL/min until the end of the run.

After optimizing separation conditions and gradient, it was time to test the method on samples. In the UHPLC method using a 2.1 mm ID, serum samples are diluted 8-fold, and 3 and 12 µL are injected in positive and negative ion modes, respectively. Until now, most optimizations were performed in positive ion mode, as this usually yields a more intense signal, making optimization easier, especially for low abundant peaks. However, when injecting 10 µL in negative ion mode on the 1 mm ID, a significant peak broadening was noted at the beginning of the chromatogram due to column overloading. Studies have shown that smaller ID columns may suffer from band brand broadening due to dead volumes[216,233]. Moreover, smaller injection volumes for columns packed with sub 2 µm particles have been recommended to improve separation efficiency and avoid overloading[222].

The internal volume of a 2.1 mm ID column is 4.4-fold larger than that of a 1 mm ID column; therefore, injecting 4-fold less volume should address the overloading issue. However, by reducing the injection volume, the amount of sample being injected was also reduced, reducing the sensitivity. To mitigate these issues, different sample concentrations were tested, injecting 1 µL in positive and 2 µL in negative ionization. In positive ionization (Figure D.11), reducing sample dilution to 6-fold and injection volume to 1 µL (4 µL of 8-fold diluted samples were injected) reduced the maximum intensity by 1.7-fold. Similarly, when further reducing sample dilution to 4-fold, the maximum intensity was decreased by 1.3-fold. However, when comparing samples diluted 2 and 8-fold, the maximum intensity was in the same order of magnitude, showing that by injecting 1 µL with samples diluted 2-fold, the obtained results are similar to those of samples diluted 8-fold with 4 µL injection volumes. Furthermore, the raw maximum intensity and the ratio between the

maximum intensity and the amount of sample used (maximum intensity per µL) can be compared

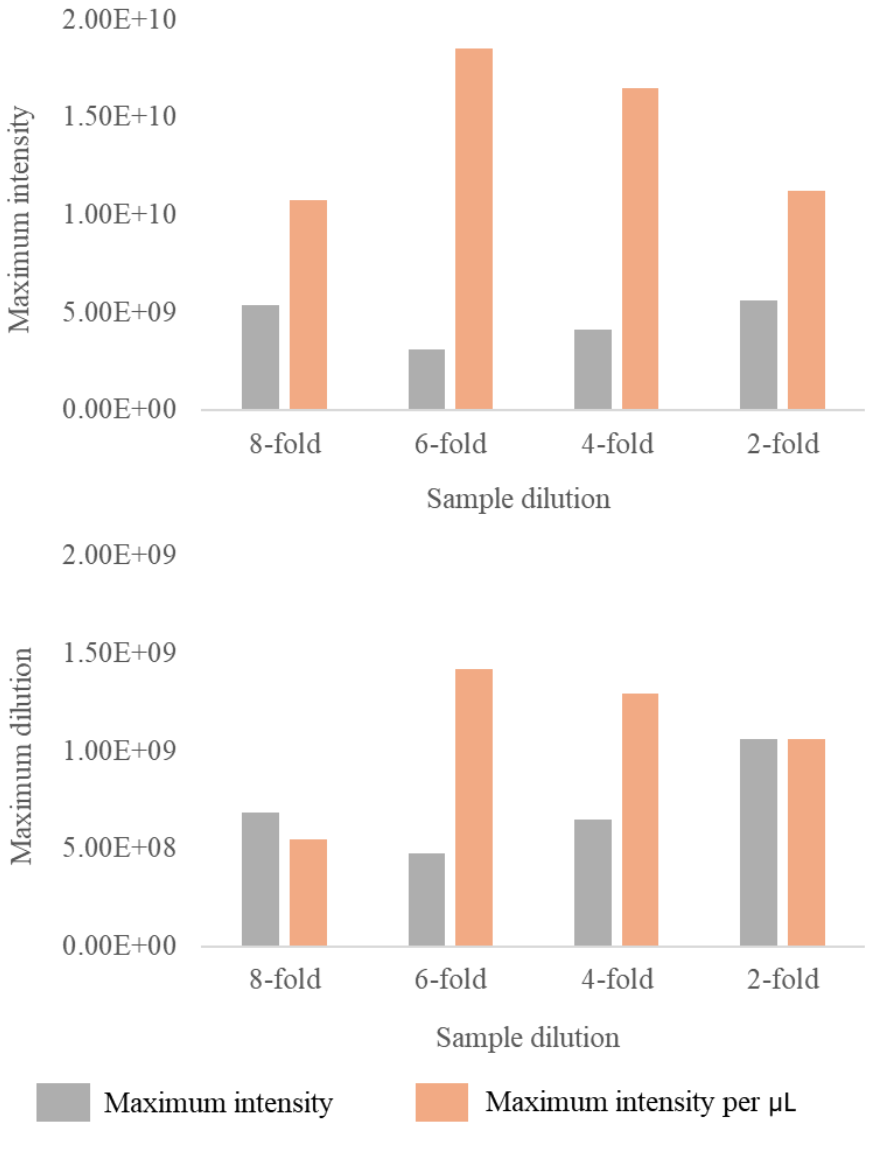

(

Figure 5.8). In positive ionization, although the 6-fold dilution has the highest intensity per µL, meaning it yields the highest intensity while using the least amount of sample, it also shows the lowest total intensity. Therefore, it might decrease sensitivity and the number of detected features. On the other hand, the 8 and 2-fold dilutions have similar maximum intensities and a similar maximum intensity per µL, yielding comparable sensitivity and detected features.

Similarly, for negative ion mode, when reducing sample dilution to 6-fold and 2 µL from 8-fold and 10 µL, the maximum intensity decreased by 1.4-fold, and then further reducing the dilution to 4-fold, the intensity decreased by 1.1-fold. Samples diluted 2-fold showed an increased intensity of 1.5-fold compared to the one obtained at the 8-fold dilution. Moreover, when comparing the maximum intensity per µL for each dilution on negative ionization, there is a similar pattern, as previously observed in positive. The 6-fold dilution yields the highest intensity using the least amount of samples. However, the highest maximum intensity is lower, leading to sensitivity loss and a lower number of detected features. On the other hand, the 2-fold dilution yields both an improvement in raw maximum intensity and maximum intensity per µL of sample. Overall, using a 2-fold sample dilution and injecting 1 and 2 µL of sample for positive and negative ionization, respectively, yields higher intensities while using less sample (*i.e.*, 1.5 µL of raw sample are used in the 2-fold dilution and 1.75 µL of raw sample are used in the 8-fold dilution).

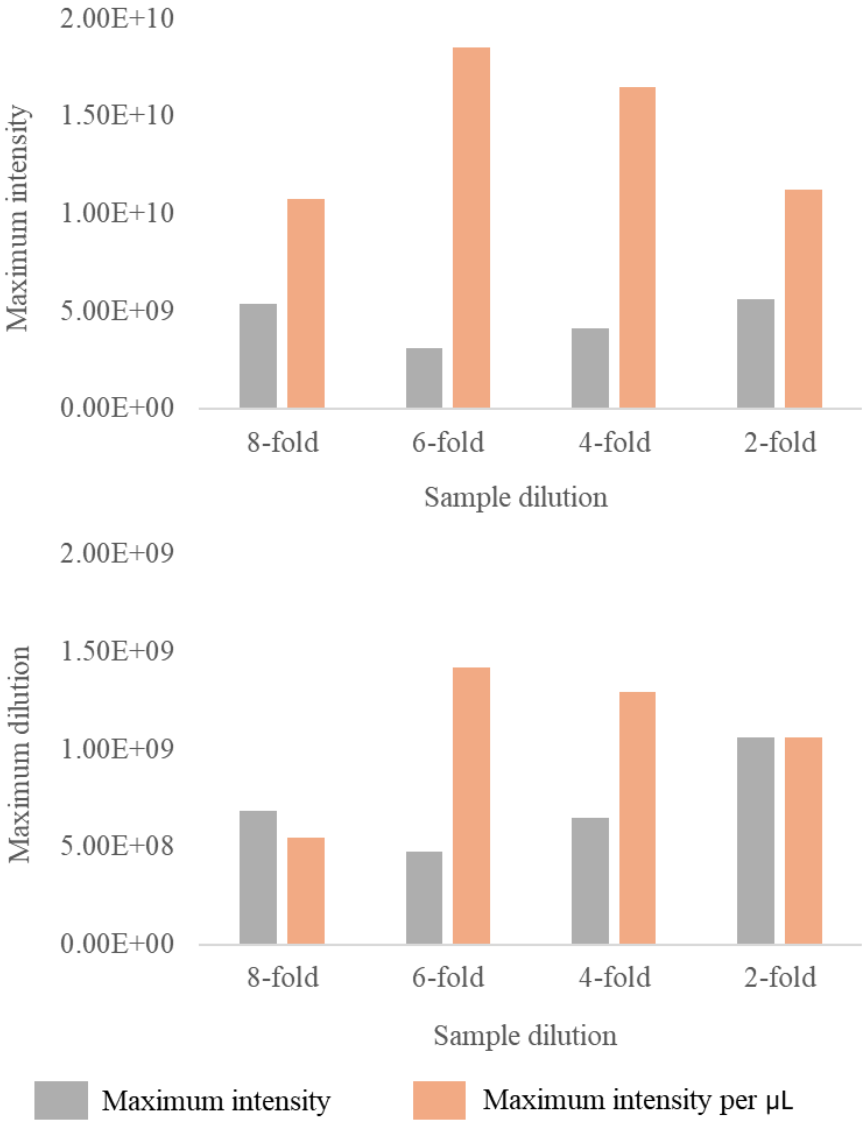

Figure 5.8. The absolute maximum intensity and maximum intensity per µL of the sample obtained for sample dilutions of 8, 6, 4, and 2-fold on a 1 mm ID UHPLC method in a) positive ionization mode and b) negative ionization mode.

The study observed a significant reduction in the intensity of the hydrophobic peaks in the 1 mm ID UHPLC method (Figure 5.6 and Figure 5.7) compared to the 2.1 mm ID method. One potential cause identified is the modifications to MPA. Previously, MPA was less hydrophilic, and our samples would be resuspended in 4:1 MPA/MPB. However, after optimizations, MPA became

more hydrophilic, and samples were reconstituted in 6:4 MPA/MPB. The study also calculated the amount of H_2O previously used to resuspend the samples and how much it was now. When samples were reconstituted to 10 µL, the final solution would have 0.9 µL of H_2O, and after optimization, it would have 1.4 µL. This increase in water content may cause lipids to be unstable in the solution, leading to sample precipitation, which can lead to issues such as column clogging[102,110,149].

To minimize these issues and improve the intensity of the hydrophobic lipid species, I resuspended LipidRep IS in different ratios of MPA and MPB. Results showed that increasing the percentage of MPB for sample resuspension improved the hydrophobic lipids' signal without affecting the present hydrophilic species or peak shapes (Figure D.13). A 2:3 MPA/MPB ratio displayed the best results, improving the hydrophobic peak intensities and intensity ratios among the peaks. Furthermore, this resuspension solvent composition now has the same amount of H_2O used in the 2.1 mm ID UHPLC method and 3 times more IPA; therefore, both hydrophilic and hydrophobic lipids should be resuspended and stable in solution until LC-MS analysis[102,110,234].

Until now, all negative ionization experiments were performed using 4500V. However, ESI arching due to the applied voltage was noted, affecting ionization stability and performance. To mitigate this, the ion source voltage was optimized for negative ionization (Figure D.14). By reducing the ionization voltage to 3500 V, peak intensities were improved, and peak shapes did not suffer significant changes.

Lastly, the performance of the 2.1 mm ID and 1 mm ID UHPLC methods were compared based on the number of detected features and the number of annotated lipid species (Figure 5.9). In the 2.1 mm ID method, 15,487 features were detected, whereas 20,865 features were detected in the 1 mm ID method, representing a 1.3-fold increase in detected features. However, it is

important to consider that a lower amount of sample is consumed in the 1 mm ID method, so if the number of detected features is normalized by the amount of raw sample used, as shown in Figure 5.9.a, the increase in detected features is 1.7-fold instead. The summed intensities for all detected features in the 2.1 mm ID UHPLC method was 1.5E11, whereas, for the 1 mm ID UHPLC method, it was 8.4E10. Although overall intensities were 1.8-fold higher in the 2.1 mm UHPLC method, considering the increased detected features (both the absolute numbers and normalized by the total injection volume), this suggests an improved separation and the potential of uncovering previously coeluting peaks[217,222].

The 1 mm ID UHPLC method yielded a total of 1,505 lipid annotations, with 1,271 annotations in Tier 1 and 234 annotations in Tier 2 (Figure 5.9.b). When comparing the absolute number of annotated lipid species, a 1.2-fold increase can be observed from what was previously annotated for the 2.1 mm ID UHPLC method, further corroborating the higher sensitivity of the 1 mm ID UHPLC method. Furthermore, by normalizing the number of annotated species by the amount of injected sample, the increase in the number of annotations is 1.6-fold, showcasing that more species can be annotated using smaller injection volumes.

Additionally, I compared unique and shared annotations between both methods. Of the total annotated lipids, 964 species were annotated in both datasets, indicating a significant overlap. However, the 1 mm ID UHPLC method annotated another 541 lipid species not present in the 2.1 mm ID method, while the 2.1 mm ID method annotated 288 unique lipid species (Figure D.16). UHPLC methods with smaller inner diameters increase sensitivity and improve separation. Therefore, previously coeluting analytes are expected to be detected using the smaller inner diameter method. Furthermore, by increasing the sensitivity and reducing coelutions, some

previously coeluting or low-intensity peaks may now be fragmenting better, leading not only to more annotations but to a difference in annotated species[106,216,217,223].

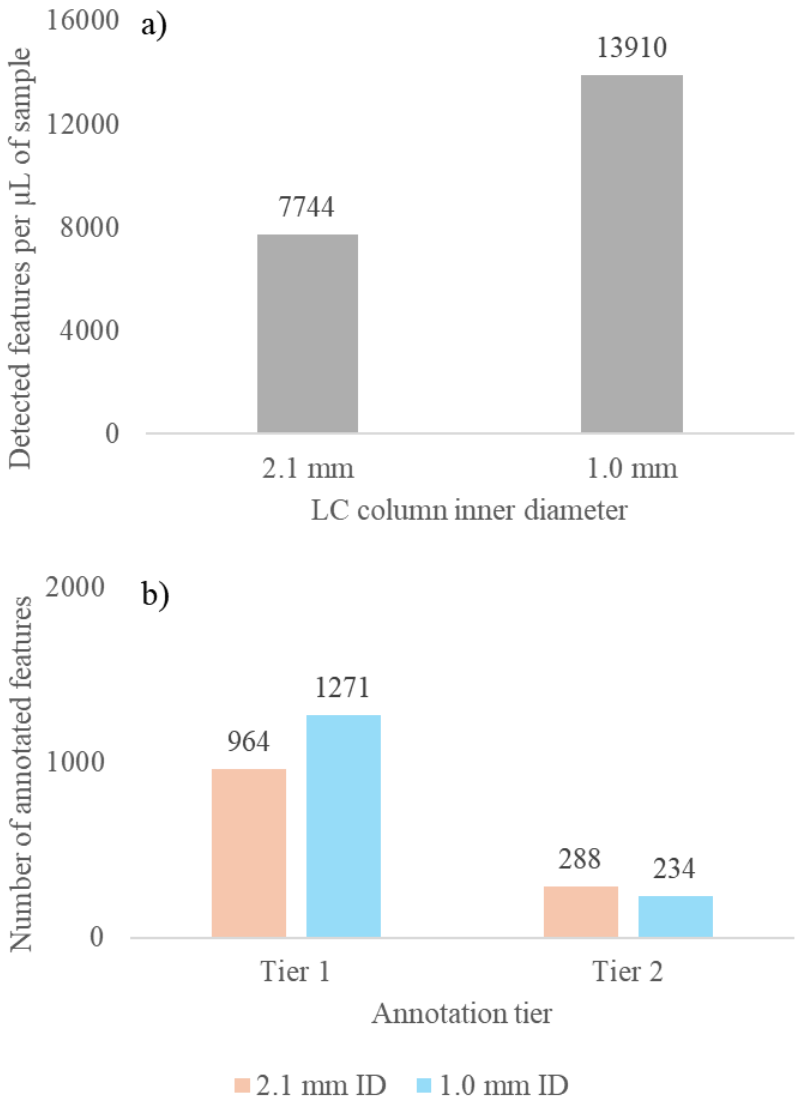

Figure 5.9. Comparison of the detected and annotated features between the 1 mm and 2.1 mm ID columns. A) Number of detected features in each UHPLC method relative to the amount of raw sample injected; b) number of annotated features for Tier 1 (MS/MS score > 500) and Tier 2 (100 < MS/MS score < 500) for each UHPLC method.

A 1 mm ID column enhances analytical performance by improving peak shapes and signal intensity. This makes it suitable for studies and clinical applications regarding biomarker discovery due to better resolution and sensitivity. However, a 2.1 mm column might be preferred for its robustness, higher sample capacity, and shorter analysis time, which can benefit routine analyses and methods requiring greater sample throughput. The choice between the two depends on the study's specific needs, balancing detailed analysis with practical considerations.

Comparing the 1.0 mm and 2.1 mm ID columns highlights the benefits and challenges of using smaller ID columns for lipidomic analysis. The 1.0 mm ID column demonstrated superior sensitivity and improved separation, particularly for low-abundance lipid species. This improvement in resolution and peak sharpness allowed for the detection of more features, providing a more comprehensive lipid profile. The smaller ID column also resulted in better-defined peaks, leading to more accurate lipid annotations.

However, the 2.1 mm ID column has its advantages, such as higher robustness, greater sample capacity, and shorter run times, making it better suited for high-throughput studies. While the 1.0 mm ID column is more sensitive, it requires careful optimization to avoid issues such as column clogging and increased pressure, particularly with more viscous solvents. Despite these challenges, the increased sensitivity and resolution of the 1.0 mm ID column make it a valuable tool for studies focused on detecting subtle changes in lipidomes and low-abundance species.

5.4. Conclusions

This study successfully optimized a UHPLC method using a 1 mm ID column coupled with an Orbitrap-MS, resulting in enhanced analytical performance with improved peak shapes, signal

intensity, and sensitivity. When comparing the optimized method with a UHPLC method using a 2.1 mm ID column, the increase in lipid annotations showcases that smaller ID columns, although less robust, can provide similar or better results using smaller amounts of sample.

Furthermore, comparing Orbitrap-MS with the QToF-MS showed that Orbitrap's higher sensitivity and resolution make it more suitable for comprehensive lipidomics studies, offering more detailed lipid profiles. However, the QToF-MS remains a more accessible and cost-effective option for some applications, highlighting the importance of selecting the right instrument based on the study's specific needs. Orbitrap-MS was particularly effective in improving the detection of low-abundance lipids such as PA, PS, and ST, providing crucial insights into various biological processes and disease states, including cancer and neurodegenerative conditions.

Despite the clear advantages of using a 1 mm ID column, such as increased resolution and sensitivity, there are some limitations. The method requires careful optimization to address ion suppression and peak broadening challenges. Additionally, the increased run time may affect sample throughput, which could be a consideration for high-throughput analyses.

Future research will include a pilot drug study to assess how this optimized method performs in high-throughput settings. This will provide valuable insights into its applicability for large-scale clinical and pharmaceutical studies, ensuring that the method can handle the demands of high-throughput analysis while maintaining accuracy and reliability.

VI

Chapter VI: Exploring the Lipidomic Impact of cisplatin and rapamycin on Non-Small Cell Lung Cancer Cells

6.1. Introduction

To date, cancer is one of the leading causes of mortality worldwide, with non-small cell lung cancer (NSCLC) being one of the most challenging types to treat. Lung cancer is among the deadliest cancers, with higher death rates than colon, breast, and pancreatic cancer combined. Over half of patients diagnosed with lung cancer die within one year of diagnosis, and the 5-year survival rate is around 17.8%. NSCLC accounts for 85% of all lung cancer cases and is classified into three types: squamous-cell carcinoma, adenocarcinoma, and large-cell carcinoma. Squamous cell carcinoma comprises 25-30% of all lung cancer cases and is strongly correlated with cigarette smoking. Adenocarcinoma, the most common type, comprises around 40% of all lung cancer and occurs in both smokers and non-smokers. Large cell carcinoma accounts for 5-10% of cases and is usually diagnosed by exclusion. These subtypes highlight the complexity and variability in NSCLC, necessitating diverse treatment approaches[235–237]. Recent advancements in targeted therapies and immunotherapy have improved outcomes for NSCLC patients, yet treatment efficacy and resistance challenges remain. Epidermal Growth Factor Receptor (EGFR) and Anaplastic Lymphoma Kinase (ALK) inhibitors have shown efficacy against specific genetic subtypes, while immunotherapy has bolstered the body's immune response against cancer cells. However, understanding the underlying metabolic changes, particularly in the lipidome, is crucial for further enhancing these therapies. Despite these advances, challenges remain in early NSCLC detection

and effective management, emphasizing the need for continuous research and tailored therapeutic strategies[237,238].

Cisplatin, a platinum-based coordination complex, is often used as a chemotherapeutic agent due to its ability to form DNA adducts that disrupt DNA replication and transcription, ultimately inducing programmed cell death[239,240]. Upon entering the cell, cisplatin undergoes hydrolysis, replacing its chloride ligands with water molecules, which allows it to bind to DNA. This binding results in cross-links, causing bends in the DNA helix and inhibiting DNA replication and transcription, thus triggering cell death[239,241]. In addition to DNA effects, cisplatin significantly impacts the metabolome and lipidome of cancer cells, leading to metabolic changes, including alterations in amino acid and nucleotide metabolism and other metabolic pathways. Studies have also shown that cisplatin can affect phospholipids and sphingolipids, influencing drug sensitivity and resistance in cancer cells[97,242].

Despite its efficacy, cisplatin is associated with side effects and drug resistance, limiting its therapeutic potential. Common side effects include nephrotoxicity, which can lead to kidney damage; neurotoxicity, resulting in nerve damage; and ototoxicity, causing hearing loss. These side effects occur due to the accumulation of cisplatin in non-cancerous cells, leading to off-target toxicities. Gastrointestinal toxicity, such as nausea and vomiting, is also prevalent, often requiring supportive treatments to manage symptoms[241–248].

Alternatively, rapamycin has also shown promise as a chemotherapic treatment by reducing cell proliferation and promoting autophagy by inhibiting the mechanistic Target of Rapamycin (mTOR) pathway[249–251]. The mTOR pathway is vital for cell growth, proliferation, and survival, and it functions as part of two distinct complexes, mTORC1 and mTORC2. Rapamycin primarily

inhibits mTORC1, leading to a decrease in protein synthesis and cell growth. Additionally, inhibiting the mTORC1 can lead to autophagy, enhancing its therapeutic effects by removing damaged organelles and proteins[251–255]. Moreover, rapamycin has been shown to prevent the formation of new blood vessels, which is crucial against tumor progression. This starves tumors of the nutrients and oxygen they need to grow and metastasize[249–251,256,257].

In combination with cisplatin, rapamycin has been shown to reduce some of the resistance mechanisms that cancer cells develop against cisplatin, potentially enhancing the overall efficacy of the treatment[249,250,258–260]. Another benefit of combining these drugs is the change in less intense cisplatin-induced side effects, as studies have reported that rapamycin can help reduce cisplatin-induced nephrotoxicity by decreasing inflammation and oxidative stress in renal tissues. These protective effects improve the body's ability to tolerate cisplatin and potentially allow higher doses or prolonged treatment, enhancing overall therapeutic efficacy[258,261,262].

Understanding the metabolic changes induced by chemotherapeutic agents is essential in determining drug efficacy and resistance. Lipids are major components of cell membrane structure, signaling pathways, and energy storage, and their dysregulation can significantly impact cancer progression and treatment outcomes[1,2,15,240,263]. Previous studies have indicated that cisplatin can alter phospholipids and sphingolipids, which are essential for cell signaling and membrane dynamics, while rapamycin has been reported to affect lipid metabolism, further underscoring the need to investigate the lipidomic changes induced by these drugs[242,251,258,264].

This study aims to analyze the changes in the lipidome of A549 cells, a model for NSCLC, following treatment with cisplatin and rapamycin, both as single agents and in combination. A previously developed high-sensitivity LC-MS method with a 1 mm ID column will be combined

with a 2DLC-MS approach to enhance lipid annotation confidence. Understanding these alterations can provide insights into the mechanisms underlying drug efficacy and resistance, potentially guiding the development of more effective cancer therapies and aiding in biomarker discovery.

6.2. Experimental

6.2.1. Reagents and Equipment

LipidRep Internal Standard Basic Mix for Tissue/Cells (Nova Medical Testing, Edmonton, AB, Canada), a mixture containing 15 deuterated lipid species from different subclasses, was used for standardization. Ammonium formate (mass spectrometry grade), LC-MS grade acetonitrile (ACN), methanol (MeOH), and dichloromethane (DCM) were purchased from Honeywell (Charlotte, North Carolina, USA). Cisplatin (cis-diamminedichloroplatinum(II)), Rapamycin (5 mM in 100% DMSO), along with LC-MS water (H_2O) and isopropanol (IPA) were obtained from Sigma-Aldrich (St. Louis, Missouri, USA.)

6.2.2. Cell Culture and Drug Treatment

A549 (ATCC CCL-185) cells were cultured in T-75 flasks using F-12k medium (Kaign's Modification of Ham's F-12 Medium) supplemented with 10% fetal bovine serum (FBS), maintained at 37 ºC in a humidified atmosphere containing 5% CO_2. The growth medium was renewed every two to three days. Cells were harvested when reaching 70% confluency, using trypsinization. Briefly, the cells were washed with warm phosphate-buffered saline (PBS). Then, 3.0 mL of 0.25% trypsin/EDTA (Hyclone, Logan, Utah, USA) was added, and the cells were

incubated at 37 ºC and 5% CO_2 for 5 minutes. To quench the reaction, 7 mL of growth medium was added to the T-75 flask. Subsequently, the cell suspensions were transferred to 15 mL sterile polypropylene tubes and centrifuged at 900 rpm for 7 minutes. The cell pellet was resuspended into 1 mL of growth medium and homogenized through gentle pipetting before the cell density was determined using a hemocytometer.

Following cell density determination, cells were diluted to facilitate aliquoting an appropriate cell density into each 6- or 96-well plate well. After 24 h of incubation, cells were treated with the drugs. Untreated control samples were included in all experiments to provide a baseline for comparison. Control wells were maintained in growth medium with 0.5% DMSO, which matches the solvent concentration in drug-treated samples. This ensures that any observed effects can be attributed to the drugs rather than the solvent. Moreover, experiments were performed in biological triplicate to ensure data robustness. This includes cell viability assays and the lipidomic analyses.

6.2.3. Drug Study

6.2.3.1.Cell Viability Assay

Cell viability was determined using the Trypan Blue assay. Briefly, detached cells were stained with Trypan Blue, which stains cells that do not have intact cell membranes (dead cells) and does not interact with the viable cells[265].

Cells were seeded in a 96-well plate at 50,000 cells/mL density for this assay. Each well received 200 µL of fresh growth medium. After 24 h of seeding the cells in the 96-well plate,

individual wells were treated with cisplatin and rapamycin with concentrations ranging from 0.5 to 500 μM and 4 to 20 μM, respectively. A stock solution of cisplatin was prepared in PBS, and treatment solutions were prepared by diluting the stock with a fresh growth medium. Meanwhile, rapamycin treatment solutions were prepared by diluting the stock with fresh growth medium, ensuring the DMSO content was less than 0.5%. Control wells were maintained in growth medium with 0.5% DMSO. Cell viability was assessed after 24 and 48 hours of drug exposure. These results were used to determine the drug treatment's inhibitory concentration (IC) values and decide which concentrations would be used in the study.

6.2.3.2.Drug Treatment

In this study, cells were treated with cisplatin (IC_{25}, IC_{50}, or IC_{75}), rapamycin (IC_{25}, IC_{50}, or IC_{75}), or a combination of rapamycin and cisplatin (IC_{25}, IC_{50}, or IC_{75}).

Following the previously described procedure, cells were seeded in a 6-well plate with a cell density of 50,000 cells/mL in each well. Twenty-four hours after seeding, 1 mL of the old growth medium was replaced with 1 mL of fresh growth medium containing one of the previously mentioned treatment conditions or no treatment for the control sample. Cells were harvested following the same procedure as above after 24 and 48 hours. Then, the cells were transferred into 2 mL sterile polypropylene vials and washed with cold PBS three times.

For quality control, a pooled sample was made by combining equal volumes of all samples, which was subsequently aliquoted into 2 mL sterile polypropylene vials. To remove any remaining PBS, samples were dried under gentle nitrogen flow, purged with nitrogen, and stored at -80º C until further analysis.

6.2.4. Sample Preparation and LC-MS Analysis

Cell lysis protocols have been previously optimized in Chapter II. Briefly, cell lysis and lipid extraction were performed using liquid-liquid extraction (LLE). Dried cell pellets and 3.5 µL of LipidRep Internal Standard Mix for Tissue/Cells were sequentially mixed with 46.3 µL of MeOH, 90 µL of DCM, and 33.1 µL of H_2O, vortexing after each solvent addition for 20 seconds. Following a 10-minute equilibration, samples were centrifuged, and an aliquot of the organic phase (76.5 µL) was dried under a gentle stream of nitrogen for 10 minutes and subsequently reconstituted in a 3:2 mix of MPA/MPB to a total volume of 17.5 µL. Pooled samples were processed using the same protocol as the samples for quality control. Samples were then placed in polypropylene inserts in autosampler vials sealed with PTFE/silicone septum at 8 ºC for a minimum of 4 hours and a maximum of 24 hours before injection.

Samples were analyzed by reversed-phase (RP) ultra-high-performance liquid chromatography (UHPLC) coupled to a high-resolution Orbitrap Exploris 240 (Thermo Fisher Scientific, Waltham, MA, USA) mass spectrometer with a heated electrospray ionization (H-ESI) source. Chromatographic separation was achieved using a Vanquish Neo system (Thermo Fisher Scientific, Waltham, MA, USA) and a Waters Acquity CSH C18 (1.7 µm, 1.0×100mm, Waters Corporation, Milford, MA, USA) column. The mobile phases were MPA (10 mM ammonium formate in 40:40:20 ACN/MeOH/H_2O) and MPB (10 mM ammonium formate in 95:5 IPA/H_2O). A gradient separation lasting 21 minutes (0 min – 15% MPB, 2.5 min – 31% MPB, 6.4 min – 37% MPB, 9.3 min – 53% MPB, 9.4 min – 53% MPB, 10.8 min – 65% MPB, 14.8 min – 75% MPB, 16.4 min – 93% MPB, 17.5 min – 98% MPB, 20 min – 98% MPB, 21 min – 15% MPB); 3 min equilibration (15% MPB); with flow rate starting at 50 µL/min until 9.3 min, reducing it to 35

µL/min from 9.3 to 9.4 min and maintaining it at 35 µL/min until the end of the run, with a column temperature of 55 °C.

Orbitrap ion source parameters were set as follows: ion voltages of 4000 and 3500 V for positive and negative modes, respectively; sheath gas at 60 arbitrary (arb) units; auxiliary gas at 15 arb units; sweep gas at 1 arb unit; ion transfer tube temperature at 300 ºC, and vaporizer temperature at 250 ºC. Full scan analysis was performed with a resolution of 240,000, an m/z range of 150 to 1500 Da, and an RF lens set to 90%. The AGC target was standard, with a maximum injection time of 60 ms and micro scans set to 2. MS/MS qualitative information was obtained for all sample injections using a resolution of 45,000, with a cycle of 5 scans and active exclusion of precursors detected for more than three consecutive spectra with a duration of 5 seconds and a mass tolerance of 10 ppm. Collision energies varied according to the precursor m/z values between 20 and 35 eV. Extra MS/MS data was acquired under different conditions to improve lipid annotation.

Injection volumes were previously optimized as 1.5 µL and 2.5 µL in the positive and negative ionization modes. Samples and blanks were prepared and injected randomly. A pooled sample was used for quality control (QC) and injected with each batch of 10 samples to ensure consistent quality control.

Lastly, pooled samples also underwent offline 2DLC analysis to increase annotation confidence. The 2DLC method used has been previously described and optimized in Chapter IV. Briefly, pooled samples were resuspended in 30:15:4:1 ACN/IPA/MeOH/H_2O before chromatographic separation and fraction collection in a 26-minute gradient separation (0 min 100% MPB; 0-2 min 100% MPB; 2-4 min 98% MPB; 4-4.5 min 98% MPB; 4.5-6 min 96% MPB; 6-8.5 min 93% MPB; 8.5-9.5 min 93% MPB; 9.5-12 min 91% MPB; 12-17 min 86% MPB; 17–25min

80% MPB; 25-26 min 20% MPB), followed by 4 min re-equilibration (0 min, 20% MPB; 0.5 min, 100 % MPB; 6 min, 100% MPB) at a 0.250 mL/min flow rate and column temperature of 45 °C, with MPA - 10 mM ammonium formate in 60:40 ACN/H_2O (v/v) and MPB - 10 mM ammonium formate in 95:3:2 ACN/MeOH/H_2O (v/v/v). Separation was carried out in an Agilent Infinity 1260 LC system coupled to a 1260 Infinity II Analytical-Scale Fraction Collector and a Waters Acquity Premier BEH Amide column (1.7 µm, 2.1×100mm, Waters Corporation, Milford, MA, USA). Fractions were individually dried under gentle nitrogen blow for 60 minutes. Dried fractions were reconstituted in 3:2 MPA/MPB (MPA - 10 mM ammonium formate in 50:40:10 MeOH/ACN/H_2O and MPB - 10 mM ammonium formate in 95:5 IPA/H_2O – RP mobile phases) and injected in RPLC-MS.

6.2.5. Data Processing, Lipid Annotation and Statistical Analyses

As described in Chapter IV, the data was processed using LipidScreener, an in-house software designed for untargeted lipidomics by The Metabolomics Innovation Centre (TMIC, Edmonton, Canada)[14]. Positive and negative ionization chromatograms were aligned using a minimum intensity cut-off of 50000 counts and a minimum peak length of six spectra. Oligomers and multiple adducts were handled within a 10-ppm m/z tolerance. Aligned features were filtered by detection in at least 80% of injections in one group before positive and negative ionization merging.

Lipid annotation followed the procedure described in Chapter IV. Briefly, a two-tier annotation approach was used for lipid annotation based on the acquired tandem mass spectrometry (MS/MS) spectra[103,182]. The acquired MS/MS spectra were compared with the MS-Dial LipidBlast

library (https://fiehnlab.ucdavis.edu/projects/ LipidBlast), the Human Metabolome Database (https:// hmdb.ca), and the MassBank of North America LC−MS/MS libraries (https://mona.fiehnlab.ucdavis.edu). An m/z tolerance of 5 mDa for the precursor ion and 15 mDa for fragments, combined with the minimum similarity between library and experimental spectra of 40%, was used to increase annotation accuracy. All annotated features were subsequently filtered based on adducts, m/z error, the carbon to double bond ratio present in the molecule, even or odd fatty acyl chains, structural modifications, and plasmenyl[14,36,103,183–187]. Annotated lipids were divided into subclasses and eight main categories following the classification system proposed by the International Lipid Classification and Nomenclature Committee (ILCNC), the Lipidomics Standards Initiative, and the LipidMaps database. Furthermore, this study did not evaluate the stereospecific configuration of glycerol derivatives and double bond positions[36,37,118,178,182].

After lipid annotation, all detected features were assigned to a fraction, or RP, if not detected in any of the 2DLC injections. The assignment was based on the feature's presence in the 2DLC injections, calculated as a percentage. The average intensity would be calculated if the detected feature was present in more than 50% of the 2DLC injections for that fraction. After calculating the average intensity for all fractions that satisfied the criteria, the fraction with the highest average intensity was assigned as the one corresponding to that feature. A feature was assigned to the RP if it did not correspond to any specific fraction. All lipid annotations were filtered based on MS/MS score and mass error, and duplicated annotations were removed, keeping the one with the highest MS/MS score and the lowest m/z error.

After removing possible duplicate annotations, using the elution pattern described in Chapter IV, assigned fractions for each annotated feature were compared to expected fractions for

each subclass to determine the annotation confidence. Only annotated features assigned to their expected fraction were used for statistical analysis.

Post-acquisition data normalization was used to mitigate ion suppression effects and other variations that might arise during sample preparation. Each annotated lipid was matched to one of the internal standards, which belonged either to the same lipid class or a similar one based on structural and retention time similarities. Normalized intensities were calculated by dividing the original peak intensity (*i.e.,* peak height) of the annotated feature by the peak intensity of the matched internal standard. Subsequently, the dataset was normalized by the median intensity ratios for all annotated features within each sample and auto-scaled before statistical analysis using MetaboAnalyst 6.0. Features exhibiting low experimental reproducibility (RSD > 30% for QCs) were excluded before statistical analysis.

The multivariate statistical analysis involved a Principal Component Analysis (PCA) and a partial least square-discriminant analysis (PLS-DA). This study's PCA score plots showcase experimental replicates for each sample, with the clustering among quality control samples indicating technical reproducibility. PLS-DA models were evaluated through leave-one-out cross-validation and permutation tests (1000 permutations), with R^2, Q^2, and p-values provided in figure captions. Univariate statistics involved Volcano Plot analysis (Fold change, FC, versus p-value for Student’s t-test with unequal variances).

6.3. Results and Discussions

6.3.1. Cell Viability Determination

The primary goal of the cell viability assay was to determine the inhibitory concentration (IC) values for cisplatin and rapamycin, representing the concentration required to inhibit cell growth by a specific percentage (*e.g.,* IC_{25} reduces cell viability by 25%)[265]. These IC values are essential for exposing cells to the desired concentrations in subsequent experiments to study the effects of these drugs. Figure 6.1 shows the cell viability assay results after 24 and 48 hours of exposure.

The dose-response for cisplatin (Figure 6.1.a) shows that as the concentration of the drug increases, cell viability drops significantly, especially at concentrations above 12.5 µM. This indicates cisplatin is very potent, with significant cell death at relatively low doses. For 24-hour exposures, cisplatin IC_{50} is 12.5 µM, whereas, for 48-hour exposure, the IC_{50} is 1 µM, corroborating that longer exposures increase the drug's effectiveness for cisplatin[260]. For rapamycin (Figure 6.1.b), the decrease in cell viability is less abrupt than that of Cisplatin. After 24 hours of exposure, the I IC_{50} for rapamycin is 4 µM; after 48 hours, it is 2 µM.

Although the same trend is observed for both drugs, higher cisplatin concentrations are required to achieve similar levels of cell death. These results suggest that lower rapamycin concentrations are needed, implying that this compound could be more efficient in treating cells derived from NSCLC than the latter. Moreover, high concentrations of cisplatin in chemotherapy regimens have been known to cause severe side effects, such as nausea and vomiting, hearing loss, and kidney damage[243,244,246,266]. On the other hand, rapamycin causes less severe side effects, such as immunosuppression-related infections and delayed wound healing[256,267,268].

Because of the differences in their mode of action, cisplatin and rapamycin affect the cancer cell and tissue lipidome and metabolome differently. Hence, studies have suggested that combination treatments with these drugs may support their actions or target different pathways in the cells[258–260,269]. Furthermore, studies have shown that combining these drugs is also beneficial, as rapamycin was observed to reduce cisplatin's potential side effects[261]. After the IC value determination, A549 cells were treated under the previously mentioned conditions before being harvested for LC-MS analysis.

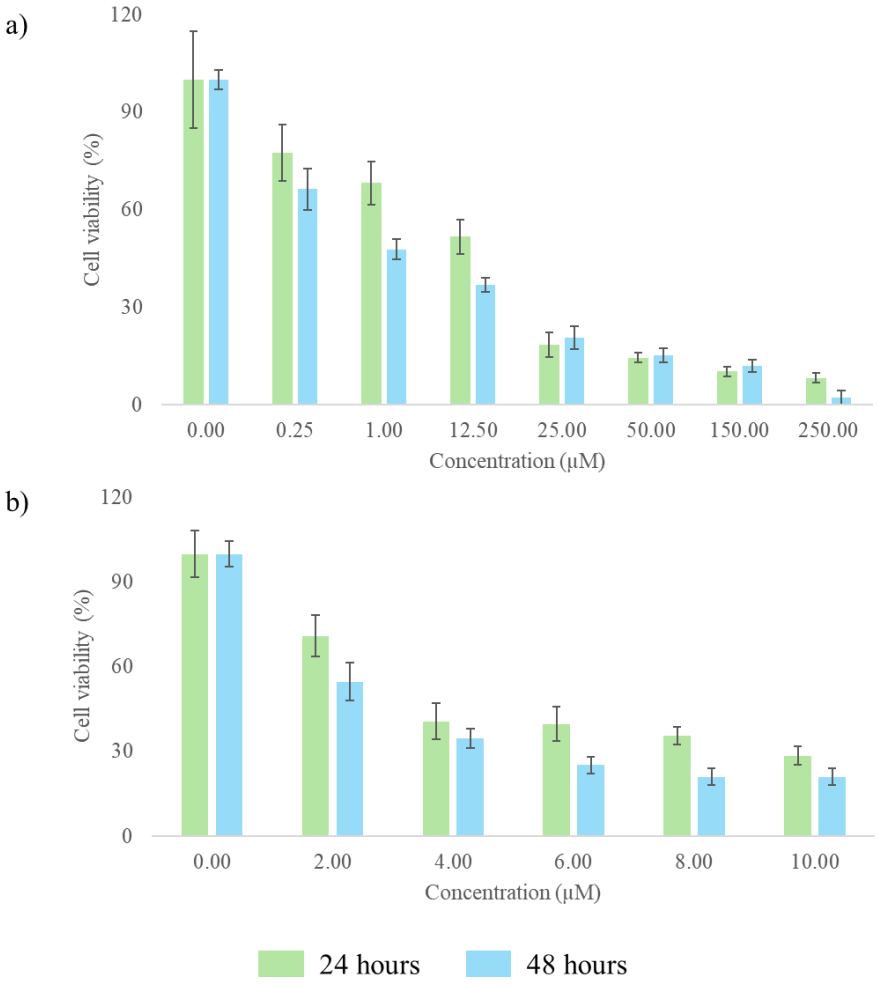

Figure 6.1. Cell viability of human non-small cell lung cancer (A549) relative to control after 24 and 48-hour exposure to different concentrations of (a) cisplatin and (b) rapamycin, using Trypan Blue to stain dead cells.

6.3.2. LC-MS Analysis and Annotation Confidence

The 1 mm ID column LC-MS method detected 9265 features after merging 6193 positive and 3072 negative ionizations. Of these, 1832 features were annotated. After removing duplicate annotations, 1076 annotations remained. Those were then assigned to one of the five fractions of the 2DLC method to determine their annotation confidence, and 94% of annotations belonged to a lipid subclass previously profiled in Chapter IV (Supp. Table 30). Twelve deuterated internal standards were detected with a minimum m/z error of 0.27 ppm and a maximum of 4.73 ppm (Figure E.1). Figure 6.2 displays the percentage of lipid annotations present in their expected fraction and the ones not.

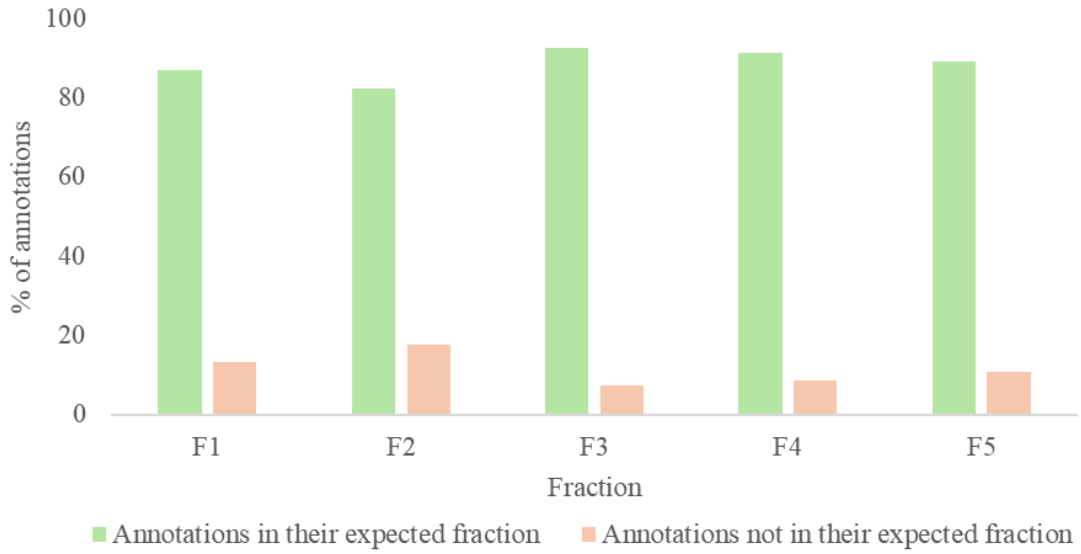

Figure 6.2. Distribution of lipid annotations in their expected fractions (green) versus those not in their expected fractions (orange) across five A549 cell sample fractions. The x-axis represents the five fractions, while the y-axis indicates the percentage of annotations.

Of all annotations belonging to a subclass previously profiled (1016 species), 82.5% were present in their expected fraction. As noted in Figure 6.2, Fraction 2 had the highest percentage of annotations not expected (17.6%), whereas fraction 3 had only 7.3%. Although some annotations were present in fractions other than the expected ones, the vast majority were in their expected fraction, indicating the method's suitability. Over 60% of all annotations detected in their expected fraction were annotated as a glycerophospholipid. In addition, 17.1% were sphingolipids, 13.7% were glycerolipids, and 2.6% were fatty acyl (Figure E.2). After careful consideration, only MS/MS annotations in their expected fraction were used for statistical analysis to increase the annotation accuracy of this study.

After alignment, 68.2% of the detected features exhibited a relative standard deviation (RSD) for QC injections lower than 30%. To improve this and reduce any possible batch effects, samples underwent batch correction using QC replicate injections, slightly increasing the percentage of features with RSDs lower than 30% to 69.9%. Post-acquisition data normalization, using the detected deuterated internal standards, significantly improved the RSD for the QC replicates, resulting in 89.9% of the detected features having RSDs lower than 30%.

The lipidome of A549 cells treated with rapamycin, cisplatin, or a combination of both was compared simultaneously, as shown in Figure 6.3. The PCA plot (Figure 6.3.a) shows that the 14 QC extraction replicates (pooled A549 cell samples) are tightly clustered, indicating consistent and reliable sample preparation. However, the high number of samples in that region makes it difficult to visualize individual replicates on the PCA plot. The dendrogram (Figure 6.3.b) provides better visualization, revealing the clustering of the QC replicates. Furthermore, although most groups are clustered around the QC replicates, injections for the combined treatment with cisplatin and

rapamycin IC_{50} are separated from the rest. For this group, there is also a sub-separation between the 24- and 48-hour samples, indicating that the exposure length affects the lipidome of the cells for this treatment condition. Furthermore, the cisplatin IC_{75} and cisplatin and rapamycin IC_{75} treatments are separated from clustered, albeit separated from other groups, indicating that cisplatin is primarily responsible for the observed changes.

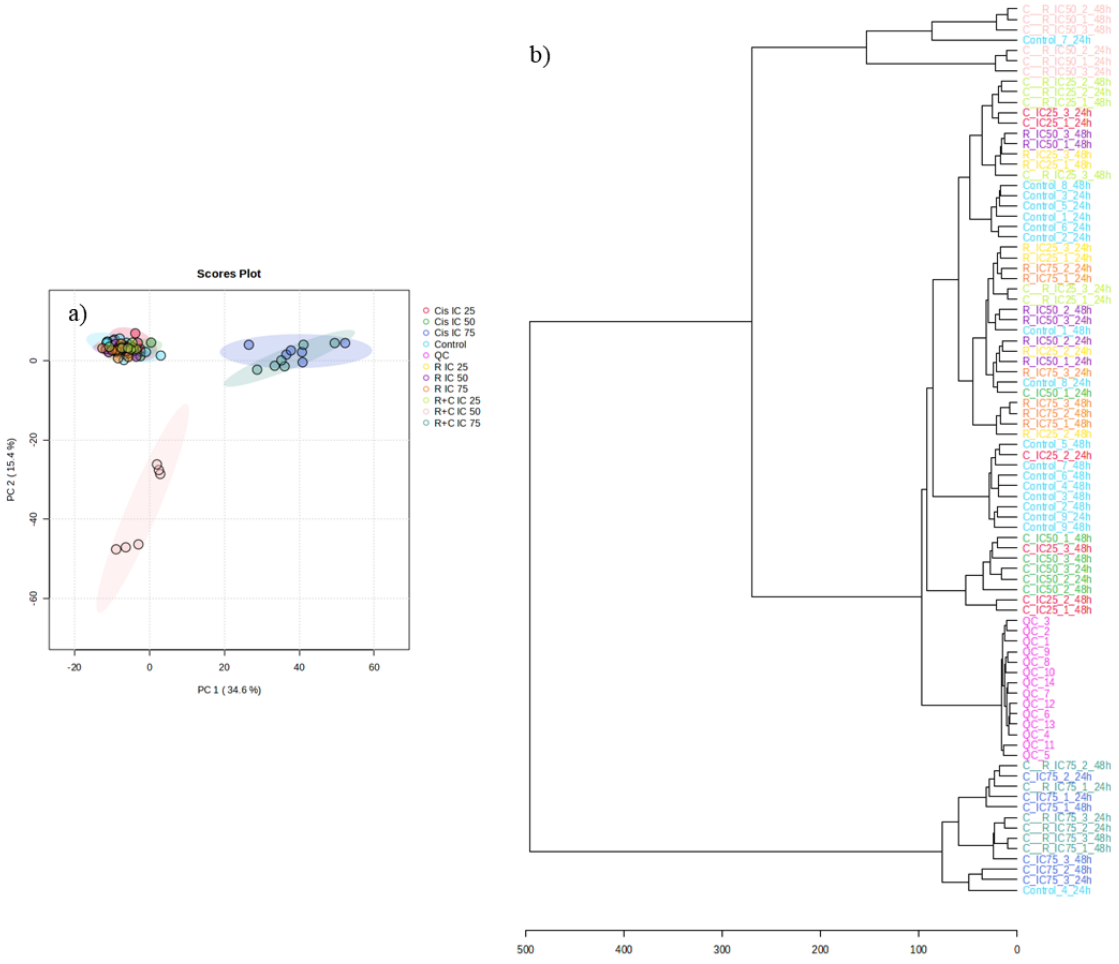

Figure 6.3. Statistical analysis for quality control of A549 cell samples treated with cisplatin (IC_{25}, IC_{50} or IC_{75}), rapamycin (IC_{25}, IC_{50} or IC_{75}), or a combination of rapamycin and cisplatin (IC_{25}, IC_{50} or IC_{75}). a) PCA score plot showcasing clustered QC extraction and injections; b) Dendrogram with injections for all samples.

To better evaluate how each treatment condition affected the samples' lipidomes, individual PCA score plots (without QCs) and PLS-DA score plots were plotted for each condition (Figure 6.4). For cisplatin, control, IC_{25}, and IC_{50} samples were clustered on the PCA (Figure 6.4.a), indicating that treating the cells with this drug for 24 or 48 hours does not significantly impact the lipidome of the cells. On the other hand, IC_{75} for cisplatin is separated from the rest, indicating that alterations in the lipidome of the cell become more noticeable at this dose. The PSL-DA score plot for cisplatin (Figure 6.4.b) did not pass the permutation test ($p=0.061$ for 1000 permutations) because of the high complexity of the dataset and the insufficient number of samples. Nevertheless, the result indicates that the lipidome of control samples differs from those of treated samples. Furthermore, IC_{25} and IC_{50} affect the lipidome similarly since they have no clear separation. However, a higher dose (IC_{75}) affects it differently since we can see a clear separation on the PLS-DA score plot (Figure 6.4.b). Furthermore, the cross-validation details for the cisplatin treatment suggest overfitting. Although the model displays a high accuracy and explained variance ($R^2=0.9746$), its predictive power is much lower ($Q^2=0.5972$), indicating the observed data should be interpreted carefully.

On the other hand, the PCA score plot for rapamycin (Figure 6.4.c) shows the treatment conditions are less clustered than those with cisplatin. The plot also indicates some separation based on treatment duration, with slight differences between 24 and 48 hours for all groups, and IC_{75} shows the most noticeable separation based on exposure length. The PLS-DA plot for rapamycin (Figure 6.4.d) separates the control samples from the treated ones. Additionally, there is some separation between IC_{75} and the other doses, but there is no clear separation between IC_{25} and IC_{50}. Although the PLS-DA analysis passed the permutation test ($p=0.038$ for 1000 permutations), the model was overfitted, as indicated by the difference between the R^2 and Q^2 values. This difference

suggests that while the model explains the dataset well, its predictive power is significantly lower. Therefore, the model cannot accurately predict the behavior of new samples, although it can still indicate trends and possible behaviors to guide future studies.

Lastly, the PCA score plot (Figure 6.4.e) shows no separation between IC25 and control samples when evaluating the combination of drugs for treatment. However, IC_{50} and IC_{75} are separated from each other and the other groups. Similar to what was observed for rapamycin, a slight separation can be observed between different exposure times, especially for IC_{50}. In the PLS-DA score plot, the treatment conditions for the combined drugs and the control samples show clear separations. Control and IC_{25} samples show no clear separation based on exposure time; however, for IC_{50} and IC_{75}, this separation is more evident, especially for IC_{50}. Moreover, although the model displays high accuracy and predictive ability (Q^2), the complexity of the dataset aligned with the difference between R^2 and Q^2 suggests the model is overfitted. The permutation test ($p < 0.001$ for 1000 permutations) indicates that the observed separation is statistically significant, indicating that the model can identify patterns in the data for this condition despite the potential overfitting.

The PLS-DA analysis suggests that treating A549 cells with cisplatin, rapamycin, or a combination of these drugs can significantly impact the lipidome, especially at higher doses. While the models suggest overfitting for all treatment conditions, the trends observed herein can help guide future studies on how these drugs alter the lipidome.

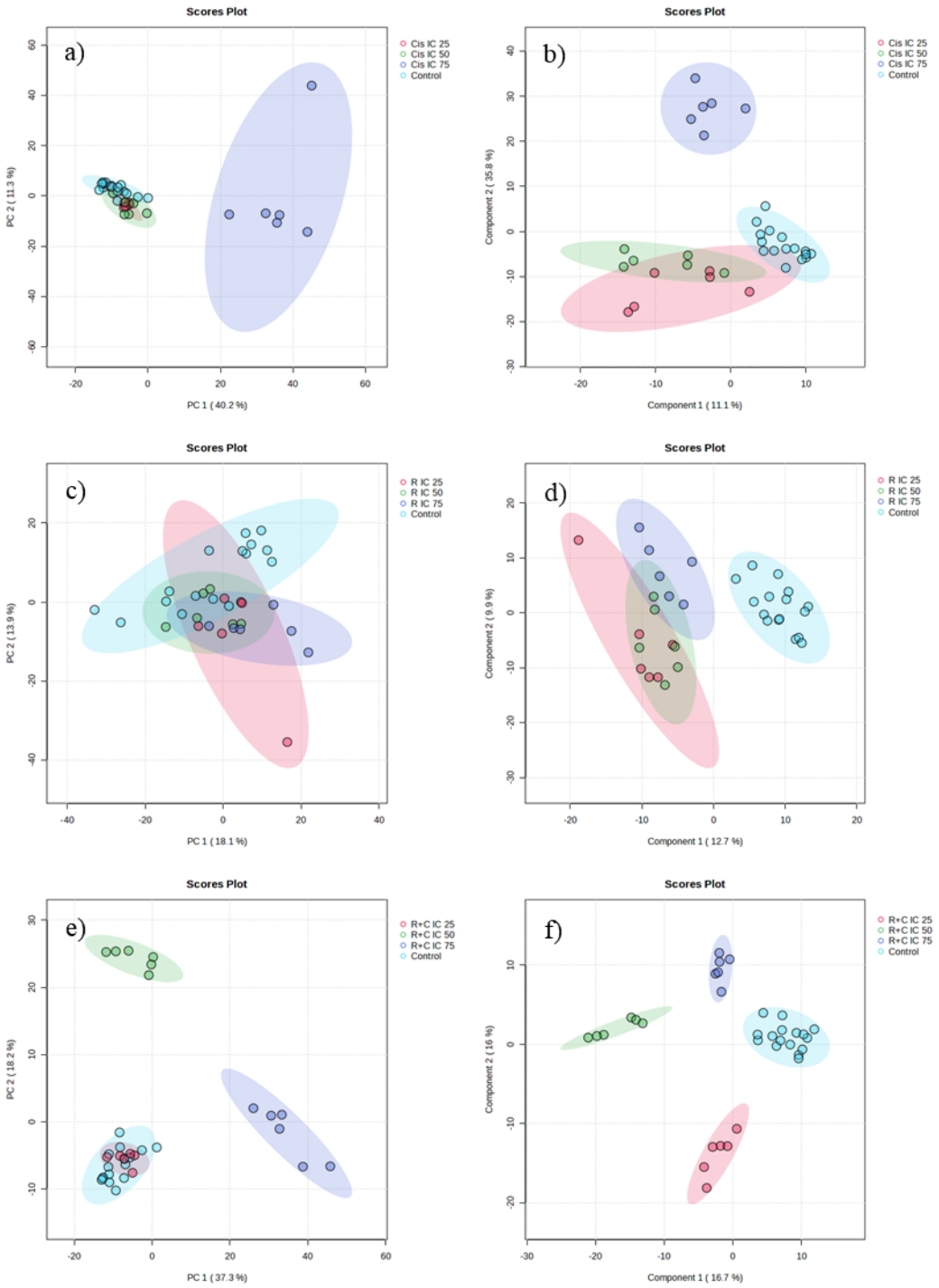

Figure 6.4. Statistical analysis for lipidomics of A549 cells treated with different doses of cisplatin and rapamycin and exposure times. a) PCA score plot for A549 cell samples treated with IC_{25} (pink), IC_{50} (green), or IC_{75} (dark blue) of cisplatin and control samples (light blue); b) PLS-DA score plot build for five components for A549 cell samples treated with IC_{25} (pink), IC_{50} (green),

or IC_{75} (dark blue) of cisplatin and control samples (light blue) R^2: 0.9746; Q^2: 0.5972 and p= 0.06 for 1000 permutations; c) PCA score plot for A549 cell samples treated with IC_{25} (pink), IC_{50} (green), or IC_{75} (dark blue) of rapamycin and control samples (light blue); d) PLS-DA score plot build for five components for A549 cell samples treated with IC_{25} (pink), IC_{50} (green), or IC_{75} (dark blue) of rapamycin and control samples (light blue) resulting in R^2: 0.9916; Q^2: 0.7630 and p= 0.04 for 1000 permutations; e) PCA score plot for A549 cell samples treated with IC_{25} (pink), IC_{50} (green), or IC_{75} (dark blue) of rapamycin and cisplatin and control samples (light blue); f) PLS-DA score plot build for five components for A549 cell samples treated with IC_{25} (pink), IC_{50}(green), or IC_{75} (dark blue) of rapamycin and cisplatin and control samples (light blue) resulting in R^2: 0.9803; Q^2: 0.8722 and p<0.001 for 1000 permutations.

Following the PLS-DA analysis, a VIP score analysis was done to identify the lipid species that most significantly contributed to the observed separations. For cisplatin treatment (Figure E.3.a), the VIP scores highlighted specific lipid species important for the observed separation between control and treated samples. Sphingomyelins (SM), TG, PE, and DG were among the most influential lipids. Moreover, changes in the normalized summed intensity for the 15 species most influenced by the separation were observed. For SM and TG, each had three species significantly affecting the separation, and in both cases, one increased and two decreased in normalized intensity. Both PE and ST species showed a decrease in normalized intensity for its species. LPC, DG, PG, and PC species increased their normalized intensities. These results suggest that the observed alterations may have been caused by the cisplatin treatment, which may have induced changes in membrane lipid composition and signaling pathways. SM and TG were the most influential subclasses, indicating that changes in sphingolipid and glycerolipid metabolism play a key role in response to cisplatin treatment. Studies have shown that cisplatin affects signaling pathways, such as cell-to-cell communications, by inducing changes in the fluidity and permeability of the lipid bilayer. It interacts with the membrane lipids, causing alterations in the

drug uptake and resistance mechanisms. This plays a crucial role in drug treatments and leads to changes in the drug's cytotoxicity[97,241,242].

The VIP score analysis for rapamycin treatment (Figure E.3.b) showed phosphatidylcholines (PC) are the major lipid species differentiating between control and treated samples. PC is one of the major components of cell membranes, indicating that treating A549 cells with rapamycin causes significant alterations in the lipid bilayer. Furthermore, SM, TG, and PE also showed significant differences between treated and control samples, indicating that treatment with rapamycin can also cause alterations in lipid storage and energy metabolism[1,249]. Most of its species also increased in normalized intensity for PC, while most SM species decreased. PE and TG showed increased normalized intensity, whereas FA decreased in its normalized intensity. Rapamycin has been reported to alter membrane composition and cellular signaling pathways, impacting lipid metabolism and cellular functions. By inhibiting mTORC1, rapamycin can reduce protein synthesis regulators' activity and influence lipids' metabolism and other macromolecules' metabolism[257,270,271].

The VIP score analysis demonstrated that SM and PE are the most important lipid subclass driving the observed separations for the combined treatment of cisplatin and rapamycin (Figure E.3.c). Here, the normalized intensities showed a decrease for most species driving the separation (SM, PI, TG, PS, and PC), whereas for DG, it increases. For PE, most of its species driving the separation showed a decreased normalized intensity, with only one of its annotations increasing. SM lipids are crucial for maintaining cell membrane integrity, facilitating signaling pathways, and influencing drug uptake and resistance. Additionally, PE lipids are important for maintaining cell membrane structure, facilitating membrane dynamics, and regulating cellular functions. The role

of these lipid species in cell signaling, protein function, and membrane stability makes them vital in cellular responses to drug treatments and potential targets for therapeutic interventions in various diseases[1,250,257,258,262,270].

The PLS-DA and VIP score analyses indicate lipidome alterations caused by drug treatments in A549 cells. These results suggest that cisplatin may disrupt sphingolipid and glycerolipid metabolism, impacting membrane lipid composition and signaling pathways. In contrast, rapamycin treatment primarily affects PC lipids, indicating significant changes in the lipid bilayer, alongside alterations in SM, TG, and PE, reflecting disruptions in lipid storage and energy metabolism. However, combined, cisplatin and rapamycin treatment affected SM and PE species the most, highlighting their roles in maintaining cell membrane integrity, facilitating signaling pathways, and influencing cellular responses to drug treatments. Results suggest that this drug treatment combination could increase therapeutic efficacy and alter resistance mechanisms, providing insights into the combined treatment's biochemical effects.

Concerning the Volcano plot analysis (Figure E.4), treatment conditions were evaluated separately against control samples to assess the effects of both dose and drug on the lipidome. In the cisplatin IC_{25} condition (Figure E.4.a), 93 species were significantly altered, mainly belonging to PC, PE, and Cer subclasses. PC lipids are important cellular membrane structure and function components, influencing cellular processes such as signaling and apoptosis. At the same time, PE is important in membrane structure and stability, and Cer plays a role in programmed cell death and cell cycle regulation. The change in these lipids suggests that cisplatin IC_{25} impacts membrane integrity and apoptotic pathways in A549 cells. These changes can impair cell viability and

promote cell death, which is consistent with the cytotoxic nature of cisplatin in cancer treatment[1,241,272].

For the IC_{50} dose (Figure E.4.b), 221 species were significantly affected, and the most affected subclasses were the same as observed for cisplatin IC_{25}. This observation indicates that higher doses of cisplatin intensify the disruption of lipid metabolism observed at lower doses; it does not disturb different subclasses, indicating it does not interfere with other cell functions. Furthermore, the consistency in the affected lipid subclasses suggests that these lipid species are sensitive to cisplatin treatment. The increased number of significantly altered lipid species at the IC_{50} dose indicates a dose-dependent intensification of the drug's impact on cellular lipidome, leading to more pronounced cellular stress and potential cytotoxicity. This dose-dependent effect is consistent with the known mechanism of cisplatin, which includes DNA damage, apoptosis, and disruption of lipid metabolism[97,241,242,262].

For cisplatin IC_{75} (Figure E.4.c), 490 significant features were observed, with PC, PE, TG, and Cer subclasses being the most affected. The large number of altered species at this higher dose indicates severe membrane integrity and signaling pathways disruption, highlighting the cytotoxic effects of high-dose cisplatin on A549 cells. Triglycerides (TG) are crucial for energy storage and lipid signaling, and the number of significantly altered TGs suggests metabolic stress and disruption of lipid homeostasis. The changes may reflect an altered energy metabolism, indicating cellular stress and damage, corroborating the known dose-dependent toxicity of cisplatin[241,242,248,272,273].

Similarly to cisplatin, in the IC_{25} dose (Figure E.4.d) for rapamycin, 100 lipid species showed significant changes, mainly Cer, PC, and FA subclasses. FA lipids are important in energy

production, membrane synthesis, and signaling pathways, and significant alteration in them may suggest a disruption in cellular energy metabolism and membrane dynamics in response to rapamycin treatment. Changes in FA levels can indicate shifts in lipid metabolism and the activation of stress responses as cells attempt to adapt to the drug-induced inhibition of the mTOR pathway. This disruption can lead to altered energy balance, impacting cell growth and survival, which aligns with the known effects of rapamycin in reducing cell proliferation and inducing autophagy[250,253,257]. At IC_{50} (Figure E.4.e), 123 lipid species were significantly altered. Similarly to what was observed for cisplatin treatments, an increase in the number of significantly altered species was observed between IC_{25} and IC_{50} doses; however, most of the altered species belonged to the previously discussed subclasses.

For rapamycin at IC_{75}, 160 species were significantly altered, with PE, PC, Cer, and LPC being the most prominent subclasses, suggesting that high drug doses can impact biological processes. Rapamycin's mechanism involves inhibiting the mTOR pathway, thereby reducing cell growth and proliferation. The significant changes in LPC – lipids involved in inflammation and cell signaling – along with alterations of other lipid subclasses highlight the extensive metabolic reprogramming and cellular stress induced by the high-dose rapamycin. These changes likely contribute to its therapeutic effects on cancer[249,250,257].

For the combined treatment using cisplatin and rapamycin at IC_{25} (Figure E.4.g), 77 significantly altered features were observed, with PC, PE, and FA subclasses being the most impacted. At IC_{50} (Figure E.4.h), the combination treatment resulted in 337 significantly altered lipids, mostly belonging to PE, PC, and Cer subclasses. This is similar to what was observed for

cisplatin treatments at IC_{25} and IC_{50}. However, the number of altered lipid species is significantly higher, indicating that using rapamycin with cisplatin increases the latter's effects.

Finally, at IC_{75} (Figure E.4.i), the combination treatment showed the highest number of significant features, with 578 changes, predominantly affecting the PC, PE, Cer, and TG subclasses. The most affected lipid subclasses for this treatment condition are very similar to what was observed for cisplatin IC_{75} alone; only the number of significantly altered species is higher, corroborating the idea that rapamycin boosts the effects of cisplatin in A549 cells. Furthermore, the extensive alteration suggests disruption of lipid homeostasis and cellular functions, confirming high-dose cisplatin and rapamycin's potent combined cytotoxic effects on A549 cells[258,259,261,262].

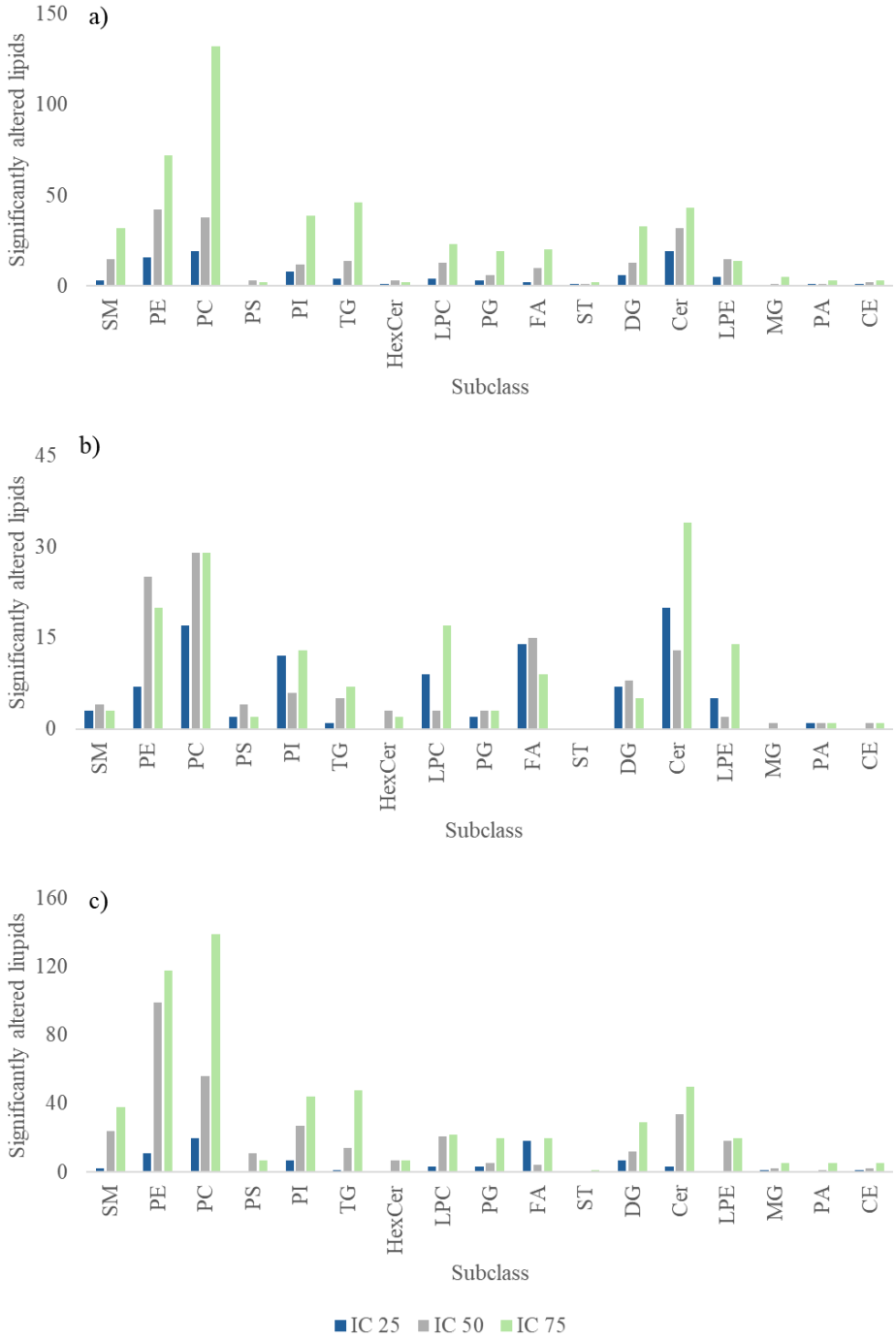

Figure 6.5. Number of significantly altered ($p<0.05$ and FC<0.67 or FC >1.5) lipid annotations between Control and treated A549 cell samples (fold-change ≤ 0.67 or ≥ 1.5 and $p < 0.05$. a) Control versus samples treated with cisplatin at IC_{25}, IC_{50}, and IC_{75}; b) Control versus samples treated with rapamycin at IC_{25}, IC_{50}, and IC_{75}; c) Control versus samples treated simultaneously with cisplatin and rapamycin at IC_{25}, IC_{50}, and IC_{75}.

6.3.3. Biological Implications

The lipidomic alterations observed in this study provide insights into the possible metabolic disruptions induced by cisplatin and rapamycin treatments in A549 cells. Cisplatin treatment significantly changed PC, PE, and Cer. These lipids play crucial roles in membrane fluidity, receptor transduction, and receptor localization, which are important in maintaining cellular homeostasis[4,46,274]. Therefore, altering these lipids could lead to dysregulation of the membrane lipid composition and disruptions of these processes. Moreover, these changes can affect cell proliferation, drug resistance mechanisms, and key cancer progression and treatment factors. In addition, the observed alterations in PC and PE species suggest membrane dynamics and cellular signaling changes, potentially leading to increased cellular stress and programmed cell death. This highlights the importance of lipid metabolism in cancer biology and underscores the therapeutic potential of targeting these pathways to improve treatment efficacy[97,241,248,249].

Moreover, combining cisplatin and rapamycin showed enhanced cytotoxic effects and lipidomic changes, suggesting an alternative approach to overcome drug resistance. Cisplatin is known for its ability to form DNA adducts, leading to programmed cell death, while rapamycin inhibits the mTOR pathway, reducing cell growth and proliferation. The combination therapy resulted in more pronounced lipid alterations, indicating a collaborative effect that enhances both drugs' efficacy. These observations suggest that combining DNA-damaging agents with mTOR inhibitors can effectively target multiple pathways in cancer cells, reducing the likelihood of resistance and improving therapeutic outcomes. Besides, studies have shown that rapamycin can be used to minimize potential side effects from the cisplatin treatment, suggesting even more advantages for the combination treatment using both drugs[241,257,258,261,262,269].

The different lipidomic profiles associated with drug treatments and dosages suggest potential biomarkers for predicting treatment response. Personalized medicine approaches can leverage these biomarkers to tailor therapies based on individual lipidomic profiles, improving therapeutic efficacy and minimizing side effects. For example, specific lipid alterations, such as altered PIs and TGs, could indicate a higher chance of response to combination therapy with cisplatin and rapamycin. Identifying and validating such biomarkers could enable personalized treatment plans, improving patient outcomes and reducing the risk of side effects associated with traditional chemotherapy[17,231,275].

6.4. Conclusions

This study explored the lipidomic alterations induced by cisplatin and rapamycin treatments in A549 cells as single agents and in combination. Our findings show significant changes in the lipid profiles of treated cells, highlighting the potential of lipidomics in understanding the metabolic disruptions caused by these chemotherapeutic agents.

The results showed that cisplatin treatment led to alterations in PC, PE, and Cer lipids, indicating changes in membrane lipid composition and signaling pathways. Similarly, rapamycin treatment primarily affected PC, SM, TG, and PE, showcasing lipid storage and energy metabolism disruptions. Cisplatin and rapamycin exhibited collaborative effects, resulting in pronounced lipid alterations and enhanced cytotoxicity compared to single-agent treatments. This combination therapy effectively targets multiple pathways in cancer cells, potentially overcoming drug resistance mechanisms. The observed synergy between cisplatin and rapamycin supports the potential of combination therapies to improve therapeutic outcomes by targeting complementary

mechanisms of action. Furthermore, the lipidomic profiles associated with different drug treatments and dosages suggest potential biomarkers for predicting treatment response. Specific lipid alterations could indicate therapeutic efficacy, allowing personalized treatment strategies.

Future research should focus on finding and validating possible biomarkers for treatment monitoring and disease progression. Exploring differences in drug action between 2D and 3D cells before *in vivo* studies should also be beneficial as it could improve the understanding of drug delivery to tissue-like samples. Moreover, in vivo or clinical studies are essential to confirm the lipidomic alterations observed in vitro and to assess the therapeutic efficacy and safety of cisplatin and rapamycin combination therapy. In addition, identifying and validating potential lipid biomarkers across a broader range of cancer cell lines and clinical samples is crucial for establishing their reliability and applicability in predicting treatment response and guiding therapies.

VII

Chapter VII: Conclusions and Future Work

Lipid molecules play diverse and crucial roles within living organisms, such as maintaining cellular structure, facilitating signaling, and storing energy. Lipidomics research is important for understanding these functions and how lipid dysregulation is associated with cancer, cardiovascular diseases, and metabolic disorders. Therefore, developing more sensitive and accurate lipidomic methods is essential for advancing our knowledge of lipid biology, identifying disease biomarkers, and improving diagnostic and therapeutic strategies.

This work focused on developing and optimizing analytical methods to improve lipidomic profiling in human samples, with potential implications for diagnostic applications. In Chapter II, a UV-Vis method was optimized to establish a reliable baseline for lipidomic analyses, ensuring high sensitivity and reproducibility. This method was successfully integrated into our UHPLC-MS platform and subsequently applied to saliva and MCF-7 cell samples. In Chapter III, comparisons were made between the method previously optimized in Chapter II and a Total Metabolite Concentration method. The potential biological implications of these normalization methods were evaluated, determining which method to use before LC-MS analysis. While normalization using total lipid quantification provided higher reproducibility and specificity for lipid-focused studies, normalization using total metabolite concentration was more suitable for broader metabolic profiling due to its higher sensitivity.

In Chapter IV, an offline two-dimensional liquid chromatography-mass spectrometry (2DLC-MS) method combining HILIC and RPLC-MS was developed and optimized to improve

lipidomics data acquisition. The 2DLC-MS method enhanced lipid class separation, reduced ion suppression, and improved the accuracy of lipid annotation. Different data processing tools (MetaboScape, MS-Dial, and LipidScreener) were evaluated to identify the most effective software for lipidomic analysis. LipidScreener provided the highest number of annotations, while MetaboScape and MS-Dial offered more precise matching of lipid species to their expected fractions. A proof-of-concept study on biological samples confirmed the method's potential for real-world applications and its ability to provide a more accurate view of the lipidome.

In Chapter V, the performance of Orbitrap-MS and QToF-MS was compared, alongside the influence of the column's inner diameter (ID) on lipidomics data. The optimization of the Orbitrap-MS ion source parameters resulted in significant improvements in signal intensity and peak shapes. This demonstrated higher sensitivity and resolution, leading to more detailed lipid profiles compared to QToF-MS. A UHPLC method using a 1 mm ID column was developed, improving lipid separation, sensitivity, and resolution compared to the traditional 2.1 mm ID column.

Lastly, Chapter VI evaluated the potential of the 1 mm ID column combined with the 2DLC-MS for high-throughput and detailed lipidomic studies to increase annotation confidence. The lipidomic changes in A549 cells, a non-small cell lung cancer (NSCLC) model, were evaluated following treatment with cisplatin and rapamycin, both as single agents and in combination. Cisplatin treatment significantly altered PC, PE, and Cer lipids, potentially impacting membrane lipid composition and signaling pathways. Rapamycin treatment affected PC, SM, TG, and PE, indicating lipid storage and energy metabolism disruptions. Combined treatment with rapamycin and cisplatin resulted in more lipid alterations and enhanced cytotoxicity than single-agent therapies, highlighting the potential for overcoming drug resistance mechanisms.

This work has advanced lipidomic profiling methodologies, demonstrating their potential for diagnostic applications and enhancing our understanding of lipid-related disease mechanisms. Future research should focus on expanding sample size and diversity to validate the findings across different biological fluids and conditions, especially for other normalization methods. Moreover, studies focusing on data processing tools for lipidomics and annotation accuracy to enhance the data quality are still required. Continued research in lipidomics will contribute to a better understanding of disease mechanisms, improve diagnostic precision, and aid in developing targeted therapies, ultimately enhancing patient outcomes.

References

(1) Van Meer, G. Cellular Lipidomics. *EMBO Journal* **2005**, *24* (18), 3159–3165. https://doi.org/10.1038/sj.emboj.7600798.

(2) Wenk, M. R. The Emerging Field of Lipidomics. *Nat Rev Drug Discov* **2005**, *4* (7), 594–610. https://doi.org/10.1038/nrd1776.

(3) Han, X. Lipidomics for Studying Metabolism. *Nat Rev Endocrinol* **2016**, *12* (11), 668–679. https://doi.org/10.1038/nrendo.2016.98.

(4) Lingwood, D.; Simons, K. Lipid Rafts As a Membrane-Organizing Principle. *Science (1979)* **2010**, *327*.

(5) Wood, P. L. Lipidomics of Alzheimer's Disease: Current Status. *Alzheimers Res Ther* **2012**, *4* (1), 1–10. https://doi.org/10.1186/alzrt103.

(6) Gross, R. W.; Han, X. Lipidomics in Diabetes and the Metabolic Syndrome. *Methods Enzymol* **2007**, *433* (07), 73–90. https://doi.org/10.1016/S0076-6879(07)33004-8.

(7) Tzelepi, V.; Gika, H.; Begou, O.; Timotheadou, E. The Contribution of Lipidomics in Ovarian Cancer Management: A Systematic Review. *Int J Mol Sci* **2023**, *24* (18). https://doi.org/10.3390/ijms241813961.

(8) Agatonovic-Kustrin, S.; Morton, D. W.; Smirnov, V.; Petukhov, A.; Gegechkori, V.; Kuzina, V.; Gorpinchenko, N.; Ramenskaya, G. Analytical Strategies in Lipidomics for Discovery of Functional Biomarkers from Human Saliva. *Dis Markers* **2019**, *2019*. https://doi.org/10.1155/2019/6741518.

(9) Yang, K.; Han, X. Lipidomics: Techniques, Applications, and Outcomes Related to Biomedical Sciences. *Trends Biochem Sci* **2016**, *41* (11), 954–969. https://doi.org/10.1016/j.tibs.2016.08.010.

(10) Koelmel, J. P.; Cochran, J. A.; Ulmer, C. Z.; Levy, A. J.; Patterson, R. E.; Olsen, B. C.; Yost, R. A.; Bowden, J. A.; Garrett, T. J. Software Tool for Internal Standard Based Normalization of Lipids, and Effect of Data-Processing Strategies on Resulting Values. *BMC Bioinformatics* **2019**, *20* (1), 1–13. https://doi.org/10.1186/s12859-019-2803-8.

(11) Ross, D. H.; Guo, J.; Bilbao, A.; Huan, T.; Smith, R. D.; Zheng, X. Evaluating Software Tools for Lipid Identification from Ion Mobility Spectrometry–Mass Spectrometry Lipidomics Data. *Molecules* **2023**, *28* (8). https://doi.org/10.3390/molecules28083483.

(12) Harris, R. A.; Leaptrot, K. L.; May, J. C.; McLean, J. A. New Frontiers in Lipidomics Analyses Using Structurally Selective Ion Mobility-Mass Spectrometry. *TrAC - Trends in Analytical Chemistry* **2019**, *116*, 316–323. https://doi.org/10.1016/j.trac.2019.03.031.

(13) Van Dijk, S. J.; Feskens, E. J. M.; Bos, M. B.; Hoelen, D. W. M.; Heijligenberg, R.; Bromhaar, M. G.; De Groot, L. C. P. G. M.; De Vries, J. H. M.; Müller, M.; Afman, L. A. A Saturated Fatty Acid-Rich Diet Induces an Obesity-Linked Proinflammatory Gene Expression Profile in Adipose Tissue of Subjects at Risk of Metabolic Syndrome. *American Journal of Clinical Nutrition* **2009**, *90* (6), 1656–1664. https://doi.org/10.3945/ajcn.2009.27792.

(14) Mujammami, M.; Aleidi, S. M.; Buzatto, A. Z.; Alshahrani, A.; AlMalki, R. H.; Benabdelkamel, H.; Al Dubayee, M.; Li, L.; Aljada, A.; Abdel Rahman, A. M. Lipidomics Profiling of Metformin-Induced Changes in Obesity and Type 2 Diabetes Mellitus: Insights

and Biomarker Potential. *Pharmaceuticals* **2023**, *16* (12). https://doi.org/10.3390/ph16121717.

(15) Eggers, L. F.; Müller, J.; Marella, C.; Scholz, V.; Watz, H.; Kugler, C.; Rabe, K. F.; Goldmann, T.; Schwudke, D. Lipidomes of Lung Cancer and Tumour-Free Lung Tissues Reveal Distinct Molecular Signatures for Cancer Differentiation, Age, Inflammation, and Pulmonary Emphysema. *Sci Rep* **2017**, *7* (1), 1–13. https://doi.org/10.1038/s41598-017-11339-1.

(16) Giallourou, N.; Urbaniak, C.; Puebla-Barragan, S.; Vorkas, P. A.; Swann, J. R.; Reid, G. Characterizing the Breast Cancer Lipidome and Its Interaction with the Tissue Microbiota. *Commun Biol* **2021**, *4* (1). https://doi.org/10.1038/s42003-021-02710-0.

(17) Santos, G. A. A.; Olave, E.; Pardi, P. C. Salivary Biomarkers in Alzheimer ´ s Disease. *International Journal of Morphology* **2020**, *38* (1), 230–234.

(18) Su, H.; Rustam, Y. H.; Masters, C. L.; Makalic, E.; McLean, C. A.; Hill, A. F.; Barnham, K. J.; Reid, G. E.; Vella, L. J. Characterization of Brain-Derived Extracellular Vesicle Lipids in Alzheimer's Disease. *J Extracell Vesicles* **2021**, *10* (7). https://doi.org/10.1002/jev2.12089.

(19) Calvano, C. D.; Ventura, G.; Sardanelli, A. M. M.; Savino, L.; Losito, I.; De Michele, G.; Palmisano, F.; Cataldi, T. R. I. Searching for Potential Lipid Biomarkers of Parkinson's Disease in Parkin-Mutant Human Skin Fibroblasts by HILIC-ESI-MS/MS: Preliminary Findings. *Int J Mol Sci* **2019**, *20* (13). https://doi.org/10.3390/ijms20133341.

(20) Kosicek, M.; Hecimovic, S. Phospholipids and Alzheimer's Disease: Alterations, Mechanisms and Potential Biomarkers. *Int J Mol Sci* **2013**, *14* (1), 1310–1322. https://doi.org/10.3390/ijms14011310.

(21) IUPAC. *Compendium of Chemical Terminology*; Gold, V., Ed.; International Union of Pure and Applied Chemistry (IUPAC): Research Triangle Park, NC, 2019. https://doi.org/10.1351/goldbook.

(22) Nelson, D. L. ,; Cox, M. M. *Lehninger Principles of Biochemistry* , 5th ed.; W.H. Freeman: New York, 2008.

(23) Garrett, R. H. ,; Grisham, C. M. *Biochemistry*, 3rd ed.; Thomson Brooks/Cole: Belmont, CA, 2005.

(24) Fahy, E.; Subramaniam, S.; Brown, H. A.; Glass, C. K.; Merrill, A. H.; Murphy, R. C.; Raetz, C. R. H.; Russell, D. W.; Seyama, Y.; Shaw, W.; Shimizu, T.; Spener, F.; Van Meer, G.; VanNieuwenhze, M. S.; White, S. H.; Witztum, J. L.; Dennis, E. A. A Comprehensive Classification System for Lipids. *J Lipid Res* **2005**, *46* (5), 839–861. https://doi.org/10.1194/jlr.E400004-JLR200.

(25) Muro, E.; Ekin Atilla-Gokcumen, G.; Eggert, U. S. Lipids in Cell Biology: How Can We Understand Them Better? *Mol Biol Cell* **2014**, *25* (12), 1819–1823. https://doi.org/10.1091/mbc.E13-09-0516.

(26) Fahy, E.; Subramaniam, S.; Murphy, R. C.; Nishijima, M.; Raetz, C. R. H.; Shimizu, T.; Spener, F.; Van Meer, G.; Wakelam, M. J. O.; Dennis, E. A. Update of the LIPID MAPS

Comprehensive Classification System for Lipids. *J Lipid Res* **2009**, *50*, 9–14. https://doi.org/10.1194/jlr.R800095-JLR200.

(27) Fahy, E.; Sud, M.; Cotter, D.; Subramaniam, S. LIPID MAPS Online Tools for Lipid Research. *Nucleic Acids Res* **2007**, *35*, 606–612. https://doi.org/10.1093/nar/gkm324.

(28) Gunstone, F. D. *Fatty Acid and Lipid Chemistry*; Springer US, 1996. https://doi.org/10.1007/978-1-4615-4131-8.

(29) Jenkins, B.; West, J. A.; Koulman, A. A Review of Odd-Chain Fatty Acid Metabolism and the Role of Pentadecanoic Acid (C15:0) and Heptadecanoic Acid (C17:0) in Health and Disease. *Molecules* **2015**, *20* (2), 2425–2444. https://doi.org/10.3390/molecules20022425.

(30) Schwingshackl, L.; Hoffmann, G. Monounsaturated Fatty Acids, Olive Oil and Health Status: A Systematic Review and Meta-Analysis of Cohort Studies. *Lipids Health Dis* **2014**, *13* (1). https://doi.org/10.1186/1476-511X-13-154.

(31) Son, S. E.; Kim, N. J.; Im, D. S. Development of Free Fatty Acid Receptor 4 (FFA4/GPR120) Agonists in Health Science. *Biomol Ther (Seoul)* **2021**, *29* (1), 22–30. https://doi.org/10.4062/biomolther.2020.213.

(32) Calder, P. C. Marine Omega-3 Fatty Acids and Inflammatory Processes: Effects, Mechanisms and Clinical Relevance. *Biochimica et Biophysica Acta (BBA) - Molecular and Cell Biology of Lipids* **2015**, *1851* (4), 469–484. https://doi.org/10.1016/J.BBALIP.2014.08.010.

(33) Saini, R. K.; Keum, Y. S. Omega-3 and Omega-6 Polyunsaturated Fatty Acids: Dietary Sources, Metabolism, and Significance — A Review. *Life Sci* **2018**, *203*, 255–267. https://doi.org/10.1016/j.lfs.2018.04.049.

(34) Djuricic, I.; Calder, P. C. Beneficial Outcomes of Omega-6 and Omega-3 Polyunsaturated Fatty Acids on Human Health: An Update for 2021. *Nutrients* **2021**, *13* (7). https://doi.org/10.3390/nu13072421.

(35) Mariamenatu, A. H.; Abdu, E. M. Overconsumption of Omega-6 Polyunsaturated Fatty Acids (PUFAs) versus Deficiency of Omega-3 PUFAs in Modern-Day Diets: The Disturbing Factor for Their "Balanced Antagonistic Metabolic Functions" in the Human Body. *J Lipids* **2021**, *2021*, 1–15. https://doi.org/10.1155/2021/8848161.

(36) Conroy, M. J.; Andrews, R. M.; Andrews, S.; Cockayne, L.; Dennis, E. A.; Fahy, E.; Gaud, C.; Griffiths, W. J.; Jukes, G.; Kolchin, M.; Mendivelso, K.; Lopez-Clavijo, A. F.; Ready, C.; Subramaniam, S.; O'Donnell, V. B. LIPID MAPS: Update to Databases and Tools for the Lipidomics Community. *Nucleic Acids Res* **2024**, *52* (D1), D1677–D1682. https://doi.org/10.1093/nar/gkad896.

(37) Liebisch, G.; Fahy, E.; Aoki, J.; Dennis, E. A.; Durand, T.; Ejsing, C. S.; Fedorova, M.; Feussner, I.; Griffiths, W. J.; Köfeler, H.; Merrill, A. H.; Murphy, R. C.; O'Donnell, V. B.; Oskolkova, O.; Subramaniam, S.; Wakelam, M. J. O.; Spener, F. Update on LIPID MAPS Classification, Nomenclature, and Shorthand Notation for MS-Derived Lipid Structures. *J Lipid Res* **2020**, *61* (12), 1539–1555. https://doi.org/10.1194/jlr.S120001025.

(38) Swinnen, J. V; Dehairs, J. A Beginner's Guide to Lipidomics. *Biochemist* **2022**, *44* (1), 20–24. https://doi.org/https://doi.org/10.1042/bio_2021_18.

(39) Farese, R. V.; Walther, T. C. Lipid Droplets Finally Get a Little R-E-S-P-E-C-T. *Cell* **2009**, *139* (5), 855–860. https://doi.org/10.1016/j.cell.2009.11.005.

(40) Lowet, M. E. The Triglyceride Lipases of the Pancreas. *J Lipid Res* **2002**, *43* (12), 2007–2016. https://doi.org/10.1194/jlr.R200012-JLR200.

(41) Rosen, E.; Spiegelman, B. Adipocytes as Regulators of Energy Balance and Glucose Homeostasis. *Nature* **2006**, *444*, 847–853. https://doi.org/10.1038/nature05483.

(42) Mérida, I.; Ávila-Flores, A.; Merino, E. Diacylglycerol Kinases: At the Hub of Cell Signalling. *Biochemical Journal* **2008**, *409* (1), 1–18. https://doi.org/10.1042/BJ20071040.

(43) Griner, E. M.; Kazanietz, M. G. Protein Kinase C and Other Diacylglycerol Effectors in Cancer. *Nat Rev Cancer* **2007**, *7* (4), 281–294. https://doi.org/10.1038/nrc2110.

(44) Blankman, J. L.; Simon, G. M.; Cravatt, B. F. A Comprehensive Profile of Brain Enzymes That Hydrolyze the Endocannabinoid 2-Arachidonoylglycerol. *Chem Biol* **2007**, *14* (12), 1347–1356. https://doi.org/10.1016/j.chembiol.2007.11.006.

(45) Mu, H.; Høy, C. E. The Digestion of Dietary Triacylglycerols. *Prog Lipid Res* **2004**, *43* (2), 105–133. https://doi.org/10.1016/S0163-7827(03)00050-X.

(46) van Meer, G.; Voelker, D. R.; Feigenson, G. W. Membrane Lipids: Where They are and How They Behave. *Nat Rev Mol Cell Biol* **2008**, *9* (124), 112–124.

(47) Brzozowski, J. S.; Jankowski, H.; Bond, D. R.; McCague, S. B.; Munro, B. R.; Predebon, M. J.; Scarlett, C. J.; Skelding, K. A.; Weidenhofer, J. Lipidomic Profiling of Extracellular Vesicles Derived from Prostate and Prostate Cancer Cell Lines. *Lipids Health Dis* **2018**, *17* (1), 1–12. https://doi.org/10.1186/s12944-018-0854-x.

(48) Schmitz, G.; Ruebsaamen, K. Metabolism and Atherogenic Disease Association of Lysophosphatidylcholine. *Atherosclerosis* **2010**, *208* (1), 10–18. https://doi.org/10.1016/j.atherosclerosis.2009.05.029.

(49) Balla, T. Phosphoinositides: Tiny Lipids With Giant Impact on Cell Regulation. *Physiol Rev* **2013**, *93*, 1019–1137. https://doi.org/10.1152/physrev.00028.2012.-Phosphoinositides.

(50) Wang, X.; Quinn, P. J. The Location and Function of Vitamin E in Membranes (Review). *Mol Membr Biol* **2000**, *17* (3), 143–156. https://doi.org/10.1080/09687680010000311.

(51) Leitinger, N. Oxidized Phospholipids as Modulators of Inflammation in Atherosclerosis. *Curr Opin Lipidol* **2003**, *14*, 421–430. https://doi.org/10.1097/01.mol.0000092616.86399.dc.

(52) Hannun, Y. A.; Obeid, L. M. Principles of Bioactive Lipid Signalling: Lessons from Sphingolipids. *Nat Rev Mol Cell Biol* **2008**, *9* (2), 139–150. https://doi.org/10.1038/nrm2329.

(53) Kolter, T.; Sandhoff, K. Sphingolipids - Their Metabolic Pathways and the Pathobiochemistry of Neurodegenerative Diseases. *Angewandte Chemie - International Edition* **1999**, *38* (11), 1532–1568.

(54) Platt, F. M.; Boland, B.; van der Spoel, A. C. Lysosomal Storage Disorders: The Cellular Impact of Lysosomal Dysfunction. *Journal of Cell Biology* **2012**, *199* (5), 723–734. https://doi.org/10.1083/jcb.201208152.

(55) Ogretmen, B. Sphingolipid Metabolism in Cancer Signalling and Therapy. *Nat Rev Cancer* **2017**, *18* (1), 33–50. https://doi.org/10.1038/nrc.2017.96.

(56) Bloch, K. E. Sterol, Structure and Membrane Function. *Crit Rev Biochem Mol Biol* **1983**, *14* (1), 47–92. https://doi.org/10.3109/10409238309102790.

(57) Miller, W. Molecular Biology of Steroid Hormone Synthesis. *Endocr Rev* **1988**, *295* (3), 295–318.

(58) Duez, H.; van der Veen, J. N.; Duhem, C.; Pourcet, B.; Touvier, T.; Fontaine, C.; Derudas, B.; Baugé, E.; Havinga, R.; Bloks, V. W.; Wolters, H.; van der Sluijs, F. H.; Vennström, B.; Kuipers, F.; Staels, B. Regulation of Bile Acid Synthesis by the Nuclear Receptor Rev-Erbα. *Gastroenterology* **2008**, *135* (2). https://doi.org/10.1053/j.gastro.2008.05.035.

(59) Herman, R. H.; Holick, M. F. Vitamin D: Importance in the Prevention of Cancers, Type 1 Diabetes, Heart Disease, and Osteoporosis. *Am J Clin Nutr* **2004**, *79*, 362–371.

(60) Lusis, A. Atherosclerosis. *Nature* **2000**, 233–241. https://doi.org/10.1038/35025203.

(61) Carson, J. A. S.; Lichtenstein, A. H.; Anderson, C. A. M.; Appel, L. J.; Kris-Etherton, P. M.; Meyer, K. A.; Petersen, K.; Polonsky, T.; Van Horn, L. Dietary Cholesterol and Cardiovascular Risk: A Science Advisory from the American Heart Association. *Circulation* **2020**, *141* (3), E39–E53. https://doi.org/10.1161/CIR.0000000000000743.

(62) Soliman, G. A. Dietary Cholesterol and the Lack of Evidence in Cardiovascular Disease. *Nutrients* **2018**, *10* (6). https://doi.org/10.3390/nu10060780.

(63) Martano, C.; Mugoni, V.; Dal Bello, F.; Santoro, M. M.; Medana, C. Rapid High Performance Liquid Chromatography–High Resolution Mass Spectrometry Methodology for Multiple Prenol Lipids Analysis in Zebrafish Embryos. *J Chromatogr A* **2015**, *1412*, 59–66. https://doi.org/10.1016/j.chroma.2015.07.115.

(64) Mladěnka, P.; Macáková, K.; Kujovská Krčmová, L.; Javorská, L.; Mrštná, K.; Carazo, A.; Protti, M.; Remião, F.; Nováková, L. Vitamin K - Sources, Physiological Role, Kinetics, Deficiency, Detection, Therapeutic Use, and Toxicity. *Nutr Rev* **2022**, *80* (4), 677–698. https://doi.org/10.1093/nutrit/nuab061.

(65) Brigelius-Flohé, R.; Traber, M. G. Vitamin E: Function and Metabolism. *The FASEB Journal* **1999**, *13* (10), 1145–1155. https://doi.org/10.1096/fasebj.13.10.1145.

(66) Dutta, S.; Whicher, J. R.; Hansen, D. A.; Hale, W. A.; Chemler, J. A.; Congdon, G. R.; Narayan, A. R. H.; Håkansson, K.; Sherman, D. H.; Smith, J. L.; Skiniotis, G. Structure of a Modular Polyketide Synthase. *Nature* **2014**, *510* (7506), 512–517. https://doi.org/10.1038/nature13423.

(67) Raetz, C. R. H.; Whitfield, C. Lipopolysaccharide Endotoxins. *Annu Rev Biochem* **2002**, *71*, 635–700. https://doi.org/10.1146/annurev.biochem.71.110601.135414.

(68) O'Donnell, V. B.; Ekroos, K.; Liebisch, G.; Wakelam, M. Lipidomics: Current State of the Art in a Fast Moving Field. *Wiley Interdiscip Rev Syst Biol Med* **2020**, *12* (1). https://doi.org/10.1002/wsbm.1466.

(69) Ivanova, P. T.; Milne, S. B.; Myers, D. S.; Brown, H. A. Lipidomics: A Mass Spectrometry Based Systems Level Analysis of Cellular Lipids. *Curr Opin Chem Biol* **2009**, *13* (5–6), 526–531. https://doi.org/10.1016/j.cbpa.2009.08.011.

(70) Wang, J.; Wang, C.; Han, X. Tutorial on Lipidomics. *Anal Chim Acta* **2019**, *1061*, 28–41. https://doi.org/10.1016/j.aca.2019.01.043.

(71) Hu, T.; Zhang, J. L. Mass-Spectrometry-Based Lipidomics. *J Sep Sci* **2018**, *41* (1), 351–372. https://doi.org/10.1002/jssc.201700709.

(72) Folch, J.; Lees, M.; Sloane Stanley, G. H. A Simple Method for the Isolation and Purification of Total Lipides from Animal Tissues. *J Biol Chem* **1957**, *226* (1), 497–509. https://doi.org/10.1016/s0021-9258(18)64849-5.

(73) Bligh, E.G. and Dyer, W. J. Canadian Journal of Biochemistry and Physiology. *Can J Biochem Physiol* **1959**, *37* (8).

(74) Matyash, V.; Liebisch, G.; Kurzchalia, T. V.; Shevchenko, A.; Schwudke, D. Lipid Extraction by Methyl-Terf-Butyl Ether for High-Throughput Lipidomics. *J Lipid Res* **2008**, *49* (5), 1137–1146. https://doi.org/10.1194/jlr.D700041-JLR200.

(75) Holčapek, M.; Ekroos, K. *Mass Spectrometry for Lipidomics: Methods and Applications*; wiley, 2023. https://doi.org/10.1002/9783527836512.fmatter.

(76) Teo, C. C.; Chong, W. P. K.; Tan, E.; Basri, N. B.; Low, Z. J.; Ho, Y. S. Advances in Sample Preparation and Analytical Techniques for Lipidomics Study of Clinical Samples. *TrAC - Trends in Analytical Chemistry* **2015**, *66*, 1–18. https://doi.org/10.1016/j.trac.2014.10.010.

(77) Bailey, L. S.; Prajapati, D. V.; Basso, K. B. Optimization of the Sulfo-Phospho-Vanillin Assay for Total Lipid Normalization in Untargeted Quantitative Lipidomic LC-MS/MS Applications. *Anal Chem* **2022**, *94* (51), 17810–17818. https://doi.org/10.1021/acs.analchem.2c03488.

(78) Lange, M.; Ni, Z.; Criscuolo, A.; Fedorova, M. Liquid Chromatography Techniques in Lipidomics Research. *Chromatographia* **2019**, *82* (1), 77–100. https://doi.org/10.1007/s10337-018-3656-4.

(79) Rampler, E.; Schoeny, H.; Mitic, B. M.; El Abiead, Y.; Schwaiger, M.; Koellensperger, G. Simultaneous Non-Polar and Polar Lipid Analysis by on-Line Combination of HILIC, RP and High Resolution MS. *Analyst* **2018**, *143* (5), 1250–1258. https://doi.org/10.1039/c7an01984j.

(80) Nasiri, A.; Jahani, R.; Mokhtari, S.; Yazdanpanah, H.; Daraei, B.; Faizi, M.; Kobarfard, F. Overview, Consequences, and Strategies for Overcoming Matrix Effects in LC-MS Analysis: A Critical Review. *Analyst* **2021**, *146* (20), 6049–6063. https://doi.org/10.1039/d1an01047f.

(81) Rustam, Y. H.; Reid, G. E. Analytical Challenges and Recent Advances in Mass Spectrometry Based Lipidomics. *Anal Chem* **2018**, *90* (1), 374–397. https://doi.org/10.1021/acs.analchem.7b04836.

(82) Mal, M.; Wong, S. A HILIC-Based UPLC/MS Method for the Separation of Lipid Classes from Plasma. *Waters Corporation*. 2011.

(83) Xu, M.; Legradi, J.; Leonards, P. Evaluation of LC-MS and LC×LC-MS in Analysis of Zebrafish Embryo Samples for Comprehensive Lipid Profiling. *Anal Bioanal Chem* **2020**, *412* (18), 4313–4325. https://doi.org/10.1007/s00216-020-02661-1.

(84) Jurowski, K.; Kochan, K.; Walczak, J.; Barańska, M.; Piekoszewski, W.; Buszewski, B. Analytical Techniques in Lipidomics: State of the Art. *Crit Rev Anal Chem* **2017**, *47* (5), 418–437. https://doi.org/10.1080/10408347.2017.1310613.

(85) Tsikas, D.; Zoerner, A. A.; Mitschke, A.; Gutzki, F. M. Nitro-Fatty Acids Occur in Human Plasma in the Picomolar Range: A Targeted Nitro-Lipidomics GC-MS/MS Study. *Lipids* **2009**, *44* (9), 855–865. https://doi.org/10.1007/s11745-009-3332-4.

(86) Wei, Q.; Cui, H.; Hu, Y.; Li, J.; Yue, S.; Tang, C.; Zhao, Q.; Yu, Y.; Li, H.; Qin, Y.; Yang, Y.; Zhang, J. Comparative Characterization of Taihe Silky Chicken and Cobb Chicken Using LC/MS-Based Lipidomics and GC/MS-Based Volatilomics. *LWT* **2022**, *163*. https://doi.org/10.1016/j.lwt.2022.113554.

(87) Eylem, C. C.; Nemutlu, E.; Dogan, A.; Acik, V.; Matyar, S.; Gezercan, Y.; Altintas, S.; Okten, A. I.; Basci Akduman, N. E. High-Throughput Single-Step Plasma Sample Extraction Optimization Strategies with Experimental Design for LC-MS and GC–MS Integrated Metabolomics and Lipidomics Analysis. *Microchemical Journal* **2022**, *179*. https://doi.org/10.1016/j.microc.2022.107525.

(88) Bhatt, K.; Dejong, T.; Dubois, L. M.; Markey, A.; Gengler, N.; Wavreille, J.; Stefanuto, P. H.; Focant, J. F. Lipid Serum Profiling of Boar-Tainted and Untainted Pigs Using GC×GC–TOFMS: An Exploratory Study. *Metabolites* **2022**, *12* (11). https://doi.org/10.3390/metabo12111111.

(89) Dias, F. F. G.; Bogusz, S.; Silva, R. S.; Fronza, M.; Hantao, L. W. Leveraging the Use of Ionic Liquid Capillary Columns and GC×GC-MS for Fatty Acid Profiling in Human

Colostrum Samples. *Anal Bioanal Chem* **2024**, *416* (1), 191–201. https://doi.org/10.1007/s00216-023-05006-w.

(90) Chollet, C.; Boutet-Mercey, S.; Laboureur, L.; Rincon, C.; Méjean, M.; Jouhet, J.; Fenaille, F.; Colsch, B.; Touboul, D. Supercritical Fluid Chromatography Coupled to Mass Spectrometry for Lipidomics. *Journal of Mass Spectrometry* **2019**, *54* (10), 791–801. https://doi.org/10.1002/jms.4445.

(91) He, B.; Zhou, T.; Liu, J. Lipidomics Study of Type 1 Diabetic Rats Using Online Phase Transition Trapping-Supercritical Fluid Extraction-Chromatography Coupled with Quadrupole Time-of-Flight Tandem Mass Spectrometry. *J Proteome Res* **2024**. https://doi.org/10.1021/acs.jproteome.4c00337.

(92) Schoeny, H.; Rampler, E.; Hermann, G.; Grienke, U.; Rollinger, J. M.; Koellensperger, G. Preparative Supercritical Fluid Chromatography for Lipid Class Fractionation—a Novel Strategy in High-Resolution Mass Spectrometry Based Lipidomics. *Anal Bioanal Chem* **2020**, *412* (10), 2365–2374. https://doi.org/10.1007/s00216-020-02463-5.

(93) Bamba, T.; Lee, J. W.; Matsubara, A.; Fukusaki, E. Metabolic Profiling of Lipids by Supercritical Fluid Chromatography/Mass Spectrometry. *J Chromatogr A* **2012**, *1250*, 212–219. https://doi.org/10.1016/j.chroma.2012.05.068.

(94) Valdes-Gonzalez, T.; Goto-Inoue, N.; Hirano, W.; Ishiyama, H.; Hayasaka, T.; Setou, M.; Taki, T. New Approach for Glyco- and Lipidomics - Molecular Scanning of Human Brain Gangliosides by TLC-Blot and MALDI-QIT-TOF MS. *Journal of Neurochemistry*. March 2011, pp 678–683. https://doi.org/10.1111/j.1471-4159.2010.07152.x.

(95) Deranieh, R. M.; Joshi, A. S.; Greenberg, M. L. Thin-Layer Chromatography of Phospholipids. *Methods in Molecular Biology* **2013**, *1033*, 21–27. https://doi.org/10.1007/978-1-62703-487-6_2.

(96) Martineau, E.; Dumez, J. N.; Giraudeau, P. Fast Quantitative 2D NMR for Metabolomics and Lipidomics: A Tutorial. *Magnetic Resonance in Chemistry* **2020**, *58* (5), 390–403. https://doi.org/10.1002/mrc.4899.

(97) Huang, Z.; Tong, Y.; Wang, J.; Huang, Y. NMR Studies of the Relationship between the Changes of Membrane Lipids and the Cisplatin-Resistance of A549/DDP Cells. *Cancer Cell Int* **2003**.

(98) Marchand, J.; Martineau, E.; Guitton, Y.; Le Bizec, B.; Dervilly-Pinel, G.; Giraudeau, P. A Multidimensional 1 H NMR Lipidomics Workflow to Address Chemical Food Safety Issues. *Metabolomics* **2018**, *14* (5). https://doi.org/10.1007/s11306-018-1360-x.

(99) Furse, S.; Williams, H. E. L.; Watkins, A. J.; Virtue, S.; Vidal-Puig, A.; Amarsi, R.; Charalambous, M.; Koulman, A. A Pipeline for Making 31 P NMR Accessible for Small- and Large-Scale Lipidomics Studies. *Anal Bioanal Chem* **2021**, No. 413, 4763–4773. https://doi.org/10.1007/s00216-021-03430-4/Published.

(100) Han, X.; Gross, R. W. Shotgun Lipidomics: Multidimensional MS Analysis of Cellular Lipidomes. *Expert Rev Proteomics* **2005**, *2* (2), 253–264. https://doi.org/10.1586/14789450.2.2.253.

(101) Fuchs, B.; Schiller, J. Application of MALDI-TOF Mass Spectrometry in Lipidomics. *European Journal of Lipid Science and Technology* **2009**, *111* (1), 83–98. https://doi.org/10.1002/ejlt.200800223.

(102) Zardini Buzatto, A.; Kwon, B. K.; Li, L. Development of a NanoLC-MS Workflow for High-Sensitivity Global Lipidomic Analysis. *Anal Chim Acta* **2020**, *1139*, 88–99. https://doi.org/10.1016/j.aca.2020.09.001.

(103) Zardini Buzatto, A.; Abdel Jabar, M.; Nizami, I.; Dasouki, M.; Li, L.; Abdel Rahman, A. M. Lipidome Alterations Induced by Cystic Fibrosis, CFTR Mutation, and Lung Function. *J Proteome Res* **2021**, *20* (1), 549–564. https://doi.org/10.1021/acs.jproteome.0c00556.

(104) Han, X.; Gross, R. W. Global Analyses of Cellular Lipidomes Directly from Crude Extracts of Biological Samples by ESI Mass Spectrometry: A Bridge to Lipidomics. *Journal of Lipid Research*. June 2003, pp 1071–1079. https://doi.org/10.1194/jlr.R300004-JLR200.

(105) Chen, J.; Xie, P.; Dai, Q.; Wu, P.; He, Y.; Lin, Z.; Cai, Z. Spatial Lipidomics and Metabolomics of Multicellular Tumor Spheroids Using MALDI-2 and Trapped Ion Mobility Imaging. *Talanta* **2023**, *265*. https://doi.org/10.1016/j.talanta.2023.124795.

(106) Wang, C. F.; Li, L. Instrument-Type Effects on Chemical Isotope Labeling LC-MS Metabolome Analysis: Quadrupole Time-of-Flight MS vs. Orbitrap MS. *Anal Chim Acta* **2022**, *1226*. https://doi.org/10.1016/j.aca.2022.340255.

(107) Bhattacharyya, D. LC-MS Innovations: Review of the Technology and Its Advancements Triple Quadrupole (QqQ) and Orbitrap-Based Mass Spectrometry Technology-Choose the Right Tools for the Right Trade. *ThermoFisher Scientiifc*. 2018.

(108) Zardini Buzatto, A.; Sarkar, I.; Van Drunen Littel-Van Den Hurk, S.; Li, L. Comprehensive Lipidomic and Metabolomic Analysis for Studying Metabolic Changes in Lung Tissue Induced by a Vaccine against Respiratory Syncytial Virus. *ACS Infect Dis* **2020**, *6* (8), 2130–2142. https://doi.org/10.1021/acsinfecdis.0c00210.

(109) Kantae, V.; Ogino, S.; Noga, M.; Harms, A. C.; Van Dongen, R. M.; Onderwater, G. L. J.; Van Den Maagdenberg, A. M. J. M.; Terwindt, G. M.; Van Der Stelt, M.; Ferrari, M. D.; Hankemeier, T. Quantitative Profiling of Endocannabinoids & Related N-Acylethanolamines in Human CSF Using Nano LC-MS/MS. *J Lipid Res* **2017**, *58* (3), 615–624. https://doi.org/10.1194/jlr.D070433.

(110) Buzatto, A. Z.; Malkawi, A.; Sabi, E. M.; Mujamammi, A. H.; Li, L.; Abdel Rahman, A. M. Tissue Lipidomic Alterations Induced by Prolonged Dexamethasone Treatment. *J Proteome Res* **2021**. https://doi.org/10.1021/acs.jproteome.0c00759.

(111) Tokiyoshi, K.; Matsuzawa, Y.; Takahashi, M.; Takeda, H.; Hasegawa, M.; Miyamoto, J.; Tsugawa, H. Using Data-Dependent and -Independent Hybrid Acquisitions for Fast Liquid Chromatography-Based Untargeted Lipidomics. *Anal Chem* **2024**, *96* (3), 991–996. https://doi.org/10.1021/acs.analchem.3c04400.

(112) Scheidemantle, G.; Duan, L.; Lodge, M.; Cummings, M. J.; Hilovsky, D.; Pham, E.; Wang, X.; Kennedy, A.; Liu, X. Data-Dependent and -Independent Acquisition Lipidomics Analysis Reveals the Tissue-Dependent Effect of Metformin on Lipid Metabolism. *Metabolomics* **2024**, *20* (3). https://doi.org/10.1007/s11306-024-02113-2.

(113) Hines, K. M.; Herron, J.; Xu, L. Assessment of Altered Lipid Homeostasis by HILIC-Ion Mobility-Mass Spectrometry-Based Lipidomics. *J Lipid Res* **2017**, *58* (4), 809–819. https://doi.org/10.1194/jlr.D074724.

(114) Hinz, C.; Liggi, S.; Griffin, J. L. The Potential of Ion Mobility Mass Spectrometry for High-Throughput and High-Resolution Lipidomics. *Curr Opin Chem Biol* **2018**, *42*, 42–50. https://doi.org/10.1016/j.cbpa.2017.10.018.

(115) Vasilopoulou, C. G.; Sulek, K.; Brunner, A. D.; Meitei, N. S.; Schweiger-Hufnagel, U.; Meyer, S. W.; Barsch, A.; Mann, M.; Meier, F. Trapped Ion Mobility Spectrometry and PASEF Enable In-Depth Lipidomics from Minimal Sample Amounts. *Nat Commun* **2020**, *11* (1). https://doi.org/10.1038/s41467-019-14044-x.

(116) Djambazova, K. V.; Klein, D. R.; Migas, L. G.; Neumann, E. K.; Rivera, E. S.; Van De Plas, R.; Caprioli, R. M.; Spraggins, J. M. Resolving the Complexity of Spatial Lipidomics Using MALDI TIMS Imaging Mass Spectrometry. *Anal Chem* **2020**, *92* (19), 13290–13297. https://doi.org/10.1021/acs.analchem.0c02520.

(117) Wilding-McBride, D.; Dagley, L. F.; Spall, S. K.; Infusini, G.; Webb, A. I. Simplifying MS1 and MS2 Spectra to Achieve Lower Mass Error, More Dynamic Range, and Higher Peptide Identification Confidence on the Bruker TimsTOF Pro. *PLoS One* **2022**, *17* (7 July). https://doi.org/10.1371/journal.pone.0271025.

(118) Liebisch, G.; Ekroos, K.; Hermansson, M.; Ejsing, C. S. Reporting of Lipidomics Data Should Be Standardized. *Biochim Biophys Acta Mol Cell Biol Lipids* **2017**, *1862* (8), 747–751. https://doi.org/10.1016/j.bbalip.2017.02.013.

(119) Tsugawa, H.; Cajka, T.; Kind, T.; Ma, Y.; Higgins, B.; Ikeda, K.; Kanazawa, M.; Vandergheynst, J.; Fiehn, O.; Arita, M. MS-DIAL: Data-Independent MS/MS Deconvolution for Comprehensive Metabolome Analysis. *Nat Methods* **2015**, *12* (6), 523–526. https://doi.org/10.1038/nmeth.3393.

(120) Koelmel, J. P.; Kroeger, N. M.; Ulmer, C. Z.; Bowden, J. A.; Patterson, R. E.; Cochran, J. A.; Beecher, C. W. W.; Garrett, T. J.; Yost, R. A. LipidMatch: An Automated Workflow for Rule-Based Lipid Identification Using Untargeted High-Resolution Tandem Mass Spectrometry Data. *BMC Bioinformatics* **2017**, *18* (1). https://doi.org/10.1186/s12859-017-1744-3.

(121) Wang, C. F.; Li, L. Unraveling the Potential of Segment Scan Mass Spectral Acquisition for Chemical Isotope Labeling LC-MS-Based Metabolome Analysis: Performance Assessment across Different Types of Biological Samples. *Anal Chim Acta* **2024**, *1288*. https://doi.org/10.1016/j.aca.2023.342137.

(122) Skotland, T.; Ekroos, K.; McDonald, J.; Ahrends, R.; Liebisch, G.; Sandvig, K. Pitfalls in Lipid Mass Spectrometry of Mammalian Samples — a Brief Guide for Biologists. *Nat Rev Mol Cell Biol* **2024**. https://doi.org/10.1038/s41580-024-00758-4.

(123) Liebisch, G.; Fahy, E.; Aoki, J.; Dennis, E. A.; Durand, T.; Ejsing, C. S.; Fedorova, M.; Feussner, I.; Griffiths, W. J.; Köfeler, H.; Merrill, A. H.; Murphy, R. C.; O'Donnell, V. B.; Oskolkova, O.; Subramaniam, S.; Wakelam, M. J. O.; Spener, F. Update on LIPID MAPS Classification, Nomenclature, and Shorthand Notation for MS-Derived Lipid Structures. *J Lipid Res* **2020**, *61* (12), 1539–1555. https://doi.org/10.1194/jlr.S120001025.

(124) Nuzzo, R. How Scientists Fool Themselves – and How They Can Stop. *Nature* **2015**, *526*, 182–185.

(125) Züllig, T.; Trötzmüller, M.; Köfeler, H. C. Lipidomics from Sample Preparation to Data Analysis: A Primer. *Anal Bioanal Chem* **2020**, *412* (10), 2191–2209. https://doi.org/10.1007/s00216-019-02241-y.

(126) Hammouri, H. M.; Sabo, R. T.; Alsaadawi, R.; Kheirallah, K. A. Handling Skewed Data: A Comparison of Two Popular Methods. *Applied Sciences (Switzerland)* **2020**, *10* (18). https://doi.org/10.3390/APP10186247.

(127) Glazier, D. S. Biological Scaling Analyses Are More than Statistical Line Fitting. *Journal of Experimental Biology* **2021**, *224* (11). https://doi.org/10.1242/jeb.241059.

(128) Hyötyläinen, T.; Orešič, M. Systems Biology Strategies to Study Lipidomes in Health and Disease. *Prog Lipid Res* **2014**, *55* (1), 43–60. https://doi.org/10.1016/j.plipres.2014.06.001.

(129) Ruiz-Perez, D.; Guan, H.; Madhivanan, P.; Mathee, K.; Narasimhan, G. So You Think You Can PLS-DA? *BMC Bioinformatics* **2020**, *21*. https://doi.org/10.1186/s12859-019-3310-7.

(130) Lee, L. C.; Liong, C. Y.; Jemain, A. A. Partial Least Squares-Discriminant Analysis (PLS-DA) for Classification of High-Dimensional (HD) Data: A Review of Contemporary Practice Strategies and Knowledge Gaps. *Analyst* **2018**, *143* (15), 3526–3539. https://doi.org/10.1039/c8an00599k.

(131) Hu, C.; Hoene, M.; Zhao, X.; Häring, H. U.; Schleicher, E.; Lehmann, R.; Han, X.; Xu, G.; Weigert, C. Lipidomics Analysis Reveals Efficient Storage of Hepatic Triacylglycerides

Enriched in Unsaturated Fatty Acids after One Bout of Exercise in Mice. *PLoS One* **2010**, *5* (10). https://doi.org/10.1371/journal.pone.0013318.

(132) Navas-Iglesias, N.; Carrasco-Pancorbo, A.; Cuadros-Rodríguez, L. From Lipids Analysis towards Lipidomics, a New Challenge for the Analytical Chemistry of the 21st Century. Part II: Analytical Lipidomics. *TrAC - Trends in Analytical Chemistry* **2009**, *28* (4), 393–403. https://doi.org/10.1016/j.trac.2008.12.004.

(133) Bowden, J. A.; Heckert, A.; Ulmer, C. Z.; Jones, C. M.; Koelmel, J. P.; Abdullah, L.; Ahonen, L.; Alnouti, Y.; Armando, A. M.; Asara, J. M.; Bamba, T.; Barr, J. R.; Bergquist, J.; Borchers, C. H.; Brandsma, J.; Breitkopf, S. B.; Cajka, T.; Cazenave-Gassiot, A.; Checa, A.; Cinel, M. A.; Colas, R. A.; Cremers, S.; Dennis, E. A.; Evans, J. E.; Fauland, A.; Fiehn, O.; Gardner, M. S.; Garrett, T. J.; Gotlinger, K. H.; Han, J.; Huang, Y.; Neo, A. H.; Hyötyläinen, T.; Izumi, Y.; Jiang, H.; Jiang, H.; Jiang, J.; Kachman, M.; Kiyonami, R.; Klavins, K.; Klose, C.; Köfeler, H. C.; Kolmert, J.; Koal, T.; Koster, G.; Kuklenyik, Z.; Kurland, I. J.; Leadley, M.; Lin, K.; Maddipati, K. R.; McDougall, D.; Meikle, P. J.; Mellett, N. A.; Monnin, C.; Moseley, M. A.; Nandakumar, R.; Oresic, M.; Patterson, R.; Peake, D.; Pierce, J. S.; Post, M.; Postle, A. D.; Pugh, R.; Qiu, Y.; Quehenberger, O.; Ramrup, P.; Rees, J.; Rembiesa, B.; Reynaud, D.; Roth, M. R.; Sales, S.; Schuhmann, K.; Schwartzman, M. L.; Serhan, C. N.; Shevchenko, A.; Somerville, S. E.; St John-Williams, L.; Surma, M. A.; Takeda, H.; Thakare, R.; Thompson, J. W.; Torta, F.; Triebl, A.; Trötzmüller, M.; Ubhayasekera, S. J. K.; Vuckovic, D.; Weir, J. M.; Welti, R.; Wenk, M. R.; Wheelock, C. E.; Yao, L.; Yuan, M.; Zhao, X. H.; Zhou, S. Harmonizing Lipidomics: NIST Interlaboratory

Comparison Exercise for Lipidomics Using SRM 1950-Metabolites in Frozen Human Plasma. *J Lipid Res* **2017**, *58* (12), 2275–2288. https://doi.org/10.1194/jlr.M079012.

(134) Mielgo-Ayuso, J.; Collado, P. S.; Urdampilleta, A.; Martínez-Sanz, J. M.; Seco, J. Changes Induced by Diet and Nutritional Intake in the Lipid Profile of Female Professional Volleyball Players after 11 Weeks of Training. *J Int Soc Sports Nutr* **2013**, *10*, 1–7. https://doi.org/10.1186/1550-2783-10-55.

(135) Shephard, R. J.; Cox, M.; West, C. Some Facrors Influencing Serum Lipid Levels in a Working Population. *Atherosclerosis* **1980**, *35*, 287–300.

(136) Ishikawa, M.; Maekawa, K.; Saito, K.; Senoo, Y.; Urata, M.; Murayama, M.; Tajima, Y.; Kumagai, Y.; Saito, Y. Plasma and Serum Lipidomics of Healthy White Adults Shows Characteristic Profiles by Subjects' Gender and Age. *PLoS One* **2014**, *9* (3). https://doi.org/10.1371/journal.pone.0091806.

(137) Wu, Y.; Li, L. Dansylation Metabolite Assay: A Simple and Rapid Method for Sample Amount Normalization in Metabolomics. *Anal Chem* **2014**, *86* (19), 9428–9433. https://doi.org/10.1021/ac503359v.

(138) Covaci, A.; Voorspoels, S.; Thomsen, C.; van Bavel, B.; Neels, H. Evaluation of Total Lipids Using Enzymatic Methods for the Normalization of Persistent Organic Pollutant Levels in Serum. *Science of the Total Environment* **2006**, *366* (1), 361–366. https://doi.org/10.1016/j.scitotenv.2006.03.006.

(139) Inouye, L. S.; Lotufo, G. R. Comparison of Macro-Gravimetric and Micro-Colorimetric Lipid Determination Methods. *Talanta* **2006**, *70* (3), 584–587. https://doi.org/10.1016/j.talanta.2006.01.024.

(140) Liu, Z.; Wang, G. Effect of Fe3+ on the Growth and Lipid Content of Isochrysis Galbana. *Chinese Journal of Oceanology and Limnology* **2014**, *32* (1), 47–53. https://doi.org/10.1007/s00343-014-3110-x.

(141) Sharma, J.; Kumar, S. S.; Bishnoi, N. R.; Pugazhendhi, A. Screening and Enrichment of High Lipid Producing Microalgal Consortia. *J Photochem Photobiol B* **2019**, *192* (January), 8–12. https://doi.org/10.1016/j.jphotobiol.2019.01.002.

(142) Schlechtriem, C.; Fliedner, A.; Schäfers, C. *Lipid Measurement*; Schmallenberg, 2009.

(143) Ramirez, M. I.; Amorim, M. G.; Gadelha, C.; Milic, I.; Welsh, J. A.; Freitas, V. M.; Nawaz, M.; Akbar, N.; Couch, Y.; Makin, L.; Cooke, F.; Vettore, A. L.; Batista, P. X.; Freezor, R.; Pezuk, J. A.; Rosa-Fernandes, L.; Carreira, A. C. O.; Devitt, A.; Jacobs, L.; Silva, I. T.; Coakley, G.; Nunes, D. N.; Carter, D.; Palmisano, G.; Dias-Neto, E. Technical Challenges of Working with Extracellular Vesicles. *Nanoscale* **2018**, *10* (3), 881–906. https://doi.org/10.1039/c7nr08360b.

(144) Hyka, P.; Lickova, S.; Přibyl, P.; Melzoch, K.; Kovar, K. Flow Cytometry for the Development of Biotechnological Processes with Microalgae. *Biotechnol Adv* **2013**, *31* (1), 2–16. https://doi.org/10.1016/j.biotechadv.2012.04.007.

(145) Niu, Y. F.; Zhang, M. H.; Li, D. W.; Yang, W. D.; Liu, J. S.; Bai, W. Bin; Li, H. Y. Improvement of Neutral Lipid and Polyunsaturated Fatty Acid Biosynthesis by

Overexpressing a Type 2 Diacylglycerol Acyltransferase in Marine Diatom Phaeodactylum Tricornutum. *Mar Drugs* **2013**, *11* (11), 4558–4569. https://doi.org/10.3390/md11114558.

(146) Ge, F.; Huang, W.; Chen, Z.; Zhang, C.; Xiong, Q.; Bowler, C.; Yang, J.; Xu, J.; Hu, H. Methylcrotonyl-CoA Carboxylase Regulates Triacylglycerol Accumulation in the Model Diatom Phaeodactylum Tricornutum. *Plant Cell* **2014**, *26* (4), 1681–1697. https://doi.org/10.1105/tpc.114.124982.

(147) Wang, X.; Liu, S. F.; Li, R. Y.; Yang, W. D.; Liu, J. S.; Lin, C. S. K.; Balamurugan, S.; Li, H. Y. TAG Pathway Engineering via GPAT2 Concurrently Potentiates Abiotic Stress Tolerance and Oleaginicity in Phaeodactylum Tricornutum. *Biotechnol Biofuels* **2020**, *13* (1). https://doi.org/10.1186/s13068-020-01799-5.

(148) Anschau, A.; Caruso, C. S.; Kuhn, R. C.; Franco, T. T. Validation of the Sulfo-Phosphovanillin (SPV) Method for the Determination of Lipid Content in Oleaginous Microorganisms. *Brazilian Journal of Chemical Engineering* **2017**, *34* (1), 19–27. https://doi.org/10.1590/0104-6632.20170341s20140222.

(149) Cheng, Y. S.; Zheng, Y.; VanderGheynst, J. S. Rapid Quantitative Analysis of Lipids Using a Colorimetric Method in a Microplate Format. *Lipids* **2011**, *46* (1), 95–103. https://doi.org/10.1007/s11745-010-3494-0.

(150) Vatassery, G. T.; Sheridan, M. A.; Krezowski, A. M.; Divine, A. S.; Bach, H. L. Use of the Sulfo-Phospo-Vanillin Reaction in a Routine Method for Determining Total Lipids in Human Cerebrospinal Fluid. *Clin Biochem* **1981**, *14* (1), 21–24. https://doi.org/10.1016/0009-9120(81)90120-X.

(151) Knight, J. A.; Anderson, S.; Rawle, J. M. Chemical Basis of the Sulfo-Phospho-Vanillin Reaction for Estimating Total Serum Lipids. *Clin Chem* **1972**, *18* (3), 199–202. https://doi.org/10.1093/clinchem/18.3.199.

(152) McMahon, A.; Lu, H.; Butovich, I. A. The Spectrophotometric Sulfo-Phospho-Vanillin Assessment of Total Lipids in Human Meibomian Gland Secretions. *Lipids* **2013**, *48* (5), 513–525. https://doi.org/10.1007/s11745-013-3755-9.

(153) Simopoulos, A. P. An Increase in the Omega-6/Omega-3 Fatty Acid Ratio Increases the Risk for Obesity. *Nutrients*. MDPI AG March 2, 2016. https://doi.org/10.3390/nu8030128.

(154) Kien, C. L.; Bunn, J. Y.; Stevens, R.; Bain, J.; Ikayeva, O.; Crain, K.; Koves, T. R.; Muoio, D. M. Dietary Intake of Palmitate and Oleate Has Broad Impact on Systemic and Tissue Lipid Profiles in Humans. *American Journal of Clinical Nutrition* **2014**, *99* (3), 436–445. https://doi.org/10.3945/ajcn.113.070557.

(155) Byreddy, A. R.; Gupta, A.; Barrow, C. J.; Puri, M. Comparison of Cell Disruption Methods for Improving Lipid Extraction from Thraustochytrid Strains. *Mar Drugs* **2015**, *13* (8), 5111–5127. https://doi.org/10.3390/md13085111.

(156) Salimetrics, L.L.C., SalivaBio, L. L. C. Saliva Collection and Handling Advice. *Methods* **2015**, *44* (0), 1–15.

(157) America, A. H. P.; Cordewener, J. H. G. Comparative LC-MS: A Landscape of Peaks and Valleys. *Proteomics* **2008**, *8* (4), 731–749. https://doi.org/10.1002/pmic.200700694.

(158) Frings, C. S.; Dunn, R. T. A Colorimetric Method for Determination of Total Serum Lipids Based on the Sulfo-Phospho-Vanillin Reaction. *Am J Clin Pathol* **1970**, *53* (1), 89–91. https://doi.org/10.1093/ajcp/53.1.89.

(159) Bakry, I. A.; Korma, S. A.; Wei, W.; Nafea, A. E.; Mahdi, A. A.; Ziedan, N. I.; Wang, X. Changes in the Fatty Acid Content of Egyptian Human Milk across the Lactation Stages and in Comparison with Chinese Human Milk. *European Food Research and Technology* **2021**, *247* (5), 1035–1048. https://doi.org/10.1007/s00217-021-03685-2.

(160) Park, J.; Jeong, H. J.; Yoon, E. Y.; Moon, S. J. Easy and Rapid Quantification of Lipid Contents of Marine Dinoflagellates Using the Sulpho-Phospho-Vanillin Method. *Algae* **2016**, *31* (4), 391–401. https://doi.org/10.4490/algae.2016.31.12.7.

(161) Bel'skaya, L. V.; Sarf, E. A.; Kosenok, V. K. Age and Gender Characteristics of the Biochemical Composition of Saliva: Correlations with the Composition of Blood Plasma. *J Oral Biol Craniofac Res* **2020**, *10* (2), 59–65. https://doi.org/10.1016/j.jobcr.2020.02.004.

(162) Li, C. H.; Haider, S.; Shiah, Y. J.; Thai, K.; Boutros, P. C. Sex Differences in Cancer Driver Genes and Biomarkers. *Cancer Res* **2018**, *78* (19), 5527–5537. https://doi.org/10.1158/0008-5472.CAN-18-0362.

(163) Uhrig, M.; Ezquer, F.; Ezquer, M. Improving Cell Recovery: Freezing and Thawing Optimization of Induced Pluripotent Stem Cells. *Cells* **2022**, *11* (5). https://doi.org/10.3390/cells11050799.

(164) Tan, H. T.; Khong, N. M. H.; Khaw, Y. S.; Ahmad, S. A.; Yusoff, F. M. Optimization of the Freezing-Thawing Method for Extracting Phycobiliproteins from Arthrospira Sp. *Molecules* **2020**, *25* (17). https://doi.org/10.3390/molecules25173894.

(165) Pispas, K.; Manthos, G.; Sventzouri, E.; Geroulia, M.; Mastropetros, S. G.; Ali, S. S.; Kornaros, M. Optimizing Phycocyanin Extraction from Cyanobacterial Biomass: A Comparative Study of Freeze–Thaw Cycling with Various Solvents. *Mar Drugs* **2024**, *22* (6), 246. https://doi.org/10.3390/md22060246.

(166) Klupczynska, A.; Plewa, S.; Kasprzyk, M.; Dyszkiewicz, W.; Kokot, Z. J.; Matysiak, J. Serum Lipidome Screening in Patients with Stage I Non-Small Cell Lung Cancer. *Clin Exp Med* **2019**, *19* (4), 505–513. https://doi.org/10.1007/s10238-019-00566-7.

(167) Eiriksson, F. F.; Nøhr, M. K.; Costa, M.; Bödvarsdottir, S. K.; Ögmundsdottir, H. M.; Thorsteinsdottir, M. Lipidomic Study of Cell Lines Reveals Differences between Breast Cancer Subtypes. *PLoS One* **2020**, *15* (4), 1–22. https://doi.org/10.1371/journal.pone.0231289.

(168) Matczuk, J.; Zendzian-Piotrowska, M.; Maciejczyk, M.; Kurek, K. Salivary Lipids: A Review. *Advances in Clinical and Experimental Medicine* **2017**, *26* (6), 1023–1031. https://doi.org/10.17219/acem/63030.

(169) Nunes, L. A. S.; Mussavira, S.; Bindhu, O. S. Clinical and Diagnostic Utility of Saliva as a Non-Invasive Diagnostic Fluid: A Systematic Review. *Biochem Med (Zagreb)* **2015**, *25* (2), 177–192. https://doi.org/10.11613/BM.2015.018.

(170) Malek, M.; Wawrzyniak, A. M.; Koch, P.; Lüchtenborg, C.; Hessenberger, M.; Sachsenheimer, T.; Jang, W.; Brügger, B.; Haucke, V. Inositol Triphosphate-Triggered Calcium Release Blocks Lipid Exchange at Endoplasmic Reticulum-Golgi Contact Sites. *Nat Commun* **2021**, *12* (1). https://doi.org/10.1038/s41467-021-22882-x.

(171) Silva, L. P.; Lorenzi, P. L.; Purwaha, P.; Yong, V.; Hawke, D. H.; Weinstein, J. N. Measurement of DNA Concentration as a Normalization Strategy for Metabolomic Data from Adherent Cell Lines. *Anal Chem* **2013**, *85* (20), 9536–9542. https://doi.org/10.1021/ac401559v.

(172) Huang, G. H.; Chen, G.; Chen, F. Rapid Screening Method for Lipid Production in Alga Based on Nile Red Fluorescence. *Biomass Bioenergy* **2009**, *33* (10), 1386–1392. https://doi.org/10.1016/J.BIOMBIOE.2009.05.022.

(173) Das, S. Recent Applications of Ninhydrin in Multicomponent Reactions. *RSC Adv* **2020**, *10* (32), 18875–18906. https://doi.org/10.1039/d0ra02930k.

(174) Zatorski, J. M.; Montalbine, A. N.; Ortiz-Cárdenas, J. E.; Pompano, R. R. Quantification of Fractional and Absolute Functionalization of Gelatin Hydrogels by Optimized Ninhydrin Assay and 1H NMR. *Anal Bioanal Chem* **2020**, *412* (24), 6211–6220. https://doi.org/10.1007/s00216-020-02792-5.

(175) Horn, P. J.; Chapman, K. D. Lipidomics in Tissues, Cells and Subcellular Compartments. *Plant Journal* **2012**, *70* (1), 69–80. https://doi.org/10.1111/j.1365-313X.2011.04868.x.

(176) Mousavi, M.; Jonsson, P.; Antti, H.; Adolfsson, R.; Nordin, A.; Bergdahl, J.; Eriksson, K.; Moritz, T.; Nilsson, L.-G.; Nyberg, L. Serum Metabolomic Biomarkers of Dementia. *Dement Geriatr Cogn Dis Extra* **2014**, *4* (2), 252–262. https://doi.org/10.1159/000364816.

(177) Lohavanichbutr, P.; Zhang, Y.; Wang, P.; Gu, H.; Nagana Gowda, G. A.; Djukovic, D.; Buas, M. F.; Raftery, D.; Chen, C. Salivary Metabolite Profiling Distinguishes Patients with Oral Cavity Squamous Cell Carcinoma from Normal Controls. *PLoS One* **2018**, *13* (9), 1–18. https://doi.org/10.1371/journal.pone.0204249.

(178) Sud, M.; Fahy, E.; Cotter, D.; Brown, A.; Dennis, E. A.; Glass, C. K.; Merrill, A. H.; Murphy, R. C.; Raetz, C. R. H.; Russell, D. W.; Subramaniam, S. LMSD: LIPID MAPS Structure Database. *Nucleic Acids Res* **2007**, *35* (SUPPL. 1). https://doi.org/10.1093/nar/gkl838.

(179) Al Habobe, H.; Haverkort, E. B.; Nazmi, K.; Van Splunter, A. P.; Pieters, R. H. H.; Bikker, F. J. The Impact of Saliva Collection Methods on Measured Salivary Biomarker Levels. *Clinica Chimica Acta* **2024**, *552*. https://doi.org/10.1016/j.cca.2023.117628.

(180) Yamaguchi, M.; Tezuka, Y.; Takeda, K.; Shetty, V. Disposable Collection Kit for Rapid and Reliable Collection of Saliva. *American Journal of Human Biology* **2015**, *27* (5), 720–723. https://doi.org/10.1002/ajhb.22696.

(181) Mung, D.; Li, L. Chemical Isotope Labeling Liquid Chromatography Mass Spectrometry for Investigating Acute Dietary Effects of Cow Milk Consumption on Human Urine Metabolome. *J Food Drug Anal* **2019**, *27* (2), 565–574. https://doi.org/10.1016/j.jfda.2018.10.007.

(182) Liebisch, G.; Vizcaíno, J. A.; Köfeler, H.; Trötzmüller, M.; Griffiths, W. J.; Schmitz, G.; Spener, F.; Wakelam, M. J. O. Shorthand Notation for Lipid Structures Derived from Mass Spectrometry. *J Lipid Res* **2013**, *54* (6), 1523–1530. https://doi.org/10.1194/jlr.M033506.

(183) Aoyagi, R.; Ikeda, K.; Isobe, Y.; Arita, M. Comprehensive Analyses of Oxidized Phospholipids Using a Measured MS/MS Spectra Library. *J Lipid Res* **2017**, *58* (11), 2229–2237. https://doi.org/10.1194/jlr.D077123.

(184) Kind, T.; Liu, K. H.; Lee, D. Y.; Defelice, B.; Meissen, J. K.; Fiehn, O. LipidBlast in Silico Tandem Mass Spectrometry Database for Lipid Identification. *Nat Methods* **2013**, *10* (8), 755–758. https://doi.org/10.1038/nmeth.2551.

(185) Lu, D.; He, A.; Tan, M.; Mrad, M.; El Daibani, A.; Hu, D.; Liu, X.; Kleiboeker, B.; Che, T.; Hsu, F.-F.; Bambouskova, M.; Semenkovich, C. F.; Lodhi, I. J. Liver ACOX1 Regulates Levels of Circulating Lipids That Promote Metabolic Health through Adipose Remodeling. *Nat Commun* **2024**, *15* (1). https://doi.org/10.1038/s41467-024-48471-2.

(186) Ma, Y.; Kind, T.; Vaniya, A.; Gennity, I.; Fahrmann, J. F.; Fiehn, O. An in Silico MS/MS Library for Automatic Annotation of Novel FAHFA Lipids. *J Cheminform* **2015**, *7* (1). https://doi.org/10.1186/s13321-015-0104-4.

(187) Wishart, D. S.; Feunang, Y. D.; Marcu, A.; Guo, A. C.; Liang, K.; Vázquez-Fresno, R.; Sajed, T.; Johnson, D.; Li, C.; Karu, N.; Sayeeda, Z.; Lo, E.; Assempour, N.; Berjanskii, M.; Singhal, S.; Arndt, D.; Liang, Y.; Badran, H.; Grant, J.; Serra-Cayuela, A.; Liu, Y.; Mandal, R.; Neveu, V.; Pon, A.; Knox, C.; Wilson, M.; Manach, C.; Scalbert, A. HMDB 4.0: The Human Metabolome Database for 2018. *Nucleic Acids Res* **2018**, *46* (D1), D608–D617. https://doi.org/10.1093/nar/gkx1089.

(188) Astarita, G.; Ahmed, F.; Piomelli, D. Lipidomic Analysis of Biological Samples by Liquid Chromatography Coupled to Mass Spectrometry. *Methods in Molecular Biology* **2009**, *579*, 201–219. https://doi.org/10.1007/978-1-60761-322-0_10.

(189) Urban, P. L. Quantitative Mass Spectrometry: An Overview. *Philosophical Transactions of the Royal Society A: Mathematical, Physical and Engineering Sciences* **2016**, *374* (2079). https://doi.org/10.1098/rsta.2015.0382.

(190) Belouafa, S.; Habti, F.; Benhar, S.; Belafkih, B.; Tayane, S.; Hamdouch, S.; Bennamara, A.; Abourriche, A. Statistical Tools and Approaches to Validate Analytical Methods: Methodology and Practical Examples. *International Journal of Metrology and Quality Engineering* **2017**, *8*. https://doi.org/10.1051/ijmqe/2016030.

(191) Wooldridge, J. M. *Introductory Econometrics: A Modern Approach*; South-Western Cengage Learning: Mason, Ohio, 2015.

(192) Zhong, H.; Fang, C.; Fan, Y.; Lu, Y.; Wen, B.; Ren, H.; Hou, G.; Yang, F.; Xie, H.; Jie, Z.; Peng, Y.; Ye, Z.; Wu, J.; Zi, J.; Zhao, G.; Chen, J.; Bao, X.; Hu, Y.; Gao, Y.; Zhang, J.; Yang, H.; Wang, J.; Madsen, L.; Kristiansen, K.; Ni, C.; Li, J.; Liu, S. Lipidomic Profiling Reveals Distinct Differences in Plasma Lipid Composition in Healthy, Prediabetic, and Type 2 Diabetic Individuals. *Gigascience* **2017**, *6* (7). https://doi.org/10.1093/gigascience/gix036.

(193) Quehenberger, O.; Dennis, E. A. The Human Plasma Lipidome. *New England Journal of Medicine* **2011**, *365* (19), 1812–1823. https://doi.org/10.1056/nejmra1104901.

(194) Neyraud, E.; Cabaret, S.; Brignot, H.; Chabanet, C.; Labouré, H.; Guichard, E.; Berdeaux, O. The Basal Free Fatty Acid Concentration in Human Saliva Is Related to Salivary Lipolytic Activity. *Sci Rep* **2017**, *7* (1). https://doi.org/10.1038/s41598-017-06418-2.

(195) Drotleff, B.; Roth, S. R.; Henkel, K.; Calderón, C.; Schlotterbeck, J.; Neukamm, M. A.; Lämmerhofer, M. Lipidomic Profiling of Non-Mineralized Dental Plaque and Biofilm by Untargeted UHPLC-QTOF-MS/MS and SWATH Acquisition. *Anal Bioanal Chem* **2020**, *412* (10), 2303–2314. https://doi.org/10.1007/s00216-019-02364-2.

(196) King, A. M.; Trengove, R. D.; Mullin, L. G.; Rainville, P. D.; Isaac, G.; Plumb, R. S.; Gethings, L. A.; Wilson, I. D. Rapid Profiling Method for the Analysis of Lipids in Human Plasma Using Ion Mobility Enabled-Reversed Phase-Ultra High Performance Liquid Chromatography/Mass Spectrometry. *J Chromatogr A* **2020**, *1611*. https://doi.org/10.1016/j.chroma.2019.460597.

(197) Song, G.; Zhu, Q.; Li, L.; Zheng, Z.; Zhao, Q.; Feng, J.; Zhang, X.; Wang, P.; Chen, K.; Shen, Q. Lipidomics Phenotyping of Clam (Corbicula Fluminea) through Graphene/Fibrous Silica Nanohybrids Based Solid-Phase Extraction and HILIC-MS Analysis. *Food Chem* **2021**, *354*. https://doi.org/10.1016/j.foodchem.2021.129565.

(198) Donato, P.; Rigano, F.; Cacciola, F.; Schure, M.; Farnetti, S.; Russo, M.; Dugo, P.; Mondello, L. Comprehensive Two-Dimensional Liquid Chromatography–Tandem Mass Spectrometry for the Simultaneous Determination of Wine Polyphenols and Target Contaminants. *J Chromatogr A* **2016**, *1458*, 54–62. https://doi.org/10.1016/J.CHROMA.2016.06.042.

(199) Shi, Y.; Li, Z.; Du, Q.; Li, W.; Liu, J.; Jia, Q.; Xue, L.; Zhang, X.; Sun, Z. UHPLC-HRMS-Based Metabolomic and Lipidomic Characterization of Glioma Cells in Response to Anlotinib. *Sci Rep* **2023**, *13* (1). https://doi.org/10.1038/s41598-023-34902-5.

(200) Surma, M. A.; Gerl, M. J.; Herzog, R.; Helppi, J.; Simons, K.; Klose, C. Flexibility of a Mammalian Lipidome-Insights from Mouse Lipidomics. **2021**. https://doi.org/10.1101/2021.05.12.443735.

(201) Hartler, J.; Tharakan, R.; Köfeler, H. C.; Graham, D. R.; Thallinger, G. G. Bioinformatics Tools and Challenges in Structural Analysis of Lipidomics MS/MS Data. *Brief Bioinform* **2013**, *14* (3), 375–390. https://doi.org/10.1093/bib/bbs030.

(202) Koelmel, J. P.; Kroeger, N. M.; Ulmer, C. Z.; Bowden, J. A.; Patterson, R. E.; Cochran, J. A.; Beecher, C. W. W.; Garrett, T. J.; Yost, R. A. LipidMatch: An Automated Workflow for Rule-Based Lipid Identification Using Untargeted High-Resolution Tandem Mass Spectrometry Data. *BMC Bioinformatics* **2017**, *18* (1). https://doi.org/10.1186/s12859-017-1744-3.

(203) Ruta, J.; Rudaz, S.; McCalley, D. V.; Veuthey, J. L.; Guillarme, D. A Systematic Investigation of the Effect of Sample Diluent on Peak Shape in Hydrophilic Interaction Liquid Chromatography. *J Chromatogr A* **2010**, *1217* (52), 8230–8240. https://doi.org/10.1016/j.chroma.2010.10.106.

(204) Chong, J.; Soufan, O.; Li, C.; Caraus, I.; Li, S.; Bourque, G.; Wishart, D. S.; Xia, J. MetaboAnalyst 4.0: Towards More Transparent and Integrative Metabolomics Analysis. *Nucleic Acids Res* **2018**, *46* (W1), W486–W494. https://doi.org/10.1093/nar/gky310.

(205) Plumb, R. S.; Isaac, G.; Rainville, P. D.; Hill, J.; Gethings, L. A.; Johnson, K. A.; Lauterbach, J.; Wilson, I. D. High Throughput UHPLC-MS-Based Lipidomics Using Vacuum Jacketed Columns. *J Proteome Res* **2022**, *21* (3), 691–701. https://doi.org/10.1021/acs.jproteome.1c00836.

(206) Triebl, A.; Trötzmüller, M.; Hartler, J.; Stojakovic, T.; Köfeler, H. C. Lipidomics by Ultrahigh Performance Liquid Chromatography-High Resolution Mass Spectrometry and Its Application to Complex Biological Samples. *J Chromatogr B Analyt Technol Biomed Life Sci* **2017**, *1053*, 72–80. https://doi.org/10.1016/j.jchromb.2017.03.027.

(207) Okazaki, Y.; Kamide, Y.; Hirai, M. Y.; Saito, K. Plant Lipidomics Based on Hydrophilic Interaction Chromatography Coupled to Ion Trap Time-of-Flight Mass Spectrometry. *Metabolomics* **2013**, *9* (SUPPL.1), 121–131. https://doi.org/10.1007/s11306-011-0318-z.

(208) Zhang, J.; Wang, Q.; Kleintop, B.; Raglione, T. Suppression of Peak Tailing of Phosphate Prodrugs in Reversed-Phase Liquid Chromatography. *J Pharm Biomed Anal* **2014**, *98*, 247–252. https://doi.org/10.1016/j.jpba.2014.05.027.

(209) Han, X.; Gross, R. W. Global Analyses of Cellular Lipidomes Directly from Crude Extracts of Biological Samples by ESI Mass Spectrometry: A Bridge to Lipidomics. *J Lipid Res* **2003**, *44* (6), 1071–1079. https://doi.org/10.1194/jlr.R300004-JLR200.

(210) Luo, X.; Gu, X.; Li, L. Development of a Simple and Efficient Method of Harvesting and Lysing Adherent Mammalian Cells for Chemical Isotope Labeling LC-MS-Based Cellular Metabolomics. *Anal Chim Acta* **2018**, *1037*, 97–106. https://doi.org/10.1016/j.aca.2017.11.054.

(211) Gu, W. yi; Liu, M. xian; Sun, B. qing; Guo, M. quan; Wu, J. lin; Li, N. Profiling of Polyunsaturated Fatty Acids in Human Serum Using Off-Line and on-Line Solid Phase Extraction-Nano-Liquid Chromatography-Quadrupole-Time-of-Flight Mass Spectrometry. *J Chromatogr A* **2018**, *1537*, 141–146. https://doi.org/10.1016/j.chroma.2018.01.015.

(212) Pellegrino, R. M.; Di Veroli, A.; Valeri, A.; Goracci, L.; Cruciani, G. LC/MS Lipid Profiling from Human Serum: A New Method for Global Lipid Extraction. *Anal Bioanal Chem* **2014**, *406* (30), 7937–7948. https://doi.org/10.1007/s00216-014-8255-0.

(213) Xu, T.; Hu, C.; Xuan, Q.; Xu, G. Recent Advances in Analytical Strategies for Mass Spectrometry-Based Lipidomics. *Anal Chim Acta* **2020**, *1137*, 156–169. https://doi.org/10.1016/j.aca.2020.09.060.

(214) Loizides-Mangold, U. On the Future of Mass-Spectrometry-Based Lipidomics. *FEBS Journal* **2013**, *280* (12), 2817–2829. https://doi.org/10.1111/febs.12202.

(215) Dams, M.; Dores-Sousa, J. L.; Lamers, R. J.; Treumann, A.; Eeltink, S. High-Resolution Nano-Liquid Chromatography with Tandem Mass Spectrometric Detection for the Bottom-Up Analysis of Complex Proteomic Samples. *Chromatographia* **2019**, *82* (1), 101–110. https://doi.org/10.1007/s10337-018-3647-5.

(216) Mejía-Carmona, K.; Soares da Silva Burato, J.; Borsatto, J. V. B.; de Toffoli, A. L.; Lanças, F. M. Miniaturization of Liquid Chromatography Coupled to Mass Spectrometry: 1. Current Trends on Miniaturized LC Columns. *TrAC - Trends in Analytical Chemistry* **2020**, *122*. https://doi.org/10.1016/j.trac.2019.115735.

(217) Lestremau, F.; Wu, D.; Szücs, R. Evaluation of 1.0mm i.d. Column Performances on Ultra High Pressure Liquid Chromatography Instrumentation. *J Chromatogr A* **2010**, *1217* (30), 4925–4933. https://doi.org/10.1016/j.chroma.2010.05.044.

(218) Cajka, T.; Fiehn, O. Increasing Lipidomic Coverage by Selecting Optimal Mobile-Phase Modifiers in LC–MS of Blood Plasma. *Metabolomics* **2016**, *12* (2), 1–11. https://doi.org/10.1007/s11306-015-0929-x.

(219) Lita, A.; Kuzmin, A. N.; Pliss, A.; Baev, A.; Rzhevskii, A.; Gilbert, M. R.; Larion, M.; Prasad, P. N. Toward Single-Organelle Lipidomics in Live Cells. *Anal Chem* **2019**, *91* (17), 11380–11387. https://doi.org/10.1021/acs.analchem.9b02663.

(220) Danne-Rasche, N.; Coman, C.; Ahrends, R. Nano-LC/NSI MS Refines Lipidomics by Enhancing Lipid Coverage, Measurement Sensitivity, and Linear Dynamic Range. *Anal Chem* **2018**, *90* (13), 8093–8101. https://doi.org/10.1021/acs.analchem.8b01275.

(221) Gadara, D.; Berka, V.; Spacil, Z. High-Throughput Microbore LC-MS Lipidomics to Investigate APOE Phenotypes. *Anal Chem* **2024**, *96*, 59–66. https://doi.org/10.1021/acs.analchem.3c02652.

(222) Werres, T.; Schmidt, T. C.; Teutenberg, T. Influence of the Column Inner Diameter on Chromatographic Efficiency in Miniaturized and Conventional Ultra-High-Performance Liquid Chromatography. *Chromatographia* **2023**, *86* (2), 143–151. https://doi.org/10.1007/s10337-023-04237-4.

(223) Wang, H.; Bennett, P. Performance Assessment of Microflow LC Combined with High-Resolution MS in Bioanalysis. *Bioanalysis* **2013**, *5* (10), 1249–1267. https://doi.org/10.4155/bio.13.93.

(224) Werres, T.; Schmidt, T. C.; Teutenberg, T. The Influence of Injection Volume on Efficiency of Microbore Liquid Chromatography Columns for Gradient and Isocratic Elution. *J Chromatogr A* **2021**, *1641*. https://doi.org/10.1016/j.chroma.2021.461965.

(225) Sun, R.; Wu, T.; Guo, H.; Xu, J.; Chen, J.; Tao, N.; Wang, X.; Zhong, J. Lipid Profile Migration during the Tilapia Muscle Steaming Process Revealed by a Transactional Analysis between MS Data and Lipidomics Data. *NPJ Sci Food* **2021**, *5* (1). https://doi.org/10.1038/s41538-021-00115-1.

(226) Venable, J. D.; Wohlschlegel, J.; McClatchy, D. B.; Sung, K. P.; Yates, J. R. Relative Quantification of Stable Isotope Labeled Peptides Using a Linear Ion Trap-Orbitrap Hybrid Mass Spectrometer. *Anal Chem* **2007**, *79* (8), 3056–3064. https://doi.org/10.1021/ac062054i.

(227) Vosse, C.; Wienken, C.; Cadenas, C.; Hayen, H. Separation and Identification of Phospholipids by Hydrophilic Interaction Liquid Chromatography Coupled to Tandem High Resolution Mass Spectrometry with Focus on Isomeric Phosphatidylglycerol and Bis(Monoacylglycero)Phosphate. *J Chromatogr A* **2018**, *1565*, 105–113. https://doi.org/10.1016/j.chroma.2018.06.039.

(228) Scigelova, M.; Hornshaw, M.; Giannakopulos, A.; Makarov, A. Fourier Transform Mass Spectrometry. *Molecular and Cellular Proteomics* **2011**, *10* (7). https://doi.org/10.1074/mcp.M111.009431.

(229) Granafei, S.; Losito, I.; Palmisano, F.; Cataldi, T. R. I. Identification of Isobaric Lyso-Phosphatidylcholines in Lipid Extracts of Gilthead Sea Bream (Sparus Aurata) Fillets by Hydrophilic Interaction Liquid Chromatography Coupled to High-Resolution Fourier-Transform Mass Spectrometry. *Anal Bioanal Chem* **2015**, *407* (21), 6391–6404. https://doi.org/10.1007/s00216-015-8671-9.

(230) Lenčo, J.; Šemlej, T.; Khalikova, M. A.; Fabrik, I.; Švec, F. Sense and Nonsense of Elevated Column Temperature in Proteomic Bottom-up LC-MS Analyses. *J Proteome Res* **2021**, *20* (1), 420–432. https://doi.org/10.1021/acs.jproteome.0c00479.

(231) Kim, M.; Legido-Quigley, C. Small Molecule Biomarkers in Alzheimer's Disease. *Ocl* **2018**, *25* (4), D404. https://doi.org/10.1051/ocl/2018027.

(232) Thermo Fisher Scientific. *Vanquish Neo System (VN-A10, VN-C10, VN-P10, VN-S10) Operating Manual (Rev. 1.0, 4822.5001-EN)*; 2021. http://www.thermofisher.com.

(233) Vanderlinden, K.; Broeckhoven, K.; Vanderheyden, Y.; Desmet, G. Effect of Pre- and Post-Column Band Broadening on the Performance of High-Speed Chromatography Columns under Isocratic and Gradient Conditions. *J Chromatogr A* **2016**, *1442*, 73–82. https://doi.org/10.1016/j.chroma.2016.03.016.

(234) Xuan, Q.; Zheng, F.; Yu, D.; Ouyang, Y.; Zhao, X.; Hu, C.; Xu, G. Rapid Lipidomic Profiling Based on Ultra-High Performance Liquid Chromatography–Mass Spectrometry and Its Application in Diabetic Retinopathy. *Anal Bioanal Chem* **2020**, *412* (15), 3585–3594. https://doi.org/10.1007/s00216-020-02632-6.

(235) Zappa, C.; Mousa, S. A. Non-Small Cell Lung Cancer: Current Treatment and Future Advances. *Transl Lung Cancer Res* **2016**, *5* (3), 288–300. https://doi.org/10.21037/tlcr.2016.06.07.

(236) Hong, Y.; Park, S.; Lee, M. K. The Prognosis of Non-Small Cell Lung Cancer Patients According to Endobronchial Metastatic Lesion. *Sci Rep* **2022**, *12* (1). https://doi.org/10.1038/s41598-022-17918-1.

(237) Casal-Mouriño, A.; Ruano-Ravina, A.; Lorenzo-González, M.; Rodríguez-Martínez, Á.; Giraldo-Osorio, A.; Varela-Lema, L.; Pereiro-Brea, T.; Miguel Barros-Dios, J.; Valdés-Cuadrado, L.; Pérez-Ríos, M. Epidemiology of Stage III Lung Cancer: Frequency, Diagnostic Characteristics, and Survival. *Transl Lung Cancer Res* **2021**, *10* (1), 506–518. https://doi.org/10.21037/tlcr.2020.03.40.

(238) Mithoowani, H.; Febbraro, M. Non-Small-Cell Lung Cancer in 2022: A Review for General Practitioners in Oncology. *Current Oncology* **2022**, *29* (3), 1828–1839. https://doi.org/10.3390/curroncol29030150.

(239) Dasari, S.; Bernard Tchounwou, P. Cisplatin in Cancer Therapy: Molecular Mechanisms of Action. *Eur J Pharmacol* **2014**, *740*, 364–378. https://doi.org/10.1016/j.ejphar.2014.07.025.

(240) Wang, D.; Lippard, S. J. Cellular Processing of Platinum Anticancer Drugs. *Nat Rev Drug Discov* **2005**, *4* (4), 307–320. https://doi.org/10.1038/nrd1691.

(241) Martinho, N.; Santos, T. C. B.; Florindo, H. F.; Silva, L. C. Cisplatin-Membrane Interactions and Their Influence on Platinum Complexes Activity and Toxicity. *Front Physiol* **2019**, *10* (JAN). https://doi.org/10.3389/fphys.2018.01898.

(242) Moreno-Gordaliza, E.; Marazuela, M. D.; Pastor, Ó.; Lázaro, A.; Gómez-Gómez, M. M. Lipidomics Reveals Cisplatin-Induced Renal Lipid Alterations during Acute Kidney Injury and Their Attenuation by Cilastatin. *Int J Mol Sci* **2021**, *22* (22). https://doi.org/10.3390/ijms222212521.

(243) Aldossary, S. A. Review on Pharmacology of Cisplatin: Clinical Use, Toxicity and Mechanism of Resistance of Cisplatin. *Biomedical and Pharmacology Journal* **2019**, *12* (1), 7–15. https://doi.org/10.13005/bpj/1608.

(244) Szturz, P.; Wouters, K.; Kiyota, N.; Tahara, M.; Prabhash, K.; Noronha, V.; Adelstein, D.; Van Gestel, D.; Vermorken, J. B. Low-Dose vs. High-Dose Cisplatin: Lessons Learned from 59 Chemoradiotherapy Trials in Head and Neck Cancer. *Front Oncol* **2019**, *9* (FEB). https://doi.org/10.3389/fonc.2019.00086.

(245) Galluzzi, L.; Senovilla, L.; Vitale, I.; Michels, J.; Martins, I.; Kepp, O.; Castedo, M.; Kroemer, G. Molecular Mechanisms of Cisplatin Resistance. *Oncogene* **2012**, *31* (15), 1869–1883. https://doi.org/10.1038/onc.2011.384.

(246) Higuchi, K.; Yanagawa, T. Evaluating Dose of Cisplatin Responsible for Causing Nephrotoxicity. *PLoS One* **2019**, *14* (4). https://doi.org/10.1371/journal.pone.0215757.

(247) Oun, R.; Moussa, Y. E.; Wheate, N. J. The Side Effects of Platinum-Based Chemotherapy Drugs: A Review for Chemists. *Dalton Transactions* **2018**, *47* (19), 6645–6653. https://doi.org/10.1039/c8dt00838h.

(248) Florea, A. M.; Büsselberg, D. Cisplatin as an Anti-Tumor Drug: Cellular Mechanisms of Activity, Drug Resistance and Induced Side Effects. *Cancers (Basel)* **2011**, *3* (1), 1351–1371. https://doi.org/10.3390/cancers3011351.

(249) Paglin, S.; Lee, N. Y.; Nakar, C.; Fitzgerald, M.; Plotkin, J.; Deuel, B.; Hackett, N.; McMahill, M.; Sphicas, E.; Lampen, N.; Yahalom, J. Rapamycin-Sensitive Pathway Regulates Mitochondrial Membrane Potential, Autophagy, and Survival in Irradiated MCF-7 Cells. *Cancer Res* **2005**, *65* (23), 11061–11070. https://doi.org/10.1158/0008-5472.CAN-05-1083.

(250) Ganesh, S. K.; Subathra Devi, C. Molecular and Therapeutic Insights of Rapamycin: A Multi-Faceted Drug from Streptomyces Hygroscopicus. *Mol Biol Rep* **2023**, *50* (4), 3815–3833. https://doi.org/10.1007/s11033-023-08283-x.

(251) Benjamin, D.; Colombi, M.; Moroni, C.; Hall, M. N. Rapamycin Passes the Torch: A New Generation of MTOR Inhibitors. *Nat Rev Drug Discov* **2011**, *10* (11), 868–880. https://doi.org/10.1038/nrd3531.

(252) Saxton, R. A.; Sabatini, D. M. MTOR Signaling in Growth, Metabolism, and Disease. *Cell* **2017**, *168* (6), 960–976. https://doi.org/10.1016/j.cell.2017.02.004.

(253) Laplante, M.; Sabatini, D. M. MTOR Signaling in Growth Control and Disease. *Cell* **2012**, *149* (2), 274–293. https://doi.org/10.1016/j.cell.2012.03.017.

(254) Lamming, D. W.; Sabatini, D. M. A Central Role for MTOR in Lipid Homeostasis. *Cell Metab* **2013**, *18* (4), 465–469. https://doi.org/10.1016/j.cmet.2013.08.002.

(255) Papadopoli, D.; Boulay, K.; Kazak, L.; Pollak, M.; Mallette, F. A.; Topisirovic, I.; Hulea, L. Mtor as a Central Regulator of Lifespan and Aging. *F1000Res* **2019**, *8*. https://doi.org/10.12688/f1000research.17196.1.

(256) Fischer, K. E.; Gelfond, J. A. L.; Soto, V. Y.; Han, C.; Someya, S.; Richardson, A.; Austad, S. N. Health Effects of Long-Term Rapamycin Treatment: The Impact on Mouse Health of Enteric Rapamycin Treatment from Four Months of Age throughout Life. *PLoS One* **2015**, *10* (5). https://doi.org/10.1371/journal.pone.0126644.

(257) Konopka, A. R.; Lamming, D. W. Blazing a Trail for the Clinical Use of Rapamycin as a GeroprotecTOR. *Geroscience* **2023**, *45* (5), 2769–2783. https://doi.org/10.1007/s11357-023-00935-x.

(258) Bae-Jump, V. L.; Zhou, C.; Boggess, J. F.; Gehrig, P. A. Synergistic Effect of Rapamycin and Cisplatin in Endometrial Cancer Cells. *Cancer* **2009**, *115* (17), 3887–3896. https://doi.org/10.1002/cncr.24431.

(259) Guo, S.; Lin, C. M.; Xu, Z.; Miao, L.; Wang, Y.; Huang, L. Co-Delivery of Cisplatin and Rapamycin for Enhanced Anticancer Therapy through Synergistic Effects and Microenvironment Modulation. *ACS Nano* **2014**, *8* (5), 4996–5009. https://doi.org/10.1021/nn5010815.

(260) Han, T. Y.; Ma, B.; Hu, B.; Xiang, L. B.; Liu, X. W. Effects of Rapamycin Combined with Cisplatin on Tumor Necrosis Factor TNF-α in MG-63 Cells. *Cell Transplant* **2020**, *29*. https://doi.org/10.1177/0963689720926153.

(261) Fang, B.; Xiao, H. Rapamycin Alleviates Cisplatin-Induced Ototoxicity in Vivo. *Biochem Biophys Res Commun* **2014**, *448* (4), 443–447. https://doi.org/10.1016/j.bbrc.2014.04.123.

(262) Alotaibi, M.; Al-Aqil, F.; Alqahtani, F.; Alanazi, M.; Nadeem, A.; Ahmad, S. F.; Lapresa, R.; Alharbi, M.; Alshammari, A.; Alotaibi, M.; Saleh, T.; Alrowis, R. Alleviation of Cisplatin-Induced Neuropathic Pain, Neuronal Apoptosis, and Systemic Inflammation in Mice by Rapamycin. *Front Aging Neurosci* **2022**, *14*. https://doi.org/10.3389/fnagi.2022.891593.

(263) Liu, Q.; Luo, Q.; Halim, A.; Song, G. Targeting Lipid Metabolism of Cancer Cells: A Promising Therapeutic Strategy for Cancer. *Cancer Lett* **2017**, *401*, 39–45. https://doi.org/10.1016/j.canlet.2017.05.002.

(264) Mejia, E. M.; Hatch, G. M. Mitochondrial Phospholipids: Role in Mitochondrial Function. *J Bioenerg Biomembr* **2016**, *48* (2), 99–112. https://doi.org/10.1007/s10863-015-9601-4.

(265) Tsaousis, K. T.; Kopsachilis, N.; Tsinopoulos, I. T.; Dimitrakos, S. A.; Kruse, F. E.; Welge-Luessen, U. Time-Dependent Morphological Alterations and Viability of Cultured Human Trabecular Cells after Exposure to Trypan Blue. *Clin Exp Ophthalmol* **2013**, *41* (5), 484–490. https://doi.org/10.1111/ceo.12018.

(266) Soni, K. K.; Kim, H. K.; Choi, B. R.; Karna, K. K.; You, J. H.; Cha, J. S.; Shin, Y. S.; Lee, S. W.; Kim, C. Y.; Park, J. K. Dose-Dependent Effects of Cisplatin on the Severity of Testicular Injury in Sprague Dawley Rats: Reactive Oxygen Species and Endoplasmic Reticulum Stress. *Drug Des Devel Ther* **2016**, *10*, 3959–3968. https://doi.org/10.2147/DDDT.S120014.

(267) Bee, J.; Fuller, S.; Miller, S.; Johnson, S. R. Lung Function Response and Side Effects to Rapamycin for Lymphangioleiomyomatosis: A Prospective National Cohort Study. *Thorax* **2018**, *73* (4), 369–375. https://doi.org/10.1136/thoraxjnl-2017-210872.

(268) Blagosklonny, M. V. Rejuvenating Immunity: "Anti-Aging Drug Today" Eight Years Later. *Oncotarget* **2015**, *6* (23), 19405–19412. https://doi.org/10.18632/oncotarget.3740.

(269) Wong, S. W.; Tiong, K. H.; Kong, W. Y.; Yue, Y. C.; Chua, C. H.; Lim, J. Y.; Lee, C. Y.; Quah, S. I.; Fow, C.; Chung, C.; So, I.; Tan, B. S.; Choo, H. L.; Rosli, R.; Cheong, S. K.; Leong, C. O. Rapamycin Synergizes Cisplatin Sensitivity in Basal-like Breast Cancer Cells through up-Regulation of P73. *Breast Cancer Res Treat* **2011**, *128* (2), 301–313. https://doi.org/10.1007/s10549-010-1055-0.

(270) Ali, E. S.; Mitra, K.; Akter, S.; Ramproshad, S.; Mondal, B.; Khan, I. N.; Islam, M. T.; Sharifi-Rad, J.; Calina, D.; Cho, W. C. Recent Advances and Limitations of MTOR Inhibitors in the Treatment of Cancer. *Cancer Cell Int* **2022**, *22* (1). https://doi.org/10.1186/s12935-022-02706-8.

(271) Perl, A.; Hanczko, R.; Lai, Z. W.; Oaks, Z.; Kelly, R.; Borsuk, R.; Asara, J. M.; Phillips, P. E. Comprehensive Metabolome Analyses Reveal N-Acetylcysteine-Responsive Accumulation of Kynurenine in Systemic Lupus Erythematosus: Implications for Activation of the Mechanistic Target of Rapamycin. *Metabolomics* **2015**, *11* (5), 1157–1174. https://doi.org/10.1007/s11306-015-0772-0.

(272) Escribá, P. V.; Busquets, X.; Inokuchi, J. I.; Balogh, G.; Török, Z.; Horváth, I.; Harwood, J. L.; Vígh, L. Membrane Lipid Therapy: Modulation of the Cell Membrane Composition and

Structure as a Molecular Base for Drug Discovery and New Disease Treatment. *Prog Lipid Res* **2015**, *59*, 38–53. https://doi.org/10.1016/J.PLIPRES.2015.04.003.

(273) Brasaemle, D. L. The Perilipin Family of Structural Lipid Droplet Proteins: Stabilization of Lipid Droplets and Control of Lipolysis. *J Lipid Res* **2007**, *48* (12), 2547–2559. https://doi.org/10.1194/jlr.R700014-JLR200.

(274) Wymann, M. P.; Schneiter, R. Lipid Signalling in Disease. *Nat Rev Mol Cell Biol* **2008**, *9* (2), 162–176. https://doi.org/10.1038/nrm2335.

(275) Ghosh, A.; Nishtala, K. Biofluid Lipidome: A Source for Potential Diagnostic Biomarkers. *Clin Transl Med* **2017**, *6* (1), 22. https://doi.org/10.1186/s40169-017-0152-7.

Appendix A

Appendix A: Supplementary Figures for Chapter II

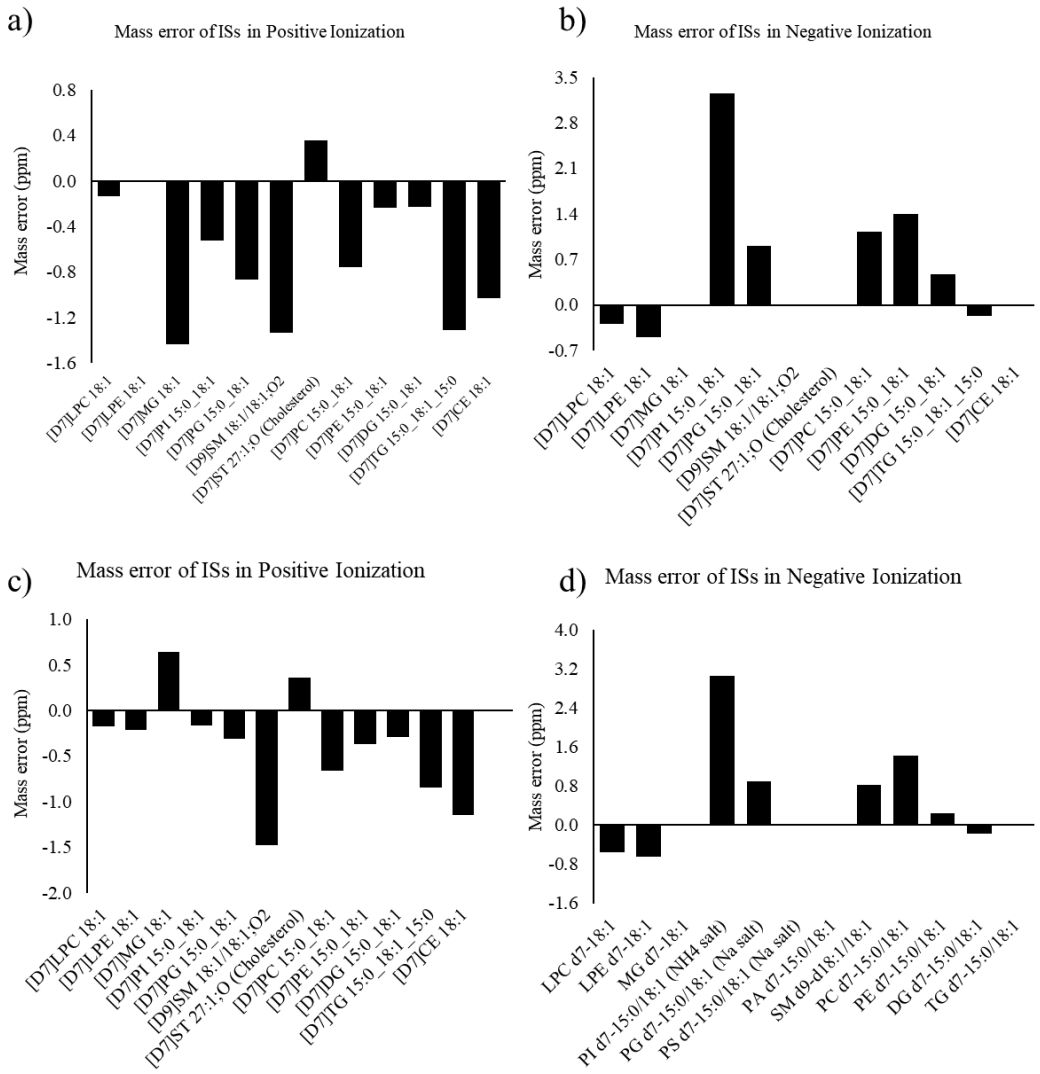

Figure A.1. Mass errors for the Avanti SPLASH Lipidomics Mass Spec standards used for the Saliva study. a) Mass errors for non-normalized saliva samples in positive ionization; b) Mass errors for non-normalized saliva samples in negative ionization; c) Mass errors for normalized saliva samples in positive ionization; d) Mass errors for normalized saliva samples in negative ionization.

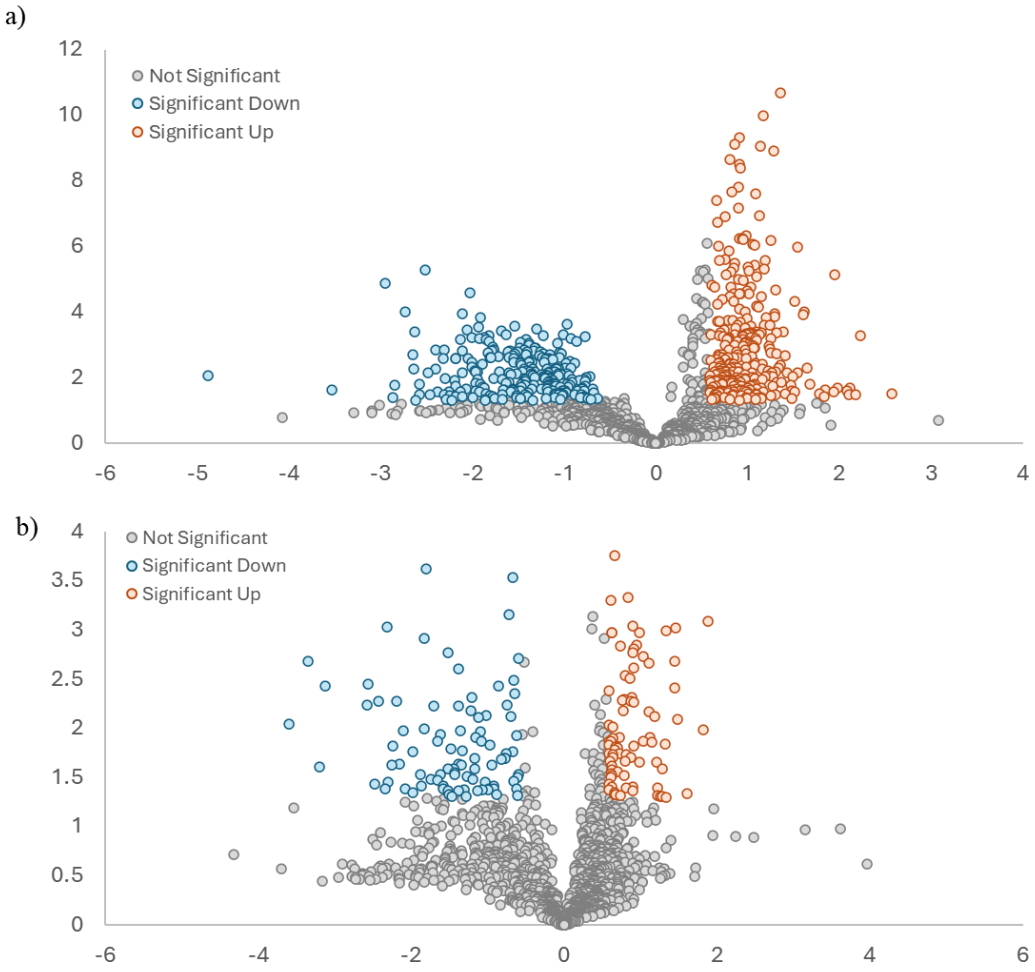

Figure A.2. Volcano plot analysis for saliva samples comparing males versus females a) Volcano plots for non-normalized saliva samples; b) Volcano plots for non-normalized saliva samples.

Figure A.3. Volcano plots for non-normalized and normalized MCF-7 and A549 cell samples. A) Volcano plots for non-normalized MCF-7 versus A549 samples; b) Volcano plots for normalized MCF-7 versus A549 samples.

Appendix B

Appendix B: Supplementary Figures for Chapter III

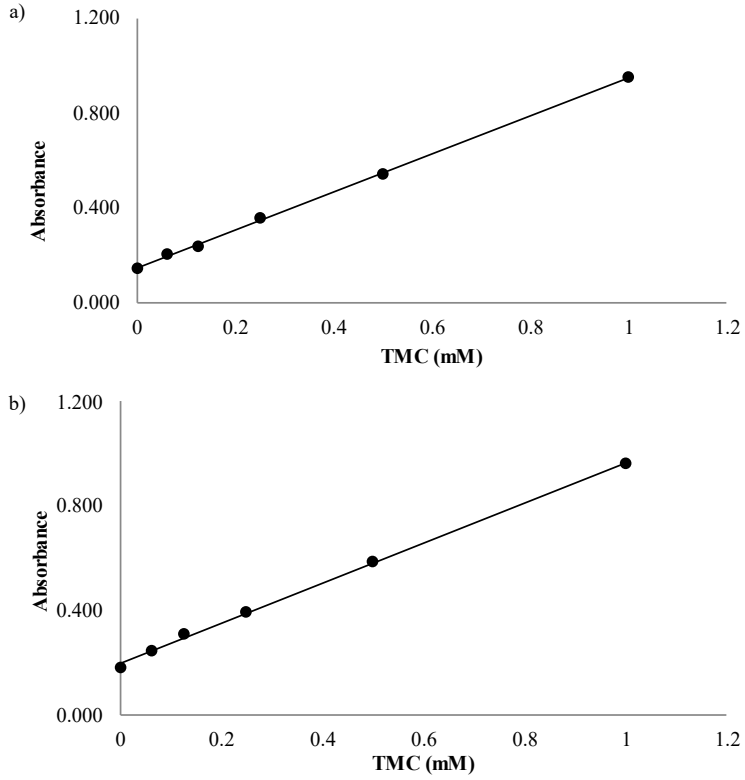

Figure B.1.Amino acid calibration curve for TMC a) Batch 1 (Abs= 0.804x + 0.1465, and R^2 = 0.9992); b) Batch 2 (Abs= 0.077x + 0.1984, and R^2 = 0.9986).

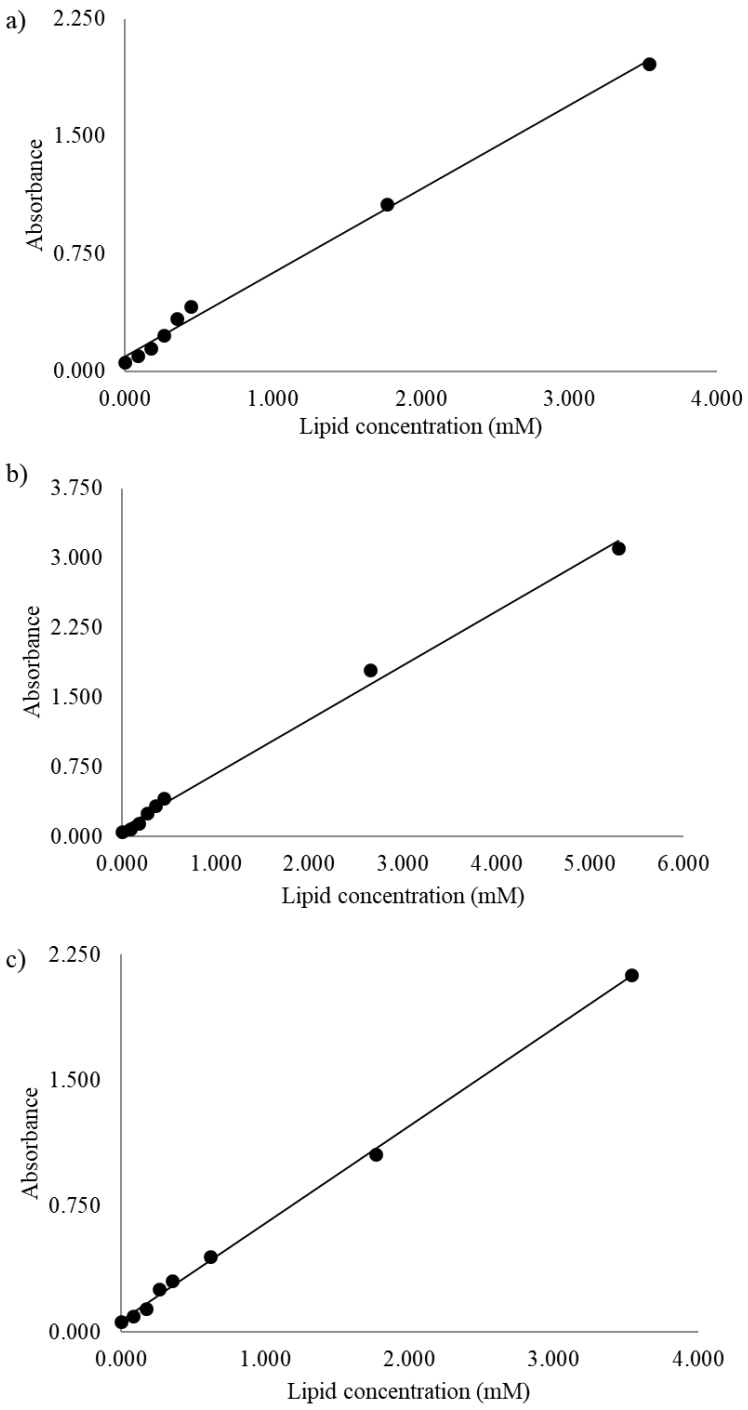

Figure B.2. Oleic acid calibration curve for TLC a) Batch 1 (Abs= 0.541x +0.0620, and $R^2 = 0.9946$); b) Batch 2 (Abs= 0.569x + 0.0871, and $R^2 = 0.9945$); c) Batch 3 (Abs= 0.580x + 0.0688, and $R^2 = 0.9984$).

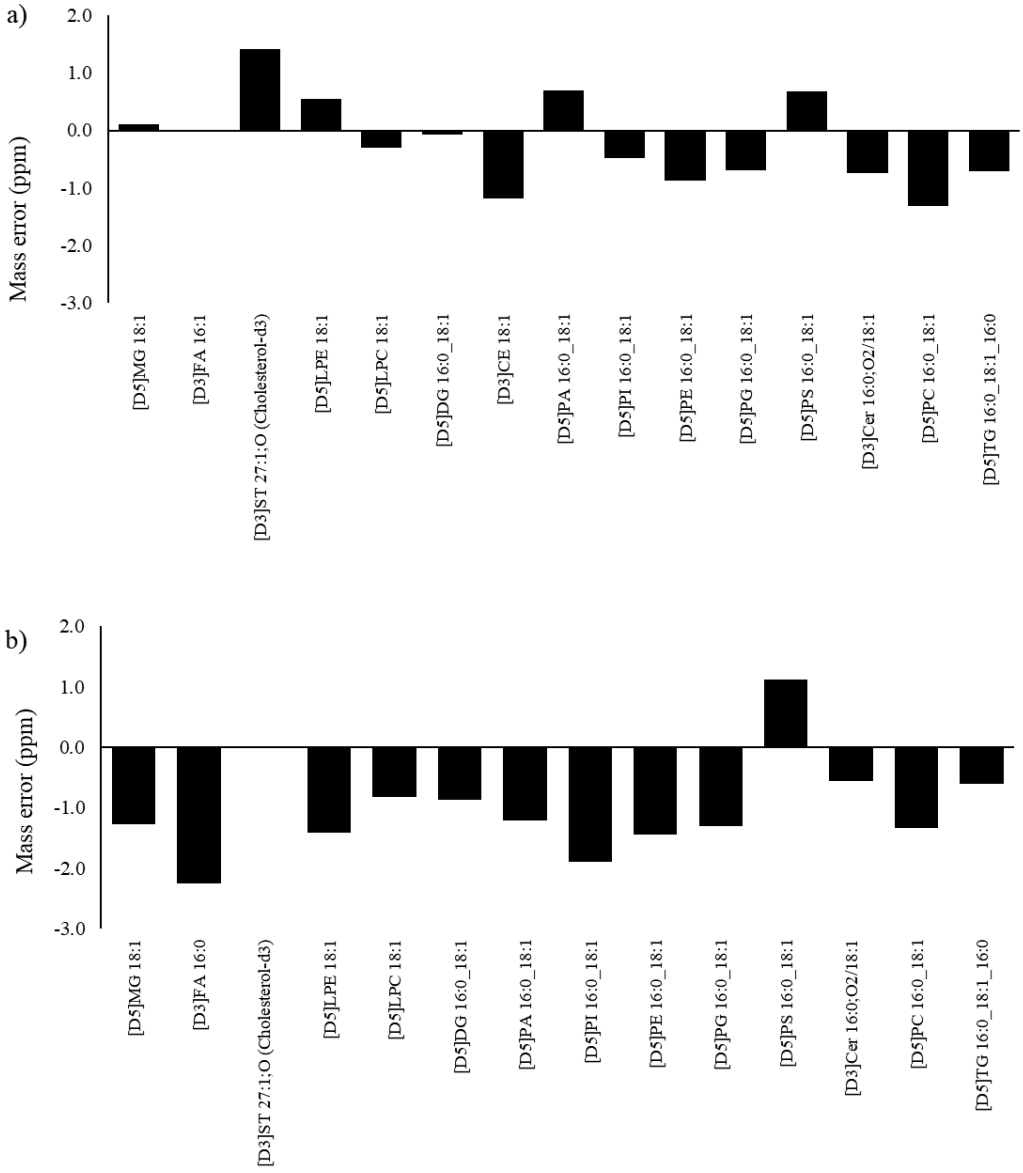

Figure B.3. Mass errors for the LipidRep Serum/Plasma Standard mix standards used for the Saliva study. a) Mass errors in positive ionization; b) Mass errors in negative ionization.

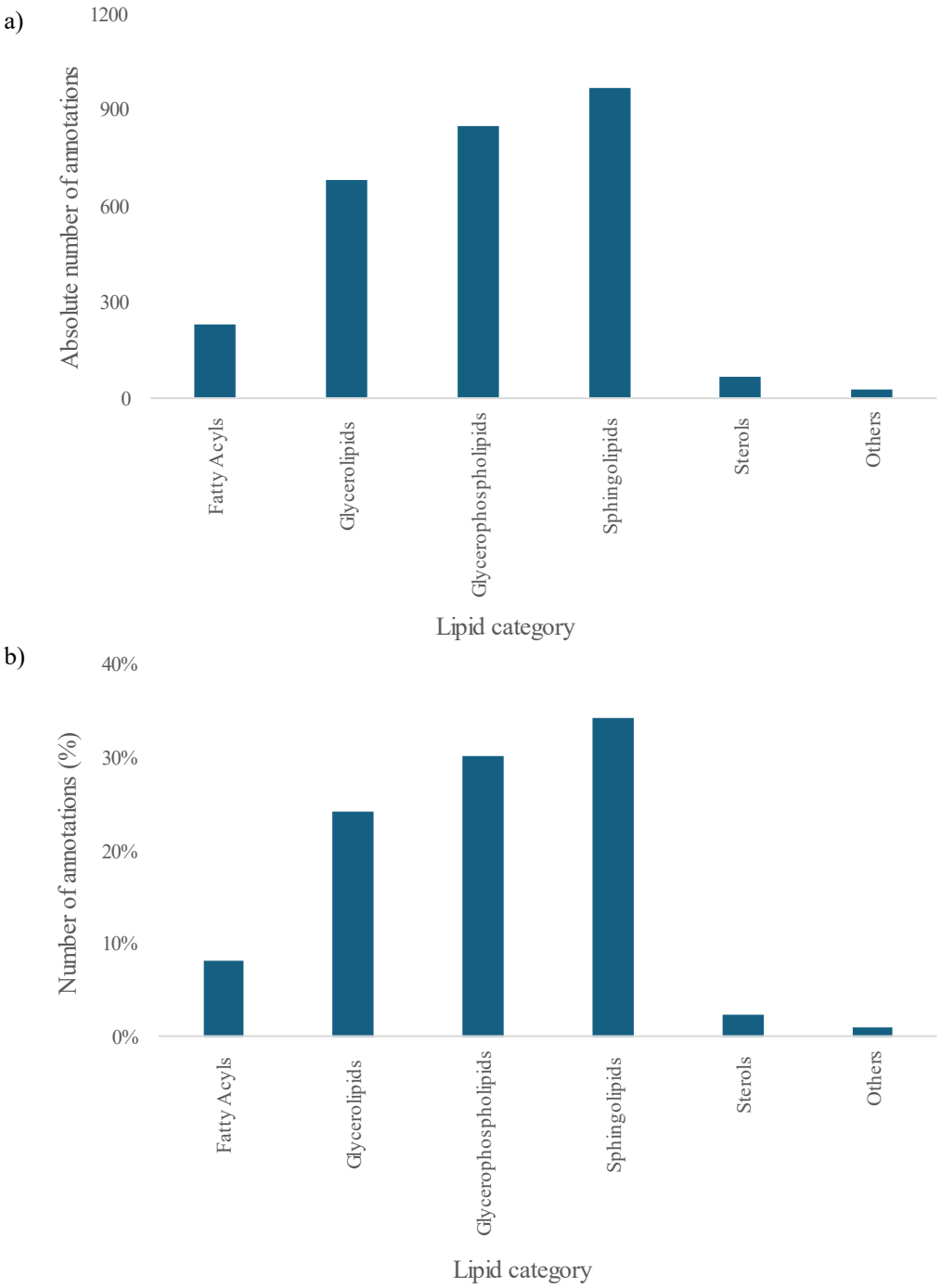

Figure B.4. Lipid annotation distribution across the different lipid categories. A) Lipid categories with absolute number of annotations per category; b) Lipid categories with percentage number of annotations per category.

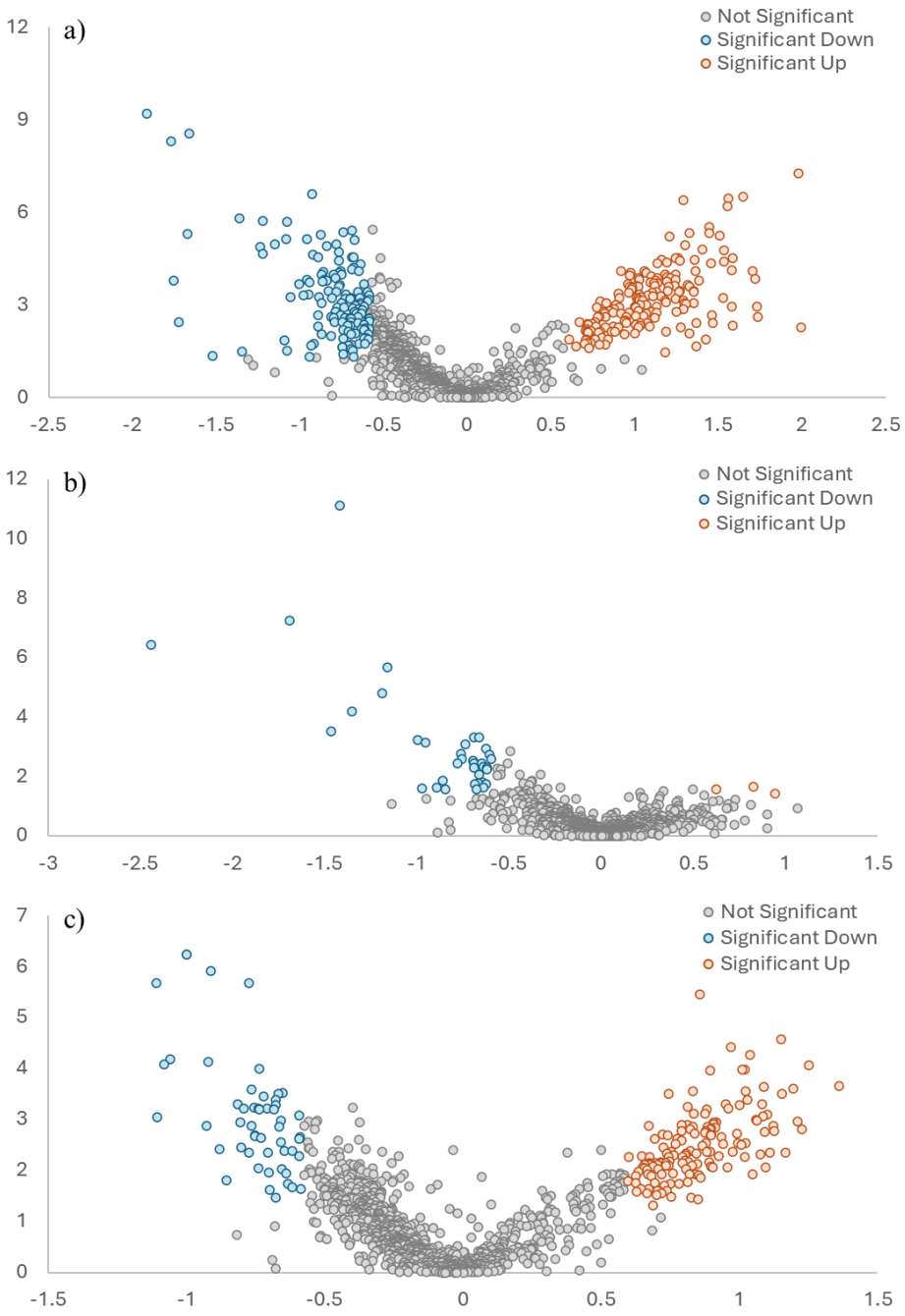

Figure B.5. Volcano plot analysis for saliva samples obtained from healthy individuals, which were analyzed by LC-MS in three conditions (Controls – not normalized samples; TMC normalized – samples normalized by total metabolite concentration; TLC normalized – samples normalized by total lipid concentration). Lipids were considered significantly altered for FC ≤ 0.67 or ≥ 1.5 and $p < 0.05$. a) Control/TLC normalized samples; b) Control/TMC normalized samples; c) TMC normalized/TLC normalized samples.

Appendix C

Appendix C: Supplementary Figures for Chapter IV

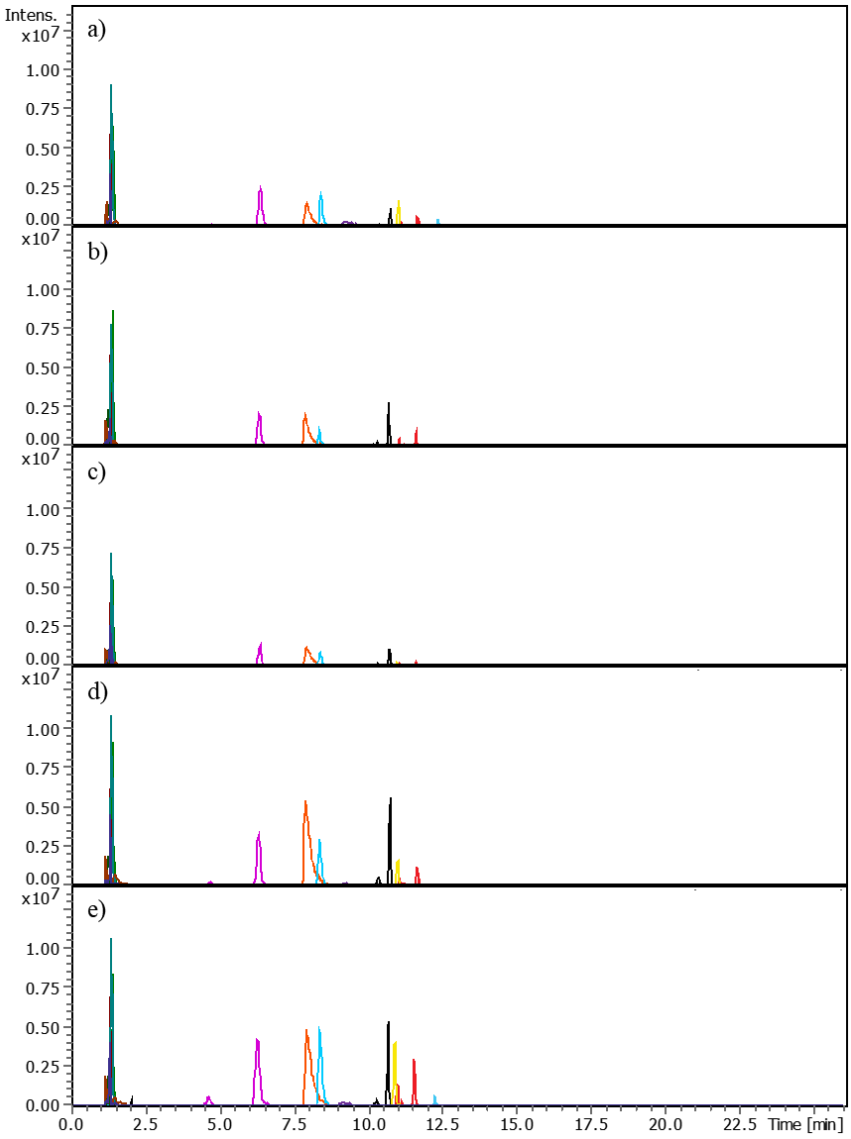

Figure C.1. Extracted Ion Chromatogram (EIC) for NovaMT Tissue Standard for the different resuspension solvents used to optimize the HILIC-MS (MPA: 10 mM NH_4COOH 50:50 ACN/H_2O; MPB: 10 mM NH4COOH 95:5 ACN/H_2O; 0.200 mL/min; 45ºC, 25 min gradient (0 min – 100% MPB, 10 min – 80% MPB, 25 min – 20% MPB); 13 min equilibration (100% MPB)) method

to improve peak shapes and separation. a) 85:15:5 ACN/IPA/H_2O; b) 10 mM NH_4COOH 95:2:3 ACN/MeOH/H_2O; c) 9:1 ACN/IPA; d) 75:25 ACN/IPA; e) 30:15:4:1 ACN/IPA/MeOH/H_2O.

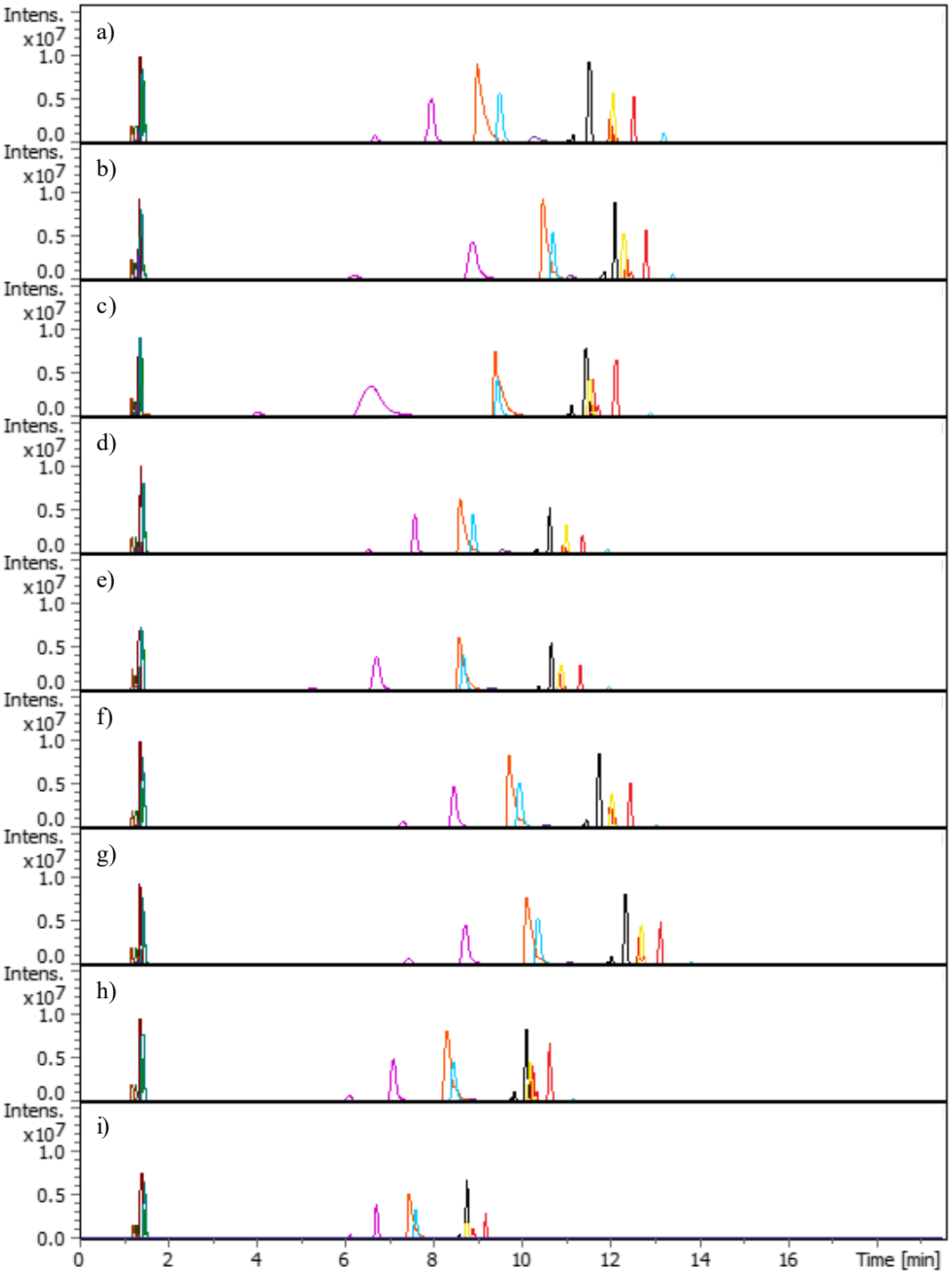

Figure C.2. Extracted Ion Chromatogram (EIC) obtained for NovaMT Tissue Standard for the gradient elution optimization of the HILIC-MS method; with MPA: 10 mM NH_4COOH 50:50 ACN/H_2O; MPB: 10 mM NH4COOH 95:5 ACN/H_2O; 0.200 mL/min; 45ºC; a) 25 min gradient (0 min – 100% MPB, 10 min – 80% MPB, 25 min – 20% MPB); 13 min equilibration (100% MPB). b) 18

min gradient (0 min – 100% MPB, 3 min – 100% MPB, 8 min – 83% MPB, 11 min – 80% MPB, 15 min – 65% MPB 18 min – 20% MPB); 8 min equilibration (100% MPB). c) 18 min gradient (0 min – 100% MPB, 2.5 min – 100% MPB, 4.5 min – 90% MPB, 15 min – 70% MPB, 18 min – 20% MPB); 8 min equilibration (100% MPB). d) 17 min gradient (0 min – 100% MPB, 8 min – 80% MPB, 15 min – 60% MPB 17 min – 20% MPB); 8 min equilibration (100% MPB). e) 18 min gradient (0 min – 100% MPB, 8 min – 80% MPB, 16 min – 50% MPB 18 min – 20% MPB); 8 min equilibration (100% MPB). f) 18 min gradient (0 min – 100% MPB, 1 min – 100% MPB, 9 min – 80% MPB, 16 min – 50% MPB 18 min – 20% MPB); 8 min equilibration (100% MPB). g) 18.5 min gradient (0 min – 100% MPB, 1 min – 100% MPB, 10 min – 80% MPB, 17 min – 50% MPB 18.5 min – 20% MPB); 8 min equilibration (100% MPB). h) 18 min gradient (0 min – 100% MPB, 7 min – 80% MPB, 15 min – 50% MPB 18 min – 20% MPB); 8 min equilibration (100% MPB). i) 18 min gradient (0 min – 100% MPB, 5 min – 80% MPB, 15 min – 50% MPB 18 min – 20% MPB); 8 min equilibration (100% MPB).

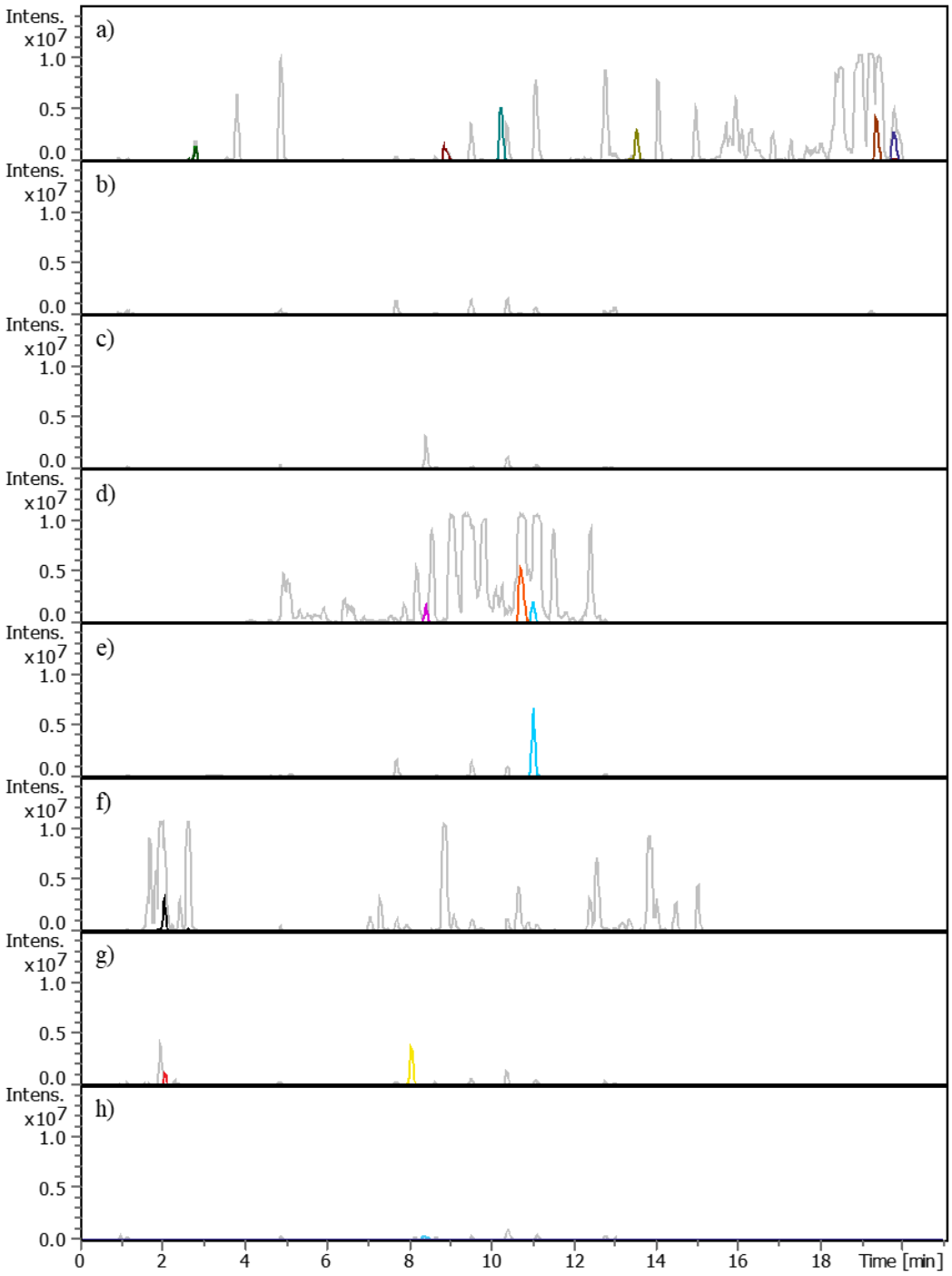

Figure C.3. Base Peak Chromatogram (BPC) for Human Serum Standard fractionated using a HILIC-MS method (MPA: 10 mM NH_4COOH 60:40 ACN/H_2O; MPB: 10 mM NH4COOH 95:2:3 ACN/MeOH/H_2O; 0.250 mL/min; 45ºC, 26 min gradient elution (0 min 100% MPB, 2 min 100% MPB, 2-4 min 98% MPB, 4.5 min 98% MPB, 6 min 96% MPB, 8.5 min 93% MPB, 9.5 min 93% MPB, 12 min 91% MPB, 17 min 86% MPB, 25min 80% MPB, 26 min 20% MPB); 4 min equilibration (100% MPB)), subsequently

injected in a RPLC-MS method (MPA: 10 mM NH_4COOH 50:40:10 MeOH/ACN/H_2O; MPB: 10 mM NH4COOH 95:5 IPA/H_2O; 0.250 mL/min; 45ºC; 20.5 min gradient (0 min – 5% MPB, 10 min – 40% MPB, 18.8 min – 98% MPB, 20.5 min – 98% MPB)); 9.5 min equilibration (5% MPB). a) F1 collection interval 0 min – 4 min. b) F2 collection interval 4 min – 9.5 min; c) F3 collection interval 9.5 min – 13 min. d) F4 collection interval 13 min – 16 min; e) F5 collection interval 16 min – 18.5 min; f) F6 collection interval 18.5 min – 21.7 min; g) F7 collection interval 21.7 min – 25 min; h) F8 collection interval 25 min – 28 min.

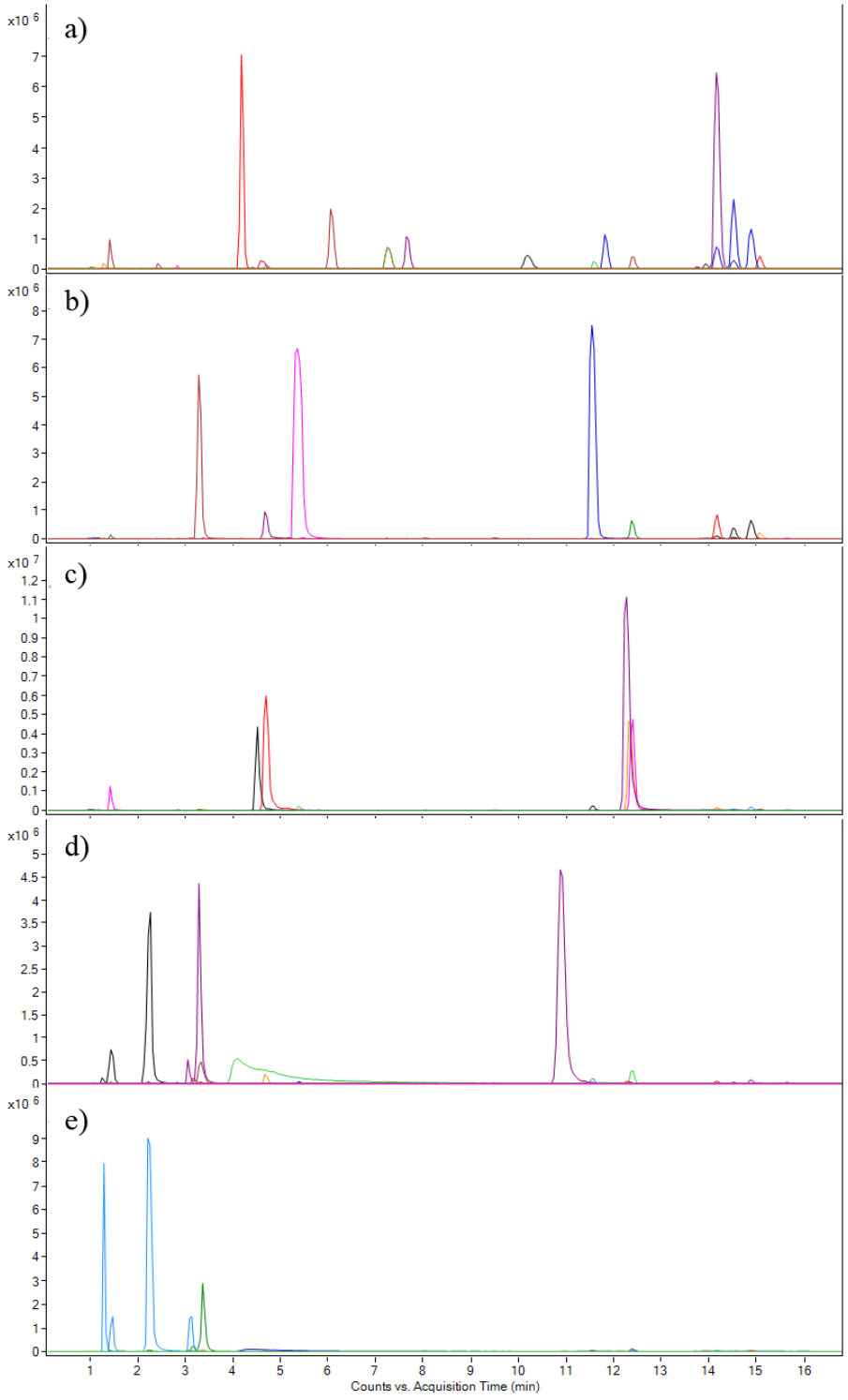

Figure C.4. Extracted Ion Chromatogram (EIC) for NovaMT Tissue Standard fractionated using a HILIC-MS method (MPA: 10 mM NH4COOH 60:40 ACN/H2O; MPB: 10 mM NH4COOH 95:2:3 ACN/MeOH/H2O; 0.250 mL/min; 45ºC, 26 min gradient

elution (0 min 100% MPB, 2 min 100% MPB, 2-4 min 98% MPB, 4.5 min 98% MPB, 6 min 96% MPB, 8.5 min 93% MPB, 9.5 min 93% MPB, 12 min 91% MPB, 17 min 86% MPB, 25min 80% MPB, 26 min 20% MPB); 4 min equilibration (100% MPB)), subsequently injected in RPLC-MS (MPA: 10 mM NH_4COOH 50:40:10 MeOH/ACN/H_2O; MPB: 10 mM NH4COOH 95:5 IPA/H_2O; 45ºC; 16-min gradient elution (0 min, 15% MPB; 0.5 min, 15% MPB; 2.3 min, 25% MPB; 9.3 min, 42% MPB, 10.1 min, 78% MPB; 12 min, 90% MPB; 13 min, 98% MPB; 14.5 min, 98% MPB; 15 min, 15% MPB); 4 min equilibration (15% MPB)), with flow rates varying from 0.300 mL/min to 0.210 mL/min. a) F1 collection interval 0 min – 5 min. b) F2 collection interval 5 min – 9.5 min; c) F3 collection interval 9.5 min – 15 min. d) F4 collection interval 15 min – 20 min; e) F5 collection interval 20 min – 25 min.

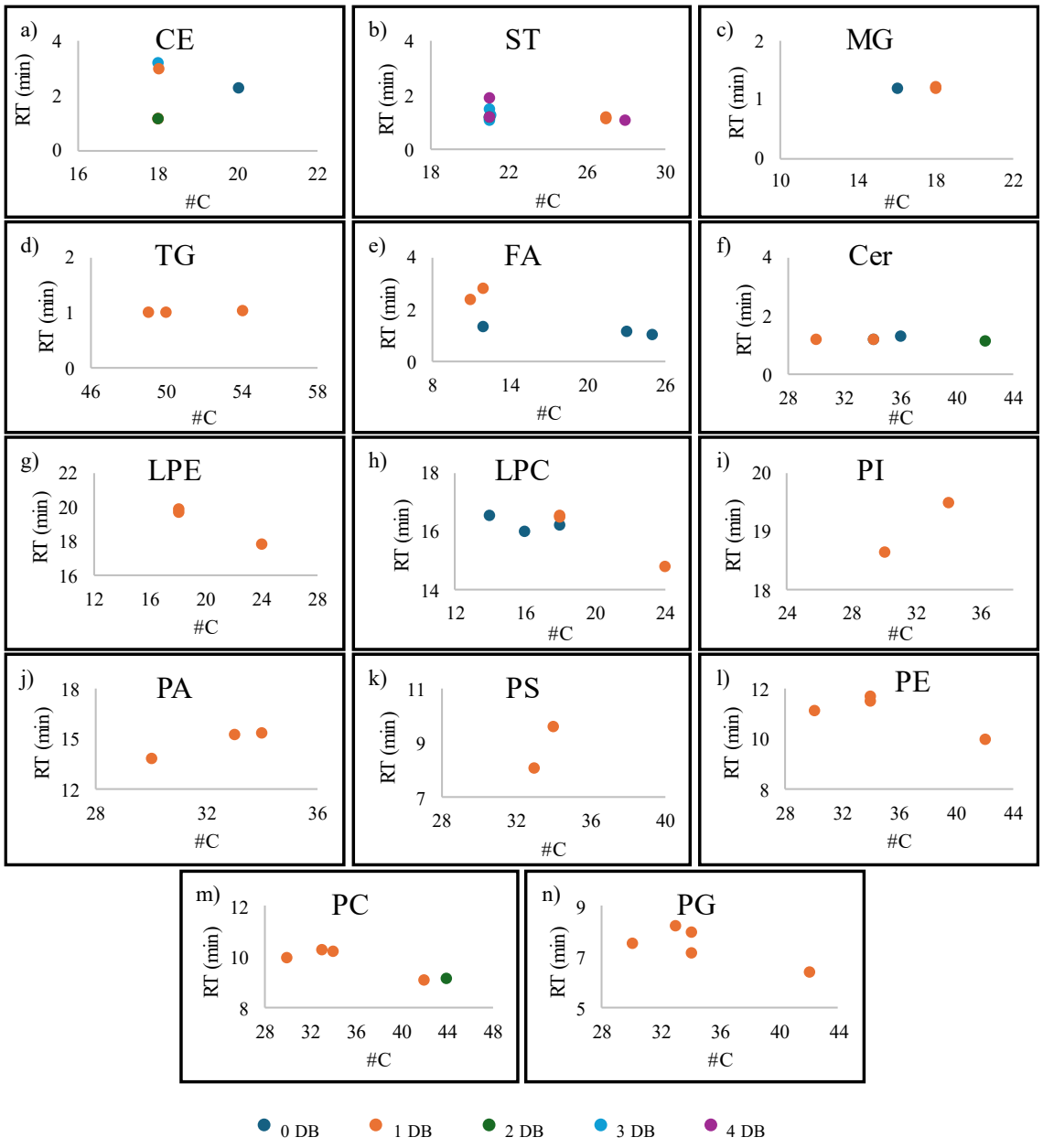

Figure C.5. Commercial Lipid Standard retention times in HILIC-MS for different subclasses with different carbons and double bonds (DB) numbers. a) CE with DB varying from 0 to 3; b) ST with DB varying from 1 to 4; c) MG with DB varying between 0 and 1; d) TG with 1 DB; e) FA with DB varying between 0 and 1; f) Cer with DB varying from 0 to 2; g) LPE with 1 DB; h) LPC with DB varying between 0 and 1; i) PI with 1 DB; j) PA with 1 DB; k) PS with 1 DB; l) PE with 1 DB; m) PC with DB varying between 1 and 2; n) PG with 1 DB.

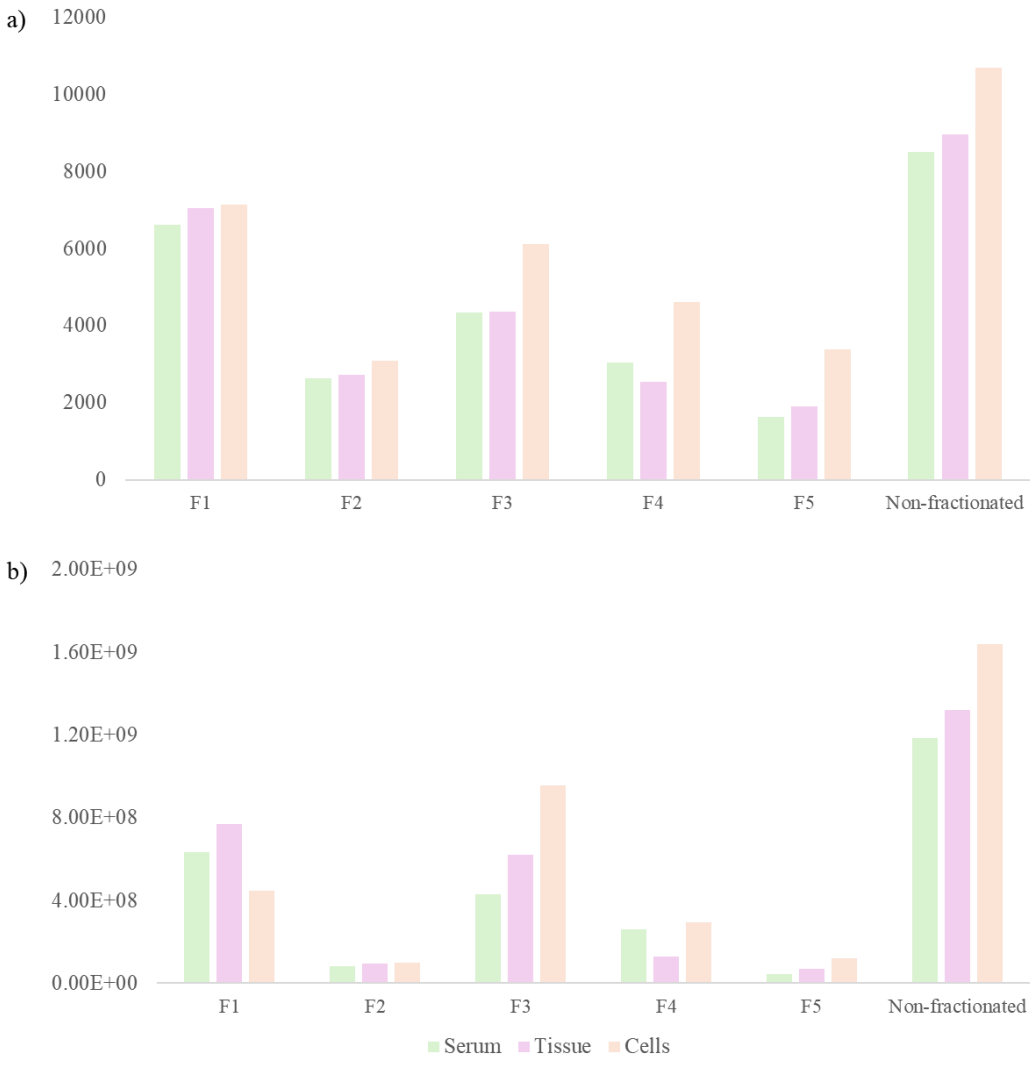

Figure C.6. Detected features, summed intensities for each fraction, and non-fractionated sample. a) Detected features for fractions (F1 through F5) and non-fractionated tissue samples; b) Summed intensities for fractions (F1 to F5) and non-fractionated samples.

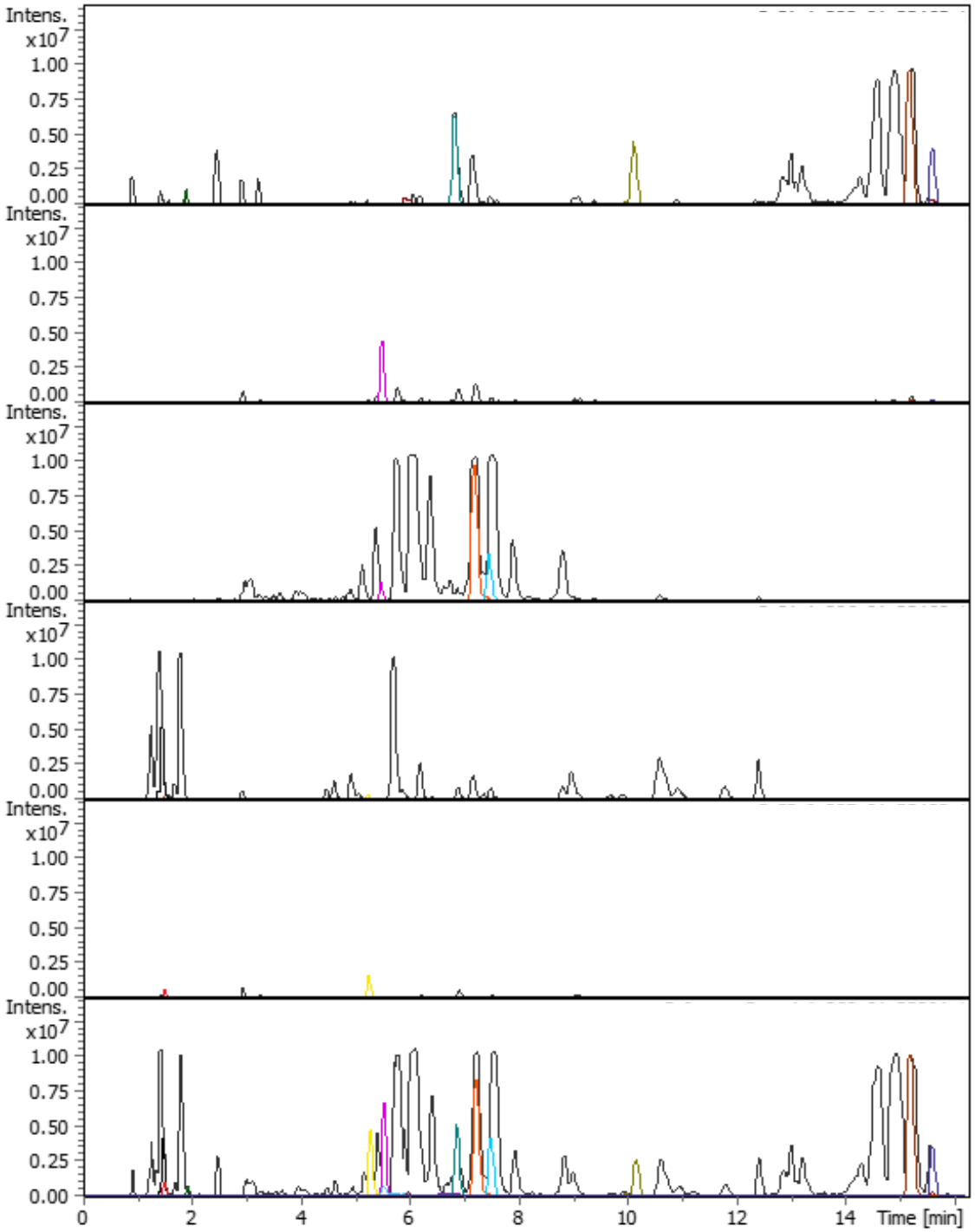

Figure C.7. Base Peak Chromatogram (BPC) for Human Serum Standard fractionated using a HILIC-MS method (MPA: 10 mM NH_4COOH 60:40 ACN/H_2O; MPB: 10 mM NH_4COOH 95:2:3 ACN/MeOH/H_2O; 0.250 mL/min; 45ºC, 26 min gradient elution (0 min 100% MPB, 2 min 100% MPB, 2-4 min 98% MPB, 4.5 min 98% MPB, 6 min 96% MPB, 8.5 min 93% MPB, 9.5 min 93%

MPB, 12 min 91% MPB, 17 min 86% MPB, 25min 80% MPB, 26 min 20% MPB); 4 min equilibration (100% MPB)), subsequently injected in RPLC-MS (MPA: 10 mM NH4COOH 50:40:10 MeOH/ACN/H_2O; MPB: 10 mM NH_4COOH 95:5 IPA/H_2O; 45ºC; 16-min gradient elution (0 min, 15% MPB; 0.5 min, 15% MPB; 2.3 min, 25% MPB; 9.3 min, 42% MPB, 10.1 min, 78% MPB; 12 min, 90% MPB; 13 min, 98% MPB; 14.5 min, 98% MPB; 15 min, 15% MPB); 4 min equilibration (15% MPB)), with flow rates varying from 0.300 mL/min to 0.210 mL/min. a) F1 collection interval 0 min – 5 min. b) F2 collection interval 5 min – 9.5 min; c) F3 collection interval 9.5 min – 15 min. d) F4 collection interval 15 min – 20 min; e) F5 collection interval 20 min – 25 min; f) Non-fractionated Human Serum Standard injected in RPLC-MS.

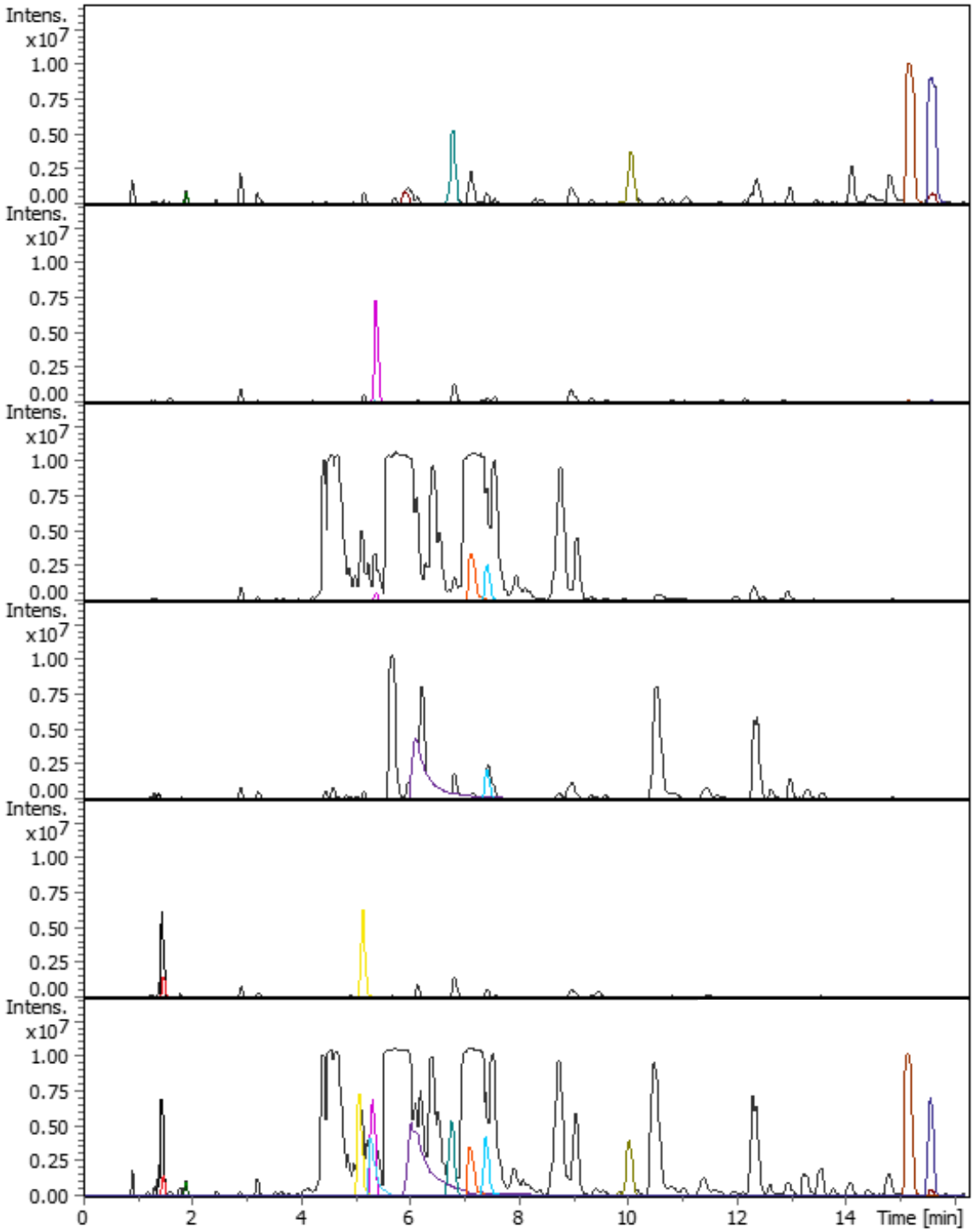

Figure C.8. Base Peak Chromatogram (BPC) for MCF-7 cells fractionated using a HILIC-MS method (MPA: 10 mM NH_4COOH 60:40 ACN/H_2O; MPB: 10 mM NH_4COOH 95:2:3 ACN/MeOH/H_2O; 0.250 mL/min; 45ºC, 26 min gradient elution (0 min 100% MPB, 2 min 100% MPB, 2-4 min 98% MPB, 4.5 min 98% MPB, 6 min 96% MPB, 8.5 min 93% MPB, 9.5 min 93% MPB, 12 min

91% MPB, 17 min 86% MPB, 25min 80% MPB, 26 min 20% MPB); 4 min equilibration (100% MPB)), subsequently injected in RPLC-MS (MPA: 10 mM NH_4COOH 50:40:10 MeOH/ACN/H_2O; MPB: 10 mM NH_4COOH 95:5 IPA/H_2O; 45ºC; 16-min gradient elution (0 min, 15% MPB; 0.5 min, 15% MPB; 2.3 min, 25% MPB; 9.3 min, 42% MPB, 10.1 min, 78% MPB; 12 min, 90% MPB; 13 min, 98% MPB; 14.5 min, 98% MPB; 15 min, 15% MPB); 4 min equilibration (15% MPB)), with flow rates varying from 0.300 mL/min to 0.210 mL/min. a) F1 collection interval 0 min – 5 min. b) F2 collection interval 5 min – 9.5 min; c) F3 collection interval 9.5 min – 15 min. d) F4 collection interval 15 min – 20 min; e) F5 collection interval 20 min – 25 min; f) Non-fractionated MCF-7 cells injected in RPLC-MS.

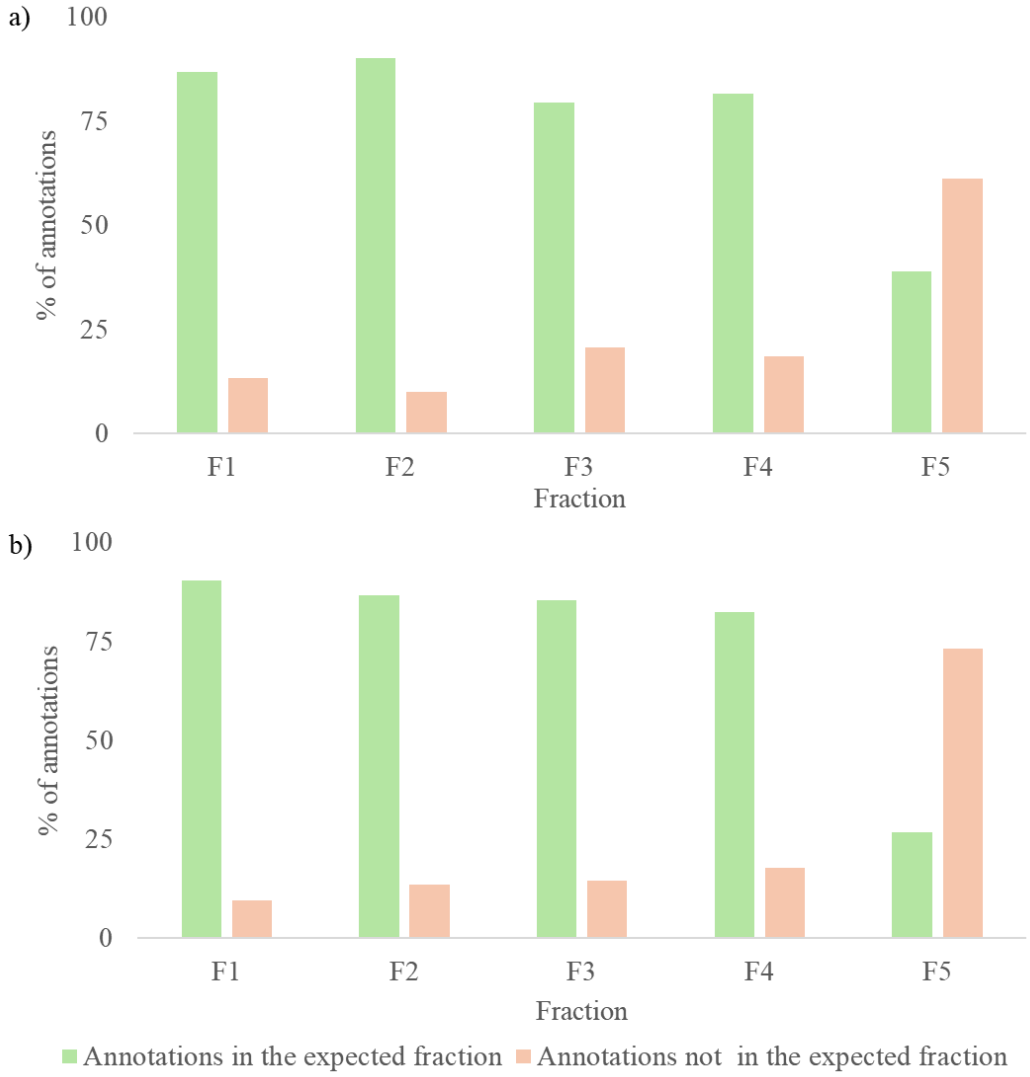

Figure C.9. Distribution of lipid annotations in their expected fractions (green) versus those not in their expected fractions (orange). The x-axis represents the five fractions, while the y-axis indicates the percentage of annotations. a) In chicken liver tissue samples; b) in MCF-7 cell samples.

Appendix D

Appendix D: Supplementary Figures for Chapter V

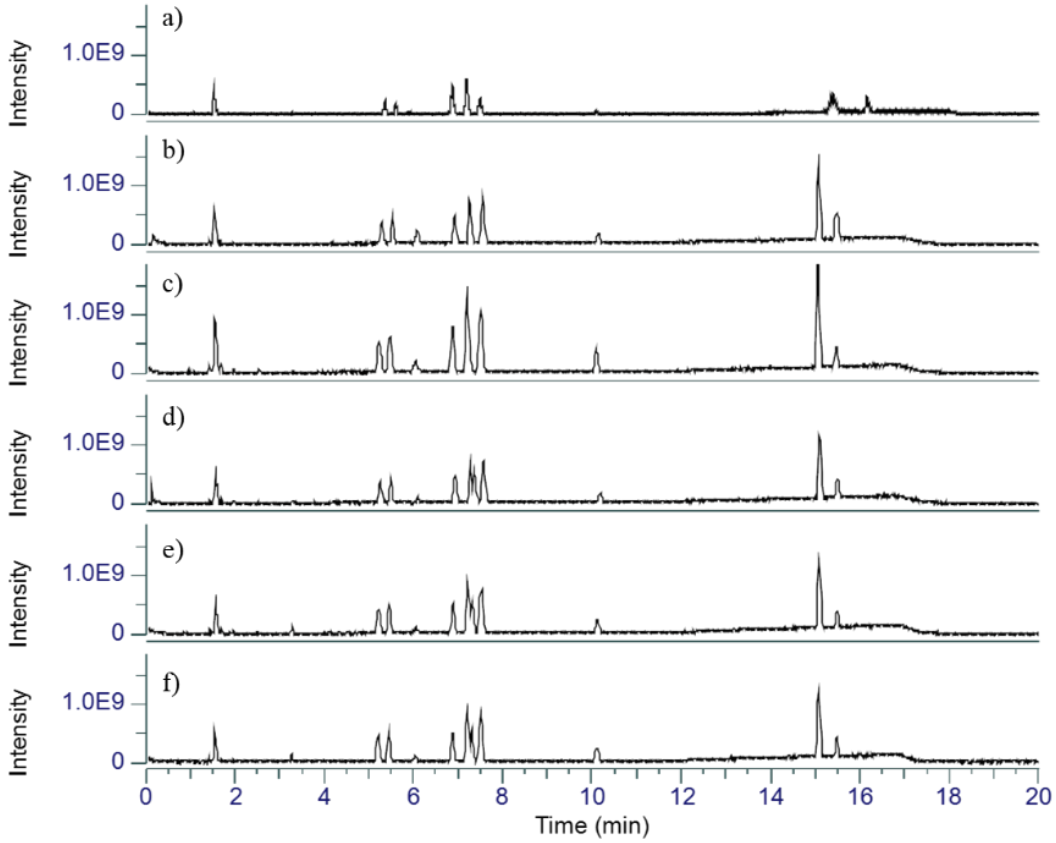

Figure D.1. Base Peak Chromatogram (BPC) for LipidRep Basic Mix Serum Standard used for ion source parameter optimizations. A) Orbitrap's default ion source parameters (Spray Voltage: 3400 V on positive; Sheath Gas: 3 Arb; Aux Gas: 2 Arb; Sweep Gas: 0 Arb; Ion Transfer Tube Temp.: 320 ºC; Vaporizer Temp.: 0 ºC); b) Optimized parameters 1 (Spray Voltage: 3500 V on positive; Sheath Gas: 70 Arb; Aux Gas: 10 Arb; Sweep Gas: 1 Arb; Ion Transfer Tube Temp.: 220 ºC; Vaporizer Temp.: 180 ºC); c) Optimized parameters 2 (Spray Voltage: 4000 V on positive; Sheath Gas: 70 Arb; Aux Gas: 10 Arb; Sweep Gas: 1 Arb; Ion Transfer Tube Temp.: 220 ºC; Vaporizer Temp.: 180 ºC); d) Optimized parameters 3 (Spray Voltage: 4000 V on positive; Sheath Gas: 70 Arb; Aux Gas: 15 Arb; Sweep Gas: 1 Arb; Ion Transfer Tube Temp.: 220 ºC; Vaporizer Temp.: 180 ºC); e) Optimized parameters 4 (Spray Voltage: 4000 V on positive; Sheath Gas: 70 Arb; Aux Gas: 20 Arb; Sweep Gas: 1 Arb; Ion Transfer Tube Temp.: 220 ºC; Vaporizer Temp.: 180 ºC); f) Optimized parameters 5 (Spray Voltage: 4000 V on positive; Sheath Gas: 60 Arb; Aux Gas: 15 Arb; Sweep Gas: 1 Arb; Ion Transfer Tube Temp.: 300 ºC; Vaporizer Temp.: 250 ºC).

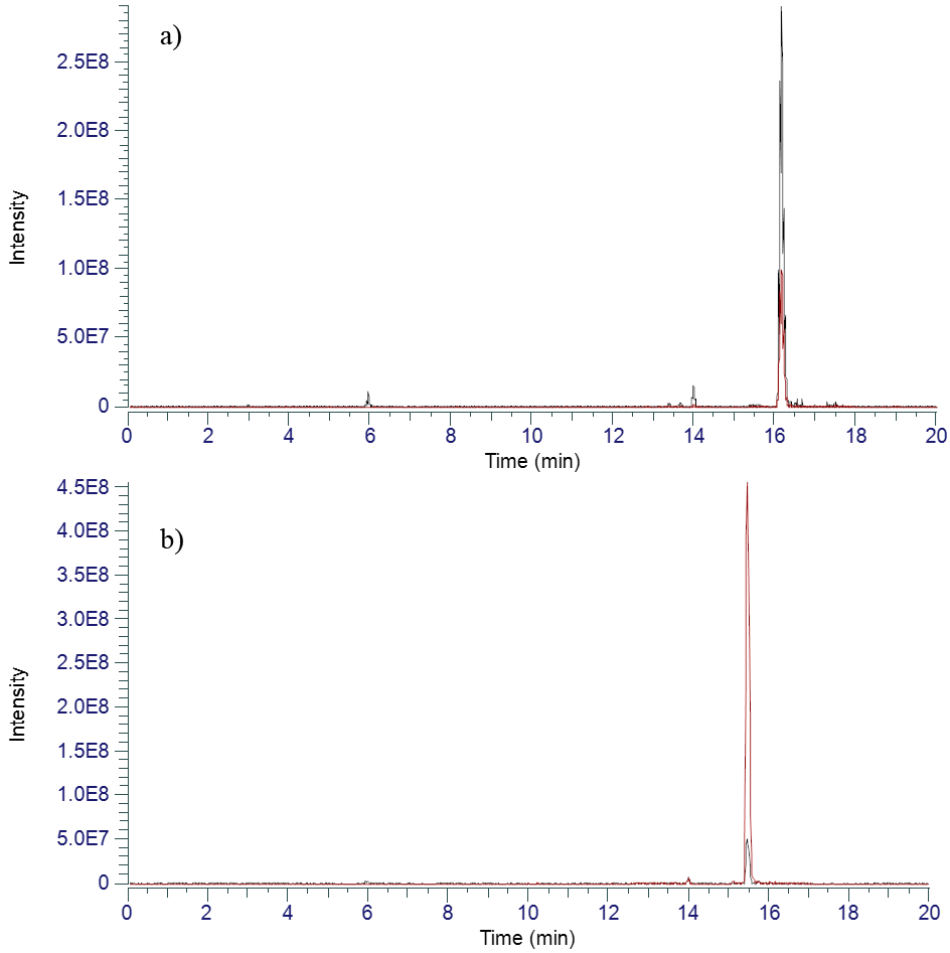

Figure D.2. Extracted Ion Chromatogram (EIC) show CE in-source fragmentation before and after ion source parameter optimizations. In black are the ICS for m/z 372.37 (in-source fragment), and in red for m/z 671.65 (main fragment). A) Orbitrap's default ion source parameters (Spray Voltage: 3400 V on positive; Sheath Gas: 3 Arb; Aux Gas: 2 Arb; Sweep Gas: 0 Arb; Ion Transfer Tube Temp.: 320 ºC; Vaporizer Temp.: 0 ºC); b) Optimized parameters 5 (Spray Voltage: 4000 V on positive; Sheath Gas: 60 Arb; Aux Gas: 15 Arb; Sweep Gas: 1 Arb; Ion Transfer Tube Temp.: 300 ºC; Vaporizer Temp.: 250 ºC).

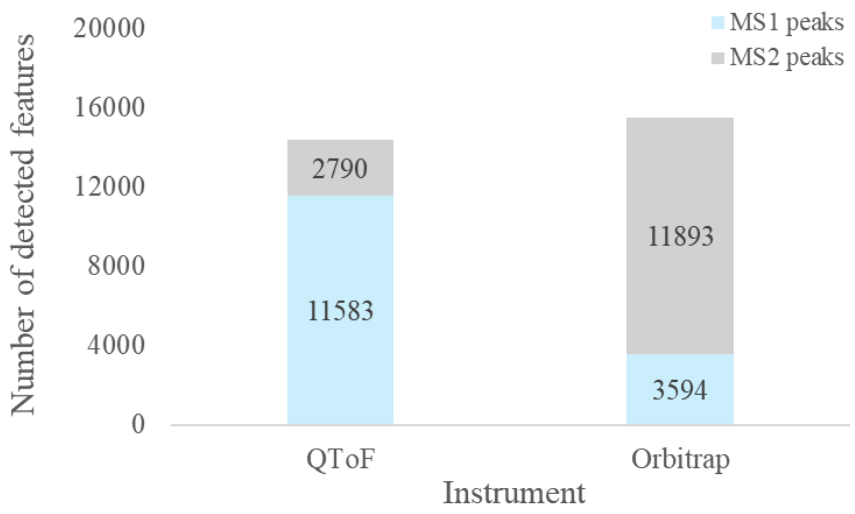

Figure D.3. Number of MS1 and MS2 detected features in Orbitrap-MS and QToF-MS using a Waters Acquity CSH Premier C18 column (1.7 µm, 2.1×100mm) at 45 ºC, MPA - 10 mM ammonium formate in 50:40:10 MeOH/ACN/H_2O and MPB - 10 mM ammonium formate in 95:5 IPA/H_2O), employing a 16-minute gradient for separation (0 min, 15% MPB; 0.5 min, 15% MPB; 2.3 min, 25% MPB; 9.3 min, 42% MPB, 10.1 min, 78% MPB; 12 min, 90% MPB; 13 min, 98% MPB; 14.5 min, 98% MPB; 15 min, 15% MPB) with an initial flow rate of 0.300 mL/min until 9.3 minutes, decreasing to 0.270 mL/min up to 10.1 minutes, and subsequently reducing further to 0.210 mL/min until the end.

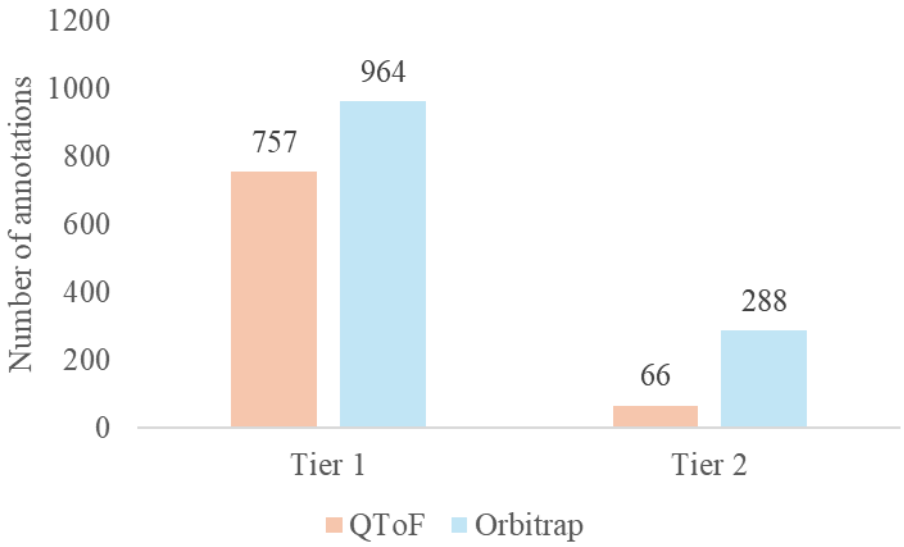

Figure D.4. Number of annotated features in Tier 1 (MS/MS score < 500) and Tier 2 (100 < MS/MS score < 500) in Orbitrap-MS and QToF-MS.

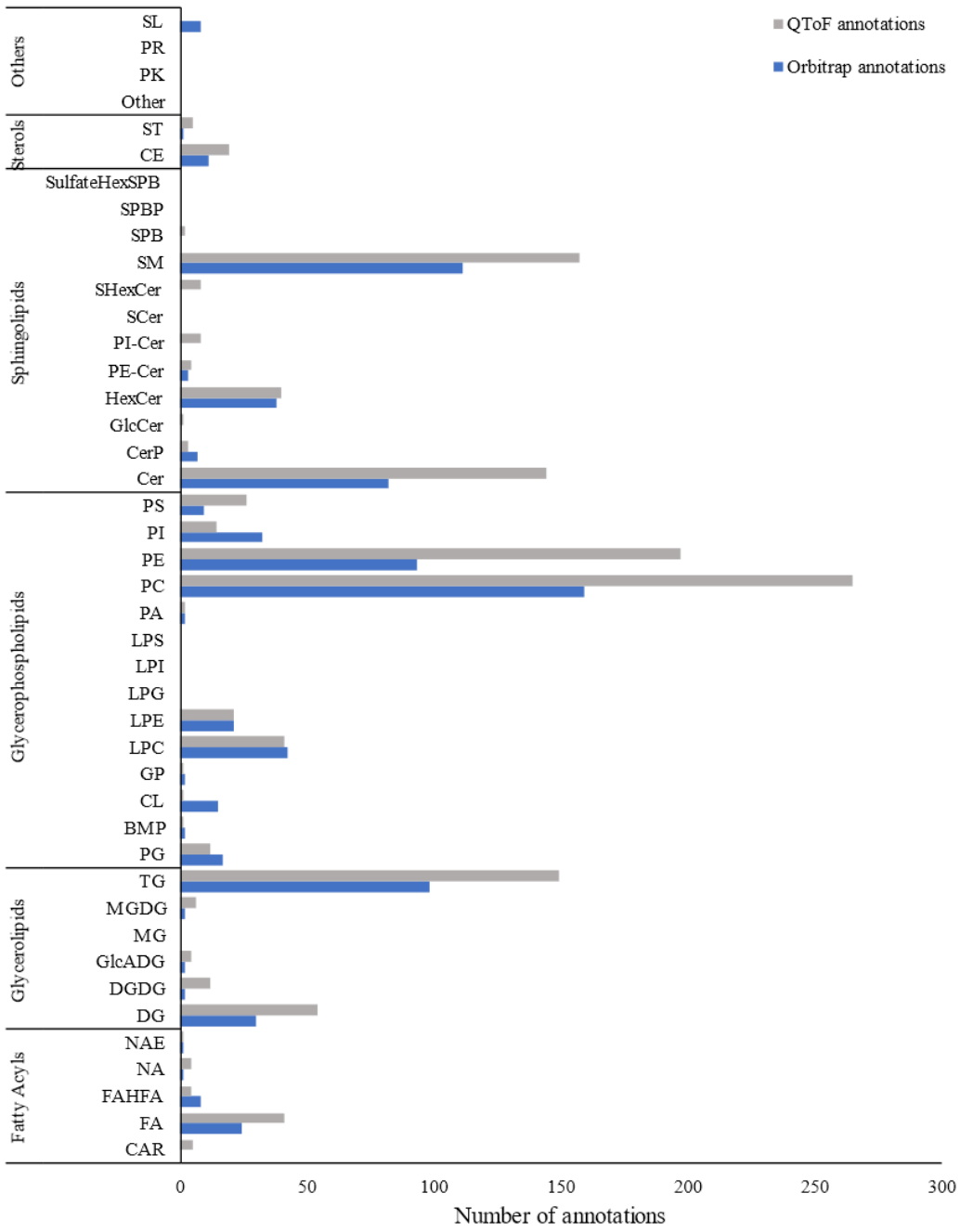

Figure D.5. Distribution of lipid annotations across various lipid subclasses for Orbitrap-MS and QToF-MS.

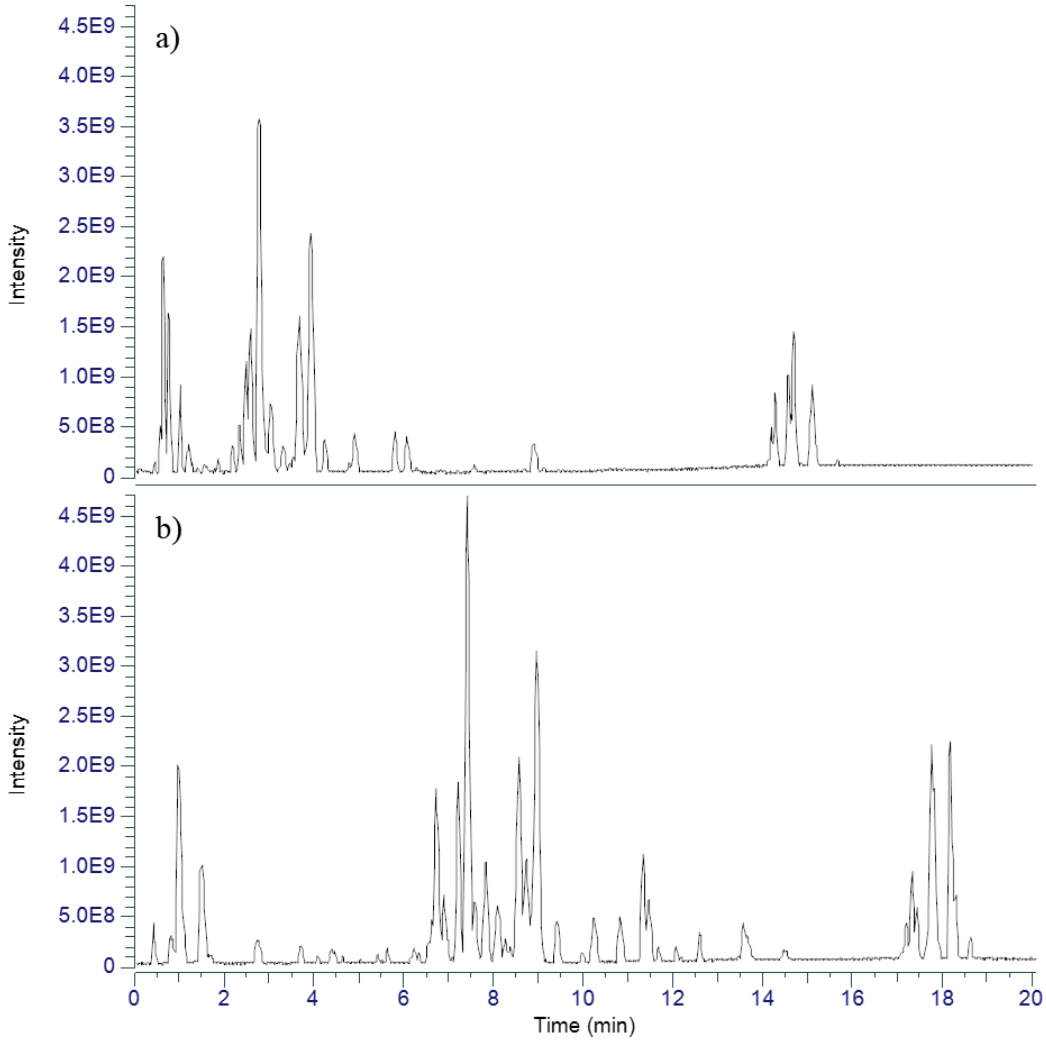

Figure D.6. Base Peak Chromatogram (BPC) for Serum samples acquired using MPB - 10mM ammonium formate in 95:5 IPA/H_2O; 16 min gradient (0 min – 15% MPB, 0.5 min – 15% MPB, 2.3 min – 25% MPB, 9.3 min – 42% MPB, 10.1 min – 78% MPB, 12 min – 90% MPB, 13 min – 98% MPB, 14.5 min – 98% MPB, 15 min – 15% MPB); 4 min equilibration (15% MPB); with flow rate starting at 100 µL/min until 10.1 min, reducing it to 80 µL/min from 10.1 to 14.5 µL/min and further reducing it to 50 µL/min until the end of the run and column oven temperature of 55 ºC. a) MPA - 10mM ammonium formate in 50:40:10 MeOH/ACN/H_2O and b) MPA - 10mM ammonium formate in 40:40:20 MeOH/ACN/H_2O.

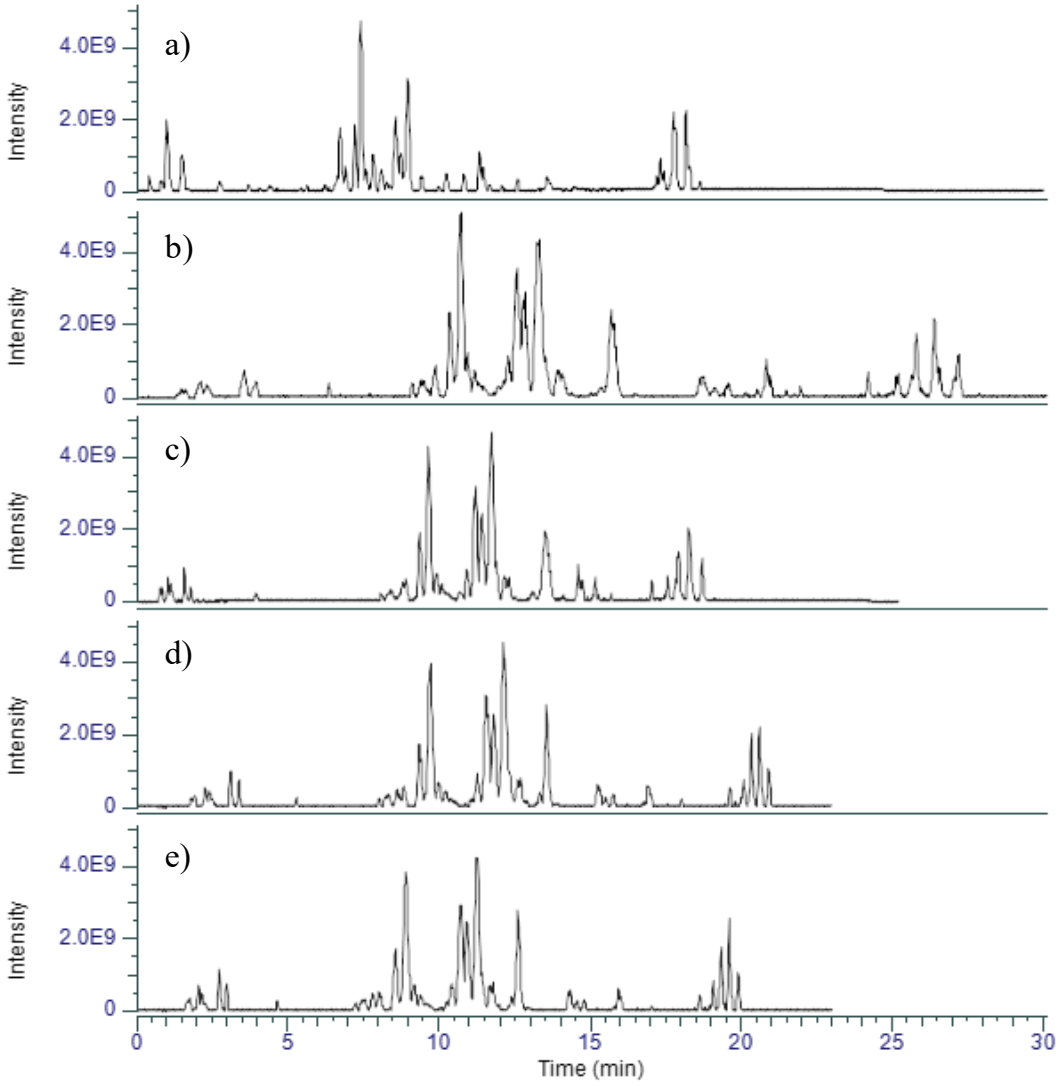

Figure D.7. Base Peak Chromatogram (BPC) for Serum samples used for the evaluation gradients 1 to 5 of the 1 mm ID UHPLC gradient optimization using MPA - 10mM ammonium formate in 40:40:20 MeOH/ACN/H_2O and MPB - 10mM ammonium formate in 95:5 IPA/H_2O and 55 ºC; a) Gradient 1 - 19 min gradient (0 min – 10% MPB, 0.5 min – 10% MPB, 2 min – 30% MPB, 7.5 min – 40% MPB, 10 min – 60% MPB, 12.9 min – 72% MPB, 13 min – 72% MPB, 13.5 min – 93% MPB, 17 min – 98% MPB, 18.5 min – 98% MPB, 19 min – 10% MPB); 4 min equilibration (15% MPB); with flow rate starting at 100 µL/min until 2 min, reducing it to 70 µL/min from 2 to 13 min, and further reducing it to 40 µL/min until the end of the run; b) Gradient 2 - 34 min gradient (0 min – 0% MPB, 0.5 min – 0% MPB, 4 min – 15% MPB, 7.5 min – 40% MPB, 5 min – 35% MPB, 10 min – 39% MPB, 17 min – 42% MPB, 19 min – 75% MPB, 27 min – 93% MPB, 31 min – 98% MPB, 33 min – 98% MPB, 34 min – 0% MPB); 4 min equilibration (0% MPB); with flow rate starting at 100 µL/min until 4 min, reducing it to 70 µL/min from 4 to 17 minutes and

further reducing it to 30 µL/min until the end of the run. c) Gradient 3 - 22.6 min gradient (0 min – 15% MPB, 1.5 min – 15% MPB, 2.5 min – 20% MPB, 2.6 min – 20% MPB, 6.6 min – 33% MPB, 12.6 min – 45% MPB, 13.1 min – 75% MPB, 18.1 min – 93% MPB, 20.1 min – 98% MPB, 21.6 min – 98% MPB, 22.6 min – 15% MPB); 4 min equilibration (15% MPB); with flow rate starting at 100 µL/min until 2.5 min, reducing it to 60 µL/min at 2.6 min until 12.6 min, and further reducing it to 35 µL/min until the end of the run. d) Gradient 4 - 24.9 min gradient (0 min – 10% MPB, 4 min – 34% MPB, 10 min – 38% MPB, 13.8 min – 55% MPB, 13.9 min – 55% MPB, 16.9 min – 75% MPB, 18.9 min – 93% MPB, 20.9 min – 98% MPB, 22.4 min – 98% MPB, 24.9 – 10% MPB); 4 min equilibration (10% MPB); with flow rate starting at 50 µL/min until 13.8 min, reducing it to 35 µL/min from until the end of the run. e) Gradient 5 - 23.9 min gradient (0 min – 10% MPB, 3 min – 34% MPB, 9 min – 38% MPB, 12.8 min – 55% MPB, 12.9 min – 55% MPB, 15.9 min – 75% MPB, 17.9 min – 93% MPB, 19.9 min – 98% MPB, 21.4 min – 98% MPB, 22.9 – 10% MPB); 4 min equilibration (10% MPB); with flow rate starting at 50 µL/min until 12.8 min, reducing it to 35 µL/min from until the end of the run.

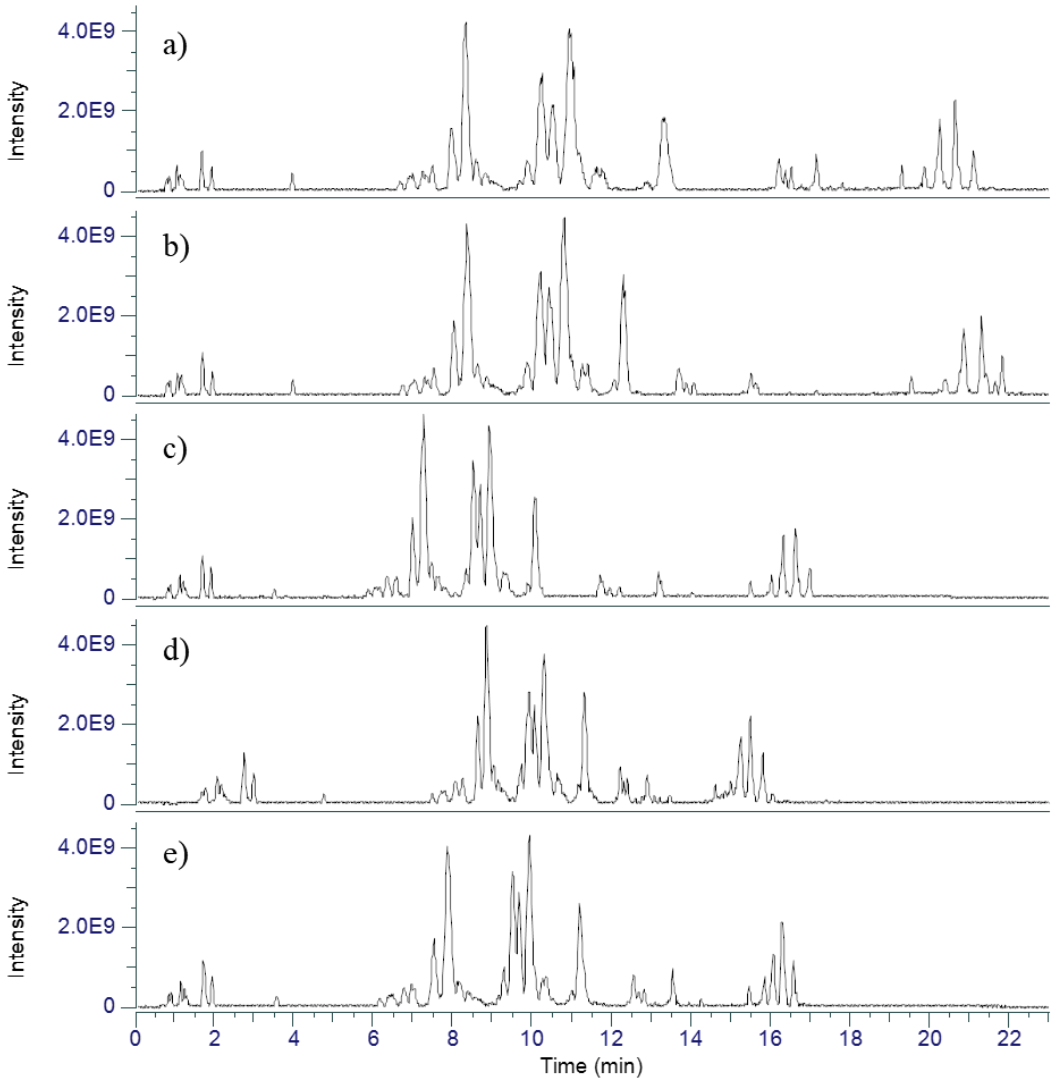

Figure D.8. Base Peak Chromatogram (BPC) for Serum samples used for the evaluation gradients 6 to 10 of the 1 mm ID UHPLC gradient optimization using MPA - 10mM ammonium formate in 40:40:20 MeOH/ACN/H_2O and MPB - 10mM ammonium formate in 95:5 IPA/H_2O and 55 ºC; a) Gradient 6 – 25.1 min gradient (0 min – 15% MPB, 1 min – 15% MPB, 2.5 min – 34% MPB, 4.5 min – 36% MPB, 8.5 min – 38% MPB, 13.5 min – 41% MPB, 13.6 min – 41% MPB, 15 min – 75% MPB, 20.6 min – 93% MPB, 22.6 min – 98% MPB, 24.1 min – 98% MPB, 25.1 min – 15% MPB); 4 min equilibration (15% MPB); with flow rate starting at 100 µL/min until 2.5 min, reducing it to 50 µL/min from 2.5 to 13.6 min, and further reducing it to 35 µL/min until the end of the run; b) Gradient 7 – 25.6 min gradient (0 min – 15% MPB, 1 min – 15% MPB, 2.5 min – 34% MPB, 6.3 min – 37% MPB, 9 min – 39% MPB, 14 min – 60% MPB, 14.1 min – 60% MPB, 17.1 min – 75% MPB, 21.1 min – 93% MPB, 23.1 min – 98% MPB, 24.6 min – 98% MPB, 25.6 min – 15% MPB); 4 min equilibration (15% MPB); with flow rate starting at 100 µL/min until 1 min,

reducing it to 50 µL/min from 1 to 14 minutes and further reducing it to 35 µL/min until the end of the run. c) Gradient 8 – 19.9 min gradient (0 min – 15% MPB, 0.5 min – 15% MPB, 1.5 min – 34% MPB, 5.7 min – 39% MPB, 10.3 min – 55% MPB, 10.4 min – 55% MPB, 12.4 min – 75% MPB, 15.4 min – 93% MPB, 17.4 min – 98% MPB, 18.9 min – 98% MPB, 19.9 min – 15% MPB); 4 min equilibration (15% MPB); with flow rate starting at 100 µL/min until 0.5 min, reducing it to 50 µL/min at 0.5 min until 10.3 min, and further reducing it to 35 µL/min until the end of the run. d) Gradient 9 – 18.9 min gradient (0 min – 15% MPB, 2.5 min – 31% MPB, 6.9 min – 37% MPB, 9.4 min – 55% MPB, 9.5 min – 55% MPB, 11.4 min – 75% MPB, 13.9 min – 93% MPB, 15.9 min – 98% MPB, 17.4 min – 98% MPB, 18.9 – 10% MPB); 4 min equilibration (10% MPB); with flow rate starting at 50 µL/min until 9.4 min, reducing it to 35 µL/min from 9.4 to 9.5 min and maintaining it until the end of the run. e) Gradient 10 - 23.9 min gradient (0 min – 15% MPB, 0.5 min – 15% MPB, 1.5 min – 34% MPB, 7.3 min – 37% MPB, 10.1 min – 55% MPB, 10.2 min – 55% MPB, 12.5 min – 75% MPB, 14.5 min – 93% MPB, 16 min – 98% MPB, 19 min – 98% MPB, 20 – 15% MPB); 4 min equilibration (15% MPB); with flow rate starting at 50 µL/min until 12.8 min, reducing it to 35 µL/min from until the end of the run.

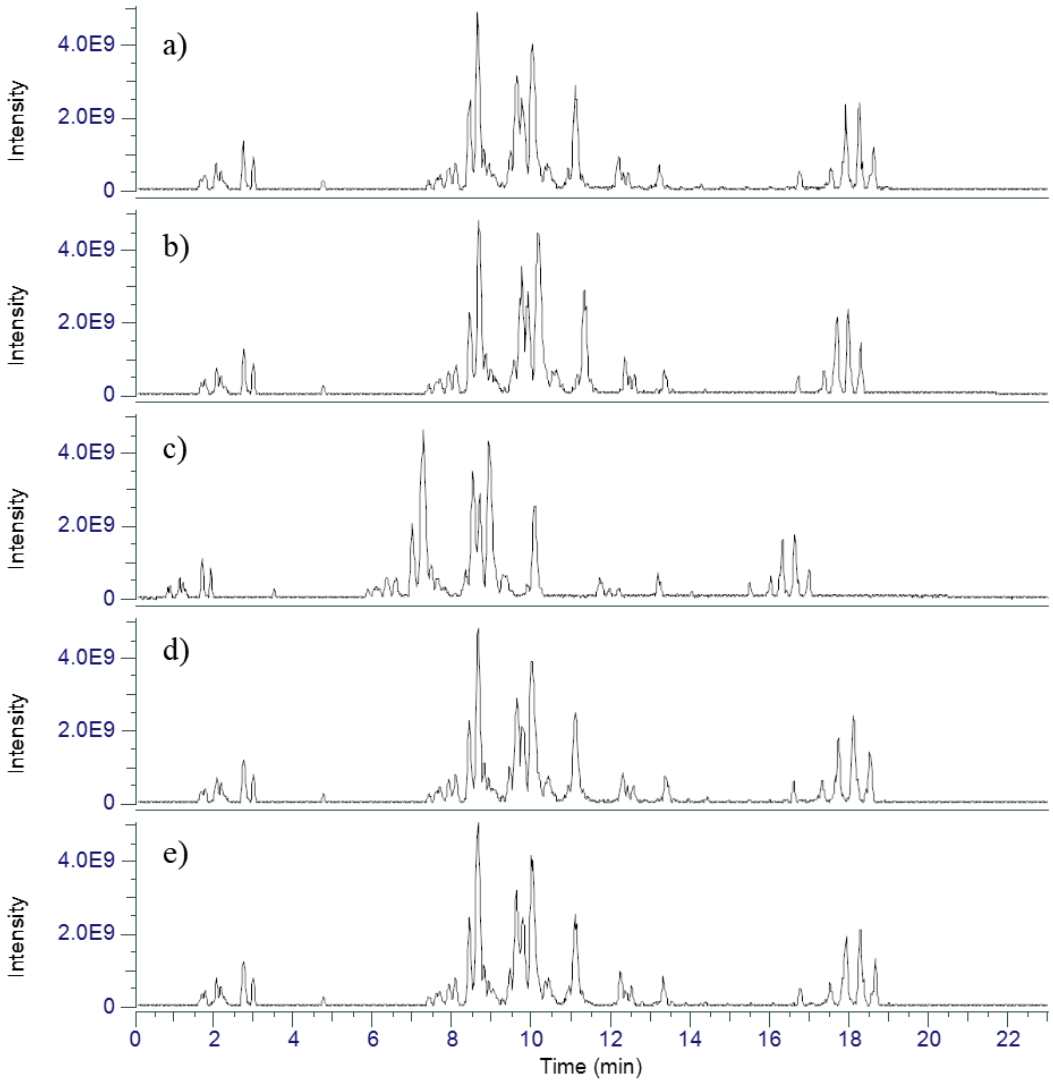

Figure D.9. Base Peak Chromatogram (BPC) for Serum samples used for the evaluation gradients 11 to 15 of the 1 mm ID UHPLC gradient optimization using MPA - 10mM ammonium formate in 40:40:20 MeOH/ACN/H_2O and MPB - 10mM ammonium formate in 95:5 IPA/H_2O and 55 ºC; a) Gradient 11 – 21.6 min gradient (0 min – 15% MPB, 2.5 min – 31% MPB, 6.4 min – 37% MPB, 9.4 min – 55% MPB, 10.8 min – 65% MPB, 15 min – 75% MPB, 16.9 min – 93% MPB, 18.1 min – 98% MPB, 20.6 min – 98% MPB, 21.6 min – 15% MPB); 4 min equilibration (15% MPB); with flow rate starting at 50 µL/min until 10.8 min, reducing it to 35 µL/min until the end of the run; b) Gradient 12 – 21 min gradient (0 min – 15% MPB, 2.5 min – 31% MPB, 6.4 min – 37% MPB, 9.3 min – 53% MPB, 9.4 min – 53% MPB, 10.8 min – 65% MPB, 14.8 min – 75% MPB, 16.4 min – 93% MPB, 17.5 min – 98% MPB, 20 min – 98% MPB, 21 min – 15% MPB); 4 min equilibration (15% MPB); with flow rate starting at 50 µL/min until 9.3 min, reducing it to 35 µL/min from 9.3 to 9.4 min and maintaining it until the end of the run; c) Gradient 13 – 19.9 min gradient

(0 min – 15% MPB, 0.5 min – 15% MPB, 1.5 min – 34% MPB, 5.7 min – 39% MPB, 10.3 min – 55% MPB, 10.3 min – 55% MPB, 10.4 min – 55% MPB, 12.4 min – 75% MPB, 15.4 min – 93% MPB, 17.4 min – 98% MPB, 18.9 min – 98% MPB, 19.9 min – 15% MPB); 4 min equilibration (15% MPB); with flow rate starting at 100 µL/min until 1.5 min, reducing it to 50 µL/min from 1.5 to 10.3 min and further reducing it to 35 µL/min from 10.4 to 10.4 min and maintaining it until the end of the run; d) Gradient 14 – 23.5 min gradient (0 min – 15% MPB, 2.5 min – 31% MPB, 6.4 min – 37% MPB, 9.3 min – 55% MPB, 9.4 min – 55% MPB, 11.3 min – 65% MPB, 14.3 min – 75% MPB, 17.2 min – 93% MPB, 19.5 min – 98% MPB, 22.5 min – 98% MPB, 23.5 – 15% MPB); 4 min equilibration (15% MPB); with flow rate starting at 50 µL/min until 9.3 min, reducing it to 35 µL/min from 9.3 to 9.4 min and maintaining it until the end of the run. e) Gradient 15 – 22.5 min gradient (0 min – 15% MPB, 2.5 min – 31% MPB, 6.4 min – 37% MPB, 9.3 min – 55% MPB, 9.4 min – 55% MPB, 11.1 min – 65% MPB, 14.8 min – 75% MPB, 17.1 min – 93% MPB, 19 min – 98% MPB, 21.5 min – 98% MPB, 22.5 min – 15% MPB); 4 min equilibration (15% MPB); with flow rate starting at 50 µL/min until 9.3 min, reducing it to 35 µL/min from 9.3 to 9.4 min and maintaining it until the end of the run.

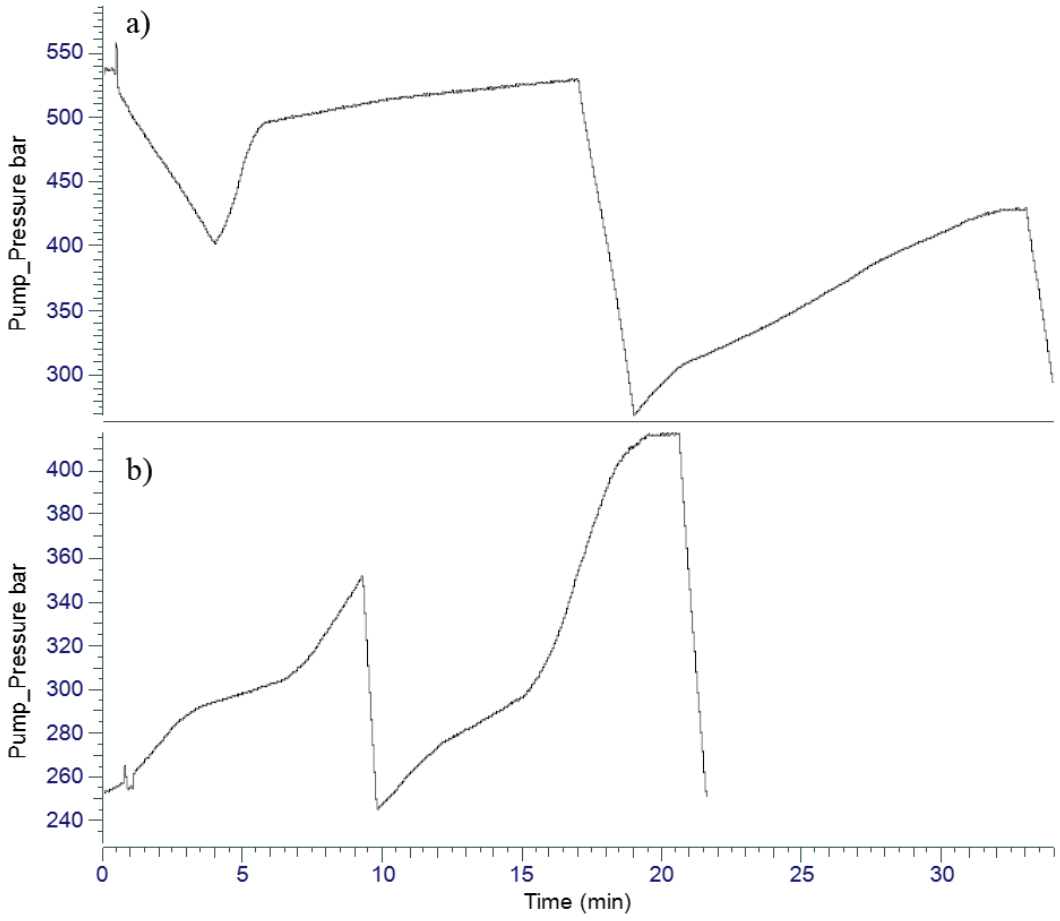

Figure D.10. Pump pressure during the gradient elution and optimization for a) Gradient 1; b) Gradient 12

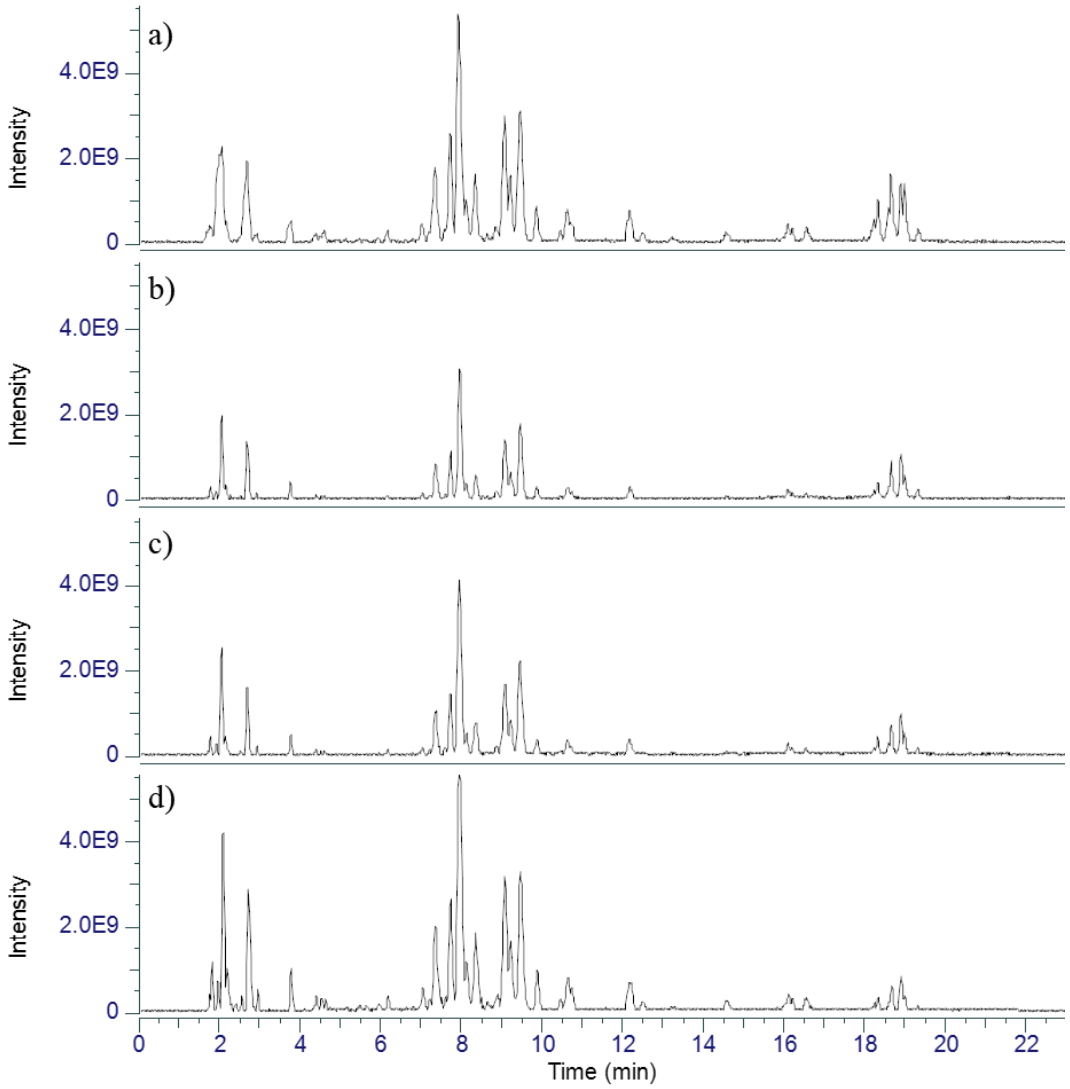

Figure D.11. Base Peak Chromatogram (BPC) for human serum samples used to evaluate sample dilution and injection volumes for positive ionization. A) Human serum samples diluted 8-fold and injected 4 µL; b) Human serum samples diluted 6-fold and injected 1 µL; c) Human serum samples diluted 4-fold and injected 1 µL; d) Human serum samples diluted 2-fold and injected 1 µL.

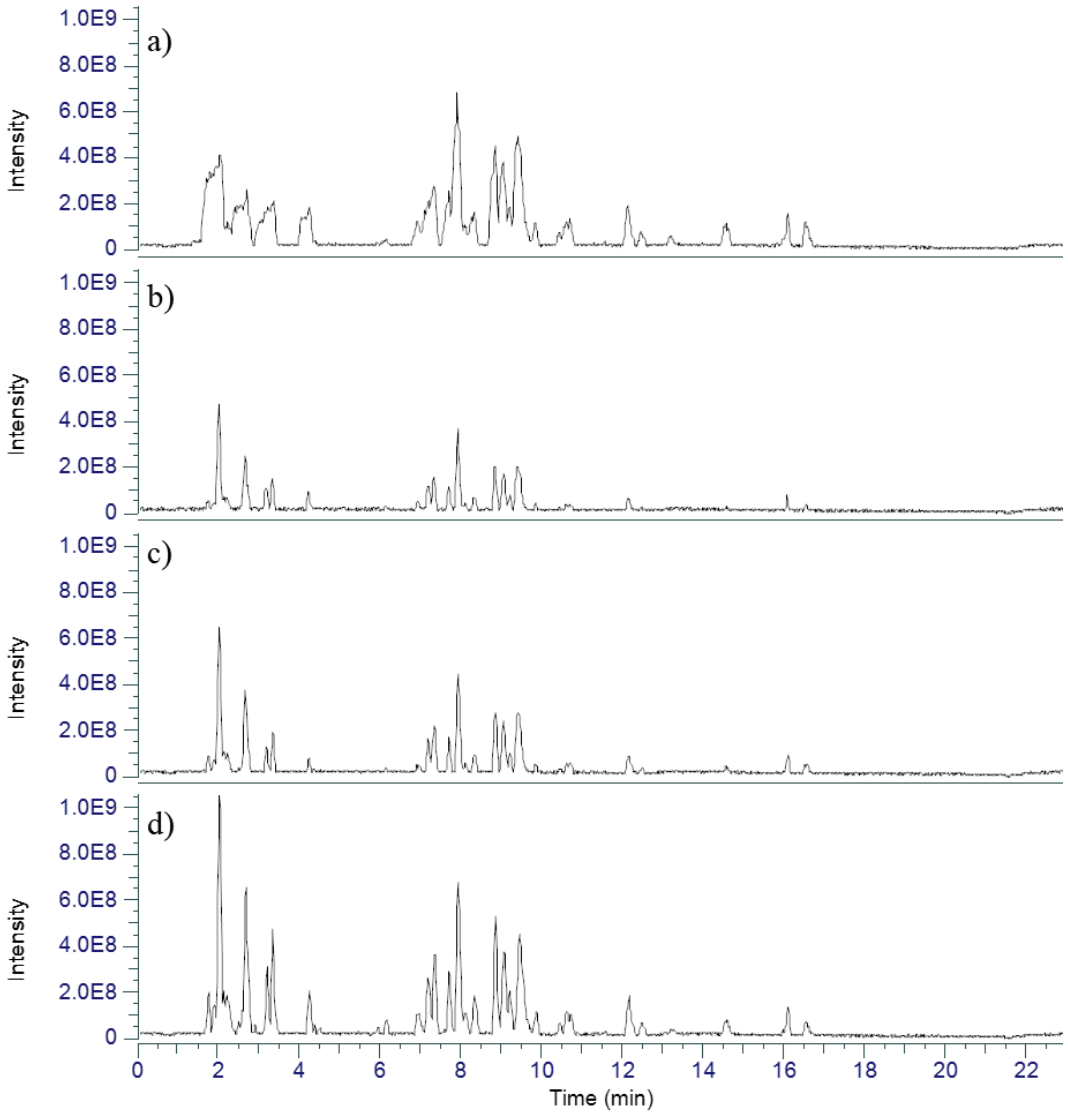

Figure D.12. Base Peak Chromatogram (BPC) for human serum samples used to evaluate sample dilution and injection volumes for negative ionization. A) Human serum samples diluted 8-fold and injected 10 µL; b) Human serum samples diluted 6-fold and injected 2 µL; c) Human serum samples diluted 4-fold and injected 2 µL; d) Human serum samples diluted 2-fold and injected 2 µL.

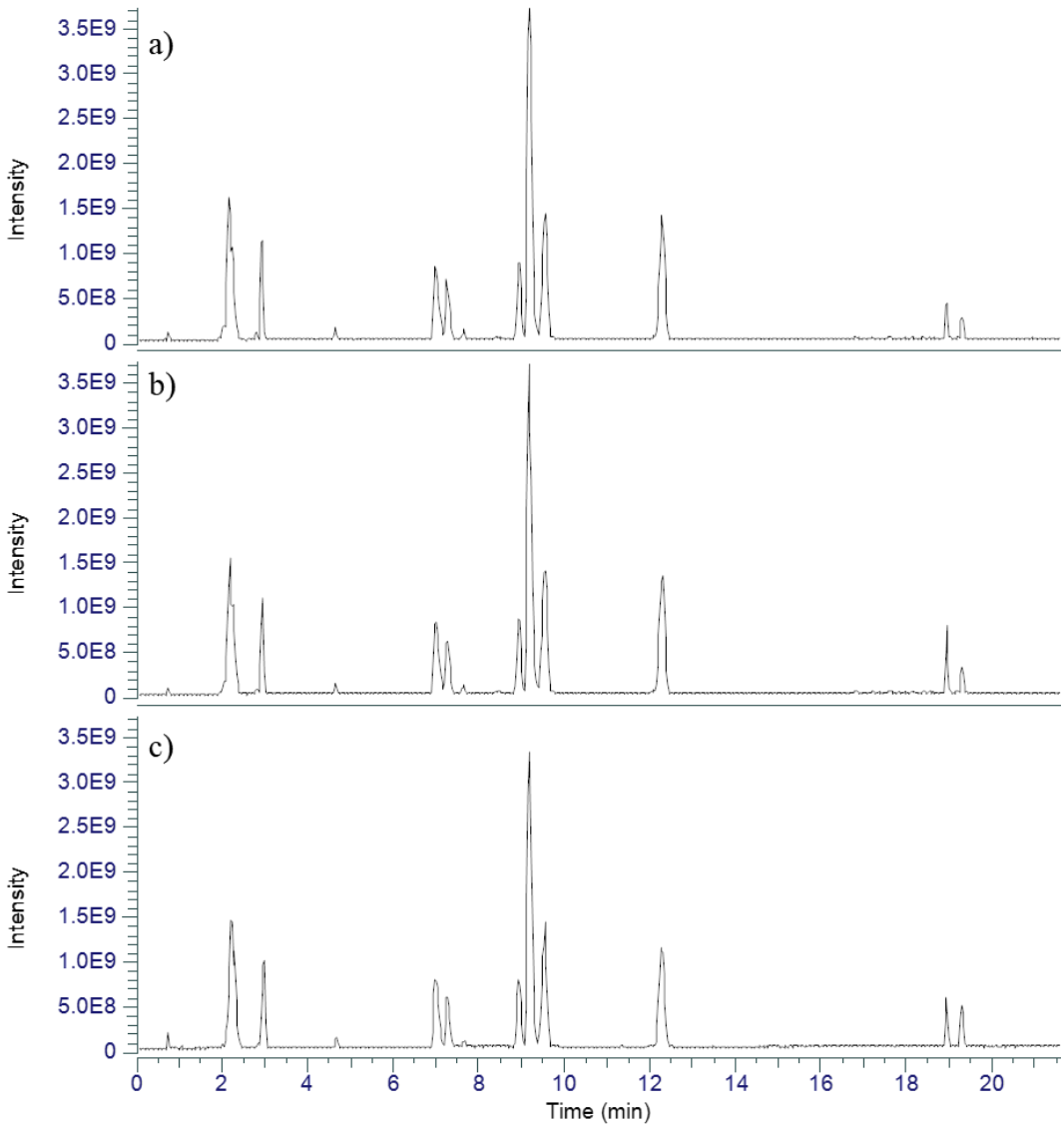

Figure D.13. Base Peak Chromatogram (BPC) for LipidRep Basic Standard mix for serum samples used to evaluate the resuspension solvent ratios. A) LipidRep IS in 3:2 MPA/MPB; b) LipidRep IS in 1:1 MPA/MPB; c) LipidRep IS in 2:3 MPA/MPB.

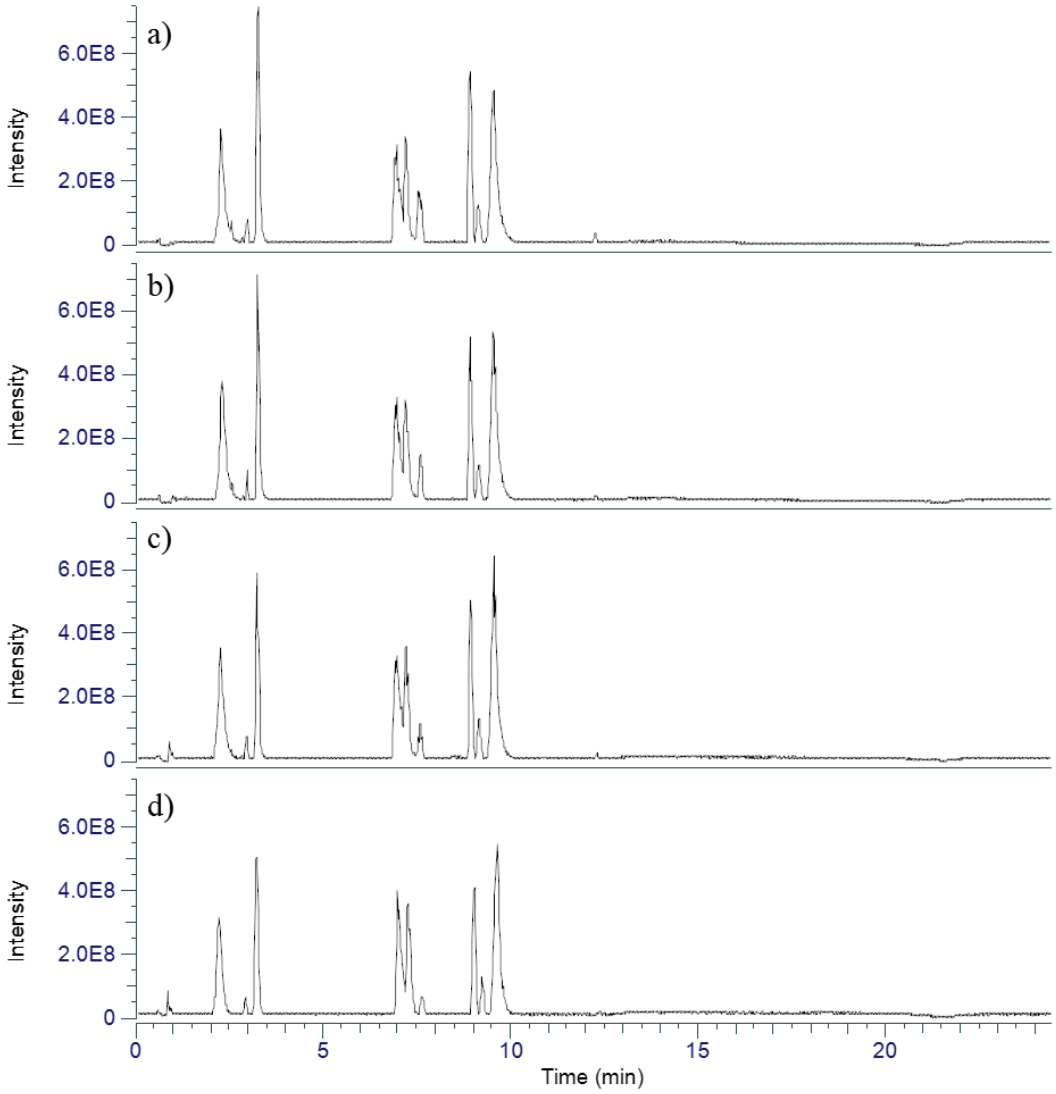

Figure D.14. Base Peak Chromatogram (BPC) for LipidRep Basic Standard mix for serum samples used to evaluate the ion source voltage for negative ionization. A) 3000 V; b) 3500 V; c) 4000 V; d) 4500 V.

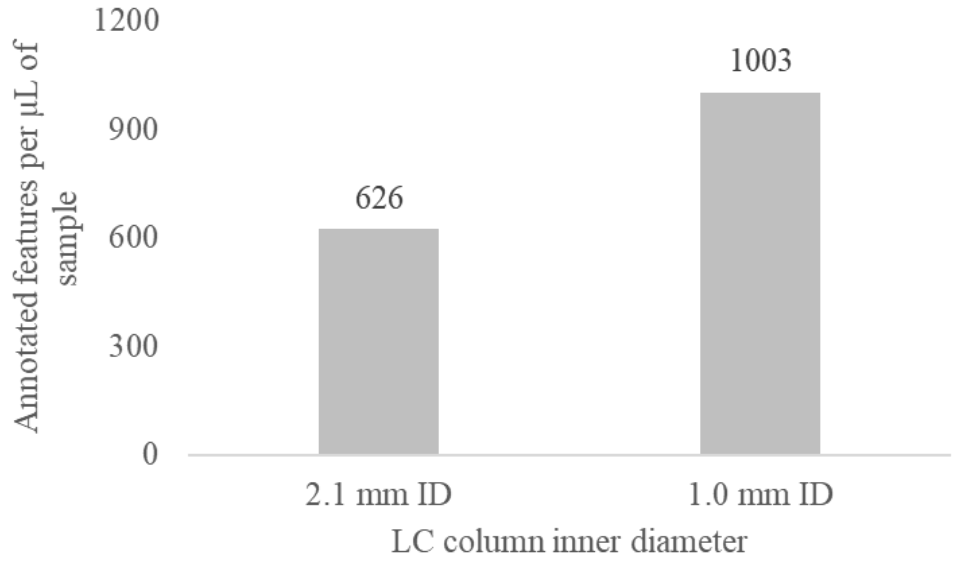

Figure D.15. Comparison between the number of MS/MS annotated features (Tier 1, MS/MS score > 500, and Tier 2, 100 < MS/MS score < 500, combined) for each UHPLC method.

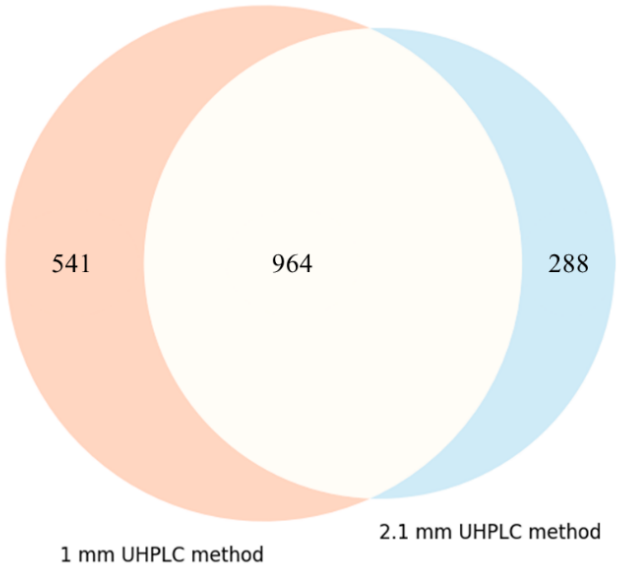

Figure D.16. Venn diagram displaying unique and shared MS/MS annotated lipid species in 1 mm ID and 2.1 mm ID UHPLC methods. The central intersection represents lipids annotated by both methods, and the outer sections denote the number of unique annotations made by each one.

Appendix E

Appendix E: Supplementary Figures for Chapter VI

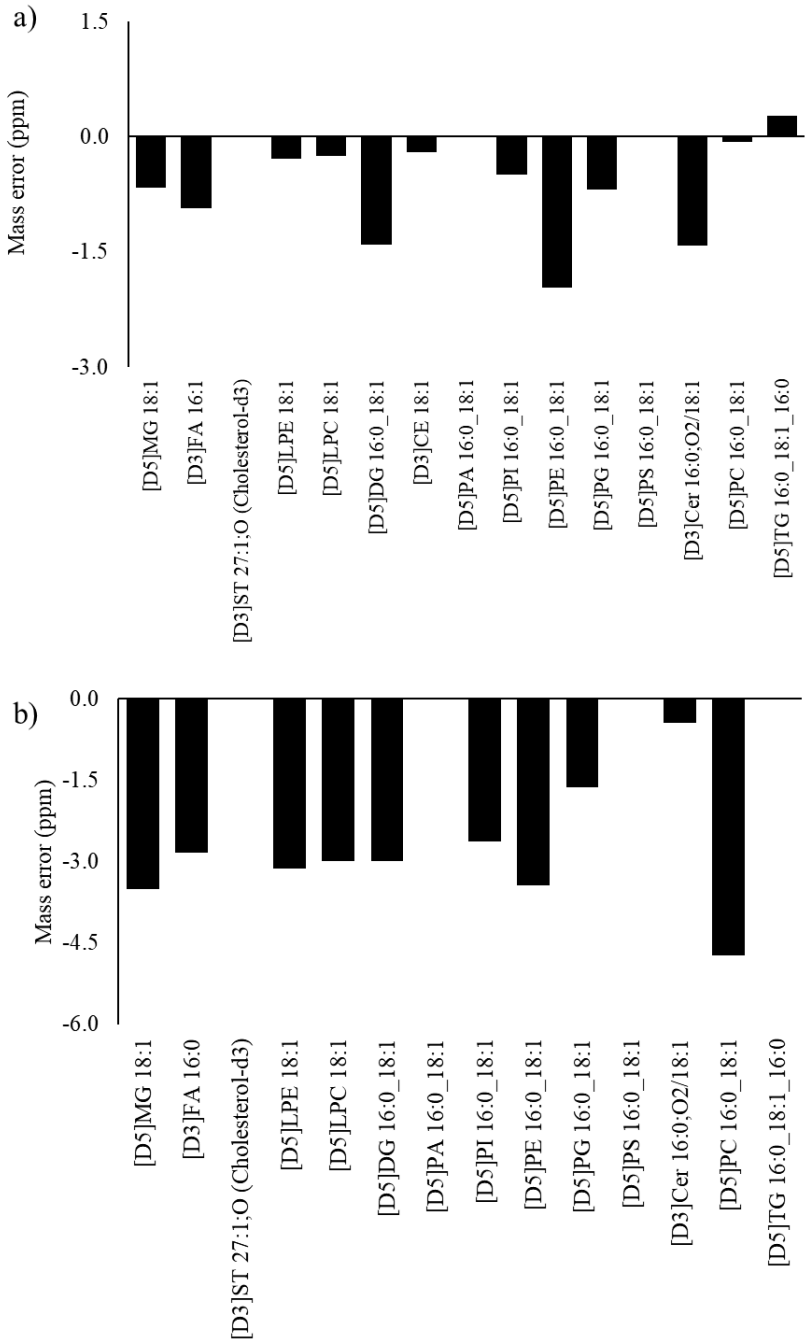

Figure E.1. Mass errors for the LipidRep Standard Mix for Tissue/Cells used in this study. a) Mass errors for A549 cell samples in positive ionization; b) Mass errors for A549 cell samples in negative ionization.

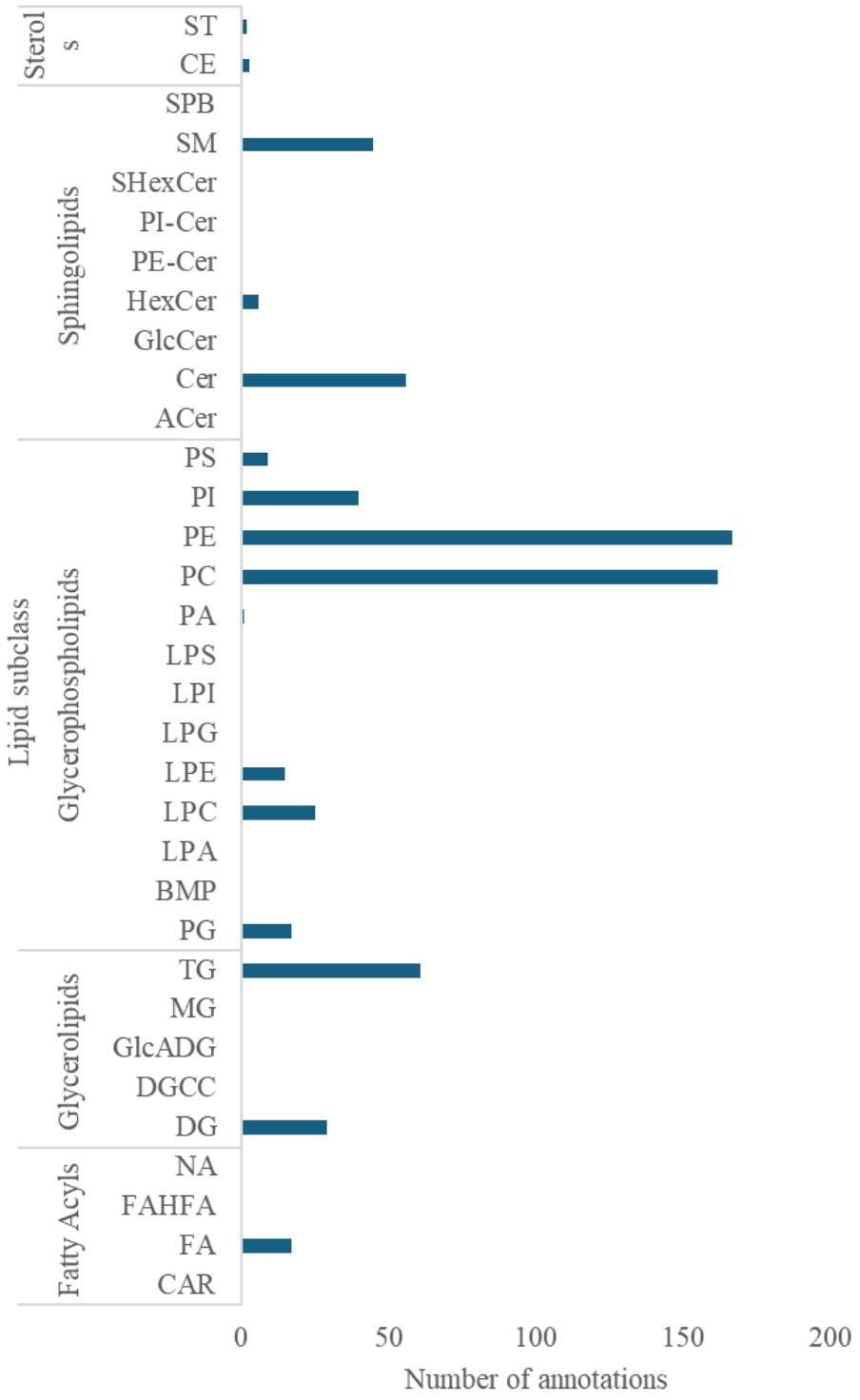

Figure E.2. Number MS/MS lipid annotation distribution across all subclasses for A549 cell samples.

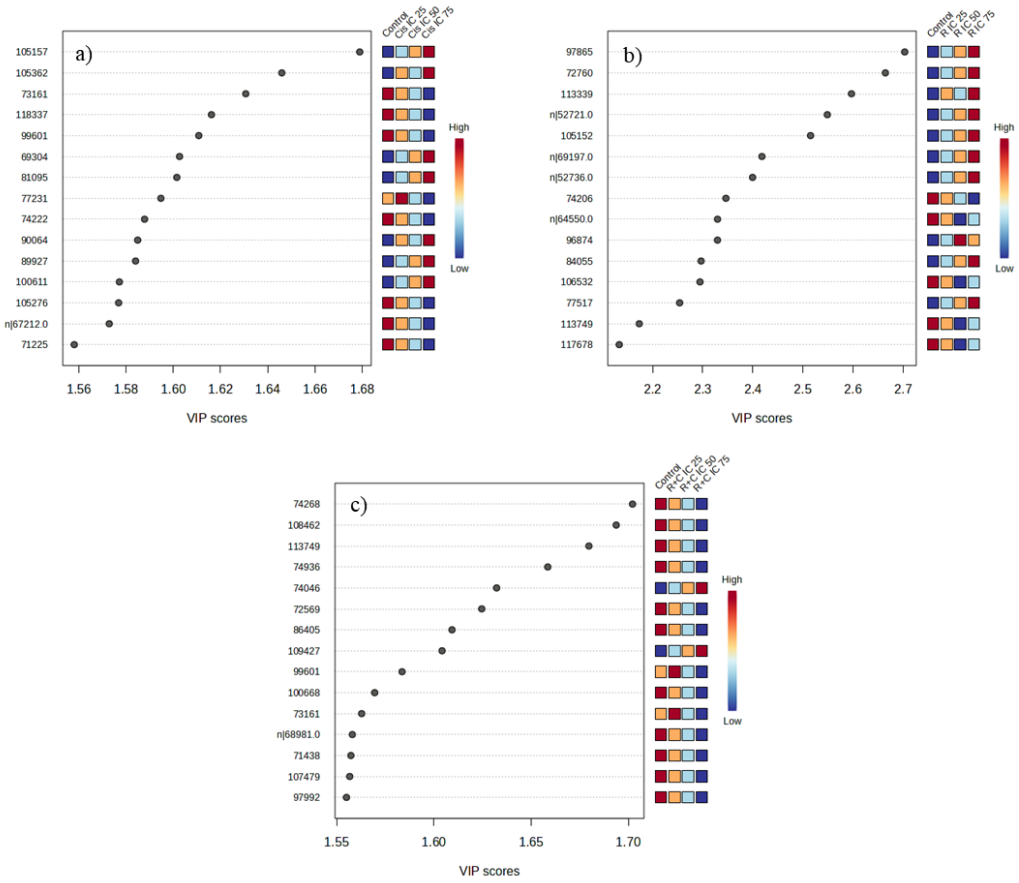

Figure E.3. PLS-DA VIP Scores for A549 cell samples: a) Control and cisplatin-treated samples; b) Control and rapamycin-treated samples; c) Control and combination treatment of rapamycin and cisplatin samples.

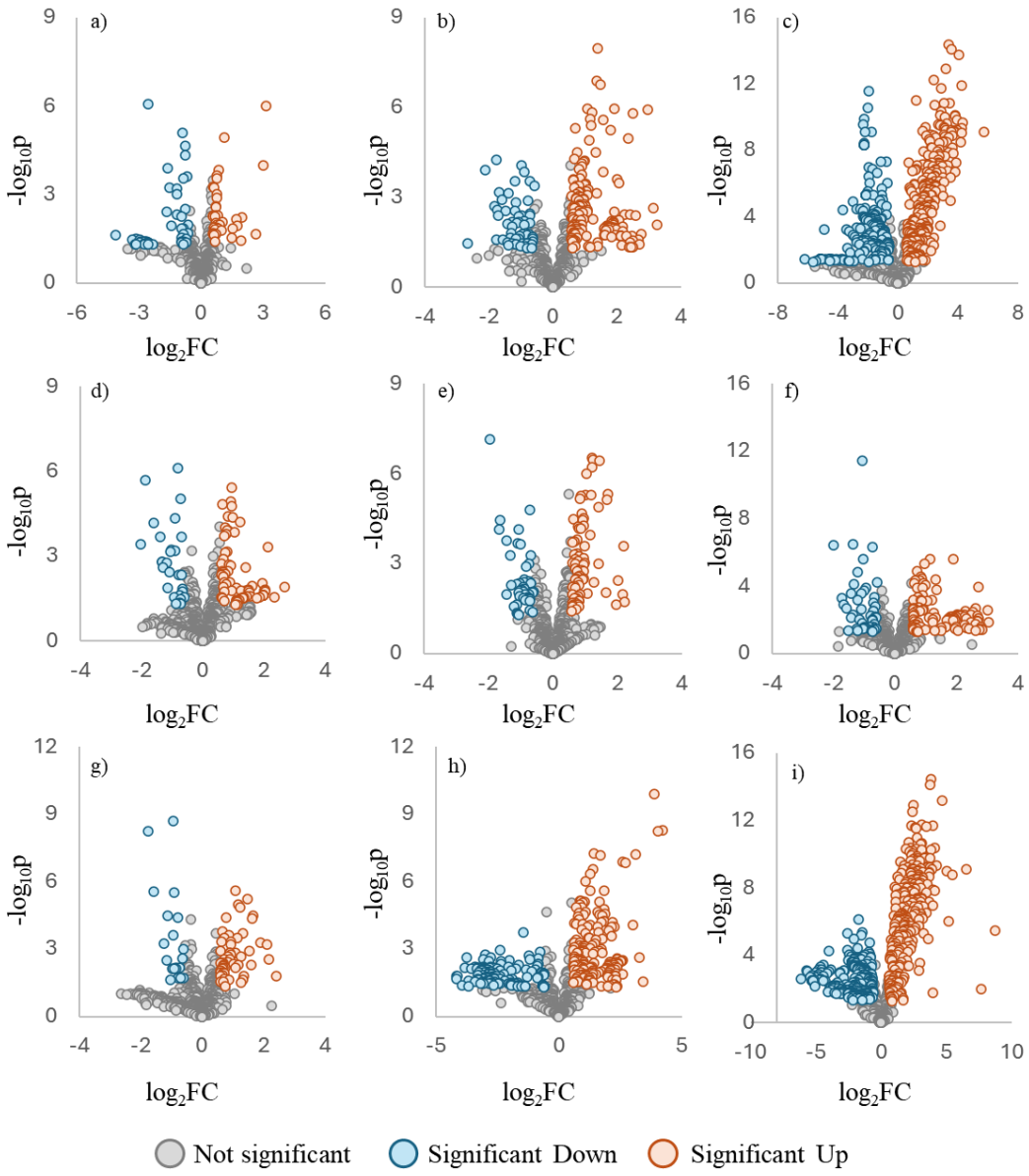

Figure E.4. A549 cell samples volcano plots a) Volcano plots for Control vs. cisplatin IC_{25} samples; b) Volcano plots for Control vs. cisplatin IC_{50} samples; c) Volcano plots for Control vs. cisplatin IC_{75} samples; d) Volcano plots for Control vs. rapamycin IC_{25} samples; e) Volcano plots for Control vs. rapamycin IC_{50} samples; f) Volcano plots for Control vs. rapamycin IC_{75} samples; g) Volcano plots for Control vs. cisplatin and rapamycin combined IC_{25} samples; h) Volcano plots for vs. cisplatin and rapamycin combined IC_{50} samples; i) Volcano plots for vs. cisplatin and rapamycin combined IC_{75} samples.